Design, Characterisation and Performance Assessment Issues of Multi-Carrier CDMA Exploiting Higher Order PSK/QAM Formats for Future Wireless Systems

Thesis Submitted in Candidature for the Degree of Doctor of Philosophy

February 2003

Nishita Hathi

Department of Electronic and Electrical Engineering
University College London
London
UK

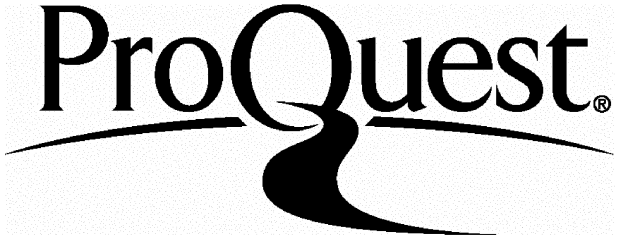

To my husband Nirav

Acknowledgements

First and foremost I am extremely grateful to my supervisors Prof. John O'Reilly and Dr. Izzat Darwazeh for their advice, guidance and support throughout the course of this study.

I would also like to express my sincere thanks to Miguel Rodrigues for his invaluable help throughout the study. A special thanks to all my colleagues in the Telecommunications Research Laboratory at UCL for making the duration of the research very enjoyable.

I am grateful to Anritsu UK and to the Engineering and Physical Sciences Research Council (EPSRC) for their financial support.

Many thanks to Alex Elsey, Mike Lee, Dan Fox, Ken Hattersley and the EMD team at Anritsu for their help and advice.

I am also indebted to my family for their support. In particular, I would like to thank my parents for their encouragement and wholehearted support and my husband for his constant help, patience and understanding.

Abstract

This thesis presents research that has addressed various design issues related to multi-carrier Code Division Multiple Access (CDMA) communication systems. The combination of multi-carrier CDMA with higher order Phase Shift Keying (PSK) and Quadrature Amplitude Modulation (QAM) mapping has been considered. The investigation has been carried out for two different multi-carrier CDMA schemes, namely, Multi-Carrier CDMA (MC-CDMA) and Multi-Carrier Direct Sequence CDMA (MC-DS-CDMA). Different architectures for combining multi-carrier CDMA with higher order PSK/QAM mapping have been developed. Their performance has been studied in terms of power efficiency, spectral efficiency and implementation complexity. As for all multi-carrier arrangements, the Peak-to-Average Power Ratio (PAPR) is of special significance and accordingly the implications for PAPR has also been investigated.

Multi-carrier CDMA signals are vulnerable to the non-linear distortion caused by non-linear elements and system components (such as High Power Amplifier (HPA)). The degradation due to non-linear effects is expected to be even more significant when higher order constellations are used. Hence, the degradation caused by HPA non-linearities on higher order PSK/QAM multi-carrier CDMA signals has been studied in terms of Bit Error Rate (BER) degradation and spectral spreading.

The high PAPR of the multi-carrier CDMA signal results in reduced system efficiency (in the presence of non-linearities). Controlling the PAPR of the multi-carrier CDMA signal is one way of improving system performance. In this work the variation of the PAPR of multi-carrier CDMA (MC-CDMA and MC-DS-CDMA) with allocation of the spreading codes has been investigated.

Overall, the theoretical, design and simulation issues addressed in this thesis provide an insight into the performance of PSK/QAM multi-carrier CDMA systems in the presence of Additive White Gaussian Noise (AWGN) and HPA non-linearities. The results obtained can be used by receiver designers, as well as system and network developers of future wireless systems.

Contents

List of Figures

List of Tables

List of Abbreviations

1G	First Generation Mobile Communications Systems
2G	Second Generation Mobile Communications Systems
3G	Third Generation Mobile Communications Systems
4G	Fourth Generation Mobile Communications Systems
A/D	Analogue-to-Digital Converter
AM/AM	Amplitude Modulation/Amplitude Modulation
AM/PM	Amplitude Modulation/Phase Modulation
AWGN	Additive White Gaussian Noise
BER	Bit Error Rate
BPSK	Binary Phase Shift Keying
CCDF	Complimentary Cumulative Distribution Function
CDMA	Code Division Multiple Access
CF	Crest Factor
CIF	Combining in Frequency
CIT	Combining in Time
CIT-SC	Combining in Time-Serial Combination
CIT-PC	Combining in Time-Parallel Combination
CP	Cyclic Prefix
DAB	Digital Audio Broadcasting
D/A	Digital-to-Analogue Converter
DFT	Discrete Fourier Transform
DS-CDMA	Direct Sequence Code Division Multiple Access
DSP	Digital Signal Processing
DVB	Digital Video Broadcasting
E_b	Average Energy per bit
EU/IST	European Union/Information Society Technologies

FDMA	Frequency Division Multiple Access
FEC	Forward Error Correction
FFH	Fast Frequency Hopping
FFT	Fast Fourier Transform
FH-CDMA	Frequency Hopping Code Division Multiple Access
FLOPS	Floating Point Operations
GP	Guard Period
GPRS	General Packet Radio Service
HD	Harmonic Distortion
HDD	Hard Decision Demapping
HPA	High Power Amplifier
IBO	Input Back-Off
ICI	Inter Carrier Interference
IDFT	Inverse Discrete Fourier Transform
IEEE	Institute of Electrical and Electronics Engineers
IFFT	Inverse Fast Fourier Transform
IMD	Intermodulation Distortion
ISI	Inter Symbol Interference
LAN	Local Area Network
MC-CDMA	Multi-Carrier CDMA
MC-DS-CDMA	Multi-Carrier Direct Sequence CDMA
MCM	Multi-Carrier Modulation
MIPS	Millions of Instructions per Second
MLSE	Maximum Likelihood Sequence Estimation
MOPS	Millions of Operations per Second
MT-CDMA	Multi-Tone CDMA
N_0	Single-sided noise power spectral density
OBO	Output Back-Off
OFDM	Orthogonal Frequency Division Multiplexing
OPS	Operations per Second
PAPR	Peak-to-Average-Power Ratio
PN	Pseudo-Noise
P/S	Parallel-to-Serial
PSD	Power Spectral Density
PSK	Phase Shift Keying
PTS	Partial Transmit Sequence
QAM	Quadrature Amplitude Modulation
QPSK	Quadrature Phase Shift Keying
RF	Radio Frequency

RLC/MAC	Radio Link Control/Medium Access Control
SFH	Slow Frequency Hopping
SLM	SeLective Mapping
SNR	Signal-to-Noise Ratio
S/P	Serial-to-Parallel
SSPA	Solid State Power Amplifier
TDMA	Time Division Multiple Access
TH-CDMA	Time Hopping Code Division Multiple Access
TWTA	Travelling Wave Tube Amplifier
W-CDMA	Wideband CDMA
WH	Walsh Hadamard
WLL	Wireless Local Loop
WWRF	Wireless World Research Forum

Chapter 1

Introduction

The third generation (3G) of mobile communications systems are currently being deployed around the world. The first 3G network was deployed in Japan by NTT DoCoMo during May 2001. In Europe, the first 3G network was deployed in the UK by MANX telecom in December 2001. Analysts predict that 3G systems deployment will be completed globally by 2006.

History indicates that mobile communication systems pass through a paradigm shift in 10 year cycles. The first generation (1G) of mobile communication systems were introduced in the early eighties, the second generation (2G) systems were introduced in the early nineties and the third generation at the beginning of this millennium. This implies that the fourth generation (4G) of mobile communication systems are expected to be introduced around 2010.

At present, there is little in the way of standardisation for 4G systems. A number of interest groups and fora are working towards formulating visions on strategic future research directions for 4G systems. These include: Wireless World Research Forum (WWRF) [1], 4G mobile forum [2] and an EU/IST initiative called *cluster on systems beyond 3G* [3]. Numerous telecoms operators and equipment manufacturers have also commenced research into 4G systems [4, 5]. In October 2002, NTT DoCoMo successfully conducted experimental fourth generation transmission (with data rates of 100 Mbps in the downlink and 20 Mbps in the uplink) in an indoor laboratory environment [6].

At present, there are many competing views on the nature of 4G systems. However, it is expected that 4G systems will be capable of providing a large variety of data rates over a wide range of propagation environments, mobility conditions, wireless devices and networks.

The data rates proposed for 4G systems vary from 10 Mbps [7] to 100 Mbps [6, 8]. However, it is expected that initial systems will provide 10-20 Mbps. The bandwidth requirement for such systems will be between 10 MHz and 100 MHz. In order to accommodate such wide

bandwidths, the systems will operate at frequencies greater than 3 GHz [9]. In [8] it is stated that frequencies as high as 40 – 60 GHz may be considered.

From the data rates suggested above, it is evident that 4G will necessitate the use of transmission schemes which can accommodate very high data rates over the "hostile" wireless channel. Multi-carrier CDMA schemes have been proposed as a strong candidate for such systems[1] [10, 11] due to the fact that they provide better performance in the presence of multipath fading as compared to traditional CDMA schemes.

Since their introduction in the early nineties, much research has been carried out into the performance of multi-carrier CDMA systems. This thesis addresses some design issues related to multi-carrier CDMA system performance. The details of the thesis structure and the contributions of the work are presented in the following sections.

1.1 Thesis structure

Following this introductory chapter, an overview of multi-carrier CDMA is presented in Chapter 2. The chapter is divided into 3 sections. The first section introduces the basics of CDMA multiple access technique. It provides a review of the pioneering developments of CDMA technology, explains the fundamentals of CDMA and describes the different CDMA techniques (namely, direct sequence spread spectrum, frequency hopping, time hopping and hybrid CDMA systems). The second section looks at Multi-Carrier Modulation (MCM). It gives a brief overview of the development of multi-carrier modulation techniques, presents the fundamentals of multi-carrier Modulation and introduces a special form of MCM technique called Orthogonal Frequency Division Multiplexing (OFDM). The final section introduces the concept of combining CDMA with MCM (multi-carrier CDMA). It reviews the different multi-carrier CDMA schemes proposed to date (namely, MC-CDMA, MC-DS-CDMA and MT-CDMA) and describes the system model and spectral characteristics of each scheme. As multi-carrier CDMA schemes will operate in a multipath environment, a brief overview of multipath is provided. The concept of cellular multi-carrier CDMA systems is also discussed together with the key properties of multi-carrier CDMA signals.

Chapter 3 and Chapter 4 explore the implications of using higher order PSK/QAM mapping on the performance of multi-carrier CDMA systems. Chapter 3 focuses on MC-CDMA and Chapter 4 focuses on MC-DS-CDMA.

There are a number of ways in which higher order PSK/QAM mapping can be incorporated into MC-CDMA systems. Two particular implementations have been considered in Chapter 3. The performance of the two implementations is measured in terms of the power efficiency, PAPR, spectral efficiency and implementation complexity. The chapter begins by presenting the two implementations considered. The subsequent section discusses the

[1] The experimental 4G system developed by NTT DoCoMo also employs a form of multi-carrier CDMA scheme: orthogonal frequency code division multiplexing technologies (described in [12]).

parameters used to assess the performance of the two implementations with different PSK/QAM formats. The performance of the two implementations is then presented and a comparison is made between the two implementations in order to determine the advantages and drawbacks of each in relation to the other.

Chapter 4 is concerned with the performance of MC-DS-CDMA incorporating higher order PSK/QAM mapping. As in the case of MC-CDMA, different implementations for combining higher order PSK/QAM mapping with MC-DS-CDMA have been considered. The performance of the different implementations in terms of power efficiency, PAPR, spectral efficiency and implementation complexity is presented and compared for the different implementations in order to identify the advantages and drawbacks of each.

Chapter 5 investigates the degradation of multi-carrier CDMA systems (MC-CDMA and MC-DS-CDMA) performance with higher order PSK/QAM mapping in the presence of HPA non-linearities. The chapter begins by presenting an overview of HPAs. In particular, it describes the various classifications of HPAs, the effects of HPA non-linearities on system performance and techniques for modelling and simulating HPA non-linearities. The subsequent section discusses the performance parameters used to analyse the effects of HPA non-linearities on the input signal (namely, BER degradation and spectral spreading). This is followed by a description of the system models used for the investigation and a discussion of the results obtained.

Chapter 6 is concerned with an investigation into the performance of multi-carrier CDMA systems with different Walsh Hadamard (WH) spreading code allocation strategies in the presence of HPA non-linearities. The chapter is divided into four sections. The first section details the concept of PAPR. It provides a description of why low PAPR is desired in a system with non-linear elements such as the HPA and discusses the analytic and simulation technique used in the literature to calculate the PAPR. The second section deals with spreading codes in CDMA systems. It provides background on spreading codes and discusses the effects of spreading code allocation on the performance of single and multi-carrier CDMA systems in terms of PAPR. The third section discusses the use of scrambling codes in CDMA based systems and provides some background into the scrambling codes employed in current CDMA systems. The final section describes the transmission scheme used for the investigation and the techniques used to allocate the WH codes to different users. The PAPR performance of both multi-carrier CDMA schemes, for different WH code allocations is investigated and presented together with the performance of both schemes in the presence of HPA non-linearities for different WH code allocations.

The thesis ends with Chapter 7. The chapter describes the main outcomes of the research and presents the concluding remarks. Suggestions for further areas of research are also proposed.

The thesis includes four appendices. Appendix A demonstrates why the simple receiver architecture proposed for implementation-2 in Chapter 3 can only successfully demodulate data for a single user case. Appendix B discusses some MATLAB™ modelling issues. Appendix C

discusses the BER degradation experience by the proposed MC-CDMA scheme in Chapter 3 in the presence of AWGN and Appendix D lists the different WH code allocations considered in Chapter 6 and presents the PAPR performance of each allocation.

1.2 Contributions to the research field

The research reported in this thesis has provided an assessment of the performance of multi-carrier CDMA systems (MC-CDMA and MC-DS-CDMA) in combination with higher order PSK/QAM formats using different architectures and in the presence of AWGN and HPA non-linearities[2]. The main contributions of the thesis are summarised below:

- Development of different architectures for incorporating higher order PSK/QAM mapping within MC-CDMA and MC-DS-CDMA schemes. In the existing architectures, higher order mapping allows the input data to be combined such that more data can be transmitted over a given symbol. In the proposed architectures, higher order mapping allows the input data to be combined such that more data can be transmitted over a given subcarrier.

- Investigation of the performance of MC-CDMA and MC-DS-CDMA incorporating higher order PSK/QAM mapping using existing and proposed architectures. The existing architectures are termed *combining in time* whereas the proposed architectures are termed *combining in frequency.* The performance matrix consists of power efficiency, PAPR, spectral efficiency and implementation complexity. Both multi-user and single user scenarios have been considered. Comparative studies of the performance of the different MC-CDMA and MC-DS-CDMA architectures are also carried out in order to identify the merits and demerits of each architecture.

- Investigation of the effects of HPA non-linearities on the performance of MC-CDMA and MC-DS-CDMA with different number of active users. The performance is analysed in terms of BER degradation and spectral spreading. Results show that in the MC-CDMA case, contrary to implicit assumptions, increasing the number of active users improves the performance of the system in the presence of HPA non-linearities. In the case of MC-DS-CDMA, it is concluded that changing the number of active users has no effect on the performance of the system in the presence of HPA non-linearities.

- Investigation of the effect of HPA non-linearities on the performance of MC-CDMA and MC-DS-CDMA with higher order PSK/QAM mapping formats. In both cases (MC-CDMA and MC-DS-CDMA), the existing implementation for incorporating higher order PSK/QAM

[2] Only one architecture has been consider for the investigation of the performance of MC-CDMA and MC-DS-CDMA systems in the presence of HPA non-linearities.

formats into multi-carrier CDMA (combining in time) has been used. The performance is analysed in terms of BER degradation and spectral spreading.

- Exploration of the influence of WH code allocation strategies on the PAPR of MC-CDMA and MC-DS-CDMA signal. It has been observed that the PAPR of MC-CDMA is significantly dependent on the allocation of WH codes (especially for small number of active users) whereas the PAPR of MC-DS-CDMA remains unchanged with the allocation of WH codes.

- Based on the observation that the PAPR of MC-CDMA signal is influenced by the allocation of the WH code, the performance of MC-CDMA and MC-DS-CDMA system in the presence of HPA non-linearities, with different WH code allocations is investigated. The results have shown that the performance of MC-CDMA in the presence of HPA non-linearities is significantly affected by the allocation of the WH code and hence appropriate allocation of the WH codes can improve the performance of MC-CDMA in the presence of HPA non-linearities. The performance of MC-DS-CDMA remains unchanged for different allocation of the WH codes.

The research work has resulted in nine publications, to date. The current research papers are listed below in the order in which they were published.

1. Nishita Hathi, "Investigating the effect of coding, interleaving and modulating GPRS RLC/MAC data", Proceedings of the London Communications Symposium 1999, pp. 65-68, London, U.K., July 1999.

2. Nishita Hathi, "Simulation of multi-carrier CDMA system for future wireless systems", Proceedings of London Communications Symposium 2000, pp. 45-48, London, U.K., September 2000.

3. N. Hathi and J. O'Reilly, "Performance assessment of higher-order MC-CDMA for 4th generation wireless systems," Proceedings of the 35th Annual Conference on Information Sciences and Systems, vol. 1, pp. 220-224 , Baltimore, U.S.A., March 2001.

4. Nishita Hathi and J. O'Reilly, "Peak-to-average power ratio in higher-order MC-CDMA", Proceedings of London Communications Symposium 2001, pp. 199-202, London, U.K., September 2001.

5. N. Hathi and J. O'Reilly, "Characterisation and performance assessment of MC-CDMA exploiting higher-order PSK/QAM formats," Proceedings of 3rd International Conference in Information, Communication and Signal Processing, Singapore, October 2001.

6. N. Hathi, M. Rodrigues, I. Darwazeh and J. O'Reilly, "Performance assessment of MC-CDMA and MC-DS-CDMA in the presence of high power amplifier non-linearities," Proceedings of IEEE Vehicular Technology Conference 2002, vol. 3, pp. 1467-1471, Birmingham, Alabama, U.S.A., May 2002.

7. N. Hathi and I. Darwazeh, "Performance of PSK/QAM multi-carrier CDMA schemes in the presence of HPA non-linearities", Proceedings of London Communications Symposium 2002, pp. 37-40, London, U.K., September 2002.

8. N. Hathi, M. Rodrigues, I. Darwazeh and J. O'Reilly, "Analysis of the influence of spreading code allocation strategies on the performance of multi-carrier CDMA systems in the presence of HPA non-linearities," Proceedings of IEEE Personal, Indoor Mobile Radio Conference 2002, vol. 3, pp. 1305-1309 , Lisbon, Portugal, September 2002.

9. N. Hathi, I. Darwazeh and J. O'Reilly, "Peak-to-average power ratio performance comparison of different spreading code allocation strategies for MC-CDMA and MC-DS-CDMA," Electronics Letters, vol. 38, no. 20, pp. 1219-1220, September 2002.

Chapter 2

Multi-carrier CDMA

The previous chapter provided an introduction to this thesis and indicated that multi-carrier CDMA is a strong candidate for future generation wireless systems as it is capable of facilitating the transmission of very high data rates over the "hostile" wireless channel. This chapter introduces the concept of multi-carrier CDMA.

The chapter is divided into 3 sections. Section 2.1 presents the basics of CDMA. It provides a review of the pioneering developments of CDMA technology. The fundamentals of CDMA technology are explained and the properties of the CDMA signal are briefly discussed. This is followed by a description of the different CDMA techniques, namely, direct sequence spread spectrum, frequency hopping, time hopping and hybrid CDMA systems.

Section 2.2 looks at multi-carrier modulation. It gives a brief overview of the development of multi-carrier modulation techniques and presents the fundamentals of multi-carrier modulation. This is followed by an introduction to a special form of MCM technique called OFDM.

Section 2.3 describes multi-carrier CDMA. Multi-carrier CDMA is a combination of CDMA and MCM. There are 3 ways in which CDMA can be combined with MCM. A review of the three schemes is presented together with a description of the system model and spectral characteristic of each scheme. As multi-carrier CDMA schemes will operate in a multipath environment, a brief overview of multipath is provided, followed by a description of the parameterisation of multi-carrier CDMA systems when operating in a multipath environment. The concept of cellular multi-carrier CDMA systems is also discussed, followed by a description of the key properties of multi-carrier CDMA signals. The chapter concludes with a summary.

2.1 Code Division Multiple Access

The basic ideas of CDMA were first introduced by Claude Shannon and Robert Pierce in 1949 [13]. The cellular application of CDMA was proposed in 1978 by Cooper and Nettleton [14]. During the 1980s, QUALCOMM [15] investigated CDMA for cellular systems, which led to the standardisation of CDMA in 1993. The first CDMA system, IS-95 [16] started operation in 1995 [15]. During recent years, wideband CDMA systems with a bandwidth of 5 MHz or over have been studied extensively throughout the world [17] for 3rd generation mobile communication systems. These include Wideband CDMA (W-CDMA) in Europe/Japan, cdma2000 [18] in the United States and TTA-I and TTA-II in Korea.

2.1.1 CDMA fundamentals

In a CDMA multiple access system, each user is assigned a unique code sequence, which is used to encode the user data. The receiver, knowing the code sequence of the individual user, decodes the received signal after reception and recovers the original data. This is possible because the cross correlation between the code of the desired user and the codes of the other users is very small [19].

The bandwidth of the code signal is chosen to be much greater then the bandwidth of the information bearing signal. Hence, the encoding process is said to enlarge (or spread) the spectrum of the signal. The resulting signal is called spread spectrum signal and CDMA is referred to as spread spectrum multiple access scheme.

A CDMA spread spectrum multiple access system must fulfil two criteria:

1. The transmission bandwidth must be much larger than the information bandwidth; and
2. The bandwidth of the transmitted signal must be independent of the bandwidth of the information signal.

One of the most important concepts of spread spectrum CDMA is the processing gain. The processing gain, G_p is given as the ratio of the transmitted signal bandwidth, B_t to information signal bandwidth B_i:

$$G_p = \frac{B_t}{B_i} \tag{2.1}$$

There are many different types of spread spectrum CDMA techniques. These can be classified in two ways: by concept or by modulation method. The first classification gives two protocol groups: averaging systems and avoidance systems (Table 2.1). Averaging systems reduce the interference in the system by averaging it over a wide time interval. Avoidance system reduces the interference by avoiding it for a large part of the time. Classifying by modulation gives four protocols (Figure 2.1): direct sequence (or pseudo-noise), frequency hopping, time hopping and hybrid methods. Direct sequence is an averaging protocol, whereas

frequency hopping and time hopping are avoidance protocols. The hybrid methods can be averaging or avoidance depending on whether or not they include DS CDMA (Table 2.1). This work focuses on classification of CDMA systems by modulation.

Table 2.1: Classification of CDMA by concept

	DS-CDMA	FH-CDMA	TH-CDMA	Hybrid CDMA
Averaging	X			X
Avoidance		X	X	X

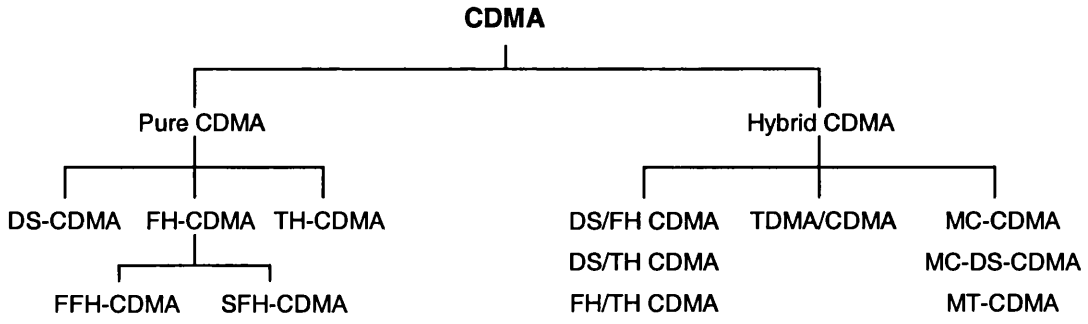

Figure 2.1: Classification of CDMA by modulation method [17]

2.1.2 CDMA systems

As shown in Figure 2.1, CDMA systems can be classified in terms of pure CDMA and hybrid CDMA. Following is a description of the different pure and hybrid CDMA systems.

2.1.2.1 Pure CDMA systems

Direct sequence (DS)

In direct sequence CDMA (DS-CDMA), the information bearing signal is directly multiplied by a spreading code signal (Figure 2.2). The spreading code signal consists of a number of code bits called "chips". The rate of the spreading code signal is much higher than the rate of the input data signal (to satisfy the 1st condition in Section 2.1.1). At the receiver, the individual user information is recovered by multiplying the down-converted received signal with a locally generated copy of the user specific spreading code signal. To be able to perform despreading, the receiver must not only know the code of the individual users but it must also synchronise the locally generated copy of the code with that of the received signal and the synchronisation must be maintained until the complete signal has been received. The main advantages and disadvantages of direct sequence CDMA are discussed in [17].

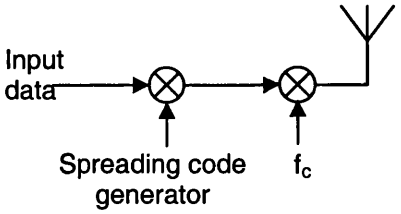

Figure 2.2: Block diagram of a DS-CDMA transmitter

Frequency Hopping (FH)

In frequency hopping CDMA (FH-CDMA), the carrier frequency of the modulated information signal is not constant but changes according to the user specific spreading code sequence. During a given time interval, T_h, the carrier frequency remains the same, but after each time interval, the carrier hops to another frequency (or stays at the same frequency). The hopping pattern is determined by the user specific spreading code. (The processing gain, G_p in this case is equal to the number of hopping frequencies.) Figure 2.3 shows the block diagram of an FH-CDMA transmitter. In this case, the data signal is first baseband modulated on to a carrier. The carrier is then converted up to transmission frequency using a fast frequency synthesizer that is controlled by the spreading code. At the receiver, the inverse process takes place to recover the transmitted data[3].

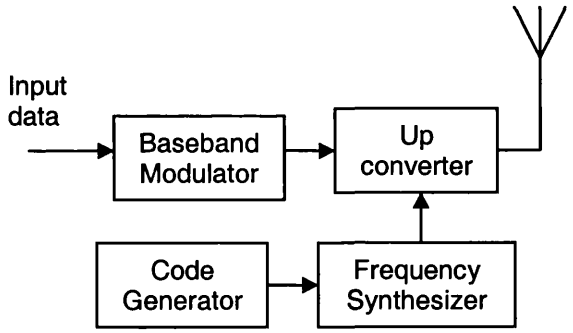

Figure 2.3: Block diagram of an FH-CDMA transmitter [17]

The frequency occupation of FH-CDMA differs considerably from a DS-CDMA system. A DS-CDMA system occupies the whole frequency band when it transmits, whereas a FH system uses only a small part of the available bandwidth when it transmits, but the location of this part differs with time. Figure 2.4 compares the time-frequency occupancy of DS-CDMA and FH-CDMA.

[3] A more detailed description of the FH-CDMA transmitter and receiver is given in Chapter 2 of [17].

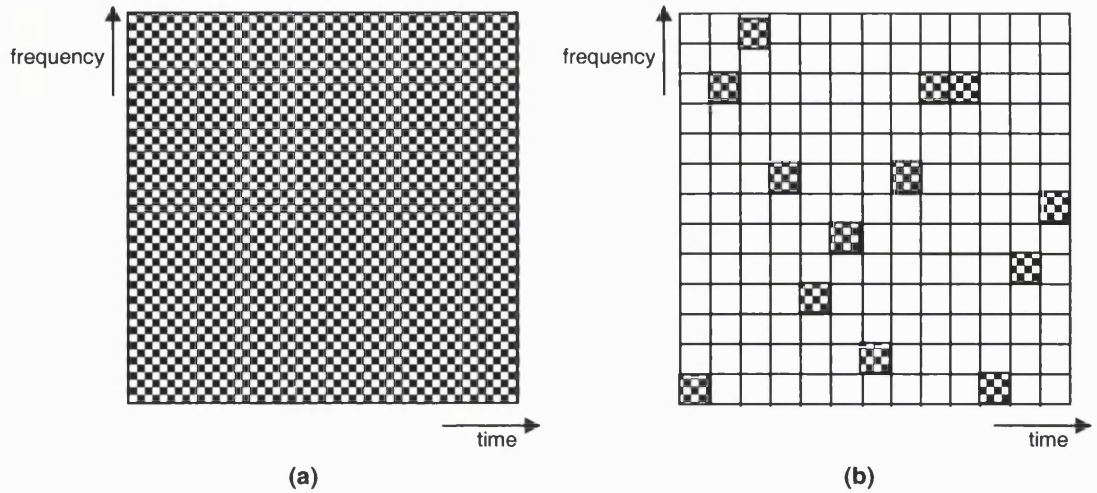

Figure 2.4: Time-frequency occupancy of: (a) DS-CDMA; (b) FH-CDMA [17]

As shown in Figure. 2.1, frequency hopping systems can be classified as Fast Frequency Hopping (FFH) and Slow Frequency Hopping (SFH). In the case of FFH, the carrier frequency changes a number of times during the transmission of one symbol ($T_h < T_{symbol}$), whereas in the case of SFH, the carrier frequency does not change for a number of symbols ($T_h > T_{symbol}$).

Time-Hopping (TH)

In time-hopping CDMA (TH-CDMA), the data signal is transmitted in bursts at time intervals determined by the user specific spreading code. The time axis is divided into frames and each frame is divided into M timeslots. During each frame, the user transmits in one of M timeslots (as shown in Figure 2.5). Which of the M timeslots is transmitted depends on the code signal assigned to the user. The processing gain is equal to the number of timeslots in each frame. The block diagram for TH-CDMA transmitter is shown in Figure 2.6.

Figure 2.5 shows the time-frequency occupancy of TH-CDMA. It is interesting to note that in this case, the transmitted signal uses the whole spectrum for short periods of time, instead of parts of the spectrum all the time (as in FH-CDMA).

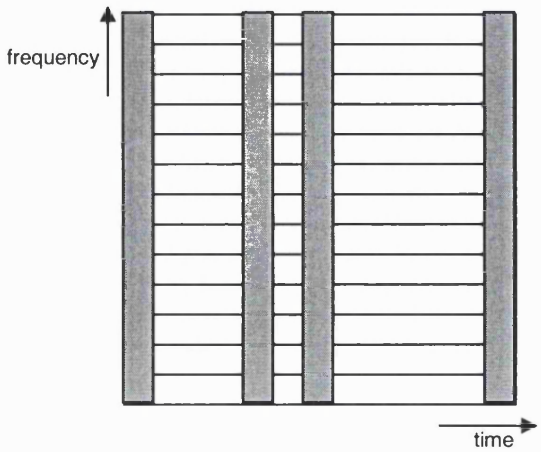

Figure 2.5: Time-frequency occupancy of TH-CDMA [17]

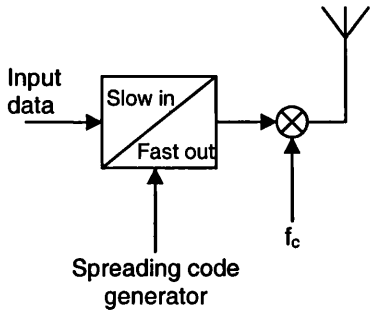

Figure 2.6: Block diagram of TH-CDMA transmitter [17]

2.1.2.2 Hybrid CDMA systems

Hybrid CDMA systems include all CDMA systems that employ a combination of two or more of the above mentioned techniques or a combination of CDMA with some other multiple access techniques (such as TDMA). The aim of such hybrid systems is to combine the specific advantages of the individual techniques. Combining the techniques listed above gives four possible hybrid systems: DS/FH, DS/TH, FH/TH and DS/FH/TH. Combining CDMA with TDMA or multi-carrier modulation gives other possible systems, such as CDMA/TDMA and multi-carrier CDMA (Figure 2.1).

2.1.3 Spreading codes in CDMA systems

In the CDMA systems described above, the main purpose of the spreading operation is to provide user separation and spectral spreading. At the transmitter, the user data is encoded (spread) using the user specific spreading code and at the receiver the desired user's data is recovered (despread) using a locally generated copy of the same user specific spreading code.

The spreading codes used for user separation should be able to provide good distinction between the signal of the desired user and signals of other users. As the separation is made by correlating the received signal with the locally generated copy of the spreading code, the cross correlation between the codes must be low. The autocorrelation of the codes must be impulsive so that the autocorrelation peak can be clearly distinguished from its sidelobes.

Spreading codes can be divided into Pseudo-Noise (PN) codes and orthogonal codes [17]. PN codes are generated using feedback shift registers whereas orthogonal codes are often generated using iterative methods. Examples of PN codes include: m-sequences, Gold codes and Kasami codes [20]. Examples of orthogonal codes include: Walsh Hadamard codes [16, 20] and complementary codes [21].

In a synchronous channel (e.g.: the downlink channel of mobile systems), some orthogonal codes, such as WH codes, provide better performance over PN codes as they have zero cross correlation for zero delay. For non-zero delays, WH codes can have large cross correlation values (Hence they are only used in synchronous applications [17]). Orthogonal codes can also achieve high spectral efficiency and allow for low complexity receiver structure.

2.1.4 Properties of spread spectrum CDMA signal

The coding and the resulting enlarged bandwidth give spread spectrum signals a number of properties that differ from the properties of narrowband signals. The main properties from a wireless communications point of view are presented here [19].

- Multiple access capability

If a number of users transmit a spread spectrum signal at the same time, the receiver will still be able to distinguish between the different users provided that each user has a unique code which has a low cross correlation with the other codes.

In the case of DS-CDMA, the multiplication of the received signal with a locally generated copy of the spreading code will only despread the signal of the desired user while the signals of the other users will remain spread over a large bandwidth. Therefore, within the information bandwidth, the power of the desired user will be much greater than the power of the other users and the desired user data can be extracted. In the FH-CDMA system, the probability of more than one user transmitting in a particular frequency band at a given time is very small due to the nature of the spreading codes. In TH-CDMA, the probability of more than one user transmitting in the same timeslot is made very small by using specific spreading codes.

- Protection against multipath interference

In a radio channel, the signals may be received over several paths due to reflection (and refraction). The signals from the different paths are all copies of the original signal but with different amplitude, phase, time delay and arrival angle, hence, the signal at the receiver will be dispersed in time. Spread spectrum CDMA has capabilities to combat this multipath interference, however, the way in which this is achieved depends very much on the CDMA technique used.

In DS-CDMA, the properties of the spreading code will treat any copy of the signal delayed by more than the chip duration as an interference signal. In the FH case, the effect of multipath will be different for each frequency band and at the receiver this effect will be averaged out. (FH-CDMA system does not combat multipath interference as well as DS-CDMA.) In the TH-CDMA case, there are no advantages in terms of protection against multipath.

- Narrowband Interference rejection

All spread spectrum CDMA systems have capabilities to combat narrowband interference. In DS-CDMA, multiplying a narrowband interference with a locally generated copy of the wideband code signal will spread the narrowband interference and hence reduce the power of the interference in the bandwidth of the desired user. In FH-CDMA, if a narrowband signal interferes on one of the hopping frequencies, the total percentage of the signal damaged is $1/G_p$ (where G_p is the processing gain of the system). In TH-CDMA, if a narrowband signal interference does occur, it will only occur in $1/G_p$ percent of the time.

2.2 Multi-carrier modulation

The CDMA schemes described in the previous section were based on serial transmission of data using a single carrier. This section introduces the concept of parallel transmission of data using multiple subcarriers.

Single carrier systems, such as DS-CDMA and FH-CDMA are limited in terms of the maximum data rate that they can support in multipath environment. As mentioned earlier, in a multipath channel, signals arrive at the receiver from different paths with different amplitude, phase, delay and arrival angle. If the differences in delay are comparable with the symbol period, delayed versions of the same signal are seen by the receiver and hence Inter Symbol Interference (ISI) occurs. As a high data rate signal has a small symbol duration, such a signal may experience severe degradation in the presence of multipath. Equalisation in the receiver can help reduce this degradation, however, this is at the cost of additional complexity. Multi-carrier modulation helps to reduce ISI without increasing the complexity of the receiver. In a multi-carrier system, the input data stream is split into a number of low rate streams and transmitted in parallel over a number of subcarriers (Figure 2.7). The symbol duration of the low rate data streams is much larger than that of the original data stream, hence, the relative delay caused by multipath is reduced. In a conventional single carrier system, the symbols are transmitted sequentially with the frequency spectrum of each data symbol occupying the entire bandwidth (Figure 2.8(a)). In a multi-carrier system, several streams of data are transmitted simultaneously, so that at any instance, several data elements are being transmitted. In such a system, the spectrum of the individual data elements occupy only a small part of the available bandwidth (as shown in Figure. 2.8(b)).

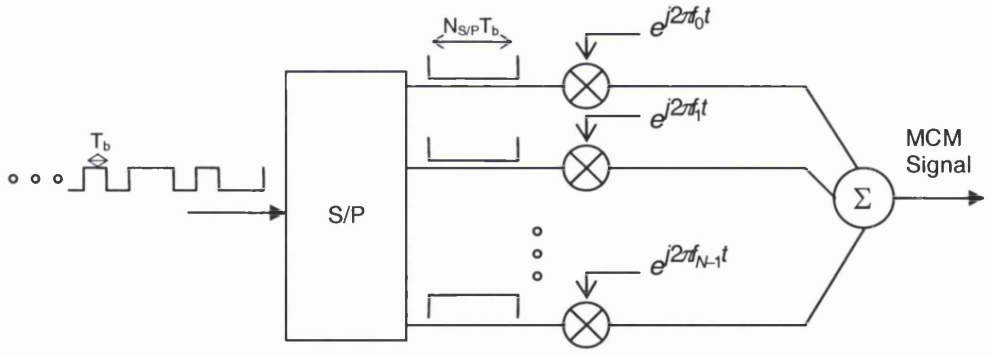

Figure 2.7: Basics of multi-carrier modulation

(a) **(b)**

Figure 2.8: Spectrum of: (a) single carrier system; (b) multi-carrier system

The concept of using multiple carriers to transmit data in parallel was first proposed by Mosier in the 1950s [22]. This method was, however, considered to be inefficient in terms of its use of the frequency spectrum, due to the fact that a guard band had to be inserted between each subcarrier. In order to overcome this inefficiency, the concept of using orthogonal subcarriers was proposed in the mid 1960s by Chang [23] and Salzberg [24]. This technique is referred to as OFDM. In 1971 Weinstein and Ebert [25] proposed an OFDM modulation and demodulation technique using Discrete Fourier Transform (DFT) to further enhance the efficiency of OFDM.

2.2.1 OFDM

The use of OFDM in wireless applications can be traced back to the 1960s, when it was used for several high frequency military systems such as KINEPLEX [22], ANDEFT [26] and KATHRYN [27]. In the 1980s, OFDM was studied for high-speed modems [28], digital mobile communications and high-density recording and in the 1990s, OFDM was investigated for wideband data communications over mobile radio channels [29], high bit rate digital subscriber lines[4] [30, 31] and digital broadcasting [32, 33].

OFDM has now been employed in numerous wireless systems such as indoor wireless LANS (HIPERLAN/2 [34], IEEE 802.11a [35]), broadband WLLs (IEEE 802.16 [36]) and digital audio and video broadcasting (DAB and DVB [32, 33]).

The basic idea of OFDM is to modulate a number of parallel data streams using orthogonal subcarriers such that they satisfy the condition given in Equation 2.2.

$$\int_0^T e^{j2\pi f_1 t} e^{-j2\pi f_2 t} dt = 0 \qquad \text{for } f1 \neq f2 \tag{2.2}$$

where T is the OFDM symbol duration and f_1 and f_2 are two subcarrier frequencies.

The orthogonality condition in Equation 2.2 is satisfied by making the subcarrier spacing equal to an integer multiple of the symbol rate, i.e., for an OFDM signal with symbol duration T, the spacing between each subcarrier should be equal to $N_{int}(1/T)$, where N_{int} is an integer. In the frequency domain this results in the spectrum of each carrier having a null at the centre frequency of each of the other subcarriers in the system (Figure 2.9(a))[5]. Maximum spectral efficiency can be achieved by making the spacing between each subcarrier equal to 1/T (as shown in Figure 2.9(b)). Note that in this case there is considerable overlapping between the spectra of the individual subcarriers, however, the information can be reliably recovered due to the fact that the subcarriers are made orthogonal to one another.

[4] In this case, OFDM is referred to as Discrete Multi-Tone (DMT).
[5] The spectrum of the OFDM signal is said to fulfii the Nyquist criterion for an ISI free pulse shape, where the pulse is present in the frequency domain and not the time domain [19].

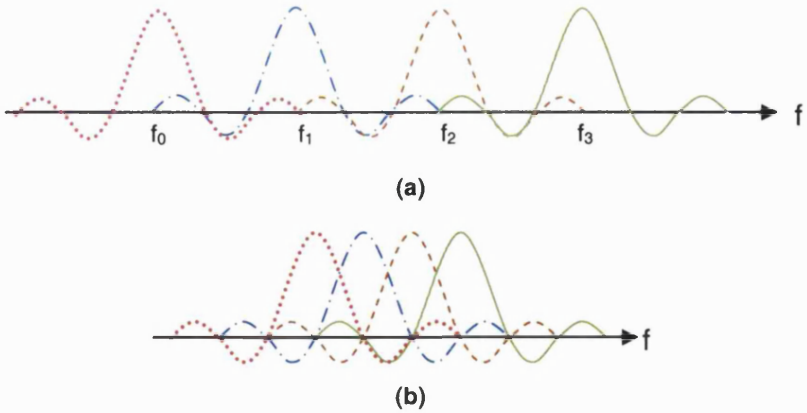

Figure 2.9: OFDM spectrum (a) Orthogonal subcarriers; (b) Orthogonal subcarriers with maximum spectral overlap

In the time domain this can be interpreted as having an integer number of cycles during the symbol period (as shown in Figure 2.10).

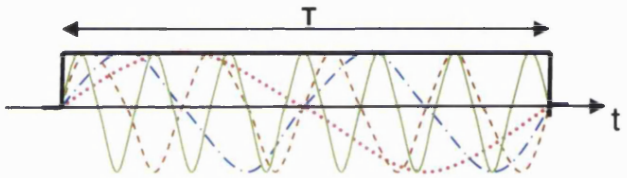

Figure 2.10: OFDM symbol with 4 subcarriers

Unlike the direct sequence spread spectrum or frequency hopping systems described in Section 2.1, OFDM does not provide any spectral spreading. The bandwidth of the OFDM signal is the same as that of the original signal. The overall system bandwidth is merely divided between the different subchannels.

Figure 2.11 shows the transmitter model for OFDM. At the input of the transmitter, the data is first Serial-to-Parallel (S/P) converted into a number of low rate data streams. The parallel outputs from the S/P converter are then modulated onto a set of orthogonal subcarriers and summed together. In order to completely eliminate the effects of ISI caused by multipath, a Guard Period (GP) is generally added at the beginning of each OFDM symbol before up-conversion and transmission.

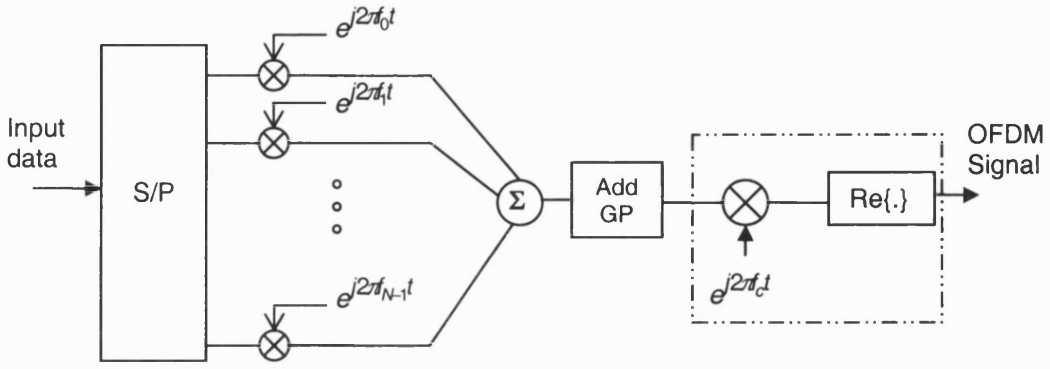

Figure 2.11: OFDM transmitter

In most OFDM based systems, the guard period is a cyclic extension of the OFDM symbol (Figure 2.12) and is referred to as the Cyclic Prefix (CP). The cyclic prefix not only eliminates the ISI but also eliminates Inter Carrier Interference (ICI) in the presence of multipath[6].

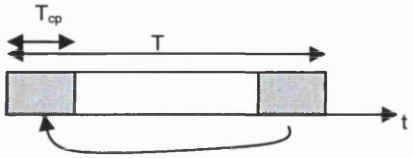

Figure 2.12: Guard period/Cyclic prefix

The insertion of the GP to the beginning of each OFDM symbol increases the spacing between the individual subcarriers from N_{int}/T to $N_{int}/(T-T_{GP})$ (This is illustrated in Figure 2.13 for the maximum overlap case). The spectrum of the transmitted OFDM signal no longer satisfies the orthogonality condition discussed above. However, at the receiver, the GP is removed from the beginning of each OFDM symbol before demodulation. Hence, the spectrum of the signal at the input of the demodulator is similar to that shown in Figure 2.9(b).

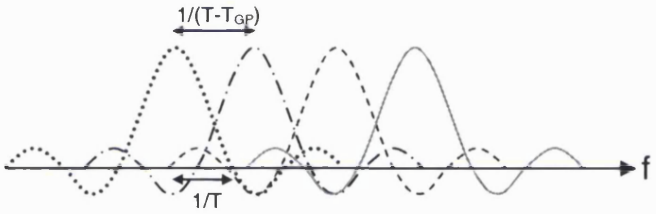

Figure 2.13: Spectrum of OFDM signal with the insertion of the guard period

Figure 2.14 shows the receiver model for OFDM. At the input, the signal is first down-converted to baseband. The GP is then removed and the signal is demodulated by multiplying it with the complex conjugate of the orthogonal subcarriers and integrating over the symbol duration.

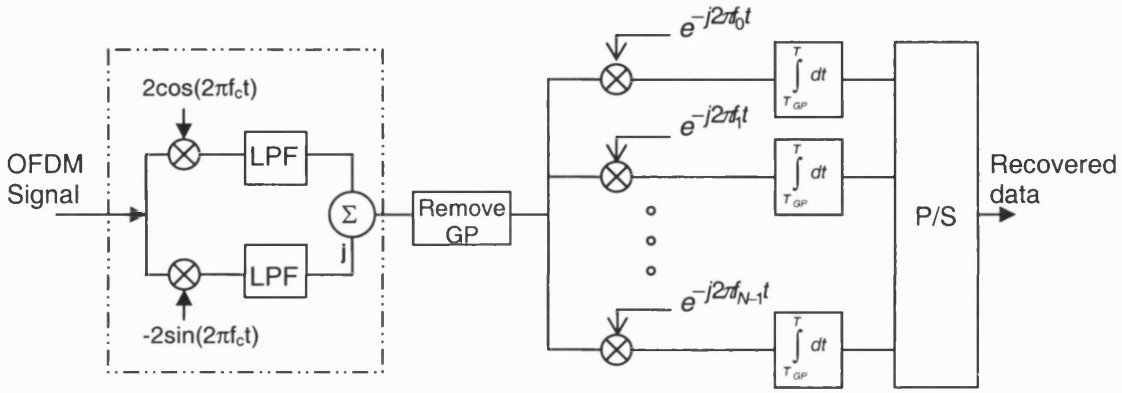

Figure 2.14: OFDM receiver

[6] A more detailed description of the basic operations of the cyclic prefix is presented in Chapter 2 of [37].

The OFDM transmitter and receiver model presented in Figure 2.11 and Figure 2.14 require banks of oscillators at the transmitter and receiver. This results in a complex system, particularly if the number of subcarriers is large. Weinstein and Ebert [25] have shown that OFDM signals can be generated and detected using an IDFT and a DFT, which greatly reduces the complexity of the system. The availability of FFT algorithms and cheap FFT chips reduces the cost and complexity of OFDM systems even further. The structure of the FFT based OFDM transmitter and receiver is shown in Figure 2.15. In this implementation the banks of oscillators at the transmitter and receiver are replaced by the IFFT and FFT, respectively. The guard period operates in the same manner as before. At the transmitter, the signal has to be converted to analogue format before transmission and at the receiver the received symbol has to be converted to digital format before demodulation. (Note that in this figure the up-conversion and down-conversion blocks have been omitted, however, in a typical system the OFDM signal at the output of the transmitter is up-converted before transmission and consequently, the received signal is down-converted before the A/D conversion.)

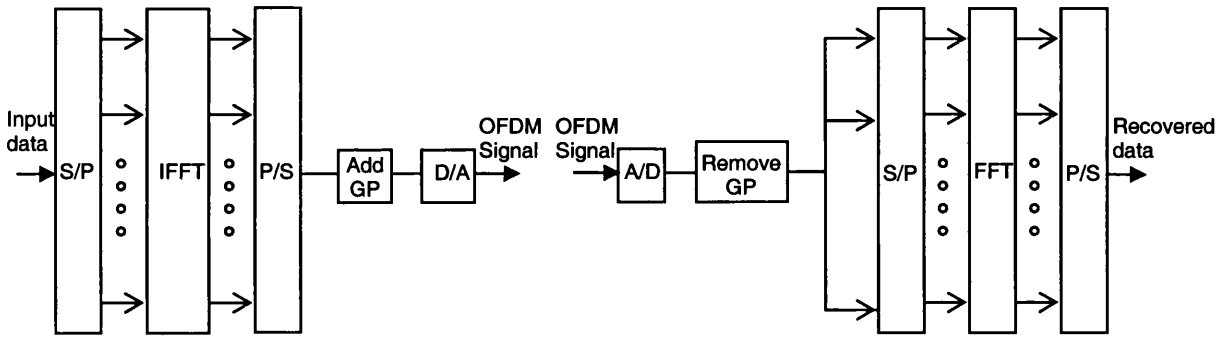

Figure 2.15: Discrete time representation of OFDM transmitter and receiver

In a practical system, the length of the IFFT/FFT is chosen to be greater than the number of subcarriers [37]. Figure 2.16 shows the spectrum of the IFFT output with the length of the IFFT set equal to the number of subcarriers. In this case, a filter with realistic passband-to-stopband transition cannot be used to recover the OFDM symbol. Hence, the length of the IFFT is increased in order to introduce a separation between the symbol spectrum and its copies. Figure 2.17 shows the spectrum of the IFFT output with the length of the IFFT set equal to N' (where N'> $N_{subcarriers}$). In this case, a filter with realistic passband-to-stopband characteristics can be used to recover the OFDM symbol.

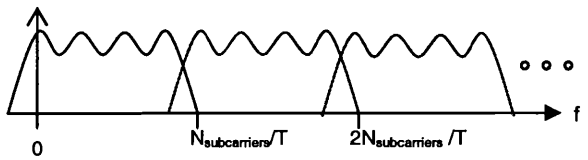

Figure 2.16: OFDM spectrum with IFFT/FFT size=$N_{subcarriers}$

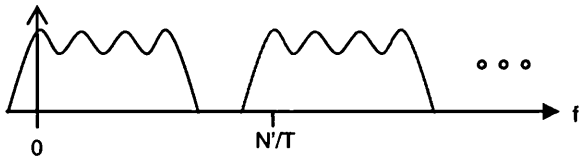

Figure 2.17: OFDM spectrum with IFFT/FFT size=N'(>$N_{subcarriers}$)

The following section introduces the concept of combining OFDM with CDMA (referred to as multi-carrier CDMA).

2.3 Multi-carrier CDMA

Due to the fact that OFDM provides good performance in a multipath channel without the need for complex equalisation techniques, the combination of OFDM and DS-CDMA has been considered for high data rate cellular systems. This combination is referred to as multi-carrier CDMA (or OFDM/CDMA).

Multi-carrier CDMA schemes were first introduced in 1993. The schemes proposed to date can be divided into 3 categories: Multi-Carrier CDMA (MC-CDMA), Multi-Carrier DS-CDMA (MC-DS-CDMA) and Multi-Tone CDMA (MT-CDMA) [38]. These schemes were proposed by different researchers, namely, MC-CDMA by N. Yee, J-P Linnartz and G Fettweis [39], K.Fazel and L. Papke [40] and A. Chouly, A. Brajal and S. Jourdan [41], MC-DS-CDMA by V. DaSilva and E. S. Sousa [42] and MT-CDMA by L. Vandendorpe [43]. A number of authors have also proposed variants of these schemes [44, 45, 46, 47].

In a multi-carrier CDMA system, each user data is first spread using a user specific spreading code (as in the case of DS-CDMA) and then modulated onto a set of subcarriers using OFDM (Figure 2.18).

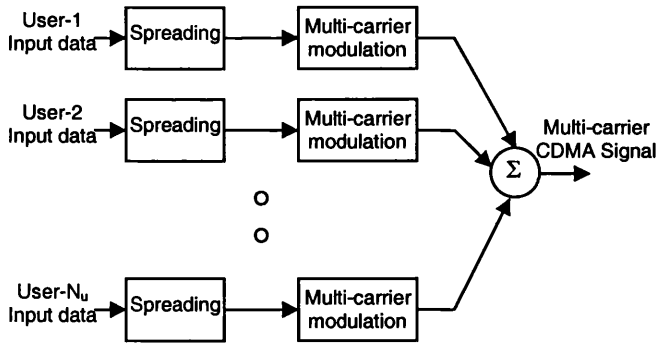

Figure 2.18: Basics of multi-carrier CDMA

The key difference between the three multi-carrier CDMA schemes (MC-CDMA, MC-DS-CDMA and MT-CDMA) is the way in which the data is spread and modulated onto the different subcarriers.

2.3.1 Multi-carrier CDMA schemes

This section describes the three multi-carrier CDMA schemes[7]. The description concentrates on the signal generation at the transmitters. The receiver conceptually reverses the transmitter function. Receiver operation is not described in this chapter but is detailed in the following chapters.

2.3.1.1 MC-CDMA

In the MC-CDMA scheme, the user data is first spread using a user specific spreading code and then each chip of the spread data is used to modulate a different subcarrier. Figure 2.19 shows the transmitter model for MC-CDMA.

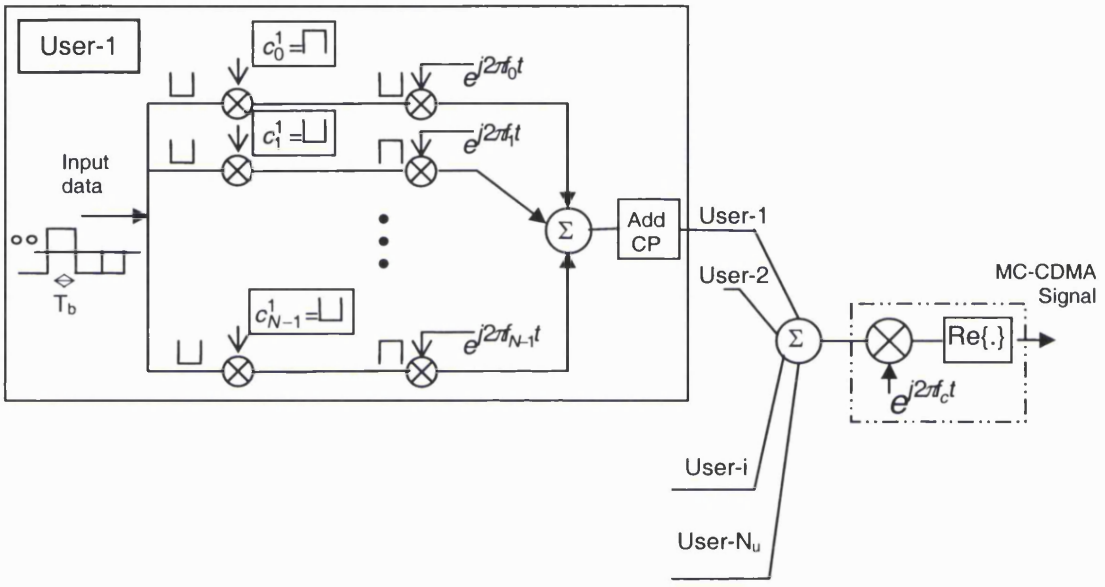

Figure 2.19: MC-CDMA transmitter

The input data is first copied into N_{code} parallel data streams (where N_{code} is the length of the spreading code). Each stream is then multiplied by a single chip of the spreading code, c_n^u (for user u and code chip n) and modulated onto a set of orthogonal subcarriers. The modulated output is summed and a cyclic prefix is added to the beginning of each MC-CDMA symbol (as in the case of OFDM) before transmission.

As each chip is mapped onto a different subcarrier, the number of subcarriers is equal to the length of the spreading code. Figure 2.20 shows the spectrum of the signal at the input and the output of the MC-CDMA transmitter[8]. In this case, the subcarrier separation, Δf is equal to $1/T_b$ (where T_b is the duration of the input data bit).

---

[7] Literature review of various aspects of multi-carrier CDMA systems relating to the work presented in this thesis has been included within the individual work chapters and is not included in this introductory section.

[8] For simplicity, it has been shown that the spectrum of each modulated subcarrier has a null at the centre frequency of each of the other modulated subcarriers. However, in a typical system, the insertion of CP will increase the subcarrier separation (as discussed in Section 2.2.1).

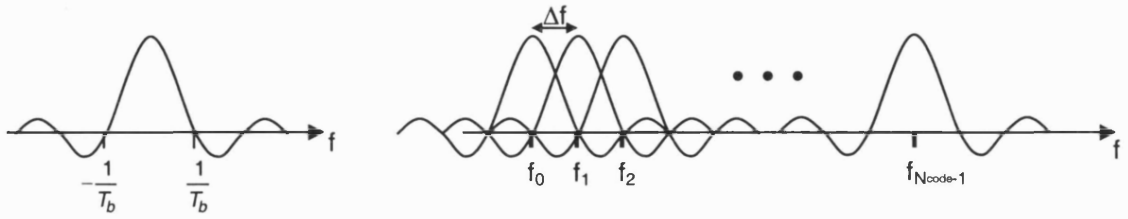

(a) (b)

Figure 2.20: Spectrum of the signal at: (a) the input; (b) the output of the MC-CDMA transmitter

In the system described above, the duration of the symbol at the output of the transmitter is the same as the duration of the symbol at the input. If the duration of the symbol is small enough to be degraded by multipath, the input signal is S/P converted before spreading and modulation (as shown in Figure 2.21[9]).

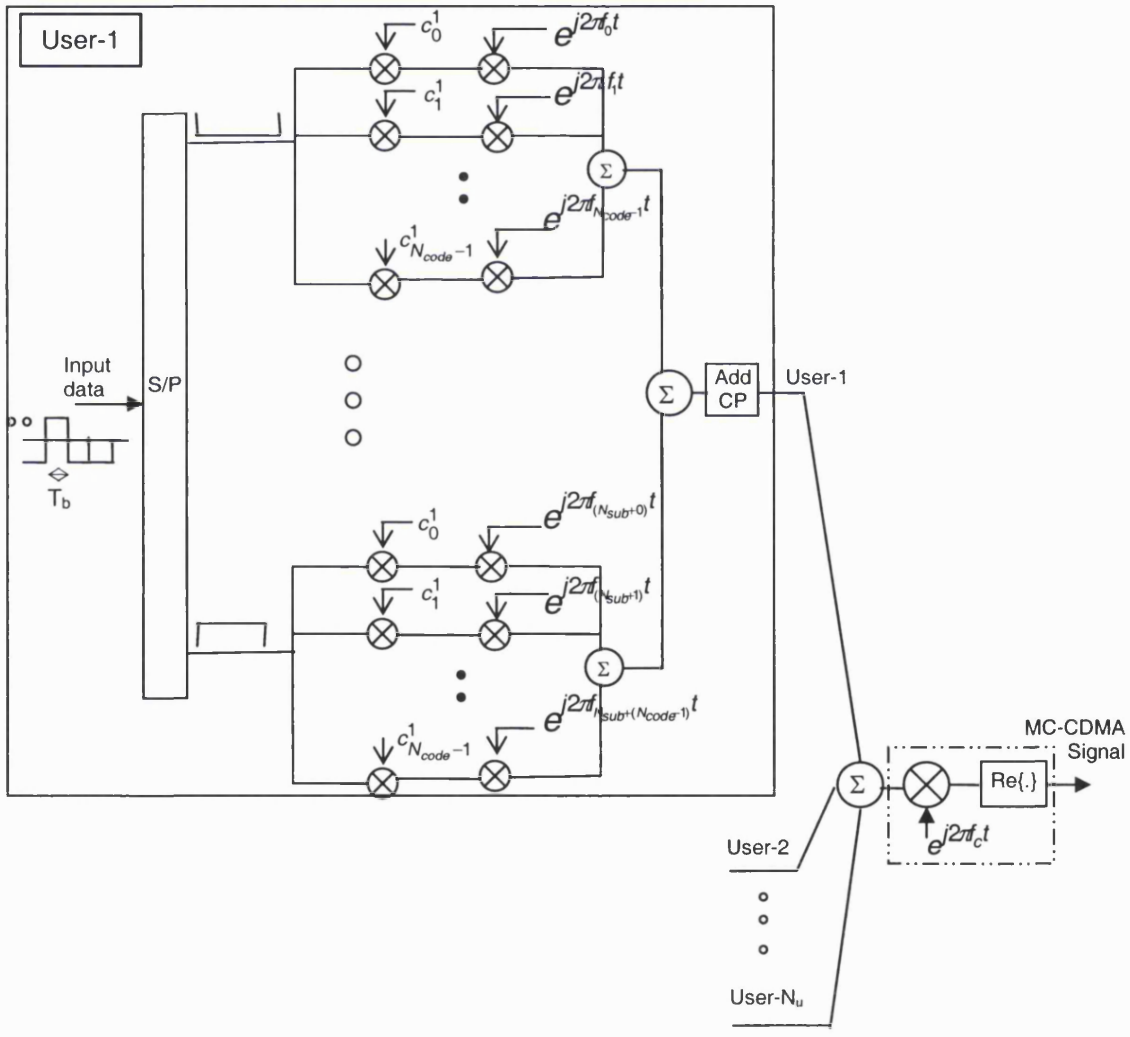

Figure 2.21: MC-CDMA transmitter with S/P converter at the input

[9] $N_{sub}=(N_{S/P}-1)*N_{code}$

In this case, the total number of subcarriers ($N_{subcarriers}$) required is equal to the product of the length of the S/P converter ($N_{S/P}$) and the length of the spreading codes (N_{code}). The spectrum of the signal at the output of the transmitter is as shown in Figure 2.22[10]. Note that in this case, the bandwidth of each individual subcarriers is narrower than the bandwidth of the input data (due to the S/P conversion). The total bandwidth of the signal at the output of the transmitter is equal to $N_{subcarriers}$ times the bandwidth of the S/P converted symbols.

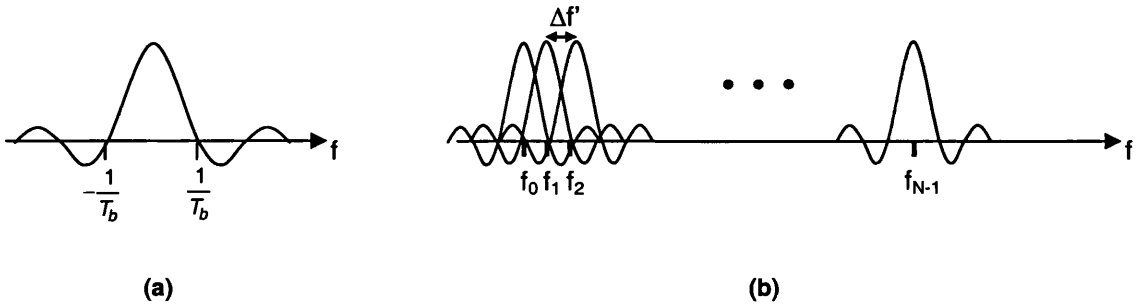

Figure 2.22: Spectrum of signal at: (a) the input; (b) the output of the MC-CDMA transmitter (with S/P converter)

The subcarrier separation, Δf' (Figure 2.22(b)) is given by:

$$\Delta f' = \frac{1}{T_b N_{S/P}} \tag{2.3}$$

where T_b is the duration of the data bit at the input of the transmitter (Figure 2.21) and $N_{S/P}$ is the length of the S/P converter.

A number of variations to the MC-CDMA scheme have been proposed in the literature. A widely used architecture is the one proposed by Kaiser [44] in which the users are grouped into blocks and each block of users transmits over a different set of subcarriers (this is explained further in Chapter 5).

2.3.1.2 MC-DS-CDMA

In the MC-DS-CDMA scheme, the user data is first S/P converted and then spread using a user specific spreading code (of length N_{code}) as shown in Figure 2.23. The parallel streams of spread data are modulated onto a set of orthogonal subcarriers as in the MC-CDMA case and a cyclic prefix is inserted between symbols before transmission.

[10] As in the previous case, for simplicity, it has been shown that the spectrum of each modulated subcarrier has a null at the centre frequency of the other modulated subcarriers. However, in a typical system, the insertion of CP will increase the subcarrier separation.

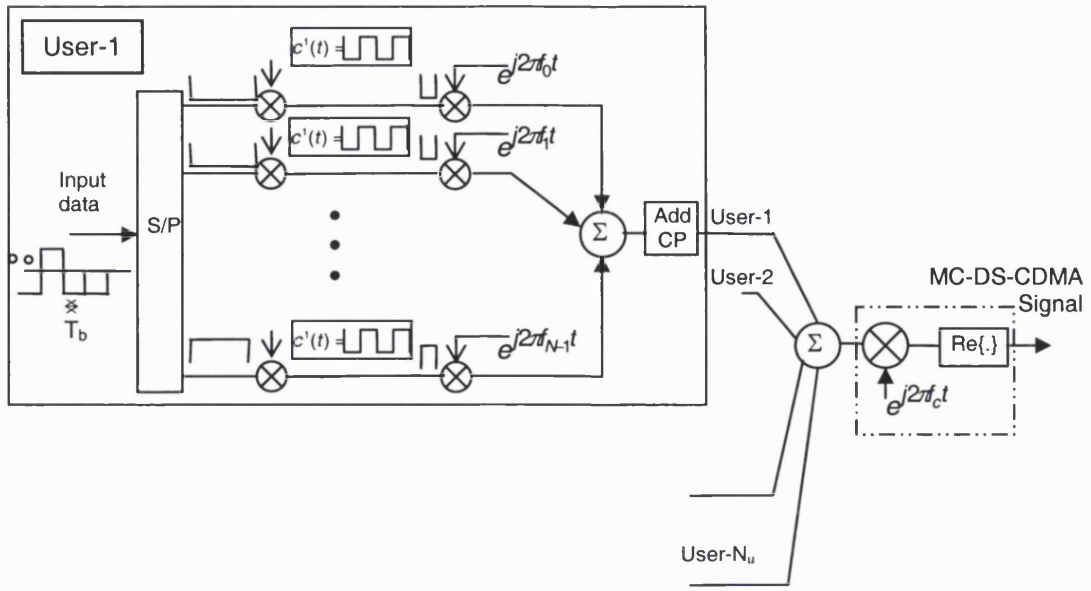

Figure 2.23: MC-DS-CDMA transmitter

In this scheme, the number of subcarriers is equal to $N_{S/P}$. $N_{S/P}$ can be equal to, less than or greater than N_{code} depending on the characteristics of the channel and the maximum number of users in the system.

The spectrum of the signal at the input and the output of the MC-DS-CDMA transmitter are presented in Figure 2.24[11]. In this case, the subcarrier separation, $\Delta f''$ is given by:

$$\Delta f'' = \frac{1}{T_b}\left(\frac{N_{code}}{N_{S/P}}\right) \tag{2.4}$$

where T_b is the duration of the data bit at the input of the transmitter in Figure 2.23, N_{code} is the length of the spreading code and $N_{S/P}$ is the length of the S/P converter.

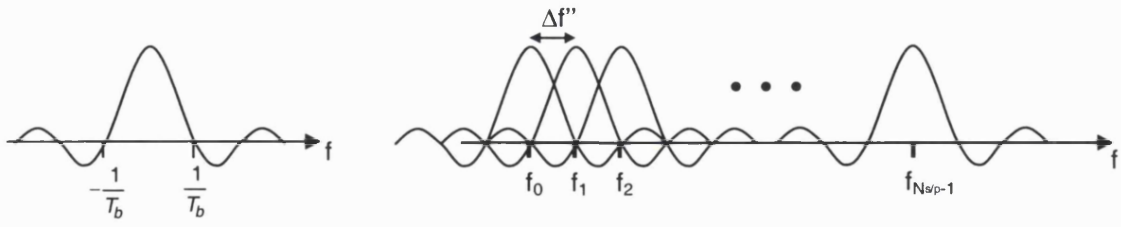

(a) **(b)**

Figure 2.24: Spectrum of signal at: (a) the input; (b) the output of the MC-DS-CDMA transmitter

A number of variations to the MC-DS-CDMA system have been proposed in the literature. In [45], an MC-DS-CDMA scheme which does not employ an S/P converter is considered. In this case the user data is spread using a user specific spreading code and the spread data is used to modulate each subcarrier. One of the key advantages of such a system is that it does

[11] Note that in a typical system, the insertion of CP will increase the subcarrier separation (as discussed in Section 2.2.1).

not require a contiguous frequency band. Hence, the available spectral gaps can be exploited efficiently. In [46] an MC-DS-CDMA scheme with larger subcarrier separation is proposed in order to yield both frequency diversity improvement and narrowband interference suppression. In [47], the performance of a multi-carrier CDMA scheme based on a combination of MC-DS-CDMA and MC-CDMA is presented.

2.3.1.3 MT-CDMA

The MT-CDMA scheme is very similar to MC-DS-CDMA, except that in this case the length of the spreading code is much greater than the number of subcarriers in the system. The main advantage of this scheme is that it can accommodate more users as compared to single carrier DS-CDMA scheme.

The transmitter model for MT-CDMA is very similar to the transmitter model for MC-DS-CDMA (Figure 2.23). The data at the input of the transmitter is first S/P converted and each branch of the parallel substream is spread with a user specific spreading code. However, as mentioned above, the length of the spreading code is much greater than the length of the spreading codes in MC-DS-CDMA. Thus, the spectrum of each subcarrier satisfies the orthogonality condition with minimum frequency separation prior to spreading operation. However, after spreading, the spectral null of each subcarrier no longer occurs at the centre frequency of each of the other subcarriers (Figure 2.25). Hence, the subcarriers experience ICI and require high complexity rake receivers.

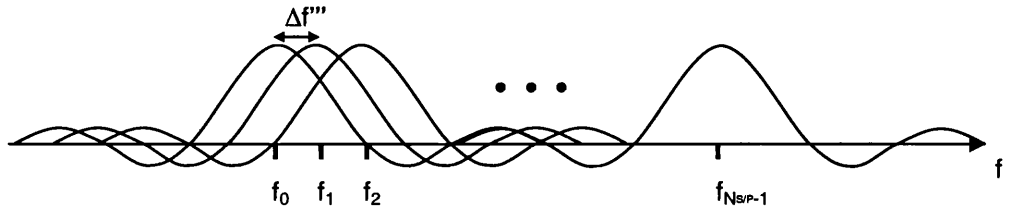

Figure 2.25: Spectrum of MT-CDMA signal

In this case, the subcarrier separation, $\Delta f'''$ is given by:

$$\Delta f''' = \frac{1}{T_b N_{S/P}} \tag{2.5}$$

It is interesting to note that in the case of MC-DS-CDMA and MT-CDMA, setting the length of the S/P converter to 1, results in a DS-CDMA system.

2.3.2 Multi-carrier CDMA systems in the presence of multipath

As multi-carrier CDMA systems will operate in a multipath environment, this section provides an overview of the multipath channel and discusses the parameterisation of the multi-carrier CDMA schemes when operated in a multipath environment.

2.3.2.1 Multipath fading

In a realistic mobile radio system, the transmitted signal arrives at the receiver through a number of different paths as it gets reflected and scattered by various obstacles. This results in the signal at the receiver consisting of a number of copies of the transmitted signal with randomly distributed amplitudes, phases, time delays and angles of arrival. The interference between these copies gives rise to some deleterious effects which are collectively known as multipath.

Effects of multipath on a transmitted signal

The effects of multipath on a signal depend on the characteristics of the multipath channel and the characteristics of the transmitted signal. In the case of high data rate signals (such as 4G signals), multipath causes dispersion in the time domain and frequency selective fading in the frequency domain.

Time dispersion occurs due to interference of various copies with different relative delays. Each multipath component arrives at the receiver with a certain delay and a certain attenuation (Figure 2.26(a)). The overall effect is a long 'tail' in the received symbol (Figure 2.26(b)) which interferes with the following symbol (known as ISI).

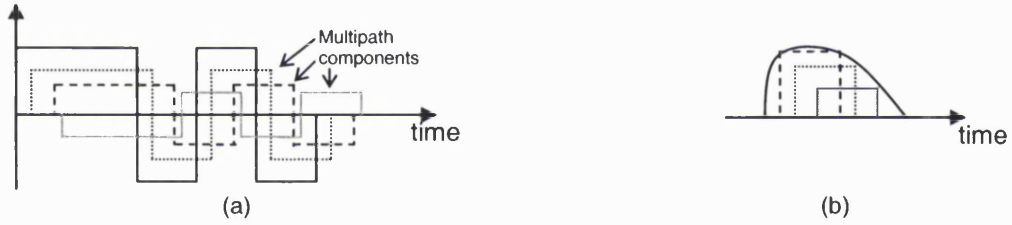

Figure 2.26: Time dispersion due to multipath

In the frequency domain, multipath causes frequency selective fading (Figure 2.27). Frequency selective fading occurs due to the interference of multiple copies with random relative phases. Frequency selective fading results in different frequency components of the transmitted signal being attenuated differently by the channel (as shown in Figure 2.27).

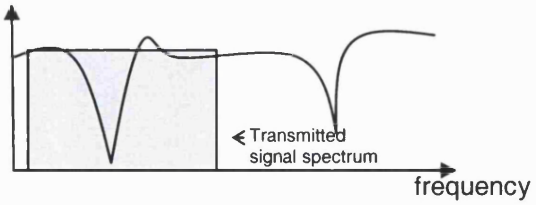

Figure 2.27: Frequency selective fading due to multipath

Multipath channel characterisation

The impulse response of a multipath channel contains all the information necessary to characterise a multipath channel and analyse any type of transmission through the channel. It

gives the attenuations and the delays of the various multipath components (relative to the first arrived component). The impulse response is generally measured in the field using channel sounding techniques (described in [48]). A typical impulse response is shown in Figure 2.28. The difference between the arrival time of the first component and the last component for which the receiver power falls below some threshold level (e.g., 20 dB) is known as the maximum excess delay of the channel (τ_{max}). The maximum excess delay is not necessarily the best indicator of how any given system will perform on the channel because some channels with the same value of τ_{max} can have very different impulse responses [50]. A more widely used measurement is the root mean squared (rms) value of the delay spread (τ_{rms})[12,13].

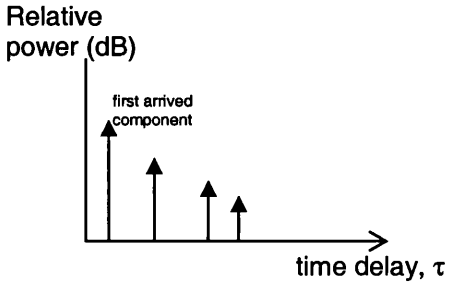

Figure 2.28: Impulse response of a multipath channel

The inverse of τ_{rms} is proportional to the coherence bandwidth, B_c[14]. The coherence bandwidth is a statistical measure of the range of frequencies over which the channel can be considered 'flat'. The coherence bandwidth of the channel determines the effect of the channel on the transmitted signal. If the coherence bandwidth is greater than the bandwidth of the signal, the signal does not experience significant time dispersion or frequency selective fading. However, if the coherence bandwidth is less than the bandwidth of the signal (as the case might be for high data rate 4G signals) the transmitted signal will experience time dispersion and frequency selective fading, resulting in signal degradation.

2.3.2.2 Parameterisation of multi-carrier CDMA for multipath channels

The key requirement for a system to operate in a multipath environment is tolerance to delay spread. In wireless communication systems, the transmitted bit rate (r_b) and the bandwidth (W) are generally specified. In multi-user systems, the maximum number of users in the system (N_{users}) is also specified. Hence, the delay spread tolerance is achieved by adjusting the transmitted symbol duration (T_{symb}).

In single carrier systems, the delay spread tolerance is achieved by making the duration of the transmitted symbol larger than τ_{rms} of the channel. Typically, the symbol duration is set to be 10 times the τ_{rms} of the channel [48, 50].

---

[12] It has been established in [49] that, for a given system, the BER performance for different multipath channels is practically identical if the τ_{rms} is the same, even if the impulse responses of the channels are different.
[13] Note that, in some references τ_{rms} is not taken to be the same as the rms of the maximum delay spread.
[14] An exact relationship between τ_{rms} and B_c does not exist. It is a function of the multipath channel.

The increased symbol duration of Multi-carrier systems (such as OFDM) mitigate the effects of multipath. Further, by setting the guard period/cyclic prefix duration to be greater than τ_{rms} of the channel, degradation due to mutipath can be eliminated. Typical values of the guard duration are 2-4τ_{rms}[15] [19].

DS-CDMA systems do not increase the duration of the transmitted symbol to combat multipath. These systems employ RAKE receivers [17] which takes advantage of the multiple paths to improve system performance. In DS-CDMA systems, the bandwidth of the transmitted signal is made to be wider than the coherence bandwidth of the channel in order to increase the number of paths arriving at the receiver. In the time domain, the transmitted symbol duration is made to be narrower than τ_{max} of the channel. The maximum number of multipath components that can be resolved by the RAKE receiver is given by [51, 52]:

$$L_{paths} = 1 + \frac{\tau_{max.}}{T_{chip}} \tag{2.6}$$

Where T_{chip} is the duration of the chip of the spreading code.

Typically, the number of resolvable paths arriving at the receiver is set to 4 [51, 52]. Hence, the chip duration of the spreading code is $\tau_{max}/3$.

Parameterisation of MC-CDMA

In order to operate the MC-CDMA system (described in section 2.3.1.1) in a multipath channel, the duration of the cyclic prefix should be set equal to 2-4 times the τ_{rms} of the channel. Once the cyclic prefix duration is set, the symbol duration can also be determined. It is desirable that the loss due to the cyclic prefix should be as small as possible. In order to achieve this, the symbol duration should be as large as possible. However, the symbol duration cannot be arbitrarily large. A practical choice is to make the symbol duration approximately 5 times the guard period in order to make the loss due to cyclic prefix approximately 1 dB[19]. As each chip of the spread data is mapped onto a different subcarrier, the number of subcarriers is equal to the length of the spreading code. In the case of MC-CDMA, the symbol duration at the output of the transmitter is the same as the duration of the data bit at the input of the transmitter (Figure 2.19). Hence, if the required symbol duration is larger than the bit duration, a S/P converter is used at the input (as shown in Figure 2.20). The number of subcarriers is then equal to the product of the length of the S/P converter and the length of the spreading code. The total bandwidth required is equal to the product of the number of subcarriers and the subcarrier separation (which is the inverse of the symbol duration less cyclic prefix duration).

[15] The exact choice depends on the type of coding and modulation. Higher order modulation is more sensitive to ICI and ISI than QPSK while heavier coding reduces the sensitivity to such interference [19].

Parameterisation of MC-DS-CDMA

In the case of the MC-DS-CDMA system described in section 2.3.1.2, the receiver can be implemented in two ways. Hence, the choice of parameters will depend on the type of receiver implementation.

The key difference between the two MC-DS-CDMA receiver implementations is the way in which the signal processing is performed. In the first implementation, the signal processing is done in a similar way to OFDM and MC-CDMA [38, 53, 46]. In this case, a guard period is employed to combat the effects of multipath fading. In the second implementation, the MC-DS-CDMA system is viewed as a special kind of DS-CDMA system and in this case a RAKE receiver is utilised on each subcarrier to mitigate the effects of multipath [52, 54, 55]. In this implementation, a guard period is not required.

In order to distinguish between the two implementations, the first implementation is often referred to as MC-DS-CDMA with frequency domain processing and the second implementation is referred to as MC-DS-CDMA with time domain processing [56].

The choice of parameter values for MC-DS-CDMA with frequency domain processing are similar to MC-CDMA. In order to operate the system in the presence of multipath, the cyclic prefix duration is set equal to $2\text{-}4\tau_{rms}$. The symbol duration is made equal to 5 times the cyclic prefix duration (in order to keep the loss due to cyclic prefix to a minimum). For a given bit rate, T_b, the symbol duration will be dependent on the number of subcarriers and the length of the spreading code (as shown in 2.3.1.2). As the bit rate ($1/T_b$) and the length of the spreading code (N_{code}) are generally specified, the number of subcarriers is equal to $T_{symb}.N_{code}/T_b$ (where T_{symb} is the required symbol duration). Once the number of subcarriers is calculated, the total bandwidth of the system is determined by multiplying the number of subcarriers by the subcarrier separation (which is the inverse of the symbol duration less cyclic prefix duration).

In order to operate MC-DS-CDMA system with time domain processing in a multipath channel, the bandwidth of each subcarrier must be made greater than the coherence bandwidth of the channel. In the time domain, the duration of the code chips (T_{chip}) must be lower than τ_{rms} of the channel. Typically, the duration of the code chips is set to be $\tau_{max}/3$ (as discussed above). In MC-DS-CDMA, T_{chip} is equal to T_{symb}. Therefore, once the chip duration is set, the number of subcarriers can be calculated for a given bit rate and spreading code length ($T_{symb}.N_{code}/T_b$). As in the previous case, the total bandwidth of the system can be determined by multiplying the number of subcarriers by the subcarrier separation (which is the inverse of the chip duration).

In a multipath channel, the MC-DS-CDMA symbol duration for the time domain processing case ($T_{symb(TD)}$) will be much narrower than the frequency domain processing case ($T_{symb(FD)}$) as $T_{symb(TD)} < \tau_{max}/3$ whereas $T_{symb(FD)} > 2\text{-}4\tau_{rms}$. Therefore the modulated subcarrier bandwidth will be much wider in the time domain processing case than the frequency domain processing case. As the bit rate and transmitted bandwidth, the time domain processing case

will require a lower number of subcarriers as compared to the frequency domain processing case. For systems employing higher order mapping, care must be taken when such systems are designed for operation in a mutipath environment since both the symbol time and overall bandwidth are functions of the mapping scheme used.

2.3.3 Multi-carrier CDMA systems in a multi-cell environment

As one of the key applications envisaged for multi-carrier CDMA is future generation cellular systems, this section discusses the operation of multi-carrier CDMA in a multi-cell environment.

In cellular systems, the service area is conceptually divided into hexagonal cells [16]. Each cell contains a base station which is linked to the mobile stations within the cell via the uplink and downlink channel. In CDMA cellular systems, neighbouring cells may share the same frequency. Hence, in order to distinguish the base stations from one another, the data transmitted from each base station is multiplied by a base station specific scrambling code [57, 58]. Figure 2.29 shows a simplified block diagram of a DS-CDMA transmitter operating in a multi-cell environment [58].

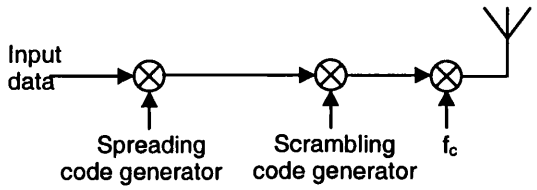

Figure 2.29: Block diagram of a DS-CDMA transmitter operating in a multi-cell environment

In CDMA based cellular systems (IS-95, W-CDMA and CDMA2000), the scrambling is achieved by multiplying the spread data by a PN code [16, 17]. In the case of IS-95 and CDMA2000, m-sequence PN codes [16] are employed for data scrambling whereas in the case of W-CDMA, gold codes are employed [17]. The chip rate of the scrambling codes is the same as that of the spreading codes and hence the scrambling operation does not cause further spectral spreading.

In the case of IS-95, W-CDMA and CDMA2000, base stations employ the same scrambling code. The differentiation between base stations is obtained by the use of a different time shift (or time offset) for each base station[16]. The length (or the period) of the scrambling code is set to 2^{15} (32768 chips). A minimum delay of 64 chips is specified between any two offsets. Hence, the number of offsets is equal to 512. (A detailed description of PN offset allocation strategy is provided in [59, 60, 61]. Alternative PN offset allocation strategies are discussed in [62]).

In order to operate the MC-CDMA and MC-DS-CDMA systems (described in Section 2.3.1.1 and 2.3.1.2) in a multi-cell environment, the data must be scrambled before

[16] In the case of m-sequence and gold codes, a time shifted version of the code is a new code.

transmission. Figure 2.30 and Figure 2.31 present the modified transmitter diagram for MC-CDMA and MC-DS-CDMA to allow for operation in a multi-cell environment (In Figure 2.30 and Figure 2.31, PN denotes the scrambling code and PN_n denotes the n^{th} chip of the scrambling code).

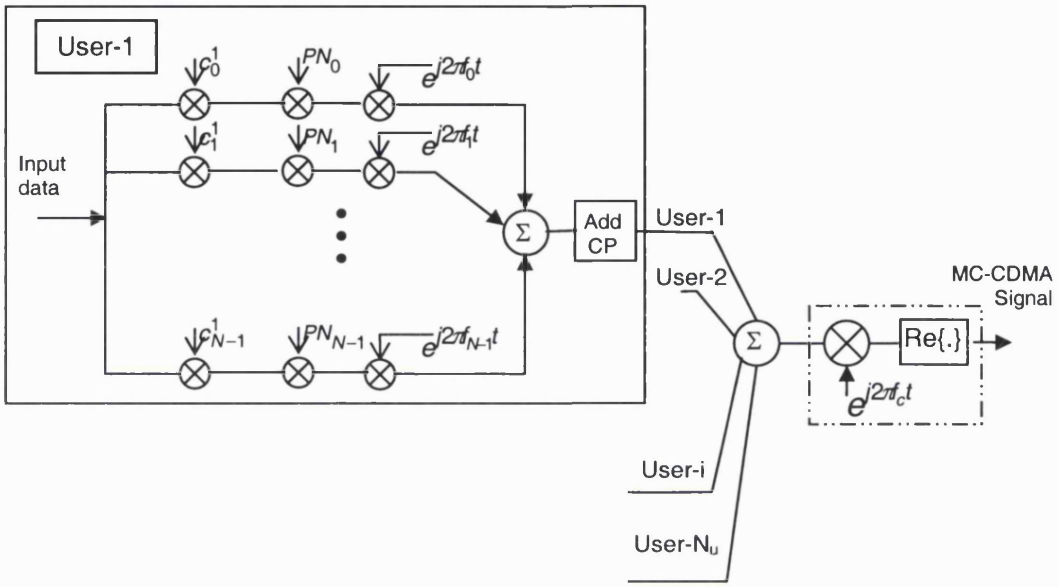

Figure 2.30: Modified MC-CDMA transmitter (with scrambling)

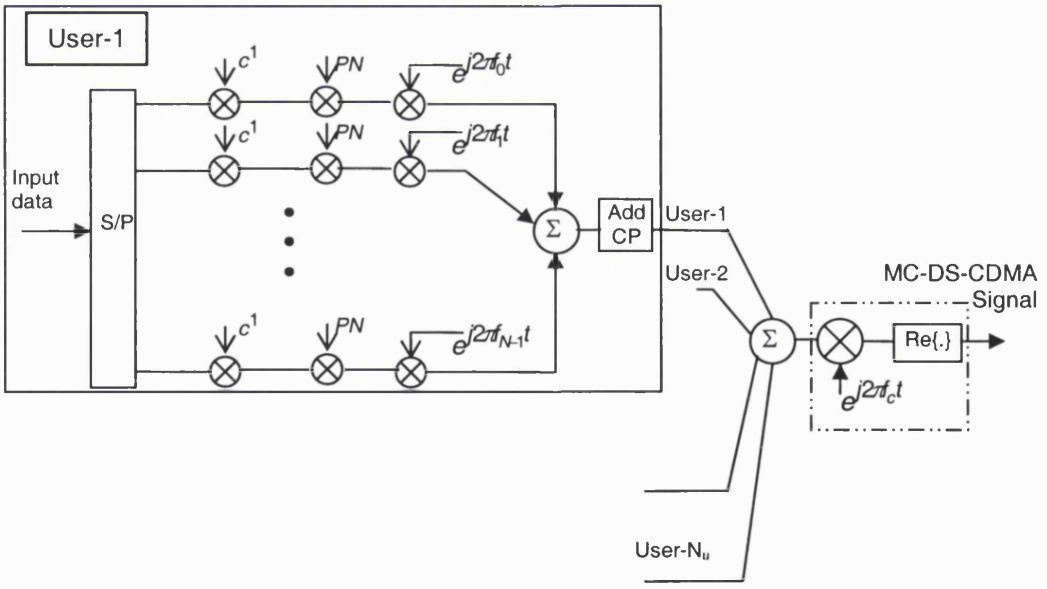

Figure 2.31: Modified MC-DS-CDMA transmitter (with scrambling)

A number of different PN codes can be considered for scrambling (base station separation) in the multi-carrier CDMA systems. These include, m-sequence codes, gold codes and kasami codes[17]. As in the existing CDMA systems, the rate of the scrambling code will be

[17] Further description of these codes is provided in Chapter 5 of [17].

the same as the rate of the spreading code. The scrambling codes must be applied synchronously to each user in order to maintain the orthogonality between the different users' data. In the case of MC-CDMA, due to the fact that the spreading is performed in the frequency domain, the length (or the period) of the scrambling code must be equal to the length of the spreading code. In the case of MC-DS-CDMA, each parallel branch can be considered to be similar to DS-CDMA and hence the length of the scrambling code can be determined in a similar way to DS-CDMA (as described in [59, 60, 61]).

2.3.4 Properties of multi-carrier CDMA signals

Multi-carrier CDMA signals exhibit the following properties:

- Multiple Access Capability

In multi-carrier CDMA, the multiplication of the user data by the code signal provides the multiple access capability. Provided that the spreading codes have a sufficiently low cross correlation, the different user's data can be separated successfully at the receiver.

- Protection against multipath

In multi-carrier CDMA, increased symbol duration and cyclic prefix insertion between each symbol provides immunity to multipath effects. If the CP duration is longer than the maximum delay spread in the system, all the time dispersion will occur within the CP and hence there is no ISI.

- Narrowband interference rejection

Any narrowband interference will only affect the information in a single subcarrier which can be recovered using Forward Error Correction (FEC).

Multi-carrier CDMA systems described in this section provide a number of advantages over single carrier CDMA systems such as DS-CDMA and FH-CDMA. These include, better immunity against multipath (due to increased symbol duration and the insertion of the cyclic prefix) and more efficient use of the spectrum (due to overlapping subcarrier spectra).

A number of authors have compared the performance of different multi-carrier CDMA schemes with DS-CDMA. In [38], the BER performance of MT-CDMA, MC-CDMA, MC-DS-CDMA and DS-CDMA is compared for the down link channel and the results show that MC-CDMA provides the best performance for different number of active users. In [52] the spectral efficiency of MC-DS-CDMA is compared with that of DS-CDMA for the downlink channel and it has been concluded that MC-DS-CDMA provides better spectral efficiency as compared to DS-CDMA. Kaiser [44] has also investigated the spectral efficiency of multi-carrier CDMA and DS-CDMA for different number of active users and has concluded that for small number of active users both schemes exhibit similar performance, however, as the number of users increases, multi-carrier CDMA outperforms DS-CDMA.

Even though multi-carrier CDMA schemes seem to be a promising alternative to DS-CDMA for future generations of wireless networks, they have two major drawbacks: vulnerability to synchronisation errors and vulnerability to non-linear distortion.

The main source of synchronisation errors in multi-carrier CDMA systems are carrier frequency offsets and symbol timing offsets [63]. Carrier frequency offsets occur due to the frequency difference between the oscillators in the transmitter and the receiver. It results in a loss of orthogonality between the different subcarriers and causes BER degradation (due to ICI). Symbol timing offset occurs due to uncertainty in establishing the multi-carrier CDMA symbol boundaries. The symbol timing offset can vary over the cyclic prefix duration without causing any ISI or ICI, however, when the timing misalignment extends over the multi-carrier CDMA symbol boundaries, ISI and ICI occur. Multi-carrier CDMA is more robust to symbol timing offset than carrier frequency offset.

As the multi-carrier CDMA signal generally consists of the sum of a large number of subcarriers, the transmitted signal may exhibit large signal excursions when such subcarriers add up coherently. Hence the signal is vulnerable to non-linear distortion caused by non-linear elements such as HPAs. The non-linear distortion manifests itself as in-band distortion and out-of-band distortion. In-band distortion causes BER degradation whereas out-of-band distortion causes spectral spreading and adjacent channel interference. In recent years, some authors [64, 65] have investigated the performance of multi-carrier CDMA in the presence of HPA nonlinearities. Techniques to reduce the PAPR of the multi-carrier CDMA signal have also been proposed in [21, 66, 67] in order to improve the performance in the presence of HPA non-linearities.

2.4 Summary

Multi-carrier CDMA is a combination of CDMA and MCM. This chapter provided background on CDMA and MCM and introduced the concept of combining the two techniques.

The chapter began with an overview of CDMA technology (Section 2.1). It detailed the fundamentals of CDMA spread spectrum technology and stated the criteria for a system to be qualified as a spread spectrum system. The key CDMA systems (namely, DS-CDMA, FH-CDMA, TH-CDMA and Hybrid CDMA) were then discussed, followed by a description of the key properties of spread spectrum CDMA.

Section 2.2 described multi-carrier modulation. It introduced the concept of parallel transmission of data over a number of subcarriers. The basic idea of OFDM was explained both in the time domain and in the frequency domain and the OFDM transmitter and receiver structures were described.

Section 2.3 presented the concept of combining DS-CDMA with OFDM. It described the three schemes proposed in the literature for combining DS-CDMA with OFDM (MC-CDMA, MC-DS-CDMA and MT-CDMA) in terms of signal generation at the transmitter and discussed some

of the advantages and drawbacks of multi-carrier CDMA schemes. It also discussed the performance of multi-carrier CDMA systems in a multipath channel and in a multi-cell environment.

The following chapters present the research work carried out, relevant to multi-carrier CDMA.

Chapter 3

Assessment of MC-CDMA exploiting higher order PSK/QAM formats

The previous chapter provided an introduction to multi-carrier CDMA. It described the basics of CDMA and MCM, introduced the concept of combining CDMA with MCM (multi-carrier CDMA) and presented the three different multi-carrier CDMA schemes.

Since their introduction in the early 1990s, much research has been carried out into the performance of multi-carrier CDMA systems in various environments, with different channel models, channel estimation techniques, equalization schemes and detection schemes [38, 41, 68]. However, most of the system models employed in these investigations have been restricted to the use of BPSK or QPSK mapping [69, 70]. Accordingly, the next two chapters explore the implications for multi-carrier CDMA system performance with higher order PSK/QAM mapping[18]. This chapter focuses on MC-CDMA and Chapter 4 focuses on MC-DS-CDMA.

The performance of single carrier systems incorporating higher order PSK/QAM mapping schemes in the presence of AWGN is well documented [71]. Using higher order mapping results in greater throughput and hence higher spectral efficiency. However, it also results in reduced power efficiency, increased complexity and for the case of QAM, increased envelope fluctuations.

The performance of multi-carrier systems (specifically OFDM) incorporating higher order PSK/QAM mapping has also been studied to some extent by Prasad [19] and others [72, 73]. Some authors have also investigated the effects of combining higher order PSK/QAM mapping with single carrier DS-CDMA [74]. However, to date there has been no significant work on the performance of multi-carrier CDMA systems combined with higher order PSK/QAM mapping.

---

[18] In this work higher order mapping is defined as M-PSK/M-QAM schemes with M>2.

Incorporating higher order mapping into MC-CDMA systems can be done in several ways. Two techniques are considered here that lead to the development of two distinct architectures for effecting such incorporation. These architectures are termed *combining in time* and *combining in frequency*. Both architectures have been studied in terms of power efficiency, PAPR, spectral efficiency and implementation complexity. The CIF architecture is only studied for a single user case due to the simplicity of the receiver structure adapted.

The chapter begins by presenting the two different architectures considered for incorporating higher order PSK/QAM within MC-CDMA. The subsequent section discusses the parameters used to investigate the performance of the two implementations[19] with different PSK/QAM formats. This is followed by an overview of the AWGN channel. The performance of the two implementations is then presented and a comparison is made between the two in order to determine the merits and demerits of each implementation. The chapter concludes with a summary.

3.1 MC-CDMA incorporating higher order mapping

This section describes the two implementations considered for combining MC-CDMA with higher order PSK/QAM mapping. In the first implementation, the PSK/QAM mapping is performed at the input of the MC-CDMA transmitter (before spreading and multi-carrier modulation) and in the second implementation, the PSK/QAM mapping is performed after signal spreading, but before multi-carrier modulation. The first implementation is referred to as *combining in time* (CIT) as increasing the order of the mapping scheme results in more data bits being transmitted over a given timeslot. The second implementation is referred to as *combining in frequency* (CIF) as increasing the order of mapping in this case results in more data chips being transmitted over a given subcarrier. The performance of the two implementations is investigated using the transmission model given in Figure 3.1. For simplicity, the channel is assumed to be a synchronous downlink channel.

Figure 3.1: Transmission model

The MC-CDMA scheme considered here is similar to the MC-CDMA scheme described in Section 2.3.1.1 with no S/P converter at the input (Figure 3.2). At the input of the MC-CDMA transmitter, the user data is first copied N_{code} times. Each copy is then multiplied by the individual chips of the spreading code, c_n^u and modulated onto a set of orthogonal subcarriers, $g_n(t)$. The modulated output is summed and synchronously added to the output of the other users. The signal is up-converted before transmission. Note that in this transmitter diagram an

[19] In this work, the term architecture and implementation are used interchangeably to describe the various models considered for incorporating higher order mapping into the multi-carrier CDMA schemes.

additional block for the CP extension has not been included as the definition of g(t) (Equation 3.3) accounts for the addition of the cyclic prefix.

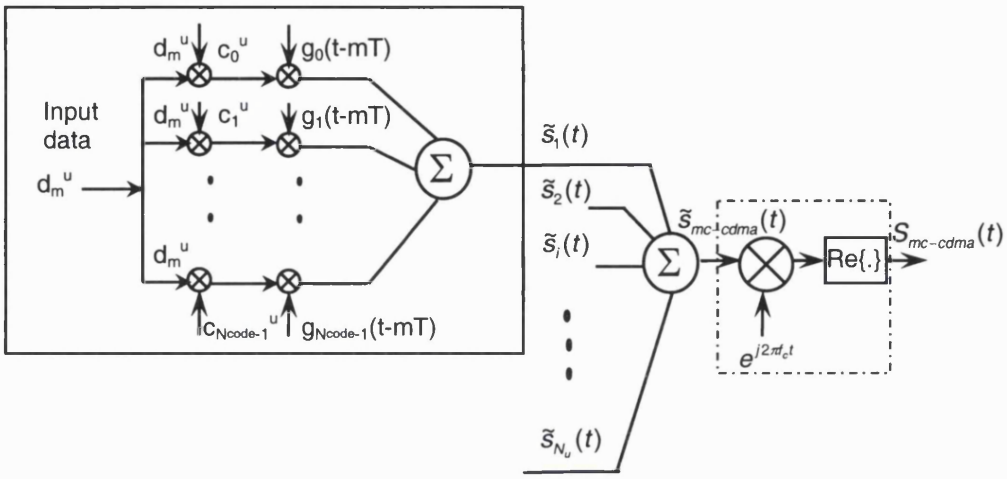

Figure 3.2: MC-CDMA transmitter

The bandpass signal at the output of the transmitter, $S_{mc-cdma}(t)$ is given by:

$$S_{mc-cdma}(t) = \mathrm{Re}\left\{\tilde{s}_{mc-cdma}(t)e^{j2\pi f_c t}\right\} \tag{3.1}$$

where $\tilde{s}_{mc-cdma}(t)$ is the equivalent baseband representation[20] [75] of $S_{mc-cdma}(t)$ (Equation 3.2) and f_c is the frequency of the carrier.

$$\tilde{s}_{mc-cdma}(t) = \sum_{u=1}^{N_u} \tilde{s}_u(t)$$
$$\tilde{s}_u(t) = \sum_{m=-\infty}^{\infty} \sum_{n=0}^{N_{code}-1} d_m^u c_n^u g_n(t - mT) \tag{3.2}$$

In the above expression, d_m^u is the input data bit in time slot m, for user u, c_n^u is the n^{th} chip of the spreading code ($c^u(t)$) for user u and $g_n(t)$ is the n^{th} subcarrier given by:

$$g_n(t) = \begin{cases} e^{\frac{j2\pi n(t-T_{cp})}{T-T_{cp}}} & t \in [0,T] \\ 0 & t \notin [0,T] \end{cases} \tag{3.3}$$

where T is the duration of the MC-CDMA symbol and T_{cp} is the duration of the cyclic prefix.

In a practical system, the multi-carrier modulation and demodulation is carried out using an IFFT and FFT, respectively. This work also employs the IFFT/FFT based implementation as it reduces simulation time and complexity. In order to reduce the simulation time further, an equivalent baseband representation [75, 76] of the bandpass signal has been used.

[20] Also referred to as complex envelope in this thesis.

System features:

Symbol mapping

The two implementations considered in this chapter (Sections 3.1.1 and 3.1.2) use M-PSK/M-QAM mapping to map a number of input bits onto a single complex value. The data at the input is first grouped into binary words of length k and then mapped onto constellation points using Gray coding. The length of the binary word (k) is dependent on the size of the constellation, M (where M is a power of 2). For a given constellation size, M, the length of the binary word, k is $\log_2(M)$. In this work higher order refers to M greater than 2.

By way of illustration, Figure 3.3 shows the constellation diagram for 16PSK and 16QAM mapping (Note, in this case M=16 and therefore $k=\log_2(16)=4$).

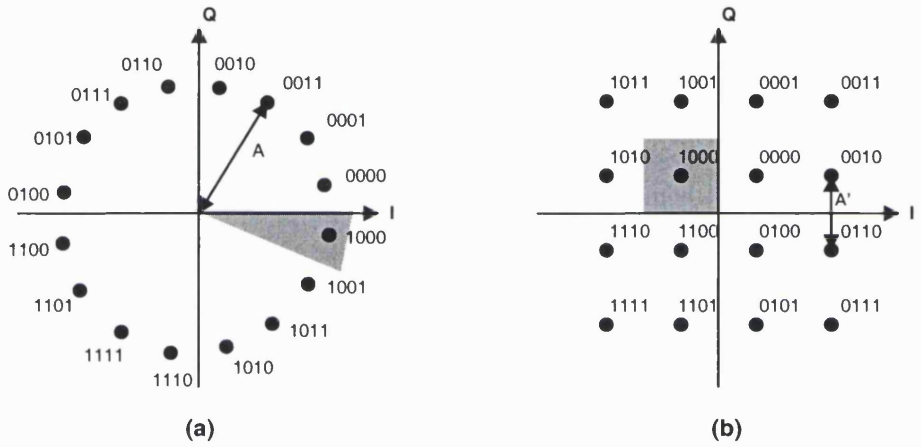

Figure 3.3: Constellation diagrams for: (a) 16PSK; (b) 16QAM

The constellation point, D for a given M-PSK mapping scheme is defined as:

$$D = Ae^{\frac{j(2\pi i+\pi)}{M}} \quad \text{i=0,1,....(M-1)} \tag{3.4}$$

where A is the amplitude of the transmitted symbol (as shown in Figure 3.3(a)).

In the case of M-QAM mapping, D is defined as:

$$D = \frac{A'}{2}(2i - K + 1) + j\frac{A'}{2}(2k - K + 1) \quad \text{i,k=0,1,....(K-1)} \tag{3.5}$$

where $K = \sqrt{M}$ and A' is the spacing between constellation points (as shown in Figure 3.3(b)).

At the receiver, the received symbols are often displaced from their original constellation points due to the effects of the channel. Hence, upon reception the received symbols are first assigned to a particular constellation point based on the decision region within which they fall and then demapped onto k bits (Shadowed region in Figure 3.3 illustrate the decision region for the constellation point corresponding to 1000). A symbol error occurs if the effects of the

channel causes the received symbol to lie outside the decision region of the corresponding transmitted symbol.

Spreading

The spreading operation provides user separation and spectral spreading, as discussed in 2.1.3. In this work, Walsh Hadamard (WH) spreading codes have been employed [16, 20, 21]. Most of the synchronous MC-CDMA systems proposed in the literature use WH codes because of their excellent cross correlation properties [17]. Other spreading codes employed in multi-carrier CDMA systems include complimentary codes [21], orthogonal gold codes [77] and Zaddoff-Chu codes [77].

The length of the WH codes is equal to the maximum number of codes in the system (i.e., there are a maximum of 32 codes of length 32). As each user is assigned a unique spreading code, the maximum number of codes is equal to the maximum number of users in the system. In this work, the maximum number of users is set to 64 [21], therefore, the length of the WH codes is equal to 64 chips.

Multi-carrier modulation

In the MC-CDMA scheme (Figure 3.2), the symbol times each chip of the spreading code is mapped onto a different subcarrier, hence the number of subcarriers is equal to the length of the spreading code (64). The separation between the subcarriers, Δf (Figure 3.4) is made equal to the symbol rate (1/T) in order to get maximum spectral overlap. Due to the insertion of the cyclic prefix, Δf is given by:

$$\Delta f = \frac{1}{T - T_{cp}} \tag{3.6}$$

where T is the duration of the transmitted MC-CDMA symbol and T_{cp} is the duration of the CP.

The bandwidth of the transmitted signal is approximately equal to $N_{code}\Delta f$ [22].

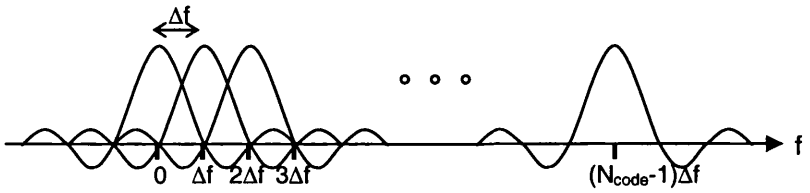

Figure 3.4: Spectrum of MC-CDMA signal

[21] In line with the IS-95 standard.

[22] In Figure 3.4, the spectrum of each modulated subcarrier has a null at the centre frequency of each of the other modulated subcarriers in the system. However, in a typical system, the insertion of the CP will increase the subcarrier separation as discussed in Section 2.2.1.

Cyclic prefix insertion

The cyclic prefix is inserted at the beginning of each MC-CDMA symbol to prevent the occurrence of ISI and ICI (as described in Section 2.2). In order to avoid ISI completely, the duration of the cyclic prefix (T_{cp}) is made greater than the rms delay spread of the system (τ_{rms}).

Inserting a CP at the beginning of each symbol introduces a loss in the SNR and an increase in the signal bandwidth. The bandwidth expansion factor is given by [37]:

$$BW_{expansion} = \frac{T}{T - T_{cp}} \tag{3.7}$$

and the loss in the SNR is given by:

$$SNR_{loss}(dB) = 10\log\left(\frac{T}{T - T_{cp}}\right) \tag{3.8}$$

In this work, the CP duration has been made equal to $1/5^{th}$ of the symbol duration in order to make SNR_{loss} approximately 1 dB. The value of the MC-CDMA symbol duration is based on the values used for OFDM based systems such as HIPERLAN/2 and IEEE 802.11a [78].

Table 3.1 summarises the main system parameters and lists the values used for the different implementations.

3.1.1 Implementation-1: Combining in time

In this implementation, higher order mapping is effected prior to the MC-CDMA modulation. (The higher order mapping and demapping are performed outside the MC-CDMA modulation and demodulation[23] (Figure 3.5)). The binary input is first mapped onto an M-PSK/M-QAM constellation point. The output is then spread and modulated onto a set of orthogonal subcarriers. The modulated signal is transmitted through an AWGN channel. At the receiver, the corrupted signal is demodulated and despread to recover the transmitted symbols. In a practical multi-carrier system, the input data is coded and interleaved before being mapped onto constellation points [19]. However, in this work, no coding or interleaving has been considered as the aim is to explore MC-CDMA architectures using higher order PSK/QAM mapping.

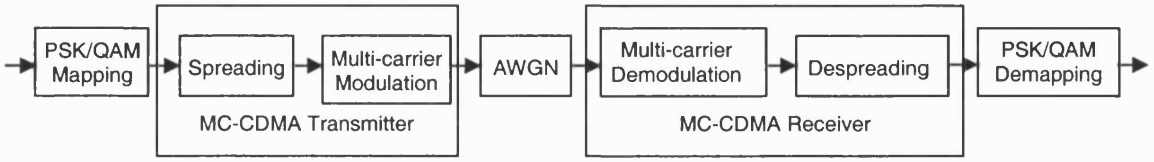

Figure 3.5: MC-CDMA implementation-1: Combining in time

[23] This implementation has been used by some authors [55, 56] for BPSK or QPSK mapping of the input data before multi-carrier modulation.

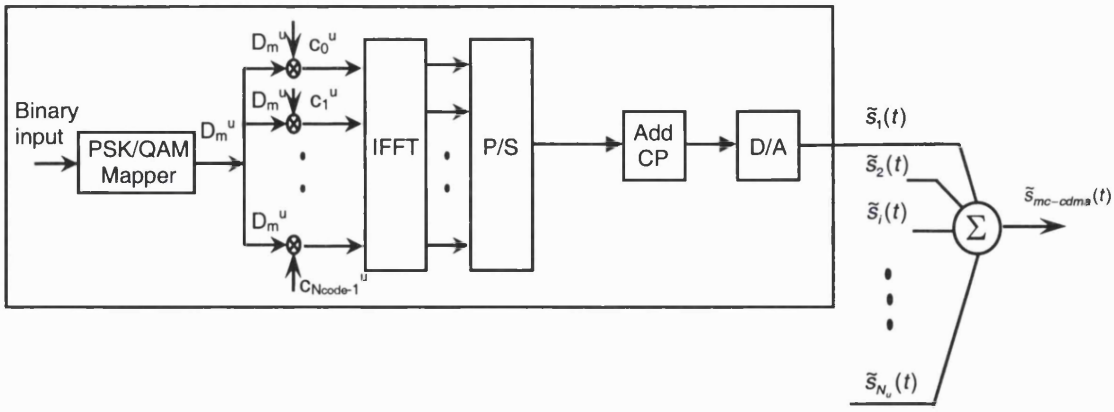

Figure 3.6: MC-CDMA implementation-1 (CIT): Transmitter

Figure 3.6 shows the equivalent baseband representation of the IFFT based implementation of the MC-CDMA transmitter with higher order mapping at the input.

The binary input is first combined into groups of k bits and mapped onto a constellation point, D by the PSK/QAM mapper. The output of the mapper is spread and mapped onto orthogonal subcarriers using the IFFT. The output of the IFFT is Parallel-to-Serial (P/S) converted and a cyclic prefix is added to the beginning of each symbol. The signal is converted into analogue format by the D/A converter before transmission.

Without any loss of generality, the equivalent baseband continuous time signal at the output of the MC-CDMA transmitter in Figure 3.6 is given by:

$$\tilde{s}_{mc-cdma}(t) = \sum_{u=1}^{N_u} \sum_{m=-\infty}^{\infty} \sum_{n=0}^{N_{code}-1} D_m^u c_n^u g_n(t - mT) \tag{3.9}$$

where D_m^u is the symbol at the output of the PSK/QAM mapper for user u, in timeslot m, c_n^u is a single chip of the spreading code and $g_n(t)$ is the n^{th} subcarrier (as defined in Equation 3.3).

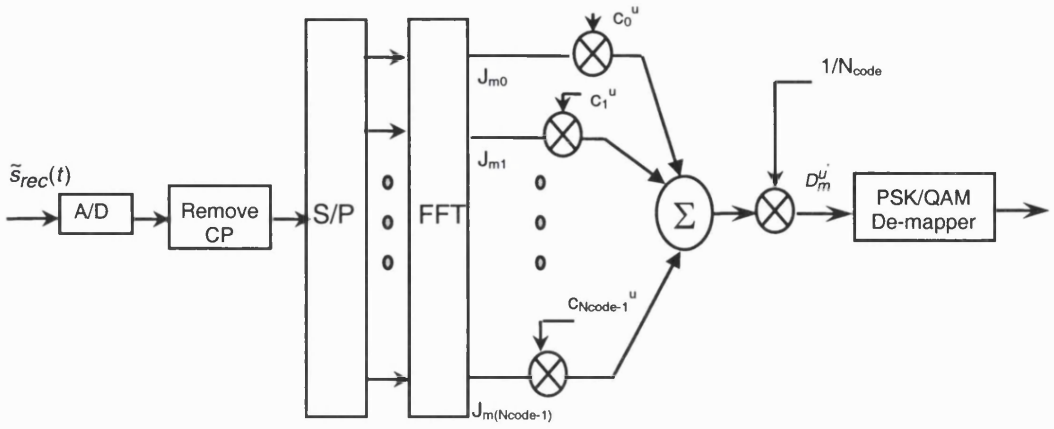

Figure 3.7: MC-CDMA implementation-1 (CIT): Receiver

The demodulation process at the receiver (Figure 3.7) is symmetrical to the modulation process at the transmitter (Figure 3.6). The complex envelope of the received signal, $\tilde{s}_{rec}(t)$ is first converted into digital format by the A/D converter. The cyclic prefix is then removed from the beginning of each symbol and the output is S/P converted and demodulated using the FFT.

The parallel output from the FFT is multiplied by the individual chips of the locally generated copy of the spreading code and summed to recover the transmitted symbol.

The recovered symbol, $D_m^{u'}$ at the output of the receiver is given by:

$$D_m^{u'} = \frac{1}{N_{code}} \sum_{n=0}^{N_{code}-1} J_{mn} c_n^u \tag{3.10}$$

where J_{mn} is the output of the FFT in timeslot m and subchannel n, c_n^u is the n^{th} chip of the spreading code for user u and N_{code} is the length of the spreading code.

3.1.2 Implementation-2: Combining in frequency

In this implementation, the higher order mapping is effected after the spreading but before the multi-carrier modulation (as shown in Figure 3.8).The input data is copied N_{code} times, spread and then combined to be mapped onto constellation points by the mapper. The complex output from the mapper is multi-carrier modulated and transmitted through the AWGN channel. The corrupted signal at the receiver is demodulated, demapped and despread to recover the transmitted data.

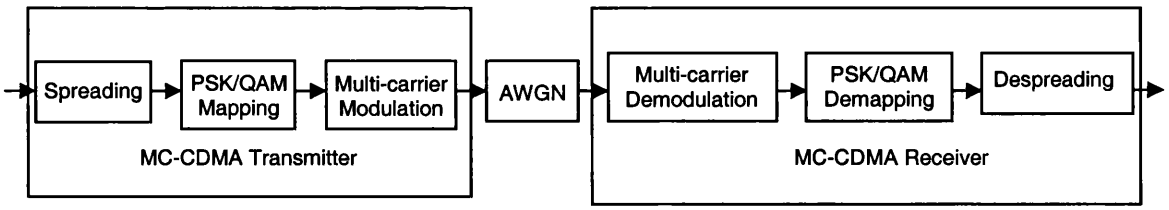

Figure 3.8: MC-CDMA implementation-2: Combining in frequency

Figure 3.9 shows the equivalent baseband transmitter model for implementation-2 (CIF). In this implementation, the binary input is first copied N_{code} times and spread by the user specific WH code. (Note that in this case, the input data is in the form of [0, 1] and therefore the spreading operation is performed by modulo 2 addition.) The spread data is then combined (in parallel) into groups of k chips and mapped onto constellation points using the PSK/QAM mapper. The output from the mapper is multi-carrier modulated using an IFFT. As in implementation-1, a cyclic prefix is added to each symbol before transmission.

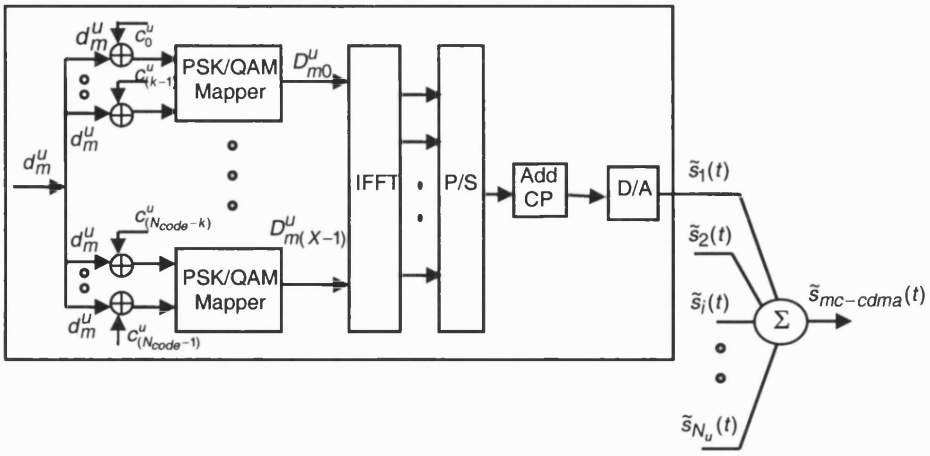

Figure 3.9: MC-CDMA implementation-2 (CIF): Transmitter

The complex envelope of the continuous time signal at the output of the transmitter, $\tilde{s}_{mc-cdma}(t)$ is given by:

$$\tilde{s}_{mc-cdma}(t) = \sum_{u=1}^{N_u} \sum_{m=-\infty}^{\infty} \sum_{x=0}^{X-1} D_{mx}^{u} g_x(t - mT) \tag{3.11}$$

where D_{mx}^{u} is the complex output of the PSK/QAM mapper for user u, in time slot m to be transmitted over subchannel x and $g_x(t)$ is the x^{th} orthogonal subcarrier given by:

$$g_x(t) = \begin{cases} e^{\frac{j2\pi x(t-T_{cp})}{T-T_{cp}}} & t \in [0,T] \\ 0 & t \notin [0,T] \end{cases} \tag{3.12}$$

Note that in this implementation, the number of subcarriers, X is dependent on k (and hence on the size of the constellation). More specifically,

$$X = \frac{N_{code}}{k} = \frac{N_{code}}{\log_2 M} \tag{3.13}$$

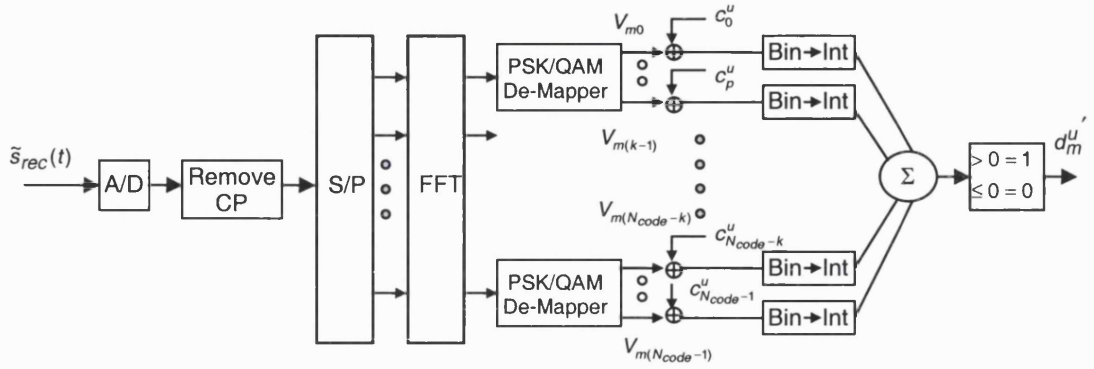

Figure 3.10: MC-CDMA implementation-2 (CIF): Receiver

Figure 3.10 shows an equivalent baseband representation of a simple receiver for CIF. As in the case of CIT, the complex envelope of the received signal is first converted into digital format with the A/D converter. The cyclic prefix is then removed from the beginning of each symbol and the output is demodulated, demapped and despread as shown in Figure 3.10.

The recovered data at the output of the receiver is given by:

$$d_m^u = \sum_{n=0}^{N_{code}-1} c_n^u \oplus V_{mn} \tag{3.14}$$

where V_{mn} is the output of the PSK/QAM demapper.

It is important to point out that the receiver model described above performs hard decision demapping (HDD) before despreading and therefore can only successfully demodulate data for a single user case (This point is developed further in Appendix-A). It is not suitable for detection in a multiuser environment. The following subsection discusses possible modifications required to operate MC-CDMA CIF in a multiuser environment.

Table 3.1: System parameters for implementation-1 and implementation-2

Parameter	CIT	CIF
Number of Users, N_{users}	64	64
Length of spreading code, N_{code}	N_{users} (64)	N_{users} (64)
Number of subcarriers, $N_{subcarriers}$	N_{code} (64)	$N_{code}/\log_2(M)$
Subcarrier spacing, Δf	$1/(T-T_{cp})$	$1/(T-T_{cp})$
Symbol duration, T	1 μs	1 μs
Cyclic prefix duration, T_{cp}	0.2 μs	0.2 μs
Spreading Code	WH Code	WH Code
Mapping Scheme	2/4/16/64PSK 16/64QAM	2/4/16PSK 16QAM
FFT size, N_{FFT}	$10*N_{subcarriers}$	$10*N_{subcarriers}$
Input sequence	m-sequence	m-sequence
Data rate	$(\log_2(M))/(T-T_{cp})$	$1/(T-T_{cp})$
Simulation duration	10000 symbols	10000 symbols

Table 3.1 summarises and compares the key parameters used for CIT and CIF. From this table it can be observed that the main difference between the parameters of the two implementations is the number of subcarriers and the data rate. In the case of CIT, increasing the order of the mapping scheme results in an increase in the data rate (but no change in the number of subcarriers and transmitter signal bandwidth), whereas in the case of CIF, increasing the order of mapping scheme results in a reduction in the number of subcarriers and the transmitted signal bandwidth (but no change in the data rate).

CIF receiver operation in a multiuser environment

In order to allow for successful multiuser demodulation, the MC-CDMA CIF receiver must be modified so that the probability of correct demodulation is maximised. This can be achieved by maximising the posterior probabilities, $P(S_m|\mathbf{S_{rec}})$ (where $\mathbf{S_{rec}}$ is the received vector and S_m is one of M transmitted symbols) [75, 76].

$P(S_m|\mathbf{S_{rec}})$ is given by:[24]

$$P(S_m|S_{rec}) = \frac{p(S_{rec}|S_m)P(S_m)}{p(S_{rec})} \tag{3.15}$$

where $p(\mathbf{S_{rec}}|S_m)$ is the conditional PDF of the received vector given S_m was transmitted, $P(S_m)$ is the priori probability of the m^{th} symbol being transmitted and $p(\mathbf{S_{rec}})$ is the PDF of the received vector.

The denominator of Equation 3.15 ($p(\mathbf{S_{rec}})$) is independent of the symbol transmitted and therefore finding the transmitted symbol that maximises $P(S_m|\mathbf{S_{rec}})$ is equivalent to finding the transmitted symbol that maximises $p(\mathbf{S_{rec}}|S_m)$.

The conditional PDF, $p(\mathbf{S_{rec}}|S_m)$ is usually referred to as the *likelihood function*. The decision criteria based on finding the symbol that maximises $p(\mathbf{S_{rec}}|S_m)$ is referred to as the *maximum likelihood criterion* and the process of maximising the likelihood function is referred to as Maximum Likelihood Sequence Estimation (MLSE).

In AWGN channels, the conditional probability, $p(\mathbf{S_{rec}}|S_m)$ is given by Equation 3.16. (Note that in order to simplify the computational complexity it is defined in terms of its natural logarithm.)

$$\ln(p(S_{rec}|S_m)) = -\frac{1}{2}N_{\dim}\ln(\pi N_0) - \frac{1}{N_0}\sum_{z=1}^{N_{dim}}(S_{rec_z} - S_{m_z})^2 \tag{3.16}$$

where N_{dim} is the dimension of the signal space.

The maximum of the natural logarithm of $p(\mathbf{S_{rec}}|S_m)$ is obtained by finding the symbol S_m which minimises the Euclidean distance (D_{Euc}) between the received symbol and the possible transmitted symbols (This is discussed further in [76]).

The Euclidean distance, D_{Euc} is given by:

$$D_{Euc} = \sum_{z=1}^{N_{dim}}(S_{rec_z} - S_{m_z})^2 \tag{3.17}$$

where N_{dim} is the dimension of the signal space.

Hence, in order to detect an M-QAM/M-PSK symbol (using MLSE), a set of M Euclidean distances are calculated and the symbol corresponding to the smallest distance is selected.

---

[24] using Bayes rule.

In a multiuser environment (such as multiuser CDMA), the likelihood function given in Equation 3.16 is modified to eliminate the interference caused by other users [76][25]. As the number of users increases, the number of Euclidean distances calculated also increases [79]. For a given M-PSK/M-QAM system, the total number of Euclidean distances calculated is equal to $M^{N_{users}}$ [80] (where N_{users} is the number of active users).

The demodulation technique described above is often employed in source/channel coded systems and multiuser systems [81, 82, 83], and is usually referred to as soft decision demodulation, due of the fact that the receiver makes use of additional information to demodulate the received signal. In coded systems, this additional information is in the form of all possible code words transmitted whereas in multiuser systems, it is in the form of data transmitted by other active users.

The main drawback of the MLSE technique is the implementation complexity, which increases with the number of active users [79]. In most practical systems, less efficient schemes (such as Minimum Mean Square Error (MMSE) and Interference Cancellation (IC) [84]) are generally employed.

The following section discusses the incorporation of Maximum Likelihood Sequence Estimation within the MC-CDMA CIF receiver to allow for successful multiuser demodulation.

Modifications to the MC-CDMA CiF receiver

The MC-CDMA CIF receiver employed in this investigation does not allow for successful multiuser demodulation due to the hard decision demapping of M-PSK/M-QAM symbols by the PSK/QAM de-mapper. In order to understand this further, consider an MC-CDMA CIF system with 2 active users and 4QAM mapping. For a given MC-CDMA symbol, the 4QAM symbol for user 1 over subcarrier 0, D^1_{m0} (refer to Figure 3.9) can be taken to be 1+1j and the 4QAM symbol for user 2 over subcarrier 0, D^2_{m0} (Figure 3.9) can be taken to be 1-1j. The symbol transmitted over subcarrier 0 will therefore be the sum of these two values, $D^1_{m0} + D^2_{m0}$ which is equal to 2+0j.

At the receiver, the symbol at the input of the first PSK/QAM de-mapper (for subcarrier 0) will be equal to D_{rec_0}=2+0j (assuming a perfect channel). The de-mapper will make a decision on D_{rec_0} based on whether the real (Re{}) and the imaginary (Im{}) part of D_{rec_0} are greater than or less than certain threshold values. In the case of 4QAM, if $Re\{D_{rec\_0}\}\geq 0$, the real part of the estimated symbol, D_{m0}' is assumed to be a 1 and if $Re\{D_{rec\_0}\}<0$, the real part of estimated symbol, D_{m0}' is assumed to be a 0. A similar comparison is used for the imaginary part. if $Im\{D_{rec\_0}\}\geq 0$, $Im\{D_{m0}'\}$ is assumed to be a 1 and if $Im\{D_{rec\_0}\}<0$, $Im\{D_{m0}'\}$ is assumed to be a

[25] This technique is referred to as Multi-User Detection (MUD).

0. If D_{rec_0}=2+0j then D'_{m0} =1+1j. Hence, it can be concluded that the hard decision performed by the PSK/QAM de-mapper results in some loss of information which consequently results in unsuccessful user separation.

In order to overcome this problem, a receiver model employing soft demodulation (using MLSE) is proposed. Figure 3.11 presents the modified receiver structure for MC-CDMA CIF with MLSE.

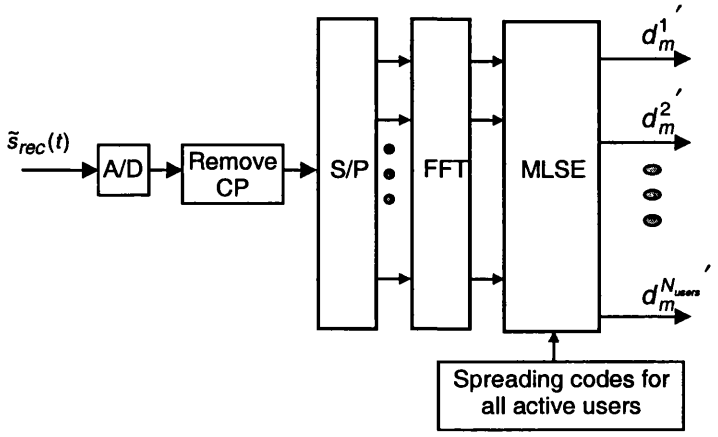

Figure 3.11: Modified MC-CDMA CIF receiver

As in the case of the original CIF receiver, the complex envelope of the received signal is first converted into digital format by the A/D converter. The cyclic prefix is then removed from the beginning of each symbol and the signal is demodulated by the FFT. The parallel output of the FFT is passed onto the MLSE which determines the data transmitted by each active user, using the knowledge of the spreading codes allocated to each active user.

In order to understand how the modified receiver model will allow for successful multiuser demodulation, consider a simple scenario with 2 active users. For a given received symbol, the data transmitted by each user will be a 1 or a 0. As the MLSE has knowledge of the spreading code allocated to each user, it can calculate all the possible symbol values transmitted by each user on each subcarrier (D^1_{m0}, D^1_{m1},..... $D^1_{m(X-1)}$, D^2_{m0}, D^2_{m1},..... $D^2_{m(X-1)}$) (refer to Figure 3.9) and thus predict the symbol transmitted on each subcarrier (($D^1_{m0}+D^2_{m0}$),($D^1_{m1}+D^2_{m1}$),.....($D^1_{m(X-1)}+D^2_{m(X-1)}$)). Hence, by calculating the Euclidian distance between the output of the FFT and the predicted symbol values (for each subcarrier) and selecting the symbols with the smallest Euclidean distance, the MLSE can estimate the transmitted M-PSK/M-QAM symbol[26] (over each subcarrier) and the data bits for each user (d^1_m, d^2_m (Figure 3.9)).

The key drawback of the modified receiver model presented in Figure 3.11 is a substantial increase in the implementation complexity with number of active users. Hence, soft

[26] This is known as a joint detection scheme.

decision/demodulation schemes with reduced implementation complexity should be investigated. The investigation and implementation of such demodulation schemes is beyond the scope of the research presented in this thesis.

3.2 Performance parameters

The most important parameters by which the effectiveness of modulation schemes can be judged are spectral efficiency and power efficiency [71]. The radio spectrum is a scarce resource and hence efficient use of the available spectrum is a key factor. The efficient use of the power is also important, particularly in mobile communications as the mobile units are battery powered. Another important consideration is implementation complexity. In mobile communications the cost and size of the mobile handset are crucial to the uptake of the system. Hence, this investigation considers the spectral efficiency, power efficiency and implementation complexity of the two implementations for different M-PSK/M-QAM formats.

3.2.1 Power efficiency

The power efficiency is quantified in terms of the achievable BER for a given bit-energy-to-noise-density ratio (E_b/N_0)[27] in AWGN.

There are a number of techniques available for the estimation of bit error rate in the simulation context [85]. In this work, the Monte Carlo technique has been employed. The Monte Carlo technique is commonly used for estimating the BER as it is simple and easy to implement. In the Monte Carlo technique, the BER is calculated as the ratio of erroneous bits received to the total number of bits received.

$$BER = \frac{Erroneous\ bits\ received}{Total\ number\ of\ bits\ received} \tag{3.18}$$

One of the main drawbacks of the Monte Carlo technique is the fact that in order to observe a BER of 10^{-k}, the simulations must be run for 10^{10k} bits. Hence, for very low BER values ($<10^{-9}$), more advanced techniques of estimation have to be considered.

3.2.2 Peak-to-average-power ratio

In a multi-carrier system, the power efficiency of the system is influenced by the envelope fluctuations of the transmitted signal, if non-linear elements such as HPAs are present in the system (This is discussed in further detail in Chapter 5). The envelope fluctuations of the transmitted signal are measured in terms of the PAPR of the signal. In general, the higher the PAPR, the higher the degradation in power efficiency in the presence of non-linearities.

---

[27] Appendix-B describes how the E_b/N_0 value is set and adjusted in the simulation.

The PAPR is defined as:

$$PAPR = \frac{P_{peak}}{P_{average}} \tag{3.19}$$

where P_{peak} is the peak power of the transmitted signal and $P_{average}$ is the average power.

The peak power of a bandpass signal, S(t) is given as the average power that would be obtained if the envelope of the equivalent baseband signal, $|\tilde{s}(t)|$ was held constant at its peak value ($\max|\tilde{s}(t)|$).This is equivalent to evaluating the average power in an unmodulated sine wave with a peak value of $\max|\tilde{s}(t)|$ [28]. Hence, the peak power of S(t), in terms of its equivalent baseband representation, $\tilde{s}(t)$ is given by [86]:

$$P_{peak} = \frac{1}{2}\left[\max|\tilde{s}(t)|\right]^2 \tag{3.20}$$

The average power of a bandpass signal, S(t) is given by:

$$P_{average} = E\left[\lim_{D_{sig.}\to\infty}\left(\frac{1}{D_{sig.}}\int_{D_{sig.}}[S(t)]^2 dt\right)\right] \tag{3.21}$$

where $D_{sig.}$ is the duration of S(t) and E[.] is the expectation operator.

The average power of S(t) in terms of its equivalent baseband representation, $\tilde{s}(t)$ is given by [76]:

$$P_{average} = E\left[\lim_{D_{sig.}\to\infty}\left(\frac{1}{D_{sig.}}\int_{D_{sig.}}\frac{1}{2}\left[\tilde{s}(t)\right]^2 dt\right)\right] \tag{3.22}$$

From Equations 3.20 and 3.22,

$$PAPR = \frac{\left[\max|\tilde{s}(t)|\right]^2}{E\left[\lim_{D_{sig.}\to\infty}\left(\frac{1}{D_{sig.}}\int_{D_{sig.}}\left[\tilde{s}(t)\right]^2 dt\right)\right]} \tag{3.23}$$

A detailed description of the PAPR is presented in Chapter 6.

[28] The average power of a sine wave with amplitude A is $A^2/2$.

3.2.3 Spectral efficiency

The spectrum of the modulated signal is usually presented as the plot of Power Spectral Density (PSD) vs. frequency (Figure 3.12). The spectral efficiency, η is defined as the data rate, r_b per unit bandwidth occupied [71].

$$\eta = \frac{r_b}{W} \tag{3.24}$$

where W is the bandwidth of the signal.

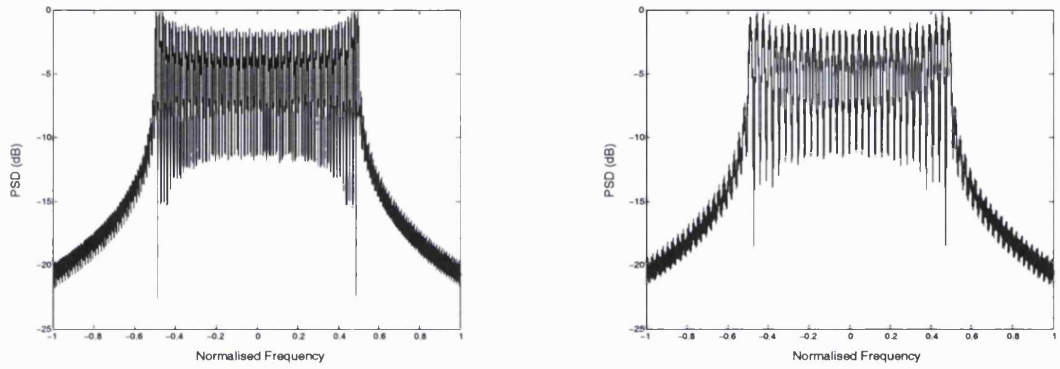

(a) (b)

Figure 3.12: PSD of transmitted signal in: (a) implementation-1; (b) implementation-2, with 4PSK mapping

3.2.4 Implementation complexity

A commonly used yardstick for assessing the implementation complexity of modulation schemes is *Millions of Instructions Per Second* (MIPS).

The MIPS can be calculated in a number of different ways and the result obtained may vary depending on the platform (DSP architecture, manufacturer etc) and scenario (worst case, average, etc).

In this work, a standard MATLAB™ library function has been used to calculate the number of floating point operations (FLOPS) required to process an MC-CDMA symbol using different mapping schemes. This value is then used to calculate the number of Operations per Second (OPS) for the different schemes.

$$OPS = \frac{FLOPS\ required\ for\ 1\ MC\ -\ CDMA\ symbol}{T} \tag{3.25}$$

where T is the duration of the MC-CDMA symbol.

It is important to point out that the values obtained here may not be comparable to the MIPS values obtained using a particular DSP platform. However, this technique has been considered sufficient to allow for a comparison between the different mapping schemes.

3.3 Additive White Gaussian Noise channel

The power efficiency of the two implementations is measured in the presence of AWGN channel and hence this section provides an overview of the AWGN channel.

The AWGN channel is the most benign channel in a communication system where the transmitted signal is corrupted by additive noise. There are several sources of noise in the communication system. The most dominant form of noise that always exists is thermal noise and hence the noise in communications channel is generally assumed to have the same characteristics as thermal noise. Thermal noise is caused by the thermal motion of charged particles (usually electrons) that are responsible for electrical conduction [86].

Thermal noise can be described as a random process with Gaussian distribution of zero mean and variance σ^2 [50]. The power spectral density of thermal noise at normal temperatures has a very flat behaviour for most of the frequencies of interest [86]. Therefore, for all practical purposes, the power spectral density of thermal noise is considered constant at all frequencies and due to this characteristic, it is referred to as white noise. *(It should be noted that in reality no physical process can have such a characteristic, since it would result in infinite power.)* Thermal noise is added to the signal and hence it is often referred to as Additive White Gaussian Noise.

3.3.1 Modelling AWGN

As discussed above, AWGN is assumed to have Gaussian distribution with zero mean and variance σ^2. The PSD of the AWGN is given by Equation 3.26 and illustrated in Figure 3.13(a).

$$\Phi_{nn}(f) = \frac{N_0}{2} \tag{3.26}$$

where $N_0/2$ is the double-sided PSD of the noise signal.

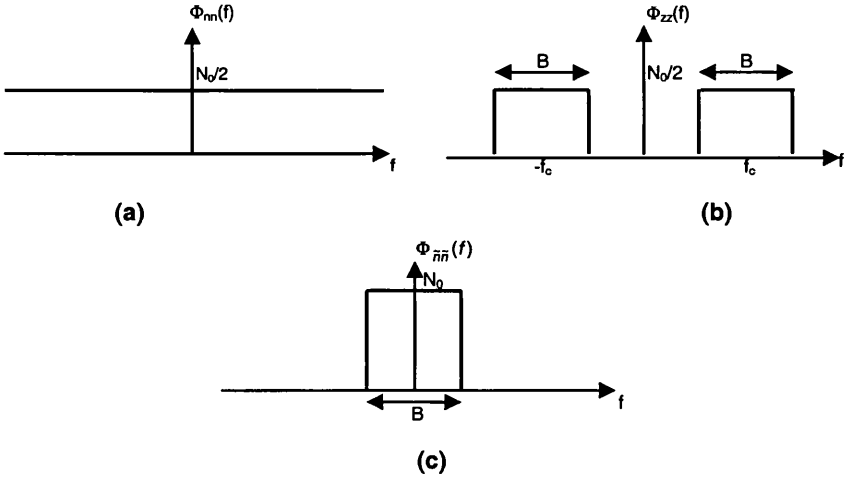

Figure 3.13: Power spectral density of: (a) AWGN; (b) band-limited AWGN; (c) complex envelope of band-limited AWGN

In a wireless communications system, the receiver usually employs filtering to remove out-of-band interference in the received signal [86]. Hence, the noise after filtering has a bandpass spectrum (Figure 3.13(b)).

The PSD of filtered AWGN is given by:

$$\Phi_{zz}(f) = \begin{cases} \frac{N_0}{2} & f_c - \frac{B}{2} < |f| \le f_c + \frac{B}{2} \\ 0 & elsewhere \end{cases} \tag{3.27}$$

In this work, the complex envelope representation of signals has been adapted and hence the complex envelope of n(t), $\tilde{n}(t)$ has been used (Figure 3.13c). It has been given in [76] that $\tilde{n}(t)$ can be modelled with PSD given by:

$$\Phi_{\tilde{n}\tilde{n}}(f) = \begin{cases} N_0 & |f| \le \frac{B}{2} \\ 0 & |f| > \frac{B}{2} \end{cases} \tag{3.28}$$

3.4 Performance of MC-CDMA incorporating higher order PSK/QAM mapping

This section presents the performance of MC-CDMA systems (CIT and CIF) in terms of the parameters described in Section 3.2.

From Table 3.1, it can be observed that for both implementations, the symbol duration has been kept the same for all mapping schemes, hence, increasing the order of mapping in CIT results in higher data rate whereas increasing the order of mapping in CIF results in reduced number of subcarriers. The following sections present the performance of CIT and CIF for 2/4/16/64PSK and 16/64QAM.

3.4.1 Performance of implementation-1 (CIT)

Figure 3.14 shows the BER performance of CIT in AWGN. The figure presents BER results for various mapping schemes with the number of active users set to 1. The theoretical performance[29] of different schemes in AWGN for single user, single carrier modulation has also been included (The performance of different mapping schemes in multiuser, multi-carrier system is considered to be similar to that of a single user, single carrier system as there is no multiuser interference (because of WH codes) and no inter-subcarrier interference (because of orthogonal subcarriers)).

[29] Burr [71] details the derivation of expressions used to calculate the theoretical BER performance of PSK/QAM schemes in AWGN.

From the graph, it can be observed that the results for various mapping schemes agree well with the theoretical values. The higher the value of M, the higher the degradation in power efficiency (due to increased number of signal states within the constellation). For a given value of M, QAM schemes give better performance as compared to PSK schemes. This is because of the fact that the distance between the constellation points in an M-QAM constellation is larger than the distance between constellation points in an M-PSK constellation, for a given transmitted power (as illustrated in Figure 3.3).

Closer observation of the results show that the simulation results for 64PSK do not agree very well with the theoretical results in the high noise regime. This is due to the fact that the theoretical results are not accurate in such a case.

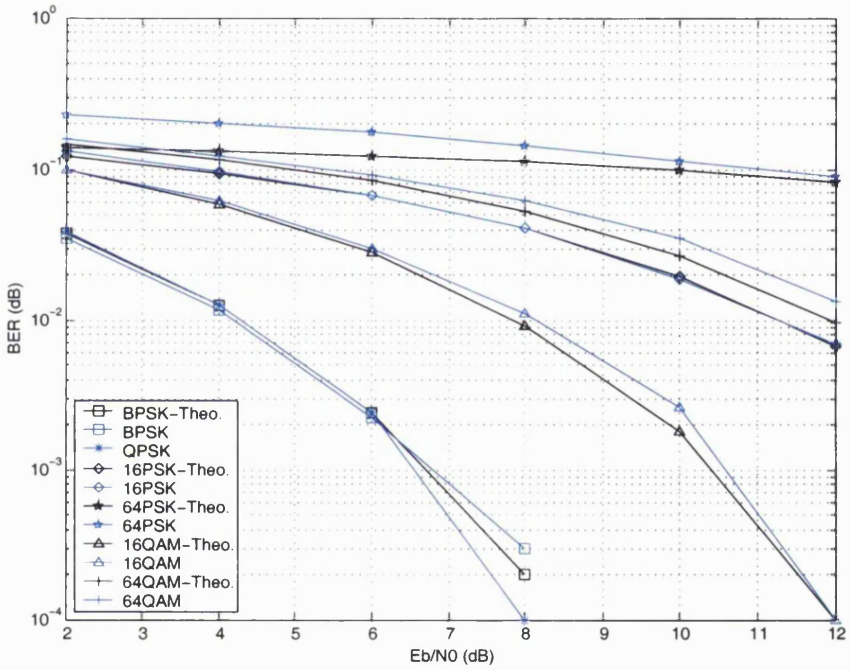

Figure 3.14: BER performance of MC-CDMA CIT in AWGN with 1 active user

The PAPR of the MC-CDMA signal at the output of the transmitted with different mapping schemes is shown in Figure 3.15. From this figure, it can be observed that as the number of active users increases the PAPR decreases (for all mapping schemes). The cause of this trend has been explained in Chapter 6. For large number of active users, the PAPR for different values of M is approximately the same for both PSK and QAM mapping schemes (with BPSK having a lower PAPR). For small number of active users, the PAPR for QAM schemes is higher than that for PSK schemes. Hence, in this implementation, using larger M-QAM constellations for greater throughput will result in an increase in the PAPR (for small number of active users), whereas using larger M-PSK constellations for greater throughput will not affect the PAPR of the transmitted signal.

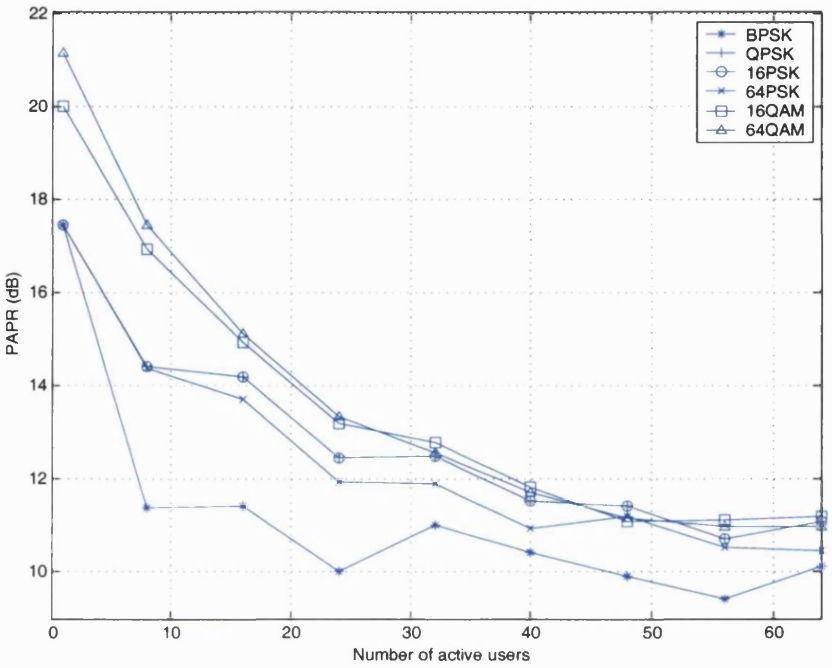

Figure 3.15: PAPR performance of MC-CDMA CIT

The implementation complexity of the MC-CDMA transceiver with different mapping schemes is presented in Figure 3.16 in terms of Millions of Operation Per Second (MOPS)[30].

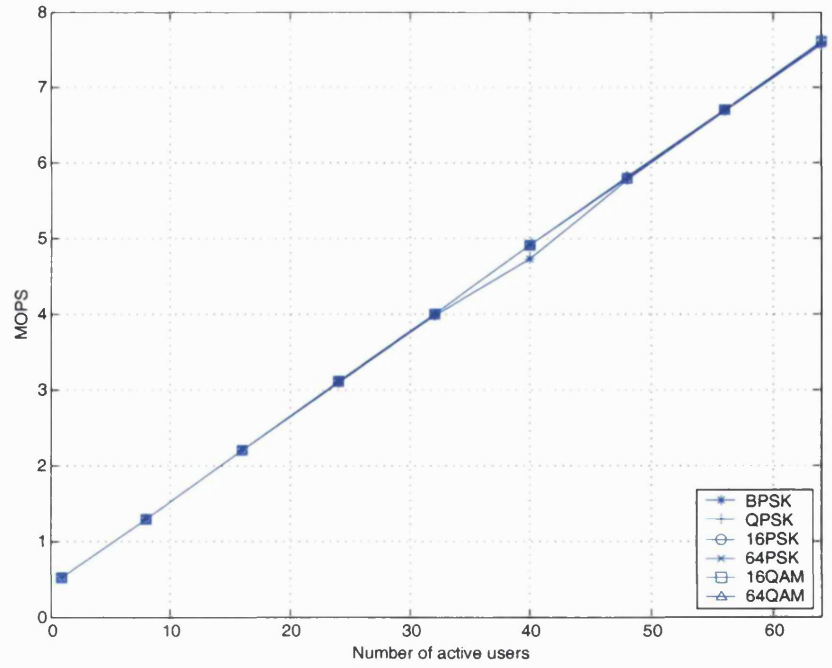

Figure 3.16: MOPS requirements for MC-CDMA CIT

[30] The MOPS value presented is the sum of the MOPS required for a transmitter with different number of active users and MOPS required for the receiver with 1 user.

Observation of Figure 3.16 shows that increasing the number of active users results in a linear increase in the MOPS requirements, as expected. The results show that the MOPS requirement for different mapping schemes is the same and hence there is no advantage in terms of implementation complexity of using one mapping scheme or another.

In this implementation, the spectrum of the transmitted signal is similar to that shown in Figure 3.4. The bandwidth of the transmitted signal (W) for the different mapping schemes is the same (as the MC-CDMA symbol duration and the number of subcarriers is kept constant), hence,

$$W = N_{code}\Delta f = \frac{N_{code}}{T - T_{cp}} \tag{3.29}$$

The data rate r_b is given by:

$$r_b = \frac{1}{T_b}$$

$$T_b = \frac{T}{k} = \frac{T}{\log_2 M}$$

Therefore,

$$r_b = \frac{1}{T_b} = \frac{\log_2 M}{T} \tag{3.30}$$

From, 3.26 and 3.27, the spectral efficiency of CIT, η is:

$$\eta = \frac{r_b}{W} = \frac{\log_2 M}{T} x \frac{(T - T_{cp})}{N_{code}} = \frac{\log_2 M}{N_{code}}\left(1 - \frac{T_{cp}}{T}\right) = \frac{k}{N_{code}}\left(1 - \frac{T_{cp}}{T}\right) \tag{3.31}$$

As N_{code}, T and T_{cp} are kept constant, the spectral efficiency of CIT increases with the size of the constellation.

3.4.2 Performance of implementation-2 (CIF)

Figure 3.18 shows the BER performance of CIF in AWGN with different mapping schemes, for one active user. The BER performance of CIF with different mapping schemes is observed to be much worse than the theoretical performance of the different schemes in AWGN (for single user, single carrier case). The degradation in performance can be attributed to the fact that the receiver performs hard decision demapping before despreading[31]. Appendix C verifies this by considering two different receiver models (with and without hard decision

[31] It has been stated in Chapter 6 of [87] that soft decision demapping can improve the BER performance of single carrier BPSK by 2 dB in an AWGN channel.

demapping) for BPSK and showing that the model with HDD generates increased errors compared to the model without HDD.

It is interesting to observe that for the mapping schemes considered (2PSK, 4PSK, 16PSK and 16QAM), the constellation of the signal at the input to the IFFT only consists of one of two possible points (i.e., the constellation of the signal transmitted over a given subcarrier consists of one of two points). This can be explained by considering a system with QPSK mapping. In this case, the input to the mapper will consist of 2 code chips (e.g., c_1 and c_2) multiplied by the input data bit. The input data bit can have one of two possible values [1 or 0]. Hence, the input to the QPSK mapper can be $1 \oplus c_1$ and $1 \oplus c_2$ or $0 \oplus c_1$ and $0 \oplus c_2$. By way of illustration, the constellation of the signal transmitted over a subcarrier for input of 0 and 1 is shown in Figure 3.17(a) and 3.17(b).

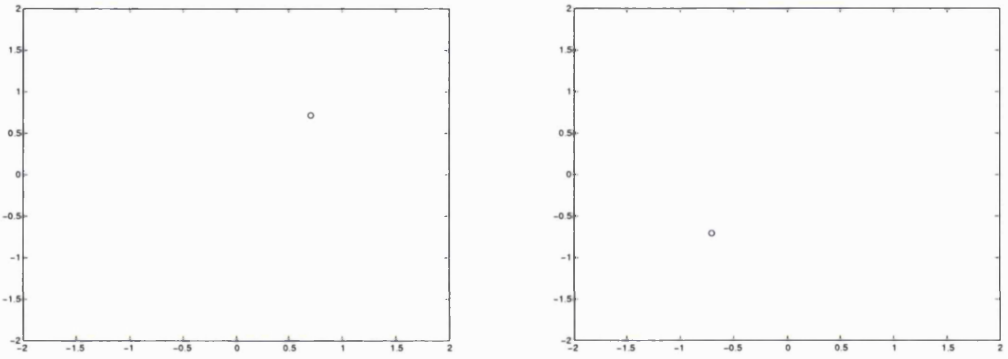

(a) (b)

Figure 3.17: Constellation of MC-CDMA/QPSK with: (a) input=0; (b) input=1

Comparing the PAPR of various mapping schemes for different number of active users shows that the PAPR is approximately the same for all cases (Figure 3.19). Hence, contrary to implicit assumptions, reducing the number of subcarriers by increasing the constellation size does not have a significant effect on the PAPR of the transmitted signal.

Figure 3.20 presents the MOPS requirement of CIF for different mapping schemes[32]. Observation of this figure shows that the MOPS requirement decreases with an increase in the constellation size. This is attributed to the fact that as the number of subcarriers decrease the number of multiplications within the IFFT/FFT also decreases. For a given M, the MOPS requirement for both PSK and QAM is the same and hence the MOPS requirement of an MC-CDMA CIF system can be decreased by using higher order M-PSK or M-QAM mapping.

[32] As in the CIT case, the MOPS value presented is the sum of the MOPS required for a transmitter with different number of active users and MOPS required for the receiver with one active user.

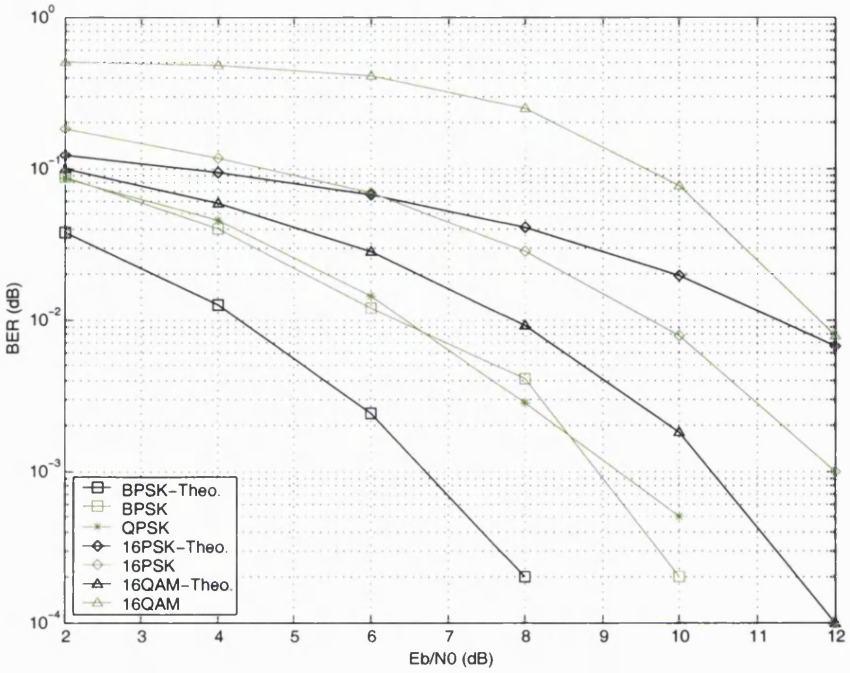

Figure 3.18: BER performance of MC-CDMA CIF in AWGN with 1 active user

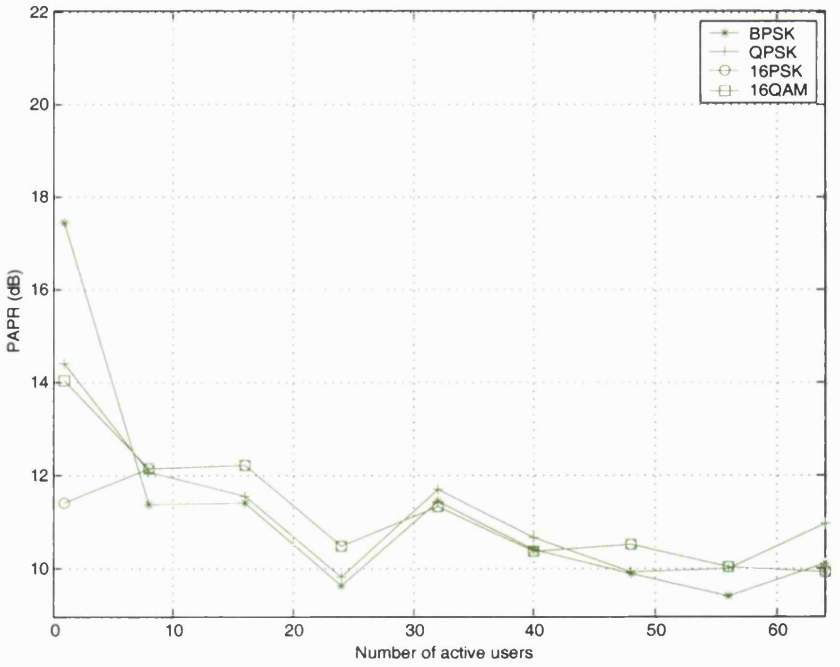

Figure 3.19: PAPR performance of MC-CDMA CIF

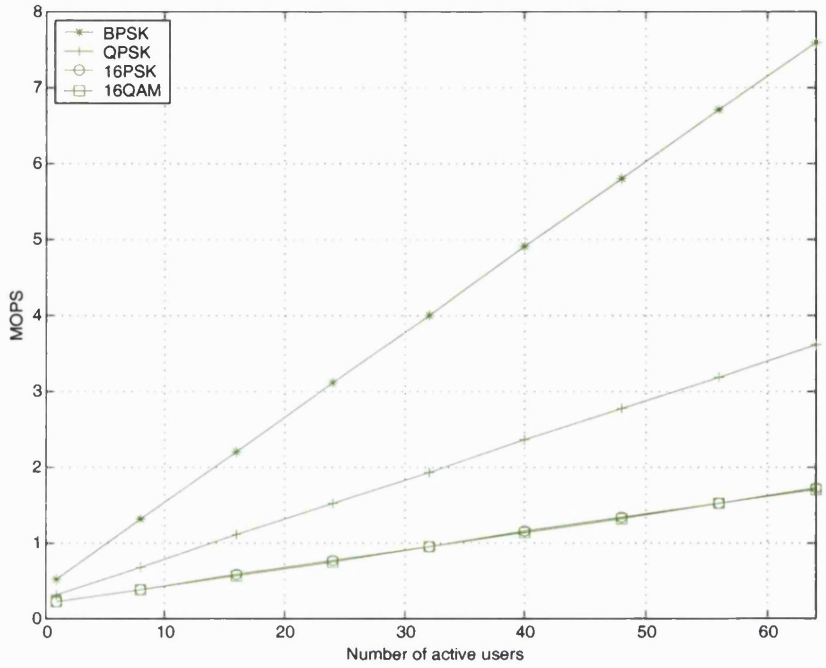

Figure 3.20: MOPS requirements for MC-CDMA CIF

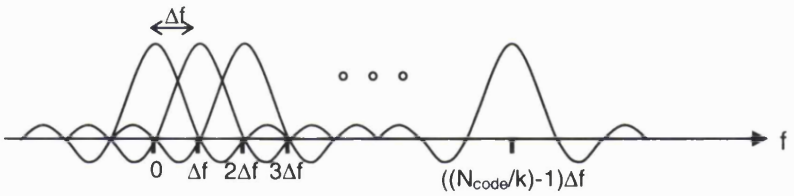

Figure 3.21: Spectrum of MC-CDMA signal for CIF [33]

The spectrum of the signal at the output of the CIF transmitter is shown in Figure 3.21.

In this case the bandwidth of the transmitted signal (W) varies with k ($\log_2$ M).

$$W = \frac{N_{code}\Delta f}{k} = \frac{N_{code}}{(\log_2 M)(T - T_{cp})} \tag{3.32}$$

The data rate is equal to the symbol rate and is independent of the constellation size:

$$r_b = \frac{1}{T_b} = \frac{1}{T} \tag{3.33}$$

[33] In Figure 3.20, the spectrum of each modulated subcarrier has a null at the centre frequency of each of the other modulated subcarriers in the system. However, in a typical system, the insertion of the CP will increase the subcarrier separation as discussed in Section 2.2.1.

Hence, the spectral efficiency of the system, η is:

$$\eta = \frac{r_b}{W} = \frac{1}{T} x \frac{(\log_2 M)(T - T_{cp})}{N_{code}} = \frac{\log_2 M}{N_{code}}\left(1 - \frac{T_{cp}}{T}\right) = \frac{k}{N_{code}}\left(1 - \frac{T_{cp}}{T}\right) \quad (3.34)$$

As in the CIT case, the spectral efficiency of CIF varies on the size of the constellation.

3.4.3 Discussion of MC-CDMA CIT and CIF systems performance

Section 3.4.1 and 3.4.2 presented the performance of CIT and CIF for different mapping schemes. In both cases, increasing the order of the mapping results in an increase in the overall bandwidth efficiency[34] of the system. In the case of CIT, this increase in bandwidth efficiency is achieved by increasing the number of bits transmitted over a given timeslot, whilst keeping the bandwidth constant (Figure 3.22(a) and 3.22(b)). In the case of CIF, increase in bandwidth efficiency is achieved by reducing the number of subcarriers, whilst keeping the number of bits transmitted over a given timeslot constant (Figure 3.22(c) and 3.22(d)).

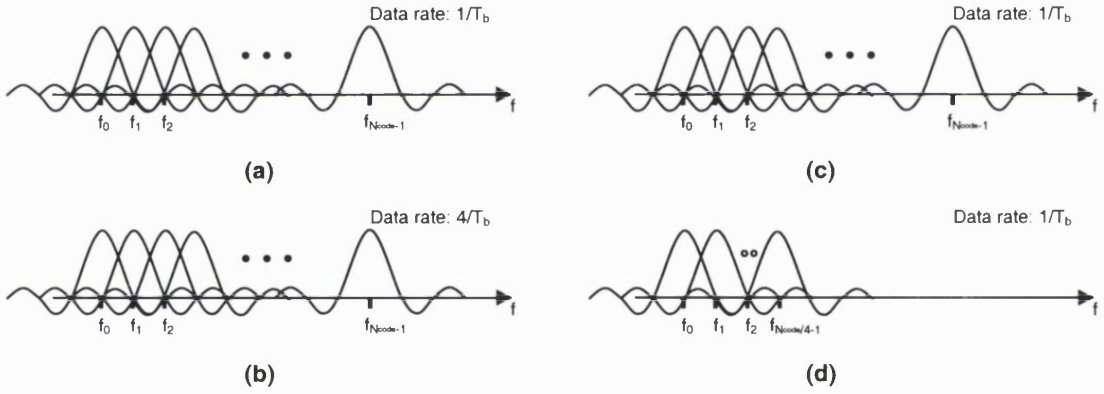

Figure 3.22: Spectrum of the transmitted MC-CDMA signal: (a) CIT with BPSK mapping; (b) CIT with 16PSK mapping; (c) CIF with BPSK mapping; (d) CIF with 16PSK mapping

In this work, the investigations have been carried out by making the MC-CDMA symbol duration constant for all mapping schemes. An alternative approach is to make the input data rate constant for all mapping schemes. In the case of CIT, making the input data rate constant would result in a reduction in the transmitted signal bandwidth with the order of mapping scheme. In the case of CIF, the input data rate is independent of the mapping schemes and hence making the input data rate constant for all mapping schemes will have no effect on the bandwidth of the transmitted signal. Comparing the two schemes for the same input data rate would result in the same bandwidth at the output of the transmitter, for a given mapping scheme (Figure 3.22). The number of subcarriers in both cases would however be different (i.e., the

[34] Bandwidth efficiency and spectral efficiency are used interchangeably in this thesis.

number of subcarriers in CIT would be equal to N_{code} whereas the number of subcarriers in CIF would be equal to N_{code}/k).

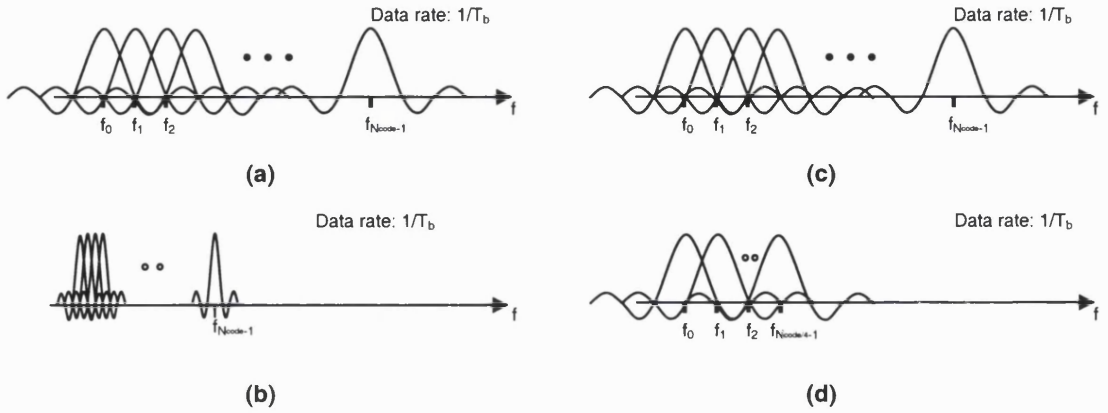

Figure 3.23: Spectrum of the transmitted MC-CDMA signal (with constant input data rate): (a) CIT with BPSK mapping; (b) CIT with 16PSK mapping; (c) CIF with BPSK mapping; (d) CIF with 16PSK mapping

Comparing the BER performance of the two implementations in the presence of AWGN, for different mapping schemes (Figure 3.24) shows that the BER performance of CIT is better than that of CIF. Further work is required on the receiver structure for CIF in order to carry out a comparison for the multiple user case. It is interesting to observe that in the case of CIT (as in the case of single user systems), QAM schemes perform better than PSK schemes, whereas in the case of CIF, PSK schemes seem to perform better than QAM schemes.

Figure 3.25 presents the PAPR variations of the two implementations for different mapping schemes. Comparison of the results reveals that the PAPR of CIF is lower than that of the CIT for all mapping schemes. However, the difference is not significant for large number of active users. In both cases, the PAPR decreases with the number of active users (This trend has been investigated in Chapter 6). It was anticipated that a reduction in the number of subcarriers would provide CIF with an advantage over CIT in terms of the PAPR, however, results show that this is not always the case.

Comparing the MOPS requirements for the two schemes (Figure 3.26) shows that for a given mapping scheme, the MOPS requirement for CIF is lower than that for CIT. As the order of mapping increases the difference between the MOPS requirements of the two implementations (for a given mapping scheme) increases. This is a consequence of the fact that in the case of CIF, increasing the order of mapping results in a reduction in the number of subcarriers and hence a reduction in the size of the FFT/IFFT.

For a given PSK/QAM scheme, the spectral efficiency of both implementations is the same. Figure 3.22 shows that as the order of mapping increases, the number of bits transmitted over the bandwidth, W increases in the case of CIT. The number of bits transmitter for different mapping schemes stays constant for CIF. However, in this case, increasing the order of mapping results in a reduction in the transmitted bandwidth (W).

The results presented in this section reveal that for a given mapping scheme each of the MC-CDMA systems has its own advantages and disadvantages and therefore the choice of combination of a system and mapping scheme should be based on the system requirements.

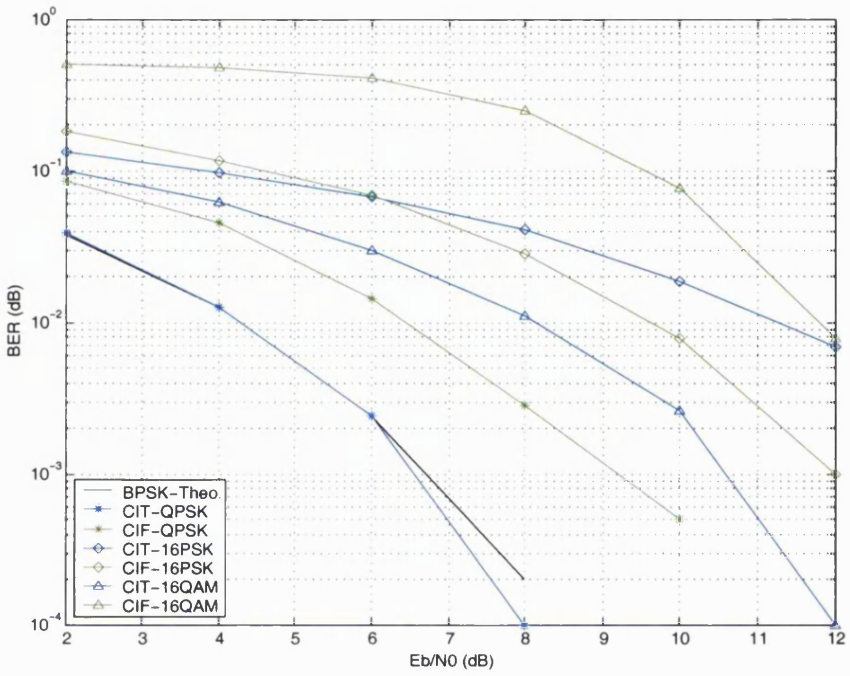

Figure 3.24: Comparison of BER performance of MC-CDMA CIT and CIF in AWGN with 1 active user

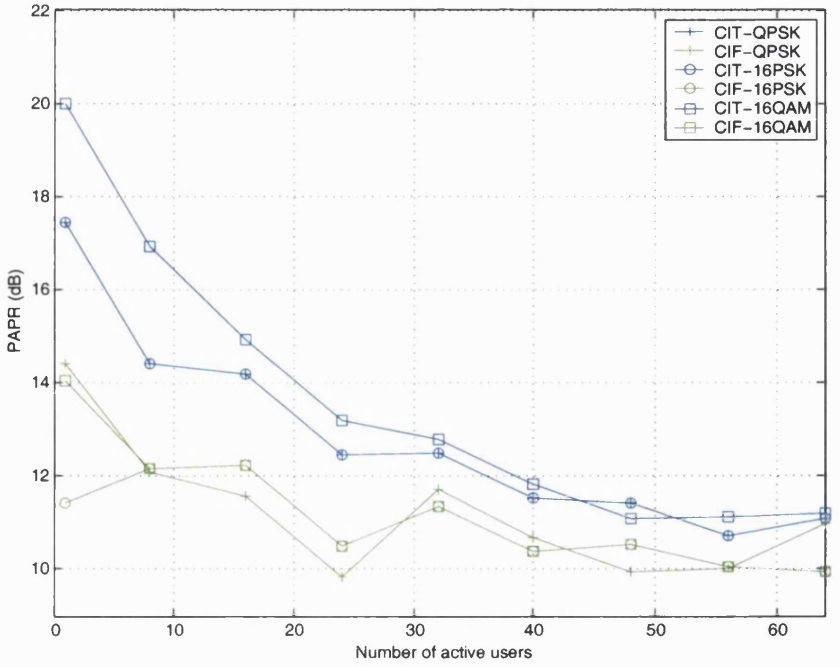

Figure 3.25: Comparison of the PAPR performance of MC-CDMA CIT and CIF

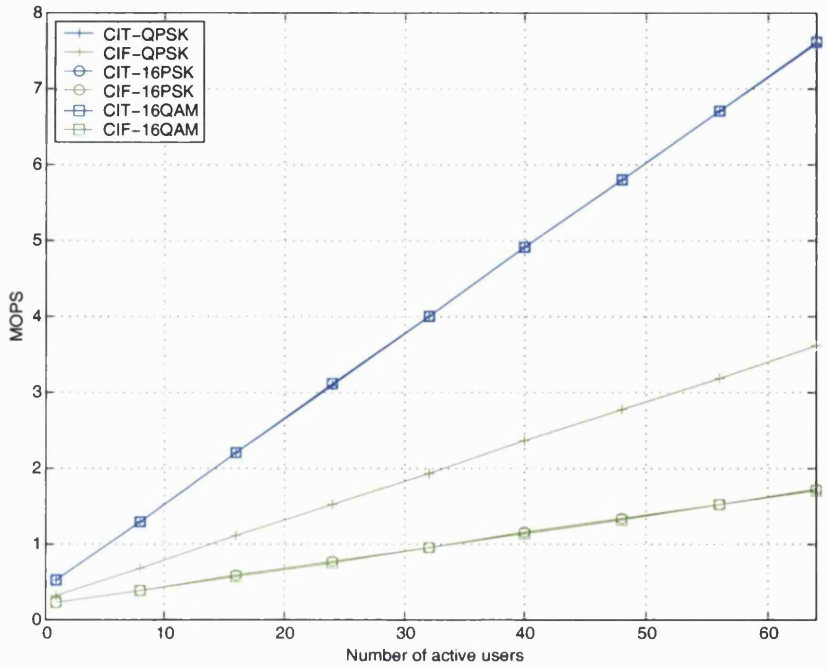

Figure 3.26: Comparison of the MOPS requirements for MC-CDMA CIT and CIF

3.5 Summary

This chapter investigated the combination of CDMA, MCM and higher order mapping. More specifically, it has investigated the combination of MC-CDMA with higher order PSK/QAM mapping. Two different implementations for incorporating higher order PSK/QAM mapping into MC-CDMA scheme were considered. In the first implementation, the mapping was performed at the input of the MC-CDMA transmitter (before signal spreading and multi-carrier modulation) and in the second implementation the mapping was performed after signal spreading, but before multi-carrier modulation. The first implementation was termed *combining in time* as increasing the order of the mapping scheme results in more data bits being transmitted over a given timeslot and the second implementation was termed *combining in frequency*.

The chapter was divided into five sections. Section 3.1 presented the two different implementations considered. The system models for both implementations were described together with system features and key parameters. Section 3.2 detailed the performance parameters used to judge the effectiveness of the two implementations (namely, power efficiency, PAPR, spectral efficiency and implementation complexity). As the power efficiency is measured in the presence of AWGN, an overview of AWGN was provided in Section 3.3. Section 3.4 presented the performance of CIT and CIF for different mapping schemes (2PSK, 4PSK, 16PSK and 16QAM) in terms of the performance parameters described in Section 3.2. The section also included a discussion on the relative merits and demerits of the two implementations with different mapping schemes.

Investigation of the performance of CIT with different mapping schemes showed that increasing the order of mapping scheme from BPSK to 4PSK/16PSK/16QAM resulted in an improvement in the spectral efficiency. However, it also resulted in a degradation in BER performance of the system (in AWGN) and some degradation in the PAPR (However, this is only significant for a small number of active users). The implementation complexity remained unchanged for all mapping schemes.

Investigation of the performance of CIF with different mapping schemes revealed that increasing the order of mapping from BPSK to 4PSK/16PSK/16QAM resulted in an improvement in spectral efficiency and implementation complexity. However, it also resulted in significant degradation of the BER performance. The PAPR remained unchanged for all mapping schemes.

Overall, for a given mapping scheme, CIT has shown to provide better BER performance as compared to CIF but CIF provided a significant reduction in implementation complexity (especially when the constellation size is large) and some reduction in the PAPR. The spectral efficiency of both schemes was the same. Further investigation is required to develop a receiver structure for CIF to allow for successful multiuser reception.

The next chapter investigates the performance of MC-DS-CDMA incorporating higher order PSK/QAM formats.

Chapter 4

MC-DS-CDMA exploiting higher order PSK/QAM formats

Chapter 3 investigated the performance of MC-CDMA incorporating different higher order PSK/QAM mapping schemes. Two different techniques for combining MC-CDMA with PSK/QAM mapping were considered (namely, CIT and CIF) and their performance was analysed in terms of power efficiency, PAPR, spectral efficiency and implementation complexity.

This chapter investigates the performance of the second multi-carrier CDMA scheme, MC-DS-CDMA, incorporating higher order PSK/QAM mapping. As in the case of MC-CDMA, different implementations for combining higher order PSK/QAM mapping with MC-DS-CDMA have been considered and their performance is analysed in terms of power efficiency, PAPR, spectral efficiency and implementation complexity.

The chapter starts by presenting the MC-DS-CDMA transmitter model and the different architectures considered for combining PSK/QAM mapping with MC-DS-CDMA. The following section describes the performance of the architectures for different PSK/QAM schemes and discusses the results for the different cases. The chapter concludes with a summary.

4.1 MC-DS-CDMA incorporating higher order mapping

This section describes the architectures considered for combining MC-DS-CDMA with higher order PSK/QAM mapping. As in the MC-CDMA case, the implementations have been categorised in terms of *combining in time* (CIT) and *combining in frequency* (CIF). In this case, two different implementations have been considered for CIT. The first CIT implementation is similar to the CIT implementation proposed for MC-CDMA, where the input is combined serially

before being spread and multi-carrier modulated. The second CIT implementation is a variant of the first in which the input data is combined in parallel before being spread and multi-carrier modulated. In order to distinguish between the two CIT implementations, the first implementation is referred to as CIT-serial combination (CIT-SC) and the second implementation is referred to as CIT- parallel combination (CIT-PC). The channel is once again assumed to be a synchronous downlink channel.

The MC-DS-CDMA scheme considered here is similar to the scheme described in Section 2.3.1.2 (Figure 4.1).

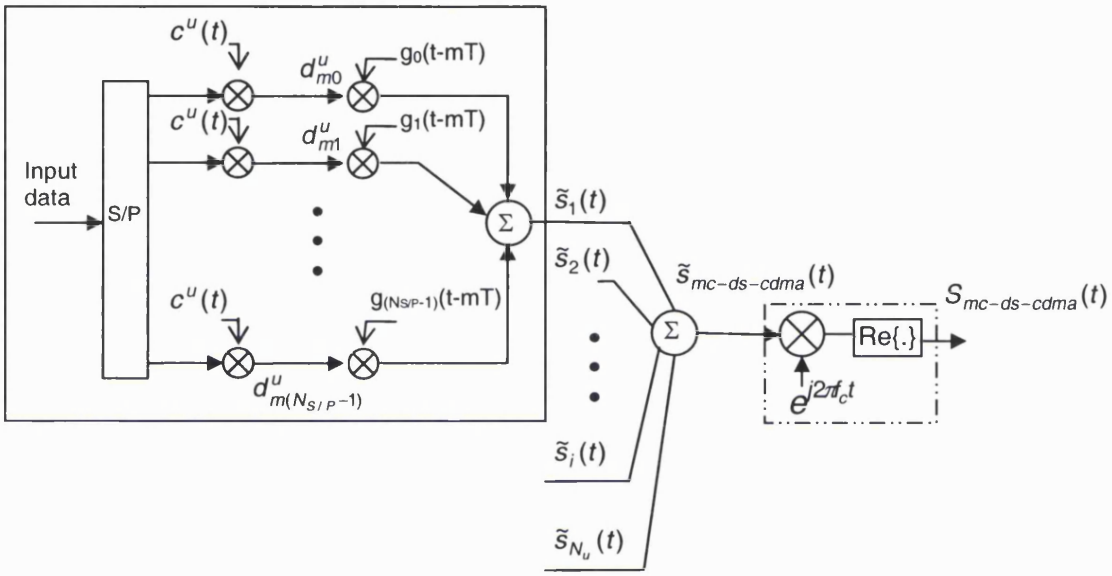

Figure 4.1: MC-DS-CDMA transmitter

At the input of the MC-DS-CDMA transmitter (Figure 4.1), the user data is first converted into parallel format using the S/P converter. The output of the S/P converter is spread by multiplying each stream by the same copy of the user specific spreading code, $c^u(t)$. The parallel streams of spread data are then modulated onto a set of orthogonal subcarriers, $g_n(t)$ and summed together. The output of the individual users is added synchronously and the signal is up-converted before transmission. Note that a separate block for cyclic prefix insertion has not been included in the diagram as this is accounted for in the definition of $g_n(t)$ (Equation 4.3).

As each parallel stream of spread data is modulated onto a different subcarrier, the number of subcarriers is equal to the length of the S/P converter ($N_{S/P}$). The length of the S/P converter can be set to be equal to, less than or greater that the length of the spreading code (N_{code}). In this work, $N_{S/P}$ has been set to be equal to N_{code} (as in the MC-CDMA case).

The MC-DS-CDMA signal at the output of the transmitter, $S_{mc\text{-}ds\text{-}cdma}(t)$ is given by:

$$S_{mc-ds-cdma}(t) = \mathrm{Re}\left\{\tilde{s}_{mc-ds-cdma}(t)e^{j2\pi f_c t}\right\} \tag{4.1}$$

where $\tilde{s}_{mc-ds-cdma}(t)$ is the equivalent baseband representation of $S_{mc-ds-cdma}(t)$ (given by Equation 4.2) and f_c is the frequency of the first subcarrier.

$$\tilde{s}_{mc-ds-cdma}(t) = \sum_{u=1}^{N_u} \tilde{s}_u(t)$$
$$\tilde{s}_u(t) = \sum_{m=-\infty}^{\infty} \sum_{n=0}^{N_{S/P}-1} d_{mn}^u g_n(t - mT) \tag{4.2}$$

In the above definition, d_{mn}^u is the data for user u to be transmitted in timeslot m and subchannel n and $g_n(t)$ is the n^{th} subcarrier given by:

$$g_n(t) = \begin{cases} e^{\frac{j2\pi n(t-T_{cp})}{T-T_{cp}}} & t \in [0,T] \\ 0 & t \notin [0,T] \end{cases} \tag{4.3}$$

where T is the duration of the MC-DS-CDMA symbol, n is the subcarrier number and T_{cp} is the duration of the cyclic prefix.

As discussed in Chapter 3, in this work the multi-carrier modulation and demodulation is performed using an IFFT in order to reduce simulation time and complexity.

System features:

Symbol mapping

In the MC-DS-CDMA implementations described in the following subsections (4.1.1.1, 4.1.1.2 and 4.1.2), the data is combined in time (or frequency) and mapped onto higher order M-PSK/M-QAM constellation points[35]. The data is first grouped into binary words of length k and then mapped onto an M-PSK/M-QAM constellation point as described in Section 3.1.

Spreading

The WH codes have been used for user separation and spreading. WH codes are commonly used in MC-DS-CDMA systems. As described in Section 3.1, the length of the WH codes is equal to the maximum number of codes in the system. As each user requires a unique code, the maximum number of codes required is equal to the maximum number of users in the system. In this investigation, the maximum number of users (and hence the length of the code) is set to 64 in order to facilitate future comparison with the MC-CDMA system described in Chapter 3.

Multi-carrier modulation

In the MC-DS-CDMA case, the number of subcarriers is equal to the length of the S/P converter ($N_{S/P}$). The bandwidth of each modulated subcarrier is dependent on N_{code}, $N_{S/P}$ and

[35] Higher order mapping is defined as M-PSK/M-QAM schemes with M>2.

T_b (as shown in Section 2.3.1.2). In this investigation, $N_{S/P}$ is set to be equal to N_{code} and therefore the bandwidth of the individual modulated subcarriers is equal to the bandwidth of the signal at the input of the MC-DS-CDMA transmitter.

The spectrum of the MC-DS-CDMA signal at the output of the transmitter is shown in Figure 4.2 [36].

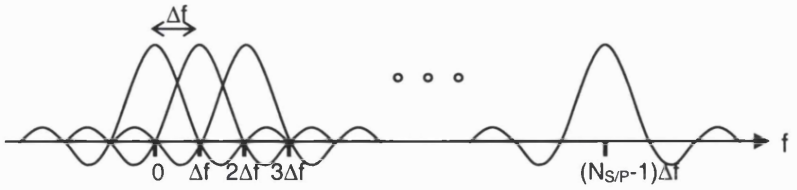

Figure 4.2: Spectrum of MC-DS-CDMA signal

As in the MC-CDMA case, the subcarrier separation, Δf is set equal to $1/(T-T_{cp})$ in order to obtain maximum spectral overlap.

The bandwidth of the MC-DS-CDMA signal at the output of the transmitter is approximately equal to $N_{S/P}\Delta f$.

Cyclic prefix insertion

The cyclic prefix insertion is performed in the same way as in the MC-CDMA case. The duration of the cyclic prefix is set equal to a $1/5^{th}$ of the symbol duration.

Table 4.1 lists the main parameters of the MC-DS-CDMA system together with the values used for the different implementations.

The following subsections describe the different implementations considered for incorporating PSK/QAM mapping in the MC-DS-CDMA scheme.

4.1.1 Implementation-1: Combining in time

In the MC-DS-CDMA system, there are two ways in which the input data can be combined and mapped onto PSK/QAM symbols before being spread and multi-carrier modulated. The first scheme is similar to the MC-CDMA CIT implementation in which the input data is combined into groups of k bits (in serial format) and mapped onto a PSK/QAM symbol before being spread and multi-carrier modulated. The second scheme is a variant of the first in which the input data is converted into parallel format (by an S/P converter) before being grouped into k bits and mapped onto a PSK/QAM symbol. As stated above, the first implementation is referred to as CIT-SC and the second implementation referred to as CIT-PC.

[36] As mentioned in the previous chapter, in Figure 4.2, the spectrum of each modulated subcarrier has a null at the centre frequency of each of the other modulated subcarriers in the system. However, in a typical system, the insertion of the CP will increase the subcarrier separation as discussed in Section 2.2.1.

For a given input data rate, the required transmission bandwidth is the same in both cases. However, in the case of CIT-SC, increasing the order of PSK/QAM mapping results in an increase in the number of data bits transmitted over a given symbol duration whereas in the case of CIT-PC, increasing the order of mapping results in an increase in the number of data bits transmitted over a given subcarrier[37].

4.1.1.1 Implementation 1a: Combining in time - serial combination

In this implementation, higher order mapping and demapping is effected outside the MC-DS-CDMA modulation and demodulation.

Figure 4.3 shows the equivalent baseband, IFFT based transmitter for MC-DS-CDMA CIT-SC. At the input of the transmitter, the user data is first mapped onto a constellation point by the PSK/QAM mapper. The output of the mapper is S/P converted and each parallel stream is multiplied by the same copy of the user specific spreading code. The spread data is multi-carrier modulated using the IFFT. The output of the IFFT is P/S converted and the cyclic prefix is added to each symbol. The signal is converted into analogue format before transmission.

With no loss of generality, the transmitted signal at the output of CIT-SC transmitter is given by:

$$\tilde{s}_{mc-ds-cdma}(t) = \sum_{u=1}^{N_u} \sum_{m=-\infty}^{\infty} \sum_{n=0}^{N_{S/P}-1} D_{mn}^{u} g_n(t - mT) \tag{4.4}$$

where D_{mn}^{u} is the transmitted symbol for user u, in timeslot m and subchannel n, and $g_n(t)$ is the n^{th} subcarrier as described in Equation 4.3.

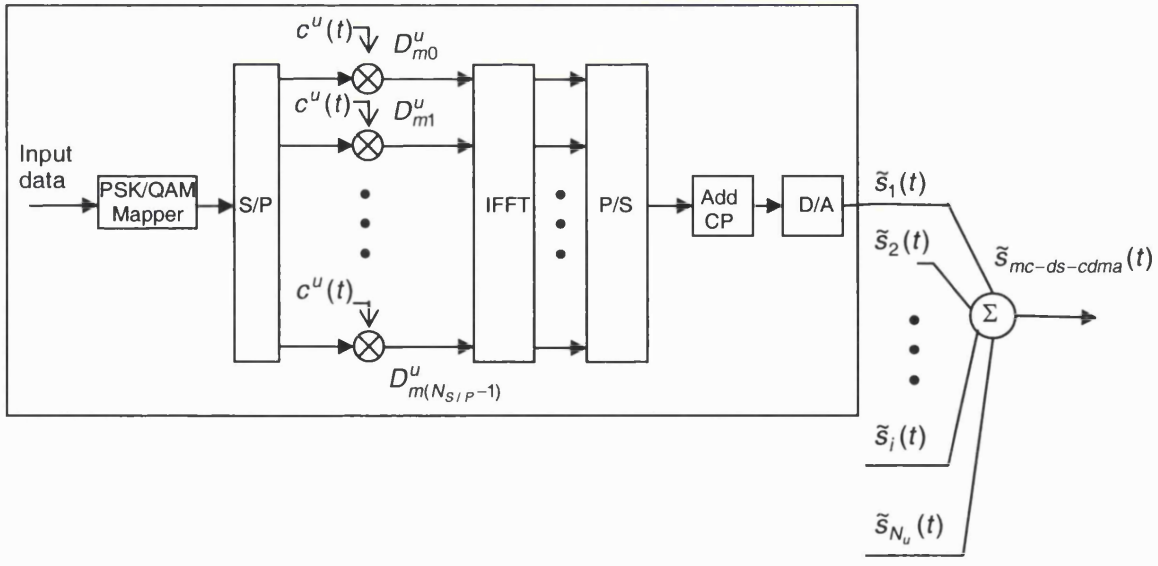

Figure 4.3: MC-DS-CDMA implementation-1a (CIT-SC): Transmitter

[37] It is important to point out that the CIF architecture also combines the data so that increasing the order of mapping results in an increase in the amount of information transmitted over a given subcarrier. However, in the case of CIF, the combination and mapping is done at chip level whereas in the case of CIT-PC, the combination is done at bit level.

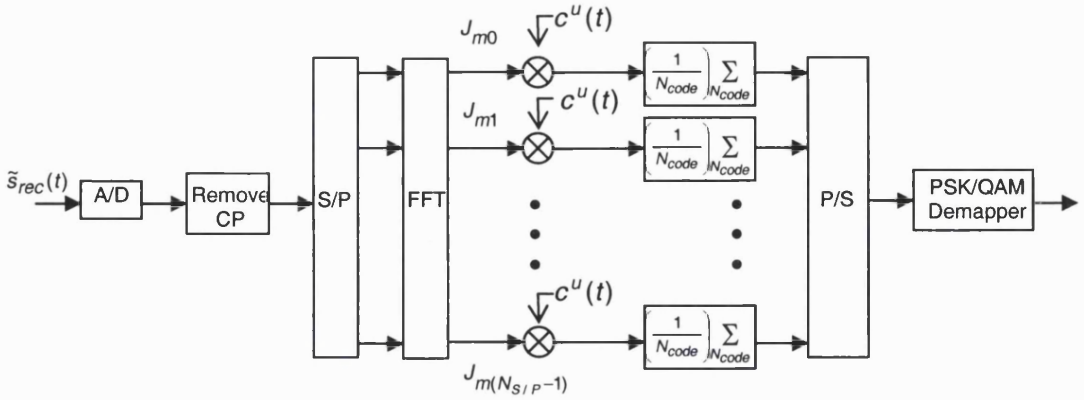

Figure 4.4: MC-DS-CDMA implementation-1a (CIT-SC): Receiver

The equivalent baseband receiver model for CIT-SC is presented in Figure 4.4. The receiver performs the inverse processes of the transmitter to demodulate the received signal. At the input of the receiver, the equivalent baseband representation of the received signal is first converted into digital format by the A/D converter. The cyclic prefix is then removed from each symbol and the signal is demodulated by an FFT. The parallel output of the FFT is despread by multiplying each stream by a locally generated copy of the spreading code ($c^u(t)$) and averaging over the length of the code. The despread data is P/S converted and demapped by the PSK/QAM demapper.

4.1.1.2 Implementation-1b: Combining in time – parallel combination

In this implementation, the higher order mapping is effected after the S/P conversion (Figure 4.5). One of the advantages of this implementation over the CIT-SC implementation is that in this case different mapping schemes can be employed for different subcarriers. Another advantage is that the higher order mapping is performed at a lower data rate.

Figure 4.5 shows the transmitter diagram for CIT-PC. In this implementation, increasing the order of mapping results in an increase in the number of parallel bits transmitted over a particular subcarrier. As the size of the S/P converter is kept constant, increasing the order of the mapping scheme results in a reduction in the number of subcarriers. The user data at the input of the transmitter is first S/P converted. The output of the S/P converter is then combined (in parallel) into groups of k bits and mapped onto constellation points using the PSK/QAM mapper. The output of the mapper is spread (by $c^u(t)$) and modulated onto a set of orthogonal subcarriers.

The continuous time signal at the output of the transmitter is:

$$\tilde{s}_{mc-ds-cdma}(t) = \sum_{u=1}^{N_u} \sum_{m=-\infty}^{\infty} \sum_{x=0}^{X-1} D_{mx}^{u} g_x(t - mT) \tag{4.5}$$

where, D_{mx}^{u} is the transmitted symbol for user u, in time slot m to be transmitted over subcarrier x and $g_x(t)$ is the x^{th} orthogonal subcarrier given by:

$$g_x(t) = \begin{cases} e^{\frac{j2\pi x(t-T_{cp})}{T-T_{cp}}} & t \in [0,T] \\ 0 & t \notin [0,T] \end{cases} \tag{4.6}$$

In this implementation, the value of X (the maximum number of subcarriers) is dependent on the order of the PSK/QAM mapping scheme (size of the constellation, M). More specifically:

$$X = \frac{N_{S/P}}{k} = \frac{N_{S/P}}{\log_2 M} \tag{4.7}$$

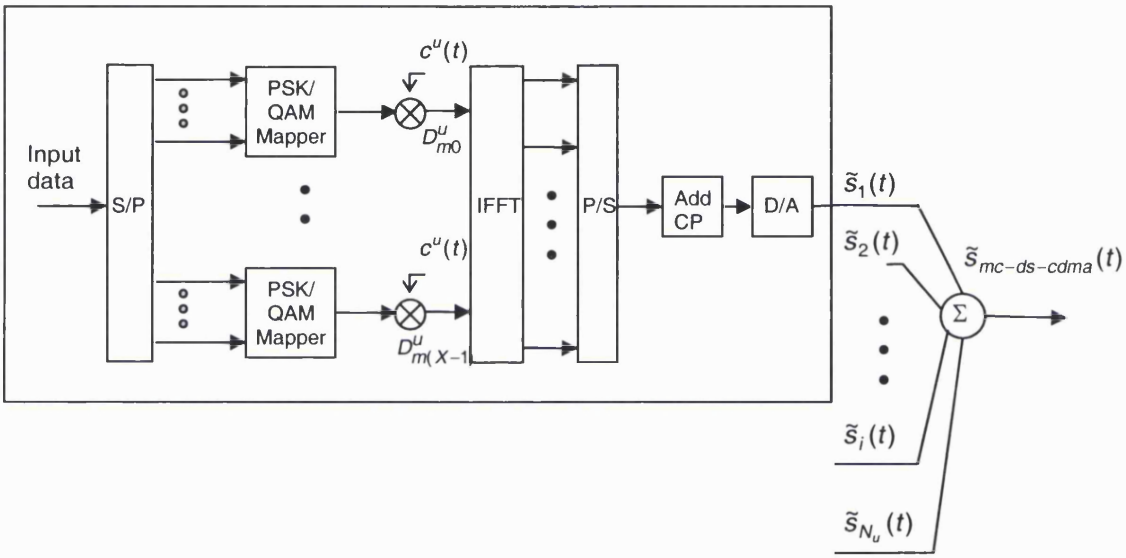

Figure 4.5: MC-DS-CDMA implementation-1b (CIT-PC): Transmitter

At the receiver (Figure 4.6), the A/D converted signal is first demodulated using the FFT. The output of the FFT is then despread and demapped to recover the transmitted data.

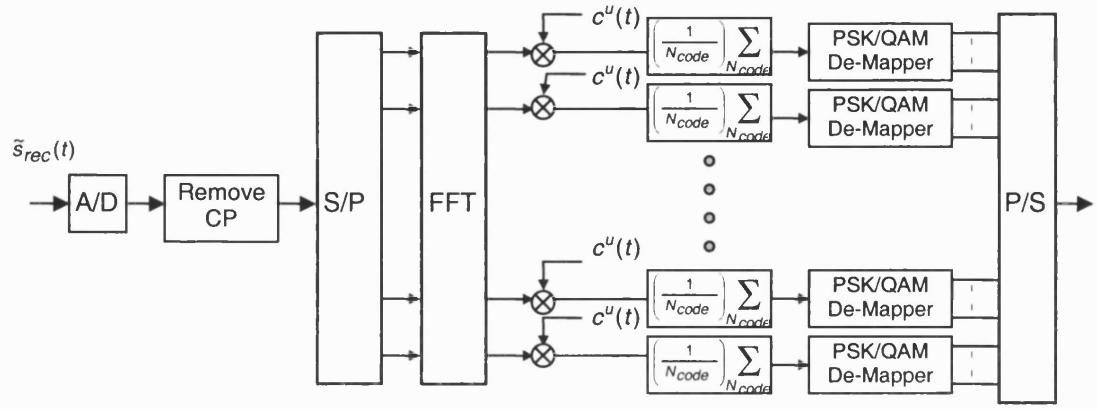

Figure 4.6: MC-DS-CDMA implementation-1b (CIT-PC): Receiver

4.1.2 Implementation-2: Combining in frequency

This implementation is similar to MC-CDMA CIF implementation (described in Section 3.1.2) in which the higher order mapping is effected after spreading. This scheme is referred to as combining in frequency as increasing the order of the mapping scheme results in an increase in the number of parallel chips transmitted over a given subcarrier[38]. As the size of the S/P converter at the input of the transmitter (Figure 4.7) is kept constant, increasing the order of the mapping scheme results in a reduction in the number of subcarriers. In this implementation, the data rate and the symbol rate are independent of the mapping scheme.

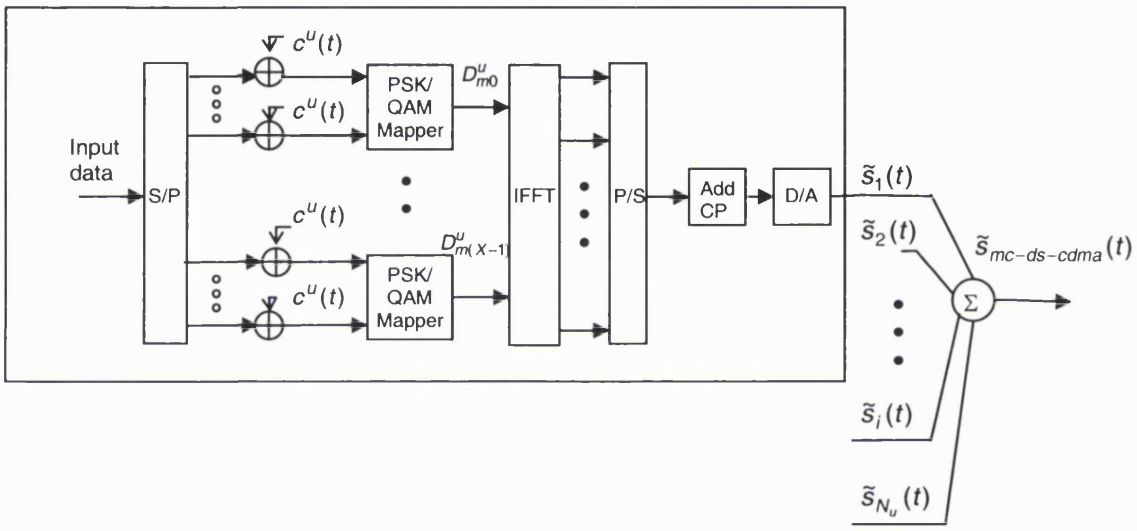

Figure 4.7: MC-DS-CDMA implementation-2 (CIF): Transmitter

Figure 4.7 shows the transmitter diagram for MC-DS-CDMA CIF. The input data is first S/P converted and spread by $c^u(t)$ (the user specific spreading code). The spread data is then combined (in parallel) into groups of k chips (where $k=\log_2 M$) and mapped onto a constellation point by the PSK/QAM mapper. The output from the mapper is multi-carrier modulated using the IFFT and the cyclic prefix is added to each symbol before transmission.

Note that in this implementation, the spreading operation is performed by modulo 2 addition and not multiplication as the input data is in the form of [0 1] and not [-1 1].

The signal at the output of the transmitter for MC-DS-CDMA CIF is given by:

$$\tilde{s}_{mc-ds-cdma}(t) = \sum_{u=1}^{N_u} \sum_{m=-\infty}^{\infty} \sum_{x=0}^{X-1} D^u_{mx} g_x(t - mT) \tag{4.8}$$

[38] Note that the CIT-PS scheme described in section 4.1.1.2 also results in an increase in the parallel data transmitted over a given subcarrier. However, as it is a variant of the CIT implementation (i.e., combining data at bit level rather than chip level) it is referred to as a CIT implementation rather than a CIF implementation.

where D_{mx}^{u} is the transmitted symbol and $g_x(t)$ is the x^{th} orthogonal subcarrier as defined in Equation 4.6.

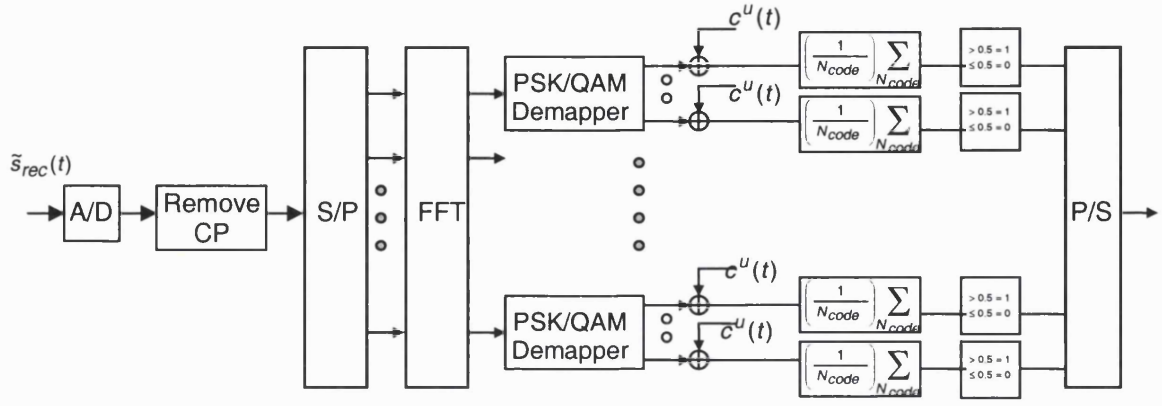

Figure 4.8: MC-DS-CDMA implementation-2 (CIF): Receiver

At the receiver (Figure 4.8), the received signal is first converted into digital format, as in the CIT implementations. The cyclic prefix is then removed from the beginning of each symbol. The data is converted into parallel format and demodulated using the FFT. The data at the output of the FFT is demapped, despread and converted back to serial format by the P/S converter.

As in the case of MC-CDMA CIF (Section 3.1.2), the simple receiver model shown in Figure 4.8 performs hard decision demapping before despreading and hence can only successfully demodulate data for the single user case. (This has been discussed for MC-CDMA in Appendix A. As the arguments for MC-DS-CDMA are similar, analysis for MC-DS-CDMA CIF has not been included in this thesis.) It is not suitable for detection in a multiuser environment and soft decision demodulation schemes should be employed to allow for successful multiuser demodulation.

The key parameters used for the three implementations are summarised in Table. 4.1. Note that in this work, the MC-DS-CDMA receiver with frequency domain processing has been employed. The choice of parameters will differ if the MC-DS-CDMA receiver with time domain processing is employed (as discussed in section 2.3.2.2).

As in the case of MC-CDMA, the investigations are carried out for the same symbol duration/symbol rate. From the table, it can be observed that the key difference between the parameters of CIT-SC, CIT-PC and CIF are the number of subcarriers and the data rate.

Table 4.1: System parameters

Parameter	CIT-SC	CIT-PC	CIF
Number of Users, N_{users}	64	64	64
Length of spreading code, N_{code}	N_{users} (64)	N_{users} (64)	N_{users} (64)
Length of the S/P Converter, $N_{S/P}$	N_{code} (64)	N_{code} (64)	N_{code} (64)
Number of subcarriers, $N_{subcarriers}$	$N_{S/P}$ (64)	$N_{S/P}/\log_2(M)$	$N_{S/P}/\log_2(M)$
Subcarrier spacing, Δf	$1/(T-T_{cp})$	$1/(T-T_{cp})$	$1/(T-T_{cp})$
Symbol duration, T	1 μs	1 μs	1 μs
Cyclic prefix duration, T_{cp}	0.2 μs	0.2 μs	0.2 μs
Spreading Code	WH Code	WH Code	WH Code
Mapping Scheme	2/4/16PSK 16QAM	2/4/16PSK 16QAM	2/4/16PSK 16QAM
FFT size, N_{FFT}	$10*N_{subcarriers}$	$10*N_{subcarriers}$	$10*N_{subcarriers}$
Input sequence	m-sequence	m-sequence	m-sequence
Data rate	$(\log_2(M))/(T-T_{cp})$	$1/(T-T_{cp})$	$1/(T-T_{cp})$
Simulation duration	10000 symbols	10000 symbols	10000 symbols

4.2 System performance

This section presents the performance of CIT-SC, CIT-PC and CIF with 2/4/16PSK and 16QAM mapping. The performance of the different mapping schemes is compared in terms of BER degradation, PAPR variation, spectral efficiency and MOPS requirements (A description of these parameters is presented in Section 3.2 and hence is not repeated here).

4.2.1 Performance of implementation-1a (CIT-SC)

The duration of the MC-DS-CDMA symbol at the output of the transmitter is set to be constant for all mapping schemes. The length of the S/P converter ($N_{S/P}$) is also constant for all mapping schemes. As the number of subcarriers is equal to the length of the S/P converter, the bandwidth of the transmitted signal is constant for all mapping schemes. Hence, in this implementation increasing the order of the mapping scheme results in an increase in the number of data bits transmitted over a given MC-DS-CDMA symbol. Figure 4.9 shows the BER performance of MC-DS-CDMA CIT-SC with various PSK/QAM mapping schemes in the presence of AWGN (for one active user). The figure also includes the theoretical BER performance of the different mapping schemes for a single carrier, single user system in AWGN. The BER performance of an MC-DS-CDMA signal is equal to the BER performance of a single carrier, single user system due to the fact that there is no multiuser interference (orthogonal WH

codes) and no inter-carrier interference (orthogonal subcarriers). Observation of Figure 4.9 shows that the simulation results agree well with the theoretical results. Increasing the constellation size results in degradation in the BER performance. Hence, in this implementation, increasing the order of mapping will increasing the throughput of the system but it will also result in an increase in the BER degradation.

The variation in the PAPR of CIT-SC with different mapping schemes is shown in Figure 4.10. The PAPR was calculated using the expression given in Equation 3.20 and is plotted as a function of the number of active users. Observation of the figure shows that increasing the order of mapping scheme has no significant effect on the PAPR for the different users. Hence in this implementation, increasing the throughput by increasing the size of the constellation has no significant implications for the PAPR of the transmitted signal.

Figure 4.11 shows the MOPS requirements for CIT-SC with different PSK/QAM schemes[39]. From the figure, it can be observed that increasing the number of active users results in a linear increase in the MOPS requirements, as expected. Changing the mapping scheme has no effect on the MOPS requirement of the system.

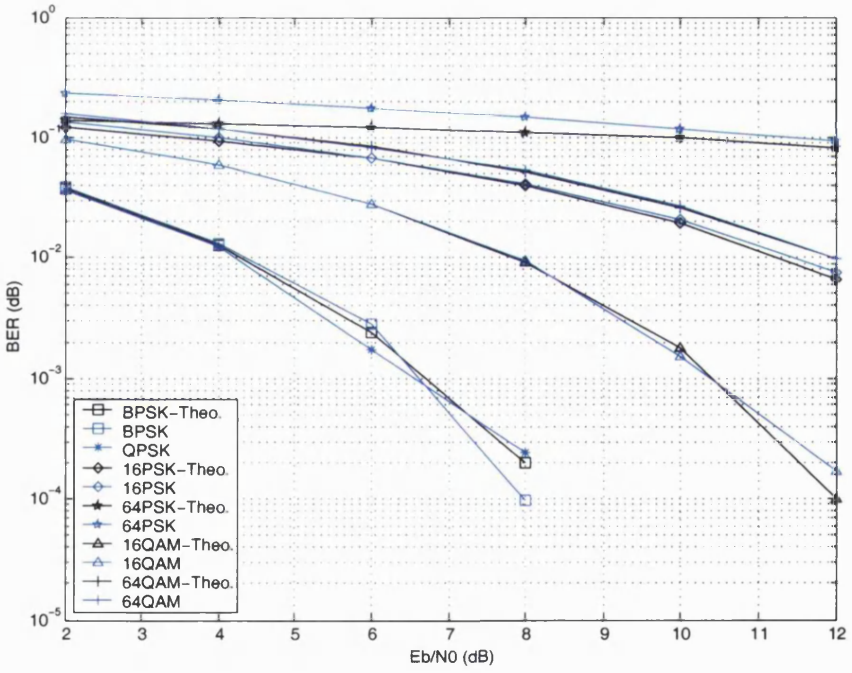

Figure 4.9: BER performance of MC-DS-CDMA CIT-SC in AWGN with 1 active user

[39] The MOPS value presented are the sum of the MOPS required for a transmitter with different number of active users and MOPS required for the receiver with 1 user.

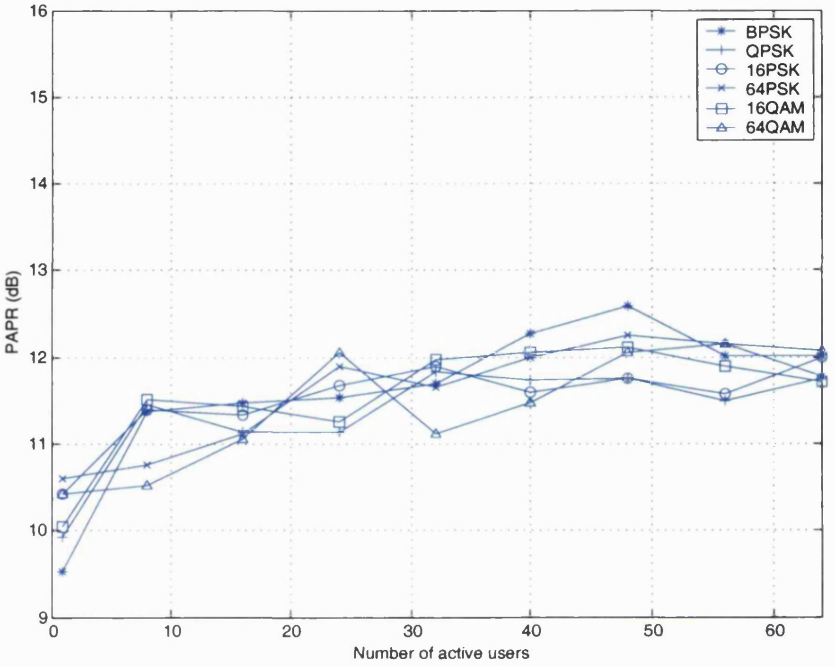

Figure 4.10: PAPR performance of MC-DS-CDMA CIT-SC

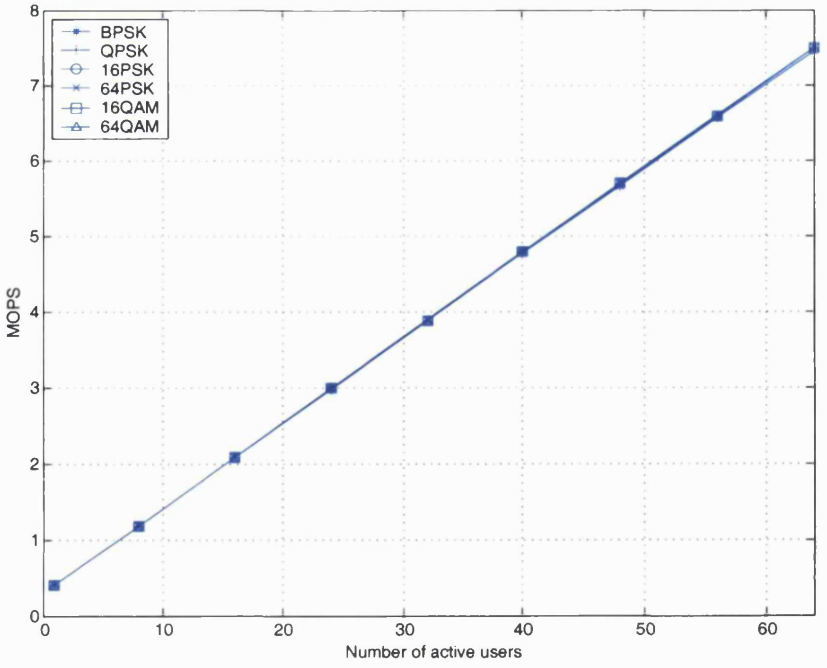

Figure 4.11: MOPS requirements for MC-DS-CDMA CIT-SC

The spectral efficiency, η is defined as:

$$\eta = \frac{r_b}{W} \tag{4.9}$$

where r_b is the input bit rate and W is the bandwidth of the transmitted signal.

In CIT-SC, the spectrum of the transmitted signal is similar to that shown in Figure 4.2. The bandwidth of the transmitted signal, W is approximately equal to $N_{S/P}\Delta f$ (where $\Delta f = 1/(T-T_{cp})$). The data rate (r_b) is k times the symbol rate (r_{symb}). Hence the spectral efficiency η is:

$$\eta = \frac{r_b}{W} = \frac{r_{symb} k}{N_{S/P}\Delta f}$$

$$r_{symb} = \frac{1}{T}$$

Therefore,

$$\eta = \frac{k}{T}\frac{(T - T_{cp})}{N_{S/P}} = \frac{k}{N_{S/P}}\left(1 - \frac{T_{cp}}{T}\right) \tag{4.10}$$

From Equation 4.10, it can be noted that the spectral efficiency of MC-DS-CDMA CIT-SC is dependent on the length of the S/P converter, the symbol duration, the CP duration and the constellation size of the mapping scheme. As the length of the S/P converter, the symbol duration and the CP duration are made constant for all mapping schemes, the spectral efficiency of CIT-SC increases with the size of the constellation (as expected).

4.2.2 Performance of implementation-1b (CIT-PC)

In this implementation, the input data rate and the transmitted MC-DS-CDMA symbol rate are independent of the mapping scheme. The symbol duration of the MC-DS-CDMA symbol at the output of the transmitter and the length of the S/P converter are made constant for all mapping schemes. Hence, increasing the order of the mapping results in a reduction in the bandwidth of the transmitted signal (due to reduction in the number of subcarriers).

The BER performance of CIT-PC with different PSK/QAM schemes (Figure 4.12) is comparable to the theoretical performance of the different mapping schemes for a single user, single carrier case (in AWGN). From Figure 4.12 it can be observed that QAM schemes perform better than PSK schemes, hence, reducing the number of subcarriers using QAM will result in lower BER degradation.

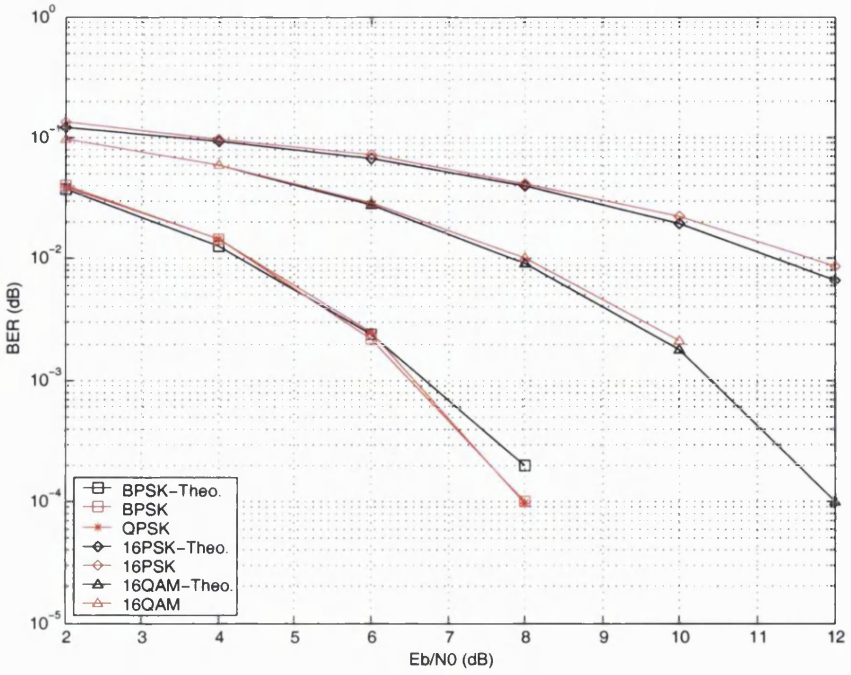

Figure 4.12: BER performance of MC-DS-CDMA CIT-PC in AWGN with 1 active user

Figure 4.13 shows the PAPR variation of CIT-PC. The variation in the PAPR of the different mapping schemes is not very significant. Hence, reducing the number of subcarriers by increasing the order of the mapping scheme has no major advantage in terms of PAPR reduction.

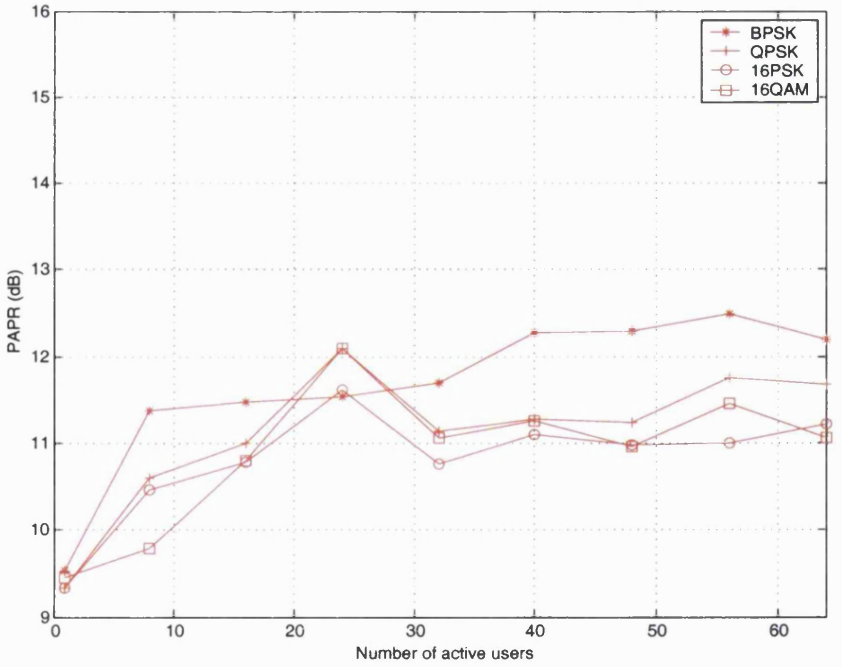

Figure 4.13: PAPR performance of MC-DS-CDMA CIT-PC

The MOPS requirements for CIT-PC reduce with the size of the constellation (Figure 4.14). Hence, in this implementation the processing requirement of the system can be reduced by increasing the size of the PSK/QAM constellation (Obviously, the reduction is more significant when the number of active users is large).

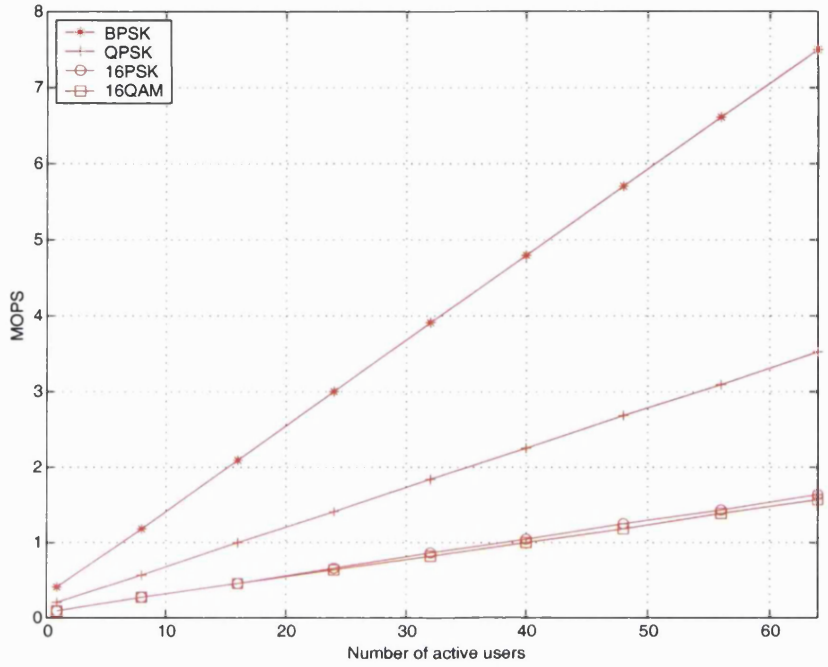

Figure 4.14: MOPS requirements for MC-DS-CDMA CIT-PC

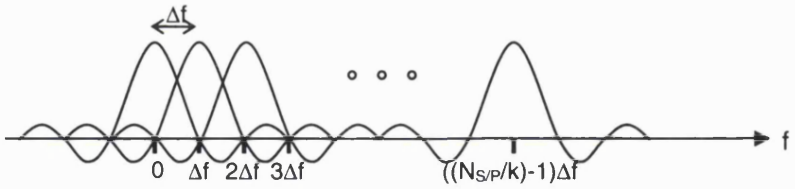

Figure 4.15: Spectrum of MC-DS-CDMA CIT-PC/CIF signal

The spectrum of the transmitted MC-DS-CDMA signal for CIT-PC is shown in Figure 4.15[40]. The total bandwidth of the transmitted signal is given by:

$$W = \frac{N_{S/P}}{k}\Delta f = \frac{N_{S/P}}{k}\frac{1}{(T - T_{cp})} \tag{4.11}$$

[40] In Figure 4.15, the spectrum of each modulated subcarrier has a null at the centre frequency of each of the other modulated subcarriers in the system. However, in a typical system, the insertion of the CP will increase the subcarrier separation as discussed in Section 2.2.1.

The data rate is equal to the symbol rate, hence

$$r_b = \frac{1}{T_b} = \frac{1}{T} \tag{4.12}$$

From Equation 4.11 and 4.12, the spectral efficiency, η of CIT-PC is:

$$\eta = \frac{r_b}{W} = \frac{1}{T}\frac{k(T - T_{cp})}{N_{S/P}} = \frac{k}{N_{S/P}}\left(1 - \frac{T_{cp}}{T}\right) \tag{4.13}$$

The spectral efficiency of CIT-PC is the same as that of CIT-SC and increases with the size of the PSK/QAM constellation.

4.2.3 Performance of implementation-2 (CIF)

As in the case of CIT-PC, the input data rate and the rate of the MC-DS-CDMA symbol at the output of the CIF transmitter are independent of the mapping scheme. Increasing the order of the mapping scheme results in a decrease in the number of subcarriers as the length of the S/P converter is made constant for all mapping schemes. The duration of the MC-DS-CDMA symbol is also set to be constant for all mapping schemes, hence, increasing the order of the mapping reduces the bandwidth of the transmitted signal (due to a reduction in the number of subcarriers).

The BER performance of CIF for different PSK/QAM schemes is shown in Figure 4.16 together with the theoretical performance for a single user, single carrier case. From the figure it can be observed that the BER performance of this implementation is much worse than theoretical. This is due to the simple receiver model adapted for this investigation. As in the case of MC-CDMA CIF, the receiver performs HDD before despreading, which results in demodulation errors. This has been verified for MC-CDMA in Appendix-C by considering two simple cases (one with HDD in the receiver and one without HDD in the receiver). The use of soft demodulation will allow for improved BER performance.

Figure 4.17 shows the PAPR variation of CIF for different number of active users with different mapping schemes. Observation of the figure shows that the PAPR for large number of active users is approximately 1 dB higher than that for small number of active users. Overall, there is not a significant difference between the PAPR of the different mapping schemes and hence it can be concluded that, contrary to expectation, reducing the number of subcarriers by increasing the size of the constellation has no benefits in terms of PAPR.

The MOPS requirements of CIF for different mapping schemes is shown in Figure 4.18. The figure shows that reducing the number of subcarriers by increasing the size of the constellation results in a reduction in the MOPS requirements. This is due to the fact that reducing the number of subcarriers results in a reduction in the size of the IFFT and FFT.

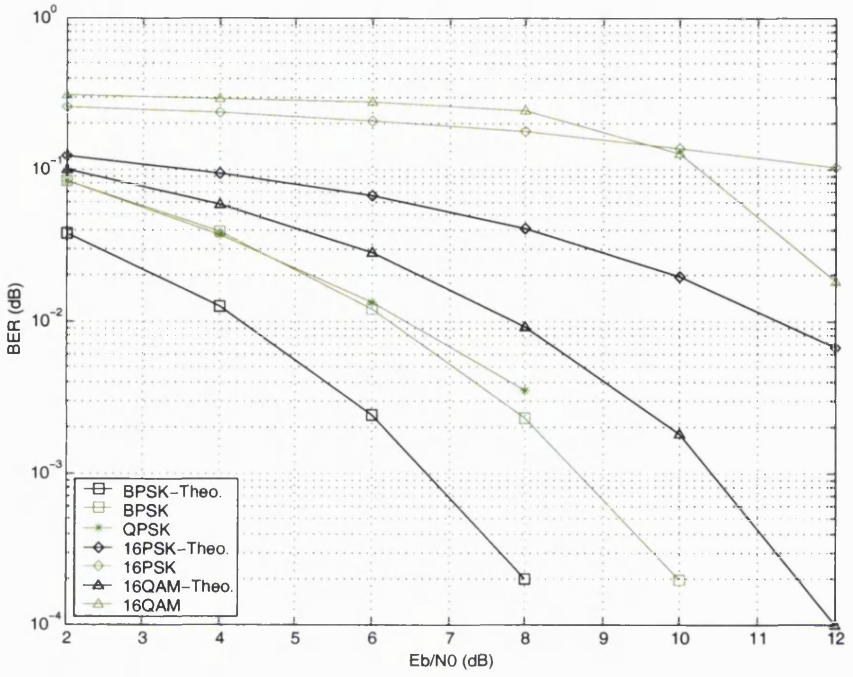

Figure 4.16: BER performance of MC-DS-CDMA CIF in AWGN with 1 active user

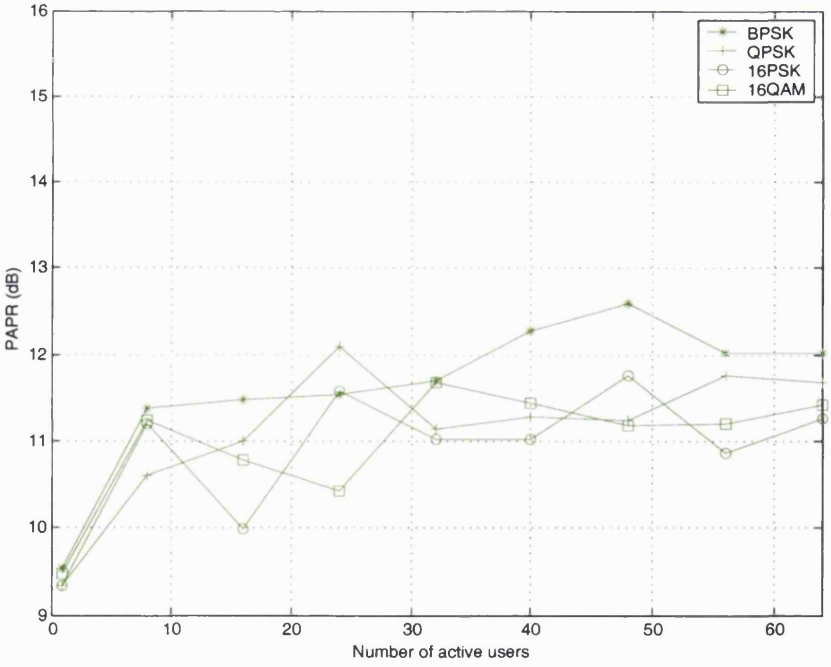

Figure 4.17: PAPR performance of MC-DS-CDMA CIF

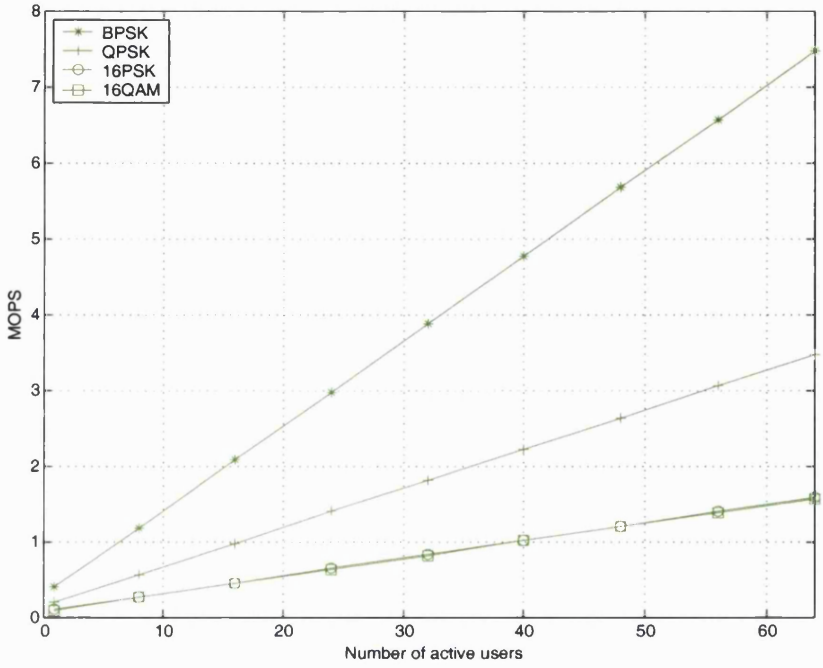

Figure 4.18: MOPS requirements for MC-DS-CDMA CIF

The spectrum of the MC-DS-CDMA signal at the output of the transmitter in Figure 4.7 is similar to that of CIT-PC (shown in Figure 4.15). The bandwidth of the signal, W is approximately $N_{S/P}\Delta f/k$. The data rate is the same as the symbol rate (1/T). Therefore, the spectral efficiency, η is given by:

$$\eta = \frac{r_b}{W} = \frac{r_{symb}}{(N_{S/P}\Delta f)/k} = \frac{1}{T}\frac{(T - T_{cp})k}{N_{S/P}} = \frac{k}{N_{S/P}}\left(1 - \frac{T_{cp}}{T}\right) \tag{4.14}$$

Equation 4.14 shows that as in the case of CIT-SC and CIT-PC, the spectral efficiency of CIF increases with k.

4.2.4 Discussion of MC-DS-CDMA CIT and CIF systems performance

The previous subsections presented the performance of the three MC-DS-CDMA implementations with different PSK/QAM mapping schemes. In all three cases, increasing the order of the mapping results in an increase in the bandwidth efficiency of the system. In the case of CIT-SC, this increase is achieved by increasing the amount of data transmitted over a given symbol. In the case of CIT-PC and CIF, this increase in bandwidth efficiency is achieved by reducing the number of subcarriers with M (whilst keeping the data transmitted over a given MC-DS-CDMA symbol constant). This is illustrated in Figure 4.19.

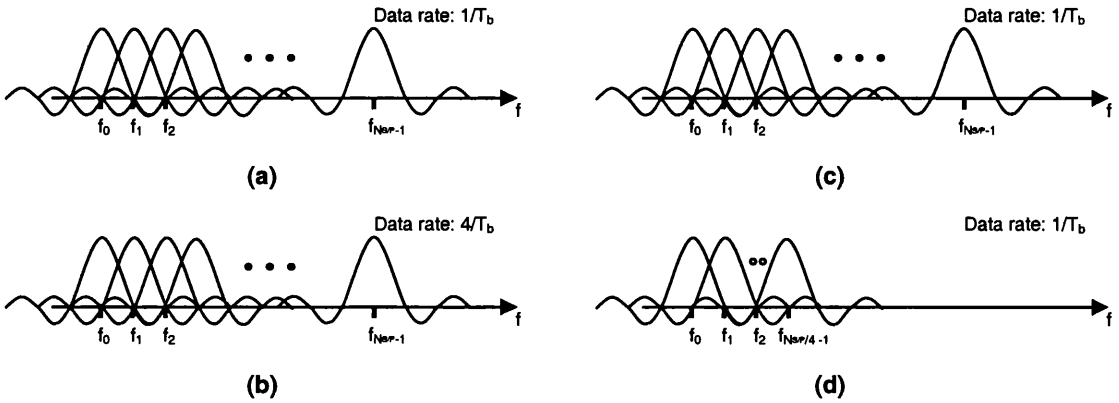

Figure 4.19: Spectrum of the transmitted MC-DS-CDMA signal: (a) CIT-SC with BPSK mapping; (b) CIT-SC with 16PSK mapping; (c) CIT-PC/CIF with BPSK mapping; (d) CIT-PC/CIF with 16PSK mapping

In this investigation, the length of the S/P converter at the input of the transmitter is made constant for all mapping schemes (equal to the length of the spreading code), however, it can be altered in step with the order of mapping schemes. For example, in the case of CIT-SC, the length of the S/P converter can be made equal to $N_{S/P}/k$ so that for all mapping schemes, the symbol rate and the data rate are the same. Increasing the order of mapping will then result in a decrease in the number of subcarriers and hence a decrease in the bandwidth of the transmitted signal. In the case of CIT-PC and CIF, the length of the S/P converter can be made equal to $kN_{S/P}$ so that the number of subcarrier for all mapping schemes stays the same. In this case, increasing the order of mapping scheme will result in an increase in the data bits transmitted over a given symbol duration.

In this investigation, the comparison between the different mapping schemes has been carried out by making the MC-DS-CDMA symbol duration constant for all mapping schemes. An alternate approach is to make the input data rate constant. In the case of CIT-SC, making the input data rate constant would result in a reduction in the transmitted signal bandwidth with the order of mapping (due to the fact that the MC-DS-CDMA symbol duration will increase with the order of mapping). In the case of CIT-PC and CIF, the input data rate and the transmitted symbol rate are independent of the mapping scheme and hence in these cases, a performance comparison in terms constant data rate will be identical to the performance comparison with constant symbol rate. Comparing the three implementations for the same input data rate would result in the same transmitted signal bandwidth (and hence the same bandwidth efficiency) for all three cases. This is illustrated in Figure 4.20. As the order of mapping increases, the bandwidth of the transmitted signal decreases in all three cases. In the case of CIT-SC, this decrease is due to an increase in the MC-DS-CDMA symbol duration (Figure 4.20(a) and 4.20(b)) whereas in the case of CIT-PC and CIF, this decrease is due to a decrease in the number of subcarriers (Figure 4.20(c) and 4.20(d)).

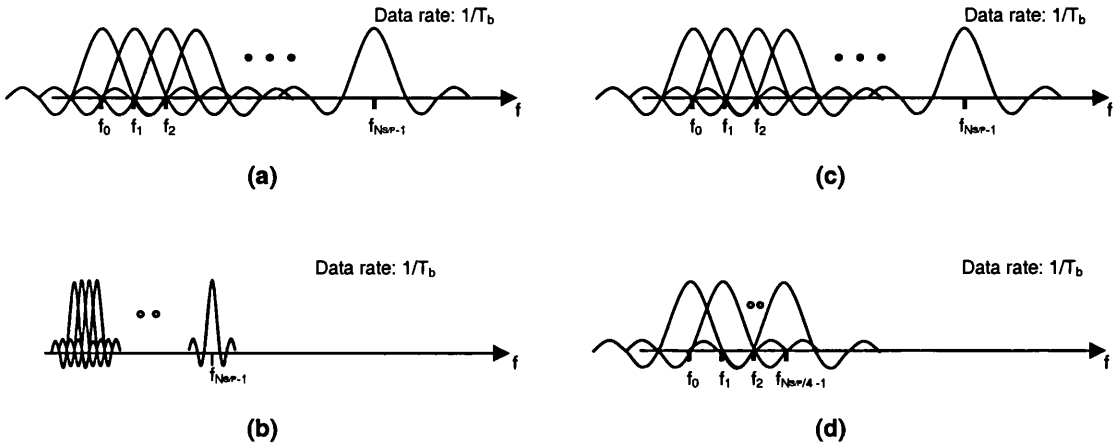

Figure 4.20: Spectrum of the transmitted MC-DS-CDMA signal (with constant Input data rate): (a) CIT-SC with BPSK mapping; (b) CIT-SC with 16PSK mapping; (c) CIT-PC/CIF with BPSK mapping; (d) CIT-PC/CIF with 16PSK mapping

Comparing the BER performance of CIT schemes and CIF (Figure 4.21) shows that CIT-SC and CIT-PC give better BER performance when compared to CIF, for a given mapping scheme (in a single user scenario). Further work is required on the receiver structure of CIF in order to carry out a comparison for the multiuser scenario.

The PAPR of all implementations with different mapping schemes is approximately the same (Figure 4.22). Hence, in terms of the PAPR, there is not a great advantage in using one implementation or another.

Comparing the MOPS requirements of the different schemes (Figure 4.23) shows that for M>2 (where M is the size of the constellation), CIT-SC has higher MOPS requirements compared to CIT-PC and CIF (for a given constellation size). This is due to the fact that in the case of CIT-PC and CIF schemes, increasing the order of mapping results in a reduction in the number of subcarriers and hence a reduction in the size of the IFFT/FFT.

Overall, the results obtained show that for a given mapping scheme, the spectral efficiency and PAPR of all three implementations are approximately the same. The BER performance for a given PSK/QAM scheme for CIT-SC and CIT-PC is better than CIF, whereas the MOPS requirements for CIT-PC and CIF are better than that of CIT-SC. For a particular mapping scheme, CIT-SC and CIT-PC give the same spectral efficiency and power efficiency (quantified in terms of BER degradation), however, CIT-SC can accommodate more data bits over an MC-DS-CDMA symbol duration whereas CIT-PC can provide reduced implementation complexity.

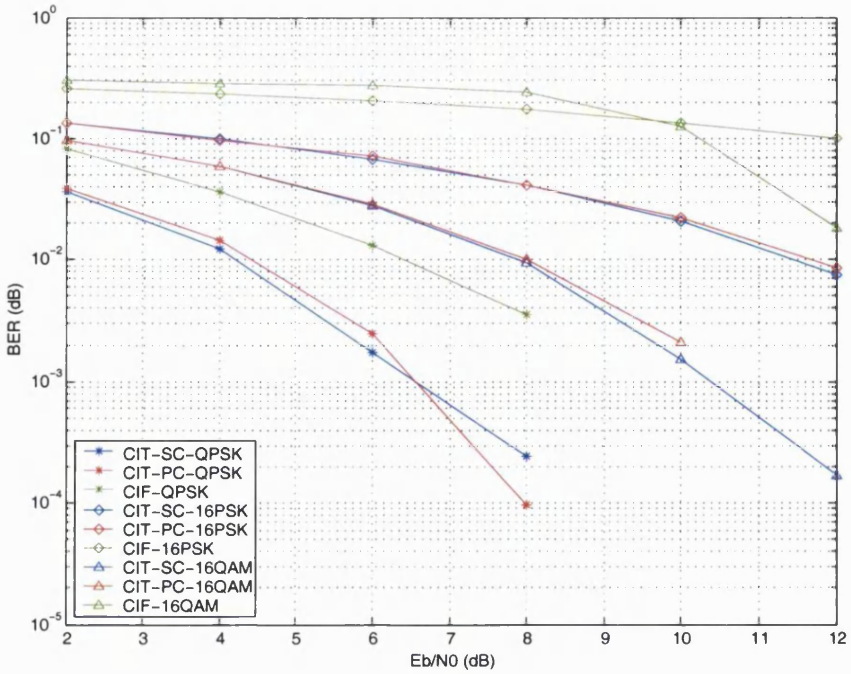

Figure 4.21: Comparison of BER performance of MC-DS-CDMA CIT-SC, CIT-PC and CIF in AWGN with 1 active user

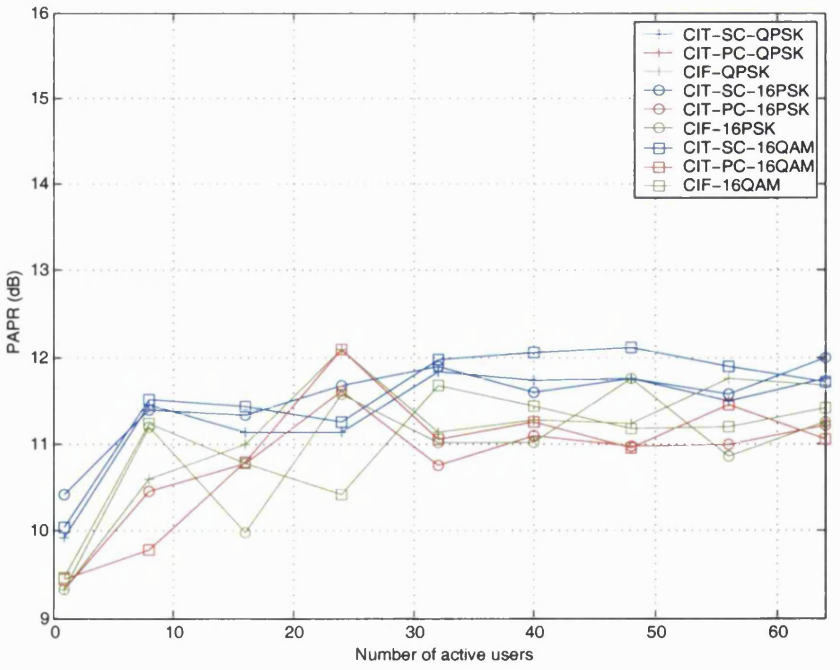

Figure 4.22: Comparison of PAPR performance of MC-DS-CDMA CIT-SC, CIT-PC and CIF

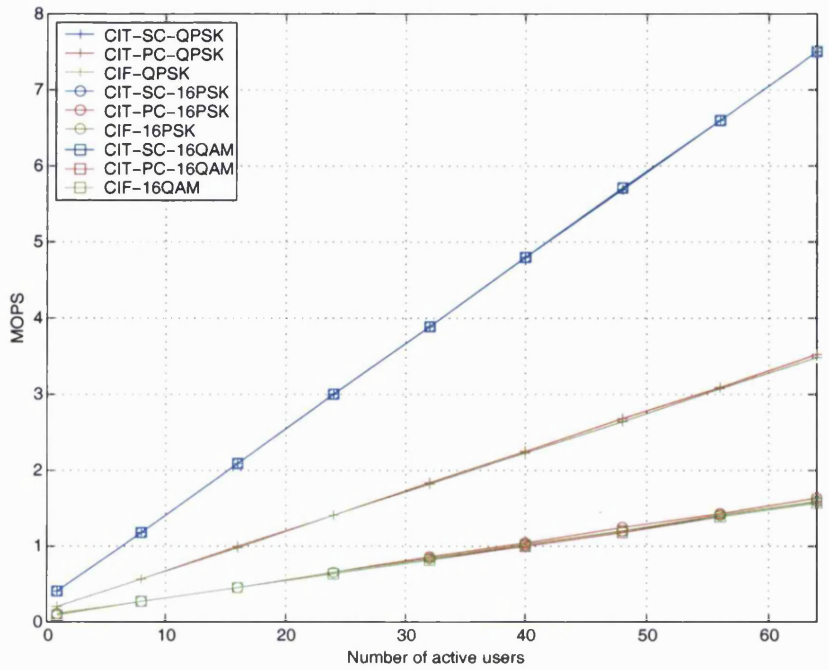

Figure 4.23: Comparison of MOPS requirements of MC-DS-CDMA CIT-SC, CIT-PC and CIF

4.3 Summary

The combination of MC-DS-CDMA with higher order PSK/QAM mapping schemes was studied in this chapter. Two different architectures for combining MC-DS-CDMA with higher order PSK/QAM mapping were investigated (namely, *combining in time* and *combining in frequency*). In the case of CIT, two implementations were proposed. The first implementation (termed CIT-SC) was similar to the CIT implementation proposed for MC-CDMA where the mapping is performed outside the MC-DS-CDMA modulation and demodulation. The second CIT implementation (termed CIT-PC) was a variant of the CIT-SC where the data is mapped after the S/P conversion instead of before (i.e., the mapping is performed at a lower rate).

The chapter was divided into 3 sections. The first section (Section 4.1) detailed the CIT and CIF implementations considered. It described the transmitter and receiver model for each implementation and listed the system features and key parameters. The second section presented and discussed the performance of the different implementations in terms of BER degradation, PAPR variation, spectral efficiency and implementation complexity, for different PSK/QAM mapping schemes. The section also included a discussion on the relative merits and demerits of the three implementations (CIT-SC, CIT-PC and CIF) with different mapping schemes.

Investigation of the performance of MC-DS-CDMA CIT-SC with different mapping schemes showed that increasing the order of the mapping scheme from BPSK to 4PSK/16PSK/16QAM resulted in an improvement in spectral efficiency at the cost of

degradation in the BER performance. The PAPR and the implementation complexity remain unchanged.

The performance of CIT-PC showed that increasing the order of mapping scheme caused a reduction in implementation complexity and improvement in spectral efficiency. The BER degradation increased with the order of mapping, however, the degradation was not as severe as in the case of CIF.

Investigation of the performance of CIF with different mapping schemes revealed that increasing the order of mapping resulted in improvement in spectral efficiency and reduction in implementation complexity. However, it also caused a significant degradation in BER performance. The PAPR for the different mapping schemes did not change significantly.

Comparison of the results obtained for the different implementations showed that for a given mapping scheme, the spectral efficiency and PAPR of all three implementations was the same. The BER performance for a given PSK/QAM scheme for CIT-SC and CIT-PC was better than CIF, whereas the MOPS requirement for CIF and CIT-PC was lower than that of CIT-SC. For a particular mapping scheme, CIT-SC and CIT-PC give the same spectral efficiency, power efficiency (quantified in terms of BER degradation) and PAPR, however, CIT-PC can provide reduced implementation complexity as compared to CIT-SC.

The next chapter investigates the performance of MC-CDMA CIT (discussed in Chapter 3) and MC-DS-CDMA CIT-SC with different PSK/QAM mapping schemes in the presence of HPA non-linearities.

Chapter 5

Performance of MC-CDMA and MC-DS-CDMA with higher order PSK/QAM mapping in the presence of HPA non-linearities

In mobile communications, one of the key goals is to maximise the coverage area of the transmitter, hence an RF amplifier (HPA) is employed in the transmitter to amplify the output signal. The HPA is generally operated close to or even in its non-linear region of operation in order to minimise the overall power consumption. In this region of operation, there are many negative effects that may result, especially if the input has varying signal amplitude. Large signal amplitudes can occasionally reach the amplifier saturation region and cause signal distortion. This distortion manifests itself as in-band distortion and out-of band distortion. In-band distortion causes BER degradation whereas out-of-band distortion results in spectral spreading and adjacent channel interference.

The effects of HPA non-linearities on the performance of OFDM systems and DS-CDMA systems have been investigated extensively [72, 73, 88, 89, 90]. However, only few researchers have investigated the effects of HPA non-linearities on the performance of multi-carrier CDMA systems [64, 65].

In [64], it has been shown that when considering the performance of MC-CDMA systems in the presence of HPA and multipath, HPA is the dominant factor in performance degradation. It is expected that the degradation due to HPA is even more notable when higher order constellations are used. (This has been shown in [72, 73] for OFDM systems.)

This chapter investigates the degradation due to HPA non-linearities of multi-carrier CDMA systems exploiting higher order PSK/QAM mapping formats. The performance is measured in terms of BER degradation and spectral spreading. The investigation is carried out

by considering only an AWGN channel in order to focus on the effects of HPA non-linearities. No coding or interleaving has been employed as the aim is to investigate the effects of higher order PSK/QAM schemes.

The chapter begins by presenting an overview of HPAs. In particular, it describes the various classifications of HPAs, the effects of HPA non-linearity on system performance and techniques for modelling and simulating HPA non-linearities. The subsequent section discusses the performance parameters used for investigating the effects of HPA on the input signal. This is followed by a description of the system models used for the investigation and discussion of the results obtained. The chapter is concluded with a summary.

5.1 High power amplifier

The high power amplifier is generally employed as the final active element in the transmitter chain and is used to increase the power of the transmitted signal. As mentioned above, the amplifier is generally operated in or near its non-linear region in order to gain maximum power transfer efficiency. However, in this region of operation an input signal with highly fluctuating amplitude (such as the multi-carrier CDMA signal) may occasionally reach the saturation region and result in distortion (This has been illustrated graphically in Figure 5.1).

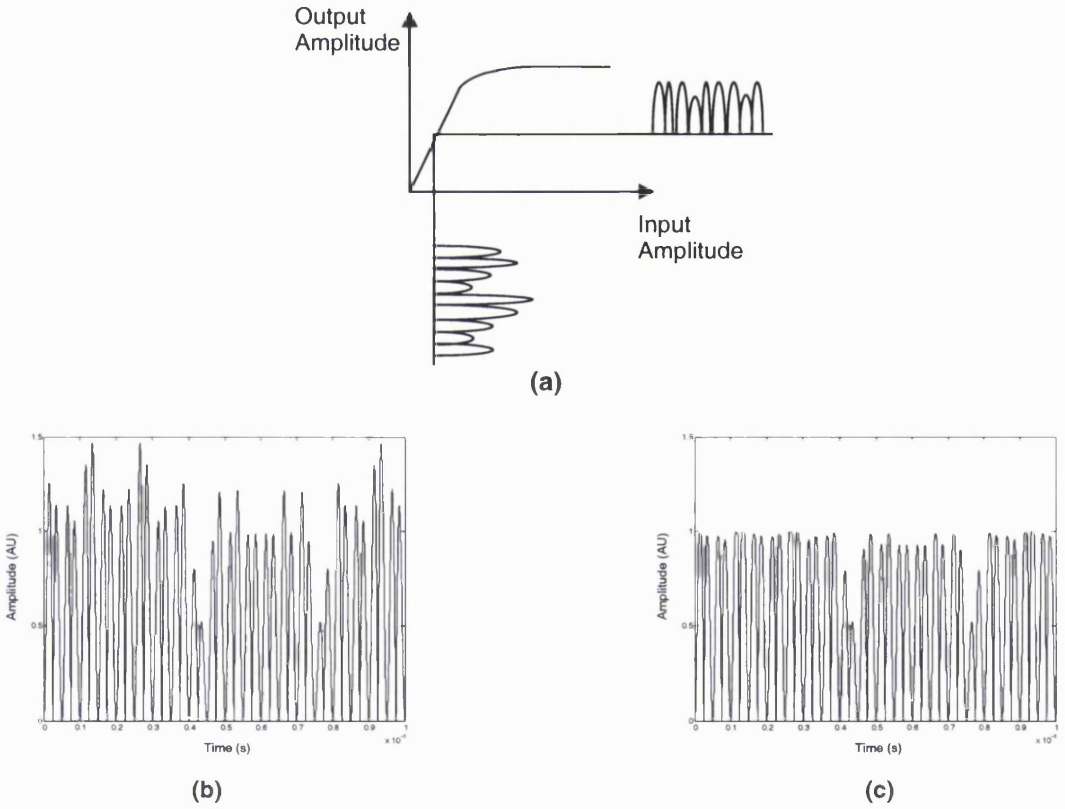

Figure 5.1: Effects of the HPA non-linearity on an input with varying amplitude: (a) graphical representation of the input-output relationship; (b) MC-CDMA signal at the input of an HPA; (c) signal at the output of the HPA (obtained through simulation)

This section describes the effects of the distortion caused by HPA non-linearities on system performance and discusses techniques for modelling and simulating HPA non-linearities.

5.1.1 HPA basics

The two most common types of HPAs in communication systems are: Travelling Wave Tube Amplifiers (TWTA) and Solid State Power Amplifiers (SSPA). TWTAs are mostly employed in high power satellite transponders whereas SSPAs (because of their size) are generally used in mobile communications.

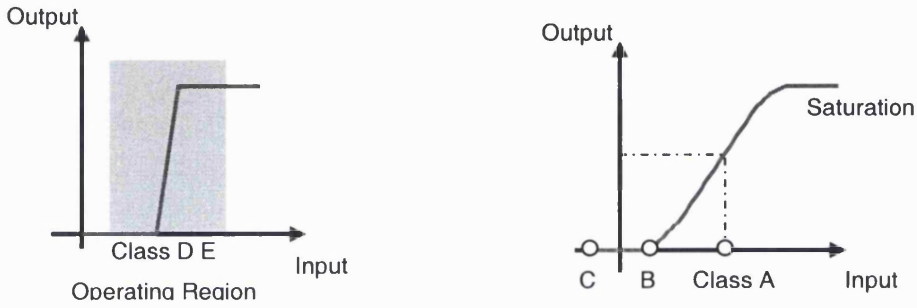

Figure 5.2: Transfer characteristics and operating points or regions of different HPA configurations [71]

The classification of HPAs is done according to the proportion of the cycle for which the amplifier conducts, which determines both the power efficiency and linearity [71, 91]. The most linear and least efficient are class A amplifiers in which the device conducts throughout the cycle. In class B, conduction is for nominally half the cycle. Class AB amplifiers usually have two devices in a push-pull configuration (each of which conducts for slightly more than half a cycle). Class C denotes conduction for less than half a cycle whereas class D and E use the output device only as a switch and hence may approach 100% efficiency. Figure 5.2 shows the transfer characteristics and operating points of the different HPA classifications. Mobile terminals generally employ class C amplifiers.

Amplifier operating point

The amplifier operating point dictates the non-linear distortion induced by the HPA. The operating point is usually identified by two parameters: Input Back-Off (IBO) and Output Back-Off (OBO).

The IBO is the level of power reduction required at the input so that the amplifier is not driven into saturation. It is defined as:

$$IBO = 10\log\left(\frac{P_{in}}{P_{sat_{in}}}\right) \tag{5.1}$$

where P_{in} is the average power of the signal at the input of the amplifier and $P_{sat_{in}}$ is the saturation power of the amplifier referred to the input (Figure 5.3).

Similarly, the OBO is the level of power reduction required at the output (with respect to the saturation power) in order to ensure that the amplifier is not driven into saturation. It is defined as:

$$OBO = 10\log\left(\frac{P_{sat_{out}}}{P_{out}}\right) \tag{5.2}$$

where $P_{sat_{out}}$ is the saturation power of the amplifier referred to the output and P_{out} is the average power of the signal at the output of the amplifier. In this work the operating point is defined in terms of the OBO[41].

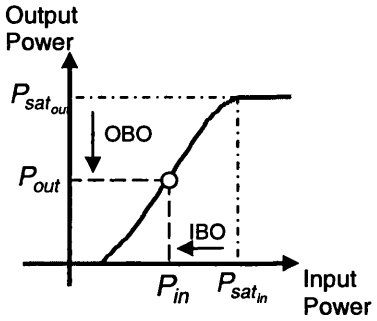

Figure 5.3: HPA operating points

The power efficiency of an HPA is very small for large back-offs. On the other hand, small back-offs give good power efficiency, but at a cost of high signal degradation (due to signal reaching the saturation region). This leads to a trade-off between maximum output power and high signal distortion.

5.1.2 Effects of HPA non-linearity on system performance

Operating in the non-linear region of the HPA produces Harmonic Distortion (HD) and Intermodulation Distortion (IMD) in the transmitted signal. The overall effect is degradation in BER performance (due to in-band distortion) and spectral spreading (due to out-of-band distortion).

The effects of the HPA on a given input signal can be explained by first considering its effect on a pure sine wave. When a pure sine wave (of frequency f_o) is amplified by the HPA, the output consists of the original wave plus some signals at other frequencies ($2f_o$, $3f_o$, $4f_o$....). The other frequencies are integer multiples of the original signal frequency and are known as

[41] The OBO of the amplifier is set by adjusting the gain of the input signal to obtain a certain P_{out}. This is explained further in Appendix B.

harmonics. The higher harmonic frequencies usually have amplitudes which are much lower than the fundamental [92].

If two closely spaced sine waves are now considered as the input to the HPA (with frequencies f_1 and f_2), the output will consist of the original frequency components (f_1 and f_2) plus signals at a number of other frequencies. These can be divided into *harmonic* components and *intermodulation* components. The harmonic components consist of signal at integer multiples of the original frequency ($2f_1$, $3f_1$.....$2f_2$, $3f_2$.....). Intermodulation components consist of signals at frequencies which are the sum and difference of original frequencies ((f_1+f_2), (f_2-f_1) .....) and signals at sum and difference of the original frequency and harmonics of the original frequencies ((f_1+3f_2), (f_2-2f_1), ($2f_2-3f_1$) .....).

Analytically, this can be expressed as follows:

If the input to the HPA is given by:

$$S(t) = \mathrm{Re}\left\{\tilde{s}(t)e^{j2\pi f_c t}\right\} = \frac{1}{2}\left[\tilde{s}(t)e^{j2\pi f_c t} + \tilde{s}^*(t)e^{-j2\pi f_c t}\right] \tag{5.3}$$

where $\tilde{s}(t)$ is the complex envelope of S(t) and f_c is the carrier frequency, then, the output of the HPA, Z(t) is given by:

$$Z(t) = \alpha S(t) + \beta S^2(t) + \gamma S^3(t) + ... \tag{5.4}$$

Substituting Equation 5.3 into Equation 5.4:

$$\begin{aligned} Z(t) = {} & \frac{\alpha}{2}\left[\tilde{s}(t)e^{j2\pi f_c t} + \tilde{s}^*(t)e^{-j2\pi f_c t}\right] \\ & + \frac{\beta}{4}\left[\tilde{s}^2(t)e^{j2(2\pi f_c)t} + 2\tilde{s}(t)\tilde{s}^*(t) + \tilde{s}^{*2}(t)e^{-j2(2\pi f_c)t}\right] \\ & + \frac{\gamma}{8}\left[\begin{array}{l}\tilde{s}^3(t)e^{j3(2\pi f_c)t} + 3\tilde{s}^2(t)\tilde{s}^*(t)e^{j2\pi f_c t} + 3\tilde{s}(t)\tilde{s}^{*2}(t)e^{-j2\pi f_c t} \\ + \tilde{s}^{*3}(t)e^{-j3(2\pi f_c)t} .....\end{array}\right] \end{aligned} \tag{5.5}$$

Of these terms, the first-order term (in α) is undistorted. The second-order term (in β) has a term at twice the carrier frequency and another at baseband. The third-order term has a component at 3 times the carrier frequency and a component at the carrier frequency.

In general, the even order terms do not generate a component at carrier frequency whilst the odd order terms do and it is these terms which produce distortion.

If two closely spaced sine waves are input to the HPA:

$$\begin{aligned} S(t) &= \mathrm{Re}\left\{\tilde{s}_1(t)e^{j2\pi f_c t} + \tilde{s}_2(t)e^{j2\pi f_d t}\right\} = \mathrm{Re}\left\{\tilde{s}_1(t)e^{j2\pi f_c t}\right\} + \mathrm{Re}\left\{\tilde{s}_2(t)e^{j2\pi f_d t}\right\} \\ &= \frac{1}{2}\left[\tilde{s}_1(t)e^{j\omega 2\pi f_c t} + \tilde{s}_1^*(t)e^{-j2\pi f_c t}\right] + \frac{1}{2}\left[\tilde{s}_2(t)e^{j2\pi f_d t} + \tilde{s}_2^*(t)e^{-j2\pi f_d t}\right] \end{aligned} \tag{5.6}$$

then the output of the HPA is given by:

$$Z(t) = \alpha S(t) + \beta S^2(t) + \gamma S^3(t) + ...$$

$$Z(t) = \frac{\alpha}{2}\left[\tilde{s}_1(t)e^{j2\pi f_c t} + \tilde{s}_1^{\,*}(t)e^{-j2\pi f_c t}\right] + \frac{\alpha}{2}\left[\tilde{s}_2(t)e^{j2\pi f_d t} + \tilde{s}_2^{\,*}(t)e^{-j2\pi f_d t}\right]$$

$$+ \frac{\beta}{4}\left[\begin{array}{l} 2\tilde{s}_1(t)\tilde{s}_1^{\,*}(t) + 2\tilde{s}_2(t)\tilde{s}_2^{\,*}(t) + \tilde{s}_1^{\,*2}(t)e^{-j2(2\pi f_c)t} + \tilde{s}_2^{\,*2}(t)e^{-j2(2\pi f_d)t} + \tilde{s}_1^{\,2}(t)e^{j2(2\pi f_c)t} + \\ \tilde{s}_2^{\,2}(t)e^{j2(2\pi f_d)t} + 2\tilde{s}_1(t)\tilde{s}_2(t)e^{j(2\pi f_c + 2\pi f_d)t} + 2\tilde{s}_1(t)\tilde{s}_2^{\,*}(t)e^{j(2\pi f_c - 2\pi f_d)t} + 2\tilde{s}_2(t)\tilde{s}_1^{\,*}(t)e^{j(2\pi f_d - 2\pi f_c)t} + \\ 2\tilde{s}_1^{\,*}\tilde{s}_2^{\,*}(t)e^{j(-(2\pi f_d)-(2\pi f_c))t} \end{array}\right]$$

$$+ .....$$

(5.7)

where (as in the case of the pure sine wave), the first-order term (in α) gives the undistorted signal. The second-order term (in β) has a component at baseband, a component at the two original carrier frequencies, a component at twice the original carrier frequencies (harmonic distortion) and various components at the sum and difference of the two original carrier frequencies (intermodulation distortion). Normally, the bandpass characteristics of the HPA will remove the higher order harmonic distortion component and the out-of-band IMD component.

5.1.3 Modelling HPA non-linearity

Non-linear elements such as HPAs are generally modelled in the time domain. HPAs can be modelled as memoryless amplifiers or amplifiers with memory. In the memoryless model, the output at a particular time is dependent on the input at that particular time (or is a function of the input with a fixed delay). In the case of models with memory, the output at time t, depends on a segment (finite or infinite) of the input signal prior to time t. Models with memory are generally difficult to obtain and are more computationally demanding than memoryless models. Hence, this investigation employs a memoryless model. The memoryless non-linearity can be modelled in two ways, using:

- Analytical based model or
- Empirical based model

An analytic model can be given in terms of the power series, quadratic function or a polynomial [50]. The choice of model depends on the parameters required to use the model in a simulation context. These parameters are obtained in practice by measurements which may or may not be simple to make.

Another way of modelling amplifier characteristics is by measuring them. It is an experimental observation that an input of:

$$\tilde{s}(t) = r(t)e^{j\phi(t)} \tag{5.8}$$

into a memoryless amplifier produces an output of the form given in Equation 5.9 [50].

$$\tilde{z}(t) = R(t)e^{j\phi(t)}e^{j\Phi(t)} \tag{5.9}$$

where $R(t) = f(r(t))$ represents a non-linear function relating the amplitude variations of the input signal to the amplitude variation of the output signal, $\phi(t)$ represents the phase of the input signal and $\Phi(t) = w(r(t))$ represents another non-linear function relating the amplitude variations of the input signal to the phase variations of the output signal. $R(t) = f(r(t))$ is referred to as the AM/AM conversion and $\Phi(t) = w(r(t))$ is referred to as the AM/PM conversion. If the input amplitude is constant, the AM/AM and AM/PM conversions do not occur [71].

The AM/AM and AM/PM characteristics of the amplifier can be measured in a number of different ways. Some of these techniques have been given in [50]. Figure 5.4 presents the simulation block diagram showing what must be done to implement the empirically based model in code.

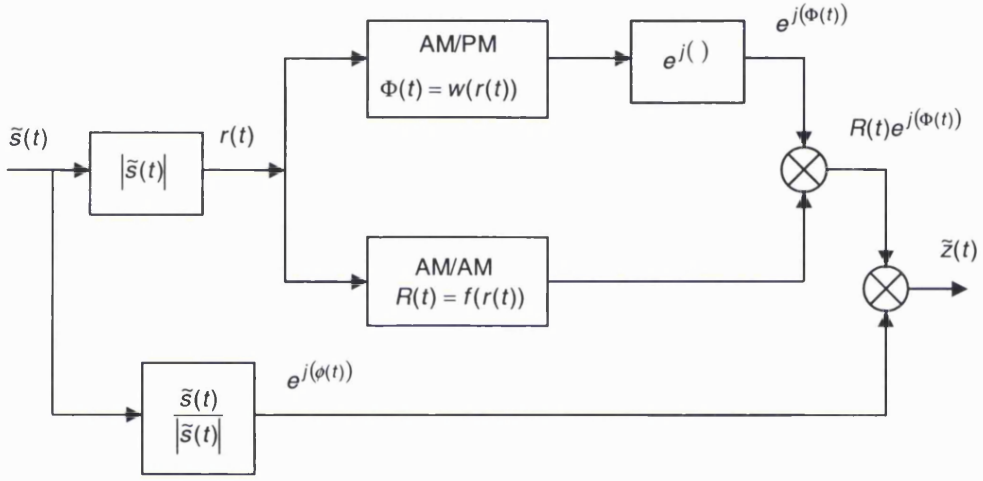

Figure 5.4: Simulation block diagram of AM/AM and AM/PM based model

As stated before, the two most common types of HPAs in communications are TWTAs and SSPAs [93, 94]. The AM/AM and AM/PM conversion functions of a typical TWTA and SSPA are shown in Figure 5.5 and Figure 5.6, respectively (Note that in the case of SSPA, the AM/PM conversion is very small and hence is neglected).

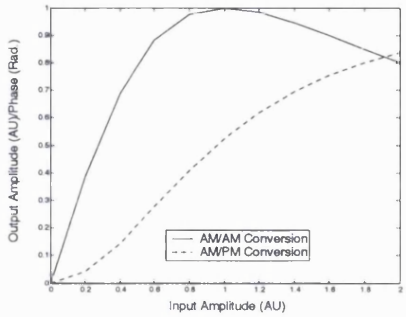

Figure 5.5: AM/AM and AM/PM conversion of TWTA

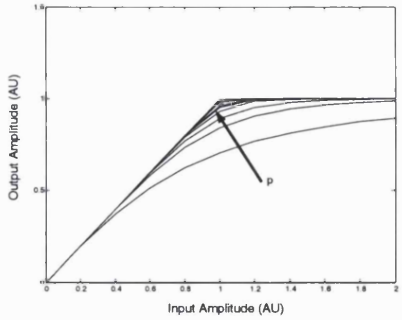

Figure 5.6: AM/AM conversion of an SSPA

Observation of Figure 5.5 and Figure 5.6 shows that the AM/AM characteristics of the TWTA are more non-linear than the SSPA.

The analytical expressions generally used to approximate the AM/AM and AM/PM conversion of TWTA are [95]:

$$R(t) = \frac{\alpha_A r(t)}{(1+\beta_A r^2(t))} \tag{5.10}$$

$$\Phi(t) = \frac{\alpha_\phi r^2(t)}{(1+\beta_\phi r^2(t))} \tag{5.11}$$

where the values of the parameters $\alpha_A, \beta_A, \alpha_\phi$ and β_ϕ are chosen to meet some pre-specified normalisation characteristics [94]. For the AM/AM conversion of the SSPA, the following approximation is generally employed [94]:

$$R(t) = \frac{\upsilon r(t)}{\left(1+\left[\left(\frac{\upsilon r(t)}{A_{sat}}\right)^2\right]^p\right)^{\frac{1}{2p}}} \tag{5.12}$$

where υ is the small signal gain of the amplifier, A_{sat} is the saturation amplitude of the amplifier referred to the output and p is an integer value which controls the smoothness of the transition from the linear region to the limiting region as shown in Figure 5.6 [94]. For large values of p, the model is perfectly linear until it reaches its maximum output level.

5.1.4 Simulation of HPA non-linearity

The most important implication of simulating a non-linear amplifier is the increase in the sampling rate. Due to the spreading of the spectrum, the sampling frequency has to be at least N_{spread} times the Nyquist rate (where N_{spread} is the order of the non-linearity being measured).

In this work a memoryless model of an SSPA has been used. The amplifier is modelled using the approximation given in Equation 5.12, where υ and $A_{sat,}$ are set to be equal to 1 and p is set equal to 5 [42] (Equation 5.13).

$$R(t) = \frac{r(t)}{\left(1 + (r(t))^{10}\right)^{\frac{1}{10}}} \tag{5.13}$$

5.2 Performance parameters

This section describes the parameters used to measure the distortion caused by HPA non-linearities.

5.2.1 Total degradation

Total degradation is used extensively as a performance measure to quantify the in-band distortion caused by the HPA [96, 97, 98]. (It is also used to provide an indication of the optimum operating point of the amplifier.)

The total degradation, T_D is defined in terms of the E_b/N_0 value required to obtain the target BER in the presence of HPA & AWGN ($E_b/N_{0(HPA)}$), the E_b/N_0 value required to obtain the target BER in the presence of AWGN ($E_b/N_{0(AWGN)}$) and the amplifier OBO (Equation 5.14).

$$T_D = \frac{E_b}{N_{0\,(HPA)}} - \frac{E_b}{N_{0\,(AWGN)}} + OBO \tag{5.14}$$

In the above expression, the value of $E_b/N_{0(AWGN)}$ is fixed for a given target BER. The value of $E_b/N_{0(HPA)}$ depends on the OBO of the amplifier. The higher the OBO, the lower the distortion caused by the HPA. Hence, the higher the OBO, the lower the E_b/N_0 value required to obtain the target BER (given as $E_b/N_{0(HPA)}$).

In this investigation, the total degradation is calculated graphically from the BER vs. E_b/N_0 plots for different OBO values. Figure 5.7 shows an illustrative BER vs. E_b/N_0 plot for MC-CDMA with OBO set equal to 2 dB. The figure also includes the theoretical BER performance of the system in the presence of AWGN[43]. The value of $E_b/N_{0(HPA)}$ and $E_b/N_{0(AWGN)}$ are obtained by noting the E_b/N_0 values for which the BER is equal to the target BER (10^{-3}).

Figure 5.8 shows an illustrative graph of total degradation plotted as a function of the amplifier OBO. From this graph it can be observed that the total degradation is high for low OBOs and high for high OBO with a minimum value at intermediate OBOs. For low OBOs, the amplifier is power efficient but it operates in its non-linear region. In this case, the major degradation is the amplifier non-linearity. For high OBO values, the amplifier is power inefficient, but it operates in its linear region. In this case, the major degradation factor is the AWGN. This

[42] The values of these parameters are typical values and are used by workers in the field [51 19 78].
[43] The derivation of the expression used to calculate the theoretical BER performance of PSK/QAM in AWGN is detailed in [71].

trade-off results in the optimum OBO value (OBO_{opt}) where the total degradation is minimum ($T_{D_{min}}$).

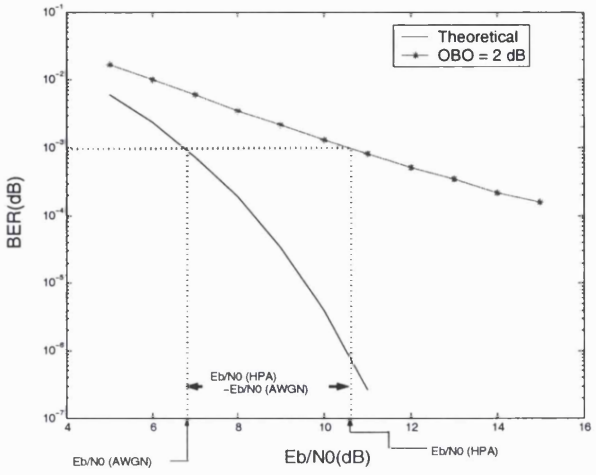

Figure 5.7: Calculating T_D using graphical techniques

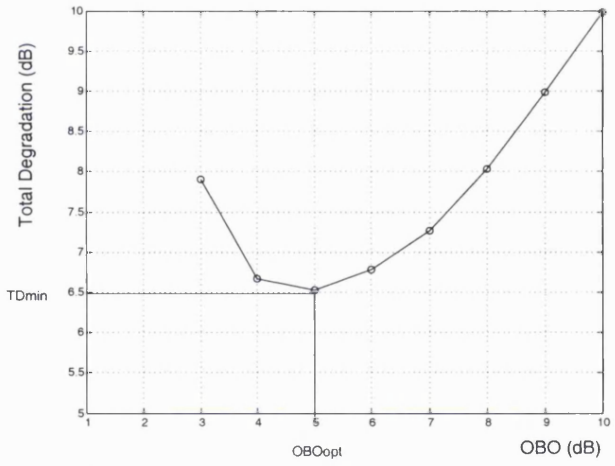

Figure 5.8: Total degradation as a function of amplifier OBO

5.2.2 Spectral spreading

Spectral spreading gives a measure of the out-of-band distortion caused by the amplifier non-linearities. The spectral spreading is calculated from an estimate of PSD of the non-linearly distorted multi-carrier CDMA signal. By way of illustration, Figure 5.9(a) and Figure 5.9(b) show the PSD of MC-CDMA and MC-DS-CDMA at the input of the amplifier (grey) and the output of the amplifier (black) for OBO=2 dB.

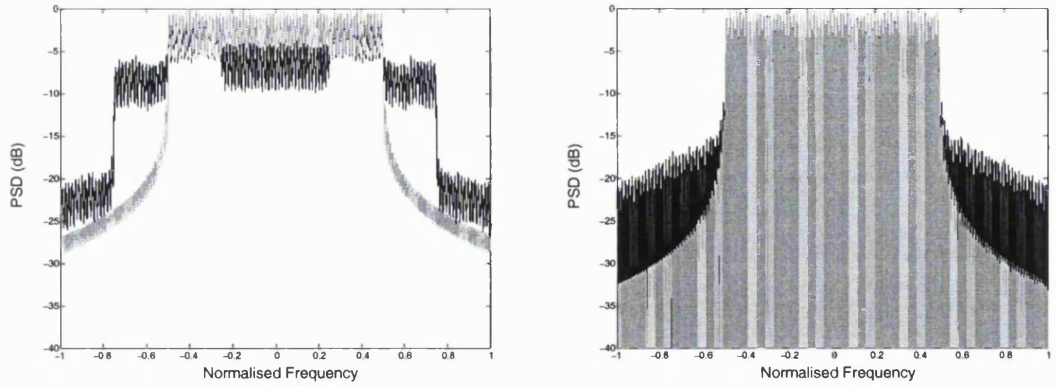

(a) (b)

Figure 5.9: PSD of: (a) MC-CDMA; (b) MC-DS-CDMA

The power spectral density of a random process, S(t) is given by:

$$\Phi_{ss}(f) = \lim_{L\to\infty} E\left[\frac{|S_L(f)|^2}{L}\right] \tag{5.15}$$

where E[.] denotes the expectation operator and $S_L(f)$ is the spectrum of the truncated version of $S_L(t)$ with duration L. Hence, the natural estimation to the power density spectrum of S(t) is:

$$\hat{\Phi}_{ss}(f) = \frac{|S_L(f)|^2}{L} \tag{5.16}$$

The precision of this estimator can be improved by observing the process over a larger duration L and by averaging the PSD with respect to a large number of realisations of the process.

In this work the multi-carrier CDMA signals have been observed over 100 symbols and the estimation has been averaged over 100 realisations of the signal. The spectrum of the signals is obtained using FFT techniques.

The spectral spreading of multi-carrier CDMA signal for different PSK/QAM formats is compared by calculating the total power in the side bands of the PSD.

5.3 System performance

The performance of MC-CDMA and MC-DS-CDMA systems using different PSK/QAM mapping schemes in the presence of HPA non-linearities is detailed in this section. Figure 5.10 shows the transmitter model used for this investigation. The multi-carrier modulated signal at the output of the transmitter is first non-linearly amplified and then corrupted by AWGN. In order to focus on the influence of the HPA non-linearity on multi-carrier CDMA signals, only an AWGN channel has been considered.

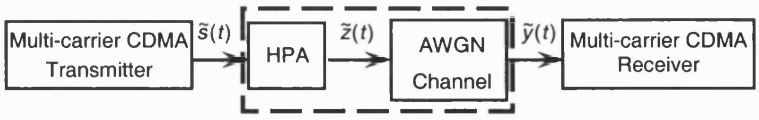

Figure 5.10: Transmission model

As mentioned in Sections 5.1.3 and 5.1.4, the HPA is modelled using a memoryless model of an SSPA. The AWGN channel is modelled in the same way as described in section 3.3. The MC-CDMA and MC-DS-CDMA systems are similar to the implementations described in Section 3.1.1 and Section 4.1.1, respectively.

The performance of both systems (MC-CDMA and MC-DS-CDMA) has been analysed for different number of active users with different PSK/QAM mapping formats.

5.3.1 MC-CDMA

The equivalent baseband representation of MC-CDMA transmitter and receiver are shown in Figure 5.11 and Figure 5.12, respectively.

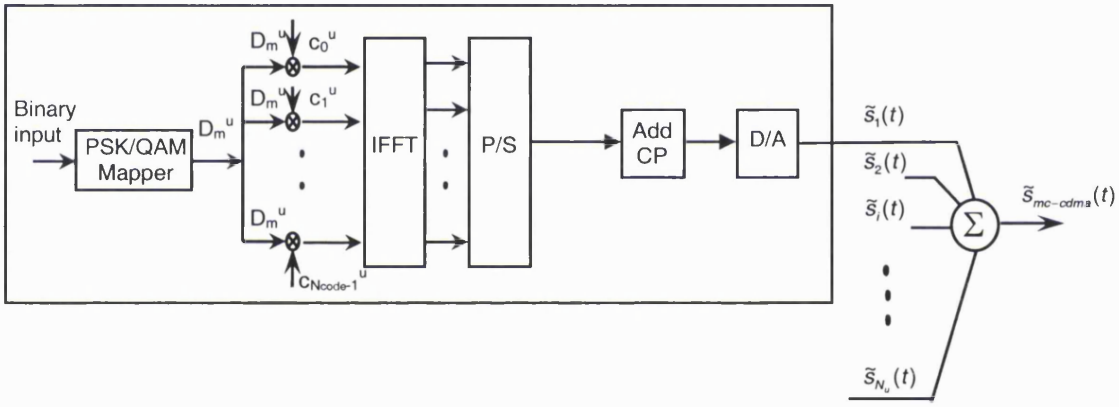

Figure 5.11: MC-CDMA transmitter

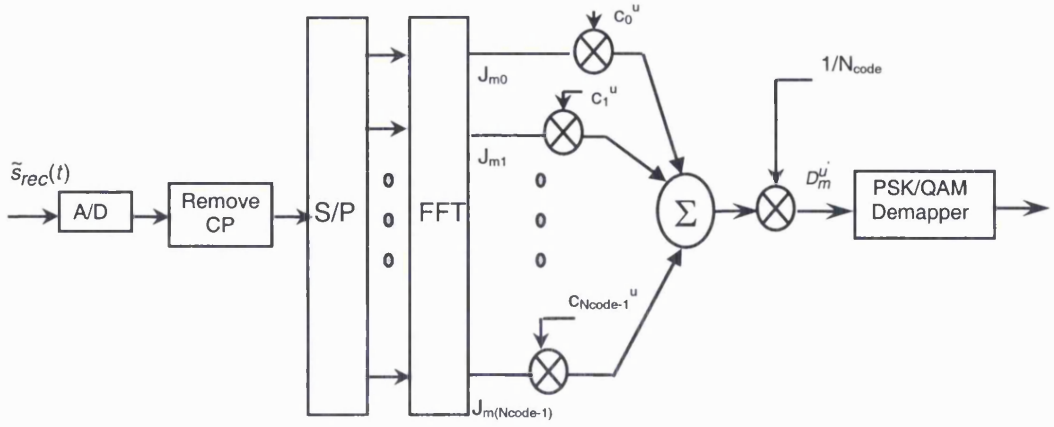

Figure 5 12: MC-CDMA receiver

As the MC-CDMA transmitter and receiver models used in this investigation are similar to those used for implementation-1 (CIT) in Chapter 3, they have not been described in detail in this chapter.

The continuous time signal at the output of the MC-CDMA transmitter, $\tilde{s}_{mc-cdma}(t)$ is given by:

$$\tilde{s}_{mc-cdma}(t) = \sum_{u=1}^{N_u} \sum_{m=-\infty}^{\infty} \sum_{n=0}^{N_{code}-1} D_m^u c_n^u g_n(t - mT) \tag{5.17}$$

where D_m^u is the PSK/QAM symbol to be transmitted in timeslot m for user u, c_n^u is the n^{th} chip of the spreading code for user u and $g_n(t-mT)$ is the n^{th} subcarrier given by:

$$g_n(t) = \begin{cases} e^{\frac{j2\pi n(t-T_{cp})}{T-T_{cp}}} & t \in [0,T] \\ 0 & t \notin [0,T] \end{cases} \tag{5.18}$$

where T is the duration of the MC-CDMA symbol, n is the subcarrier number and T_{cp} is the duration of the cyclic prefix.

The system parameters used in this investigation are similar to the parameters used in Chapter 3 and Chapter 4 and have been summarised in Table 5.1.

Table 5.1: MC-CDMA and MC-DS-CDMA system parameter

Parameter	Value	Parameter	Value
Number of Users, N_{users}	64	Mapping Scheme	2/4/16PSK 16 QAM
Length of spreading code, N_{code}	N_{users} (64)	FFT size, N_{FFT}	N_{spread}*10*$N_{subcarriers}$
Number of subcarriers, $N_{subcarriers}$	N_{code} (64)	Input sequence	m-sequence
Subcarrier spacing, Δf	$1/(T-T_{cp})$	Data rate	$(\log_2(M))/(T-T_{cp})$
Symbol duration, T	1 μs	Simulation duration	10000 symbols
Cyclic prefix duration, T_{cp}	0.2 μs	Spreading Code	WH Code
Oversampling Factor, N_{spread}	7		

The performance of MC-CDMA in the presence of SSPA non-linearity has been analysed for 1, 16 and 32 active users and for BPSK, QPSK[44], 16PSK and 16QAM mapping schemes.

[44] QPSK and 4PSK are used interchangeably throughout the thesis

Performance of MC-CDMA with different number of active users

Figure 5.13 presents the total degradation, T_D of MC-CDMA with BPSK mapping for different number of active users. The total degradation is calculated using the technique described in Section 5.2.1. Observation of the figure reveals that increasing the number of active users results in a decrease in the total degradation of the system, i.e., the total degradation for 1 user is much higher than the total degradation for 16 or 32 users and the total degradation of 16 users is higher than that of 32 users. This observation can be justified by studying the Complimentary Cumulative Distribution Function (CCDF) of the MC-CDMA signal amplitudes at the input of the HPA. Figure 5.13 plots the CCDF of the signal amplitudes at the input of the HPA, as a function of the normalised amplitude ($(|\tilde{s}(t)|/\sigma)$, where σ is the standard deviation of the amplitudes). From this figure, it can be seen that the signal amplitudes for a single user case are much higher than those for 16 or 32 users and hence the probability of the signal reaching the saturation region of the amplifier is also higher for the single user case. Overall, as the number of active users increases the signal amplitude decreases.

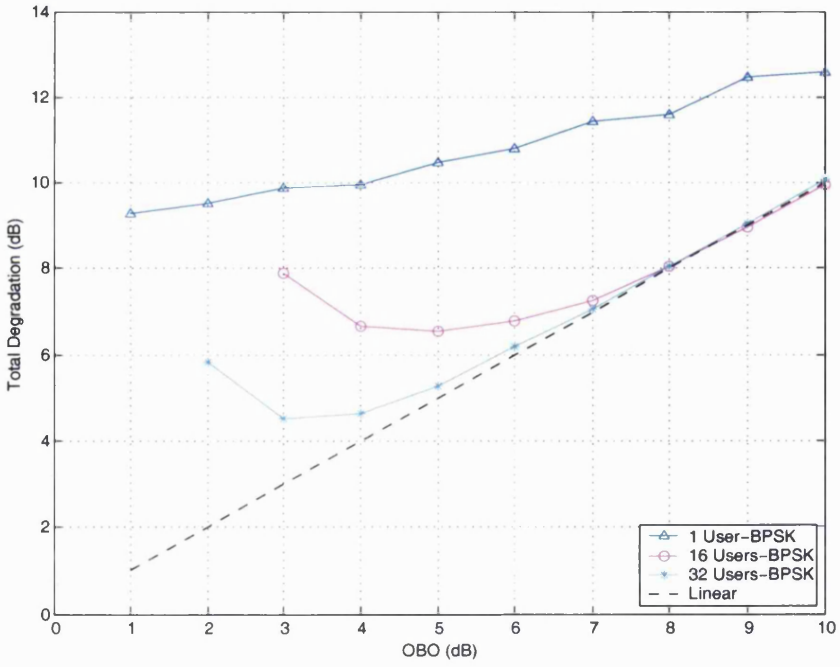

Figure 5.13: Total degradation of MC-CDMA in the presence of SSPA non-linearities with different number of active users

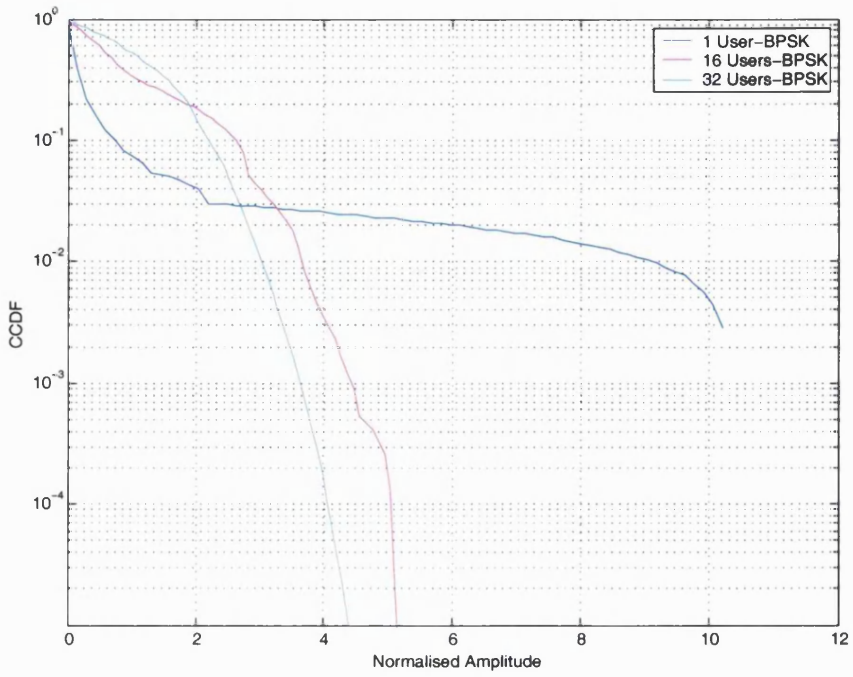

Figure 5.14: CCDF of the normalised amplitudes of MC-CDMA/BPSK signal at the output of the transmitter, with different number of active users

Similar investigation has been undertaken by Fazel and Kaiser in [65]. It is interesting to note that the results presented in [65] indicate that the total degradation of multi-carrier CDMA in the presence of SSPA non-linearities increases with the number of active users. This is the inverse of the trend observed above (In this investigation, $T_{D_{min}}$ for 1 user and 32 users is 9 dB and 4.5 dB, respectively whereas in [65], $T_{D_{min}}$ for 1 user and 32 users is 1dB and 3dB, respectively). A comparison between the system models for the two cases reveals that in the scheme proposed by Fazel and Kaiser (described in [44]), all active users do not transmit on the same set of subcarriers (Figure 5.15). In this implementation, the total number of subcarriers, N are grouped into B blocks. The data from each block is transmitted in parallel over N subcarriers. Each block has a maximum user capacity of N/B users. A simplified transmitter model of this implementation is presented in Figure 5.15.

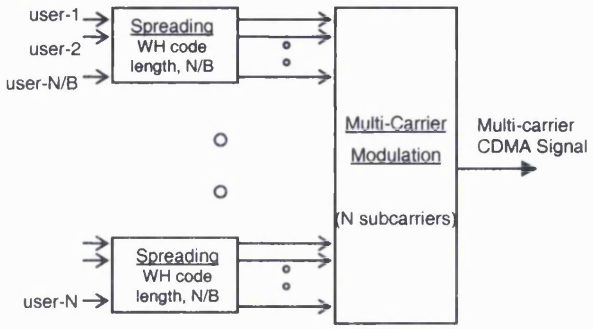

Figure 5.15: Simplified transmitter diagram for MC-CDMA scheme investigated in [65]

The first N/B users (user 1 to user N/B) are transmitted over N/B subcarriers. If the number of active users exceeds N/B, the second block is employed and the number of subcarriers increases to 2N/B. When the number of users exceeds 2N/B, the third block is employed. Hence, the number of subcarriers (and therefore the variation in signal amplitude) increase with the number of active users.

The power in the adjacent sidebands of the non-linearly amplified MC-CDMA signal is shown in Figure 5.16 for different amplifier OBO values (with number of active users set equal to 16 and 32). Observation of the figure shows that increasing the OBO results in lower spectral spreading as the effects of amplifier non-linearities decrease under these circumstances. Increasing the number of active users also results in a decrease in the spectral spreading. This is due to the dependence of MC-CDMA signal amplitudes on the number of active users (Figure 5.14). It is also interesting to note that the spectral spreading of the output signal for different number of active users at the optimum operating point is approximately the same in both cases.

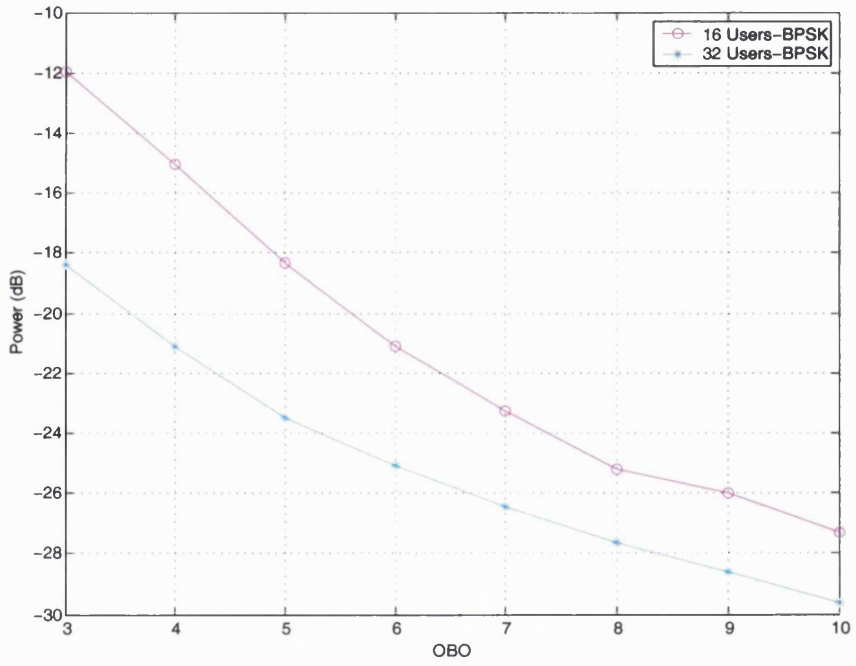

Figure 5.16: Power in the adjacent sidebands of the non-linearly amplified MC-CDMA signal for different OBOs, with different number of active users

Table 5.2 lists the optimum OBO for the different MC-CDMA and MC-DS-CDMA system together with the minimum total degradation at each point.

Performance of MC-CDMA with different mapping schemes

Figure 5.17 shows the total degradation of MC-CDMA with different PSK/QAM schemes. Observation of this figure reveals that changing the modulation format from BPSK to QPSK

does not have a significant effect on the total degradation of the system. The optimum operating point of the HPA remains unaltered, however, the value of $T_{D_{min}}$ increases by approximately 1 dB (Table 5.2). Changing the modulation format from BPSK to 16PSK and 16QAM increases $T_{D_{min}}$ by 4dB and moves OBO_{opt} from 5dB to 10dB. This is due to the fact that for a given OBO, the average power of the signal at the input of the HPA is the same for all mapping schemes. Hence, the distance between the constellation points, in the case of larger constellations (such as 16PSK and 16QAM) is smaller than the distance between constellation points in the case of smaller constellations (such as BPSK). Therefore, the BER is greater in the case of the larger constellations.

It is also interesting to observe that in the presence of non-linearities, the performance of 16PSK is better than 16QAM whereas in the presence of AWGN, 16QAM performs better than 16PSK (as shown in Chapter 3).

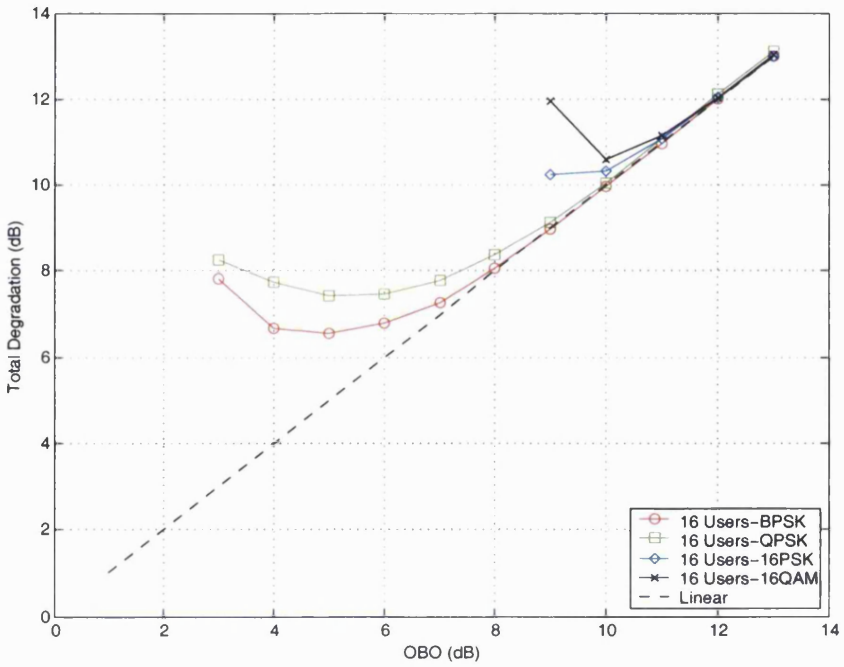

Figure 5.17: Total degradation of MC-CDMA system in the presence of SSPA non-linearities for different mapping schemes, with 16 active users

Figure 5.18 shows the power in the adjacent sidebands for MC-CDMA with different PSK/QAM mapping schemes. As expected, the spectral spreading reduces as the OBO increases. For a given OBO, the power in the adjacent sidebands for all mapping schemes is about the same, with BPSK being approximately 1 dB lower. This trend can be explained by the fact that the CCDF of the MC-CDMA signal amplitudes is about the same for all mapping schemes (Figure 5.19) and hence the probability of the signal reaching the non-linear region of the SSPA and causing out-of-band distortion is the same for all schemes.

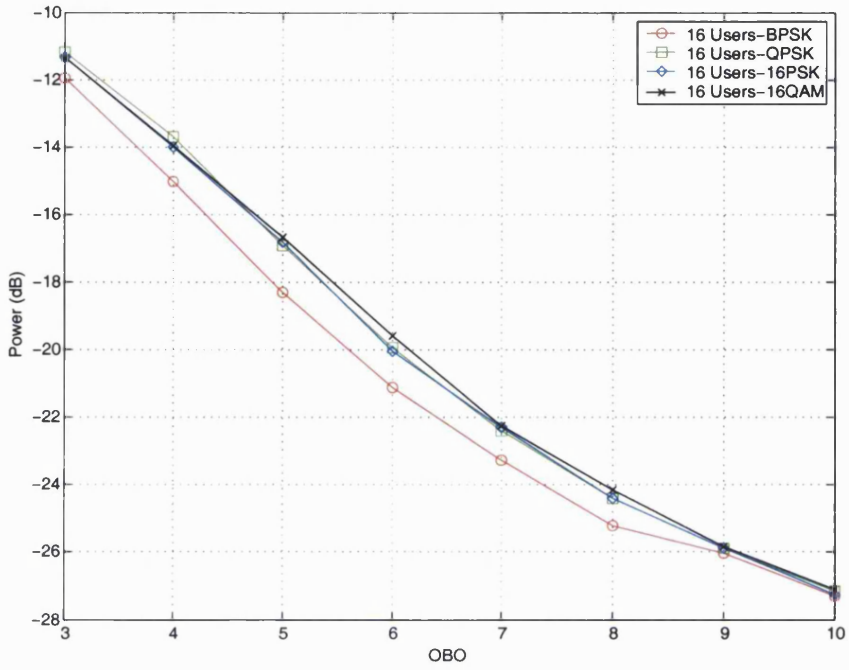

Figure 5.18: Power in the adjacent sidebands of the non-linearly amplified MC-CDMA signal for different OBOs, with different mapping schemes

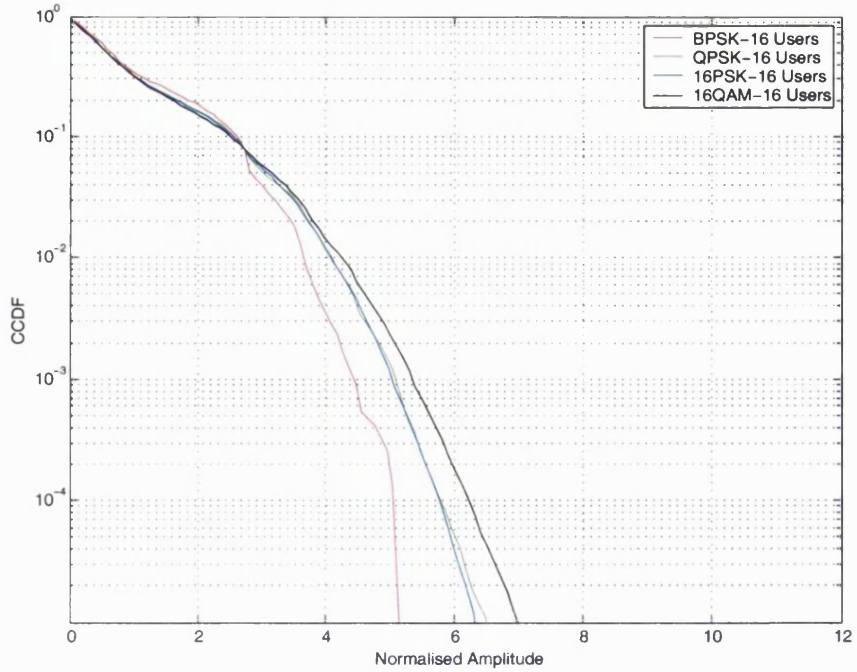

Figure 5.19: CCDF of the normalised amplitudes of MC-CDMA signal at the output of the transmitter for different PSK/QAM schemes, with 16 active users

5.3.2 MC-DS-CDMA

The equivalent baseband representation of the transmitter and receiver model of MC-DS-CDMA used in this analysis is presented in Figure 5.20 and Figure 5.21, respectively. The transmitter and receiver models employed in this work are similar to implementation-1a (CIT-SC) in Chapter 4.

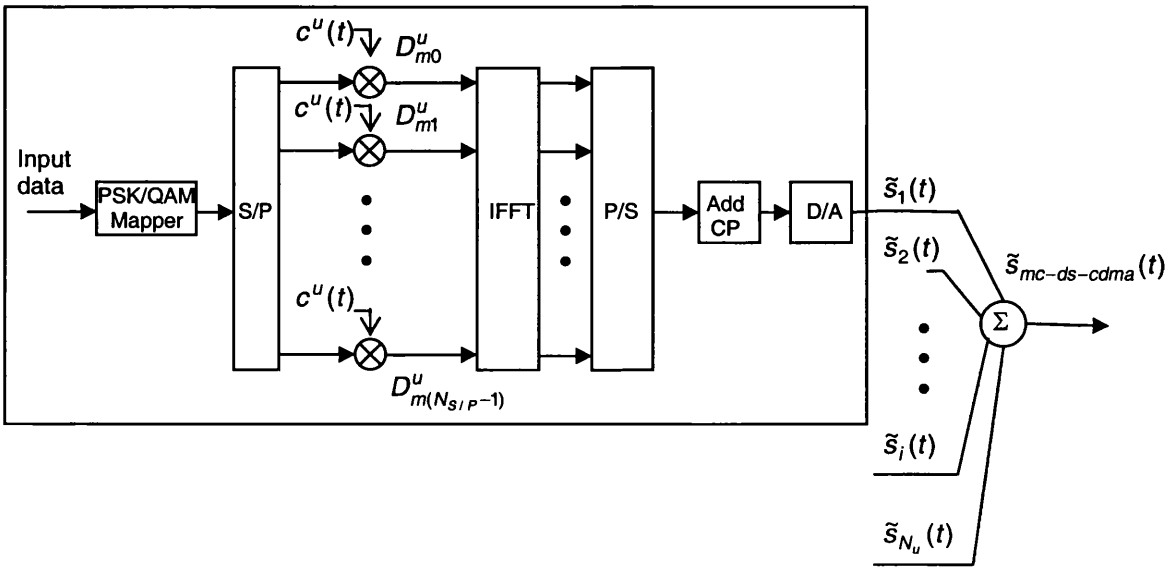

Figure 5.20: MC-DS-CDMA transmitter

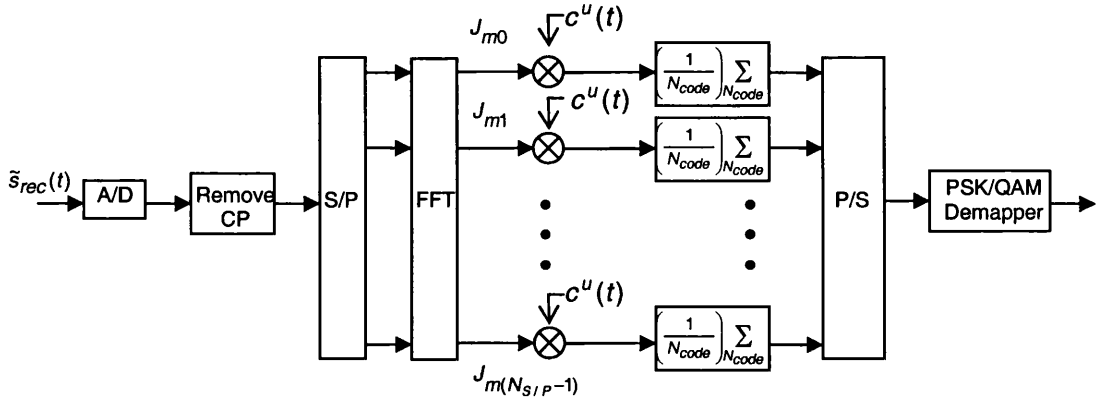

Figure 5.21: MC-DS-CDMA receiver

The signal at the output of the MC-DS-CDMA transmitter, $\tilde{s}_{mc-ds-cdma}(t)$ is given by:

$$\tilde{s}_{mc-ds-cdma}(t) = \sum_{u=1}^{N_u} \sum_{m=-\infty}^{\infty} \sum_{n=0}^{N_{S/P}-1} D_{mn}^{u} g_n(t - mT) \tag{5.19}$$

where D_{mn}^{u} is the transmitted symbol for user u, in time slot m and subcarrier n, $c^u(t)$ is the WH code for user u and $g_n(t)$ is the n^{th} subcarrier (as defined in Equation (5.18)).

As in the MC-CDMA case, the performance of the MC-DS-CDMA system in the presence of SSPA non-linearity has been investigated for 1, 16 and 32 active users and for BPSK, QPSK, 16PSK and 16QAM mapping.

Performance of MC-DS-CDMA with different number of active users

Figure 5.22 shows the total degradation, T_D of the MC-DS-CDMA signal in the presence of SSPA non-linearities for different number of active users (with BPSK mapping). Observation of the figure shows that increasing the number of active users does not result in a significant change in the total degradation of the system, i.e., the total degradation for 1 user is approximately the same as the total degradation for 16 or 32 users. This result can be explained by the fact that increasing the number of users in the MC-DS-CDMA case does not result in a significant change in the CCDF of the MC-DS-CDMA signal amplitudes at the input of the HPA (Figure 5.23). Hence, the probability of the signal reaching the non-linear region of the SSPA is same for different number of active users.

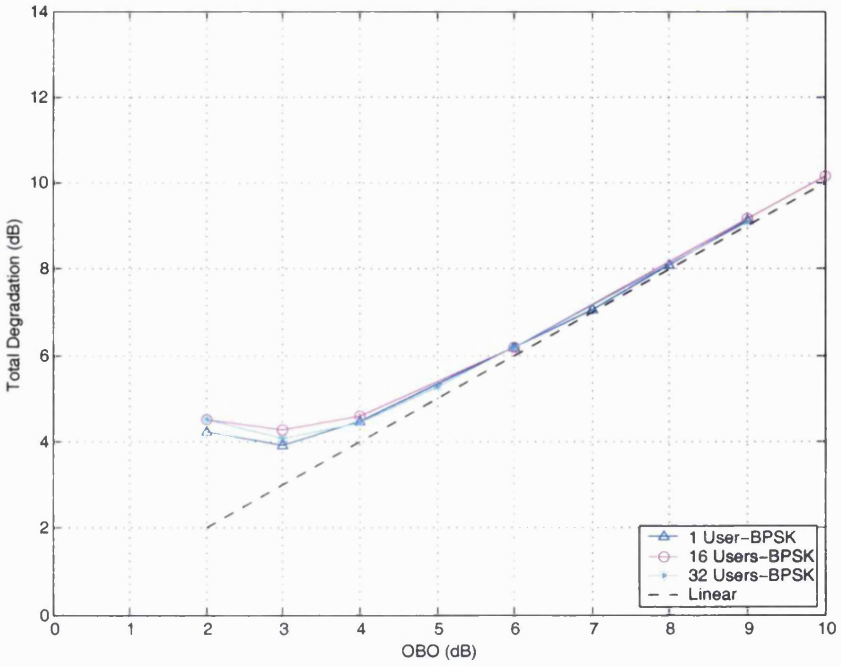

Figure 5.22: Total degradation of MC-DS-CDMA/BPSK in the presence of SSPA non-linearity with different number of active users

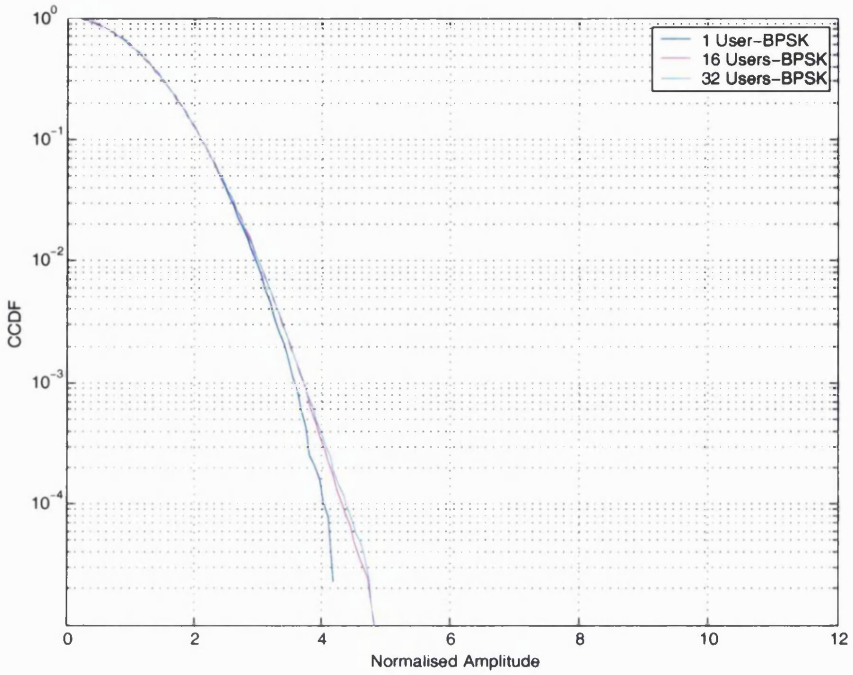

Figure 5.23: CCDF of the normalised amplitudes of MC-DS-CDMA/BPSK signal at the output of the transmitter, with different number of active users

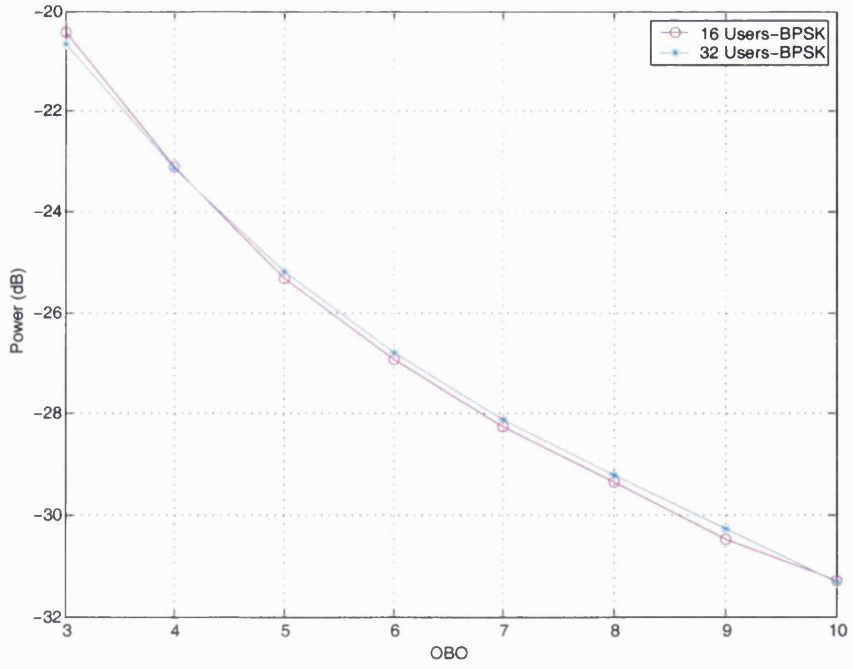

Figure 5.24: Power in the adjacent sidebands of the non-linearly amplified MC-DS-CDMA signal for different OBOs, with different number of active users

The spectral spreading of the non-linearly amplified MC-DS-CDMA signal (in terms of the power in the adjacent sidebands) for 16 and 32 active users is given in Figure 5.24. For a given

OBO value, the power in the adjacent sidebands is the same for 16 and 32 users. Again, this result is due to the fact that the CCDF of the MC-DS-CDMA signal amplitudes does not vary with number of active users (Figure 5.23).

Performance of MC-DS-CDMA with different mapping schemes

Figure 5.25 presents the total degradation of MC-DS-CDMA with 16 active users for different mapping schemes. Observation of the figure reveals that changing the mapping scheme from BPSK to QPSK does not alter the optimum operating point of the HPA nor does it increase $T_{D_{min}}$ (Table 5.2). However, changing the mapping from BPSK to 16PSK and 16QAM increases $T_{D_{min}}$ and moves OBO_{opt} by 3dB and 2dB, respectively. As explained in the case of MC-CDMA, in order to compare the performance of different mapping schemes for the same OBO, the power of the MC-DS-CDMA signal, at the input of the HPA has to be the same for all schemes. For higher order constellations, this results in a reduction in the distance between constellation points and hence produces an increase in the BER.

The out-of-band distortion of MC-DS-CDMA signal remains unchanged for all mapping schemes (Figure 5.26). This is due to the fact that the CCDF of the MC-DS-CDMA signal amplitude (Figure 5.27) at the input of the HPA is the same for all mapping schemes and hence the probability of the signal reaching the non-linear region and causing out-of-band distortion is the same for all mapping schemes.

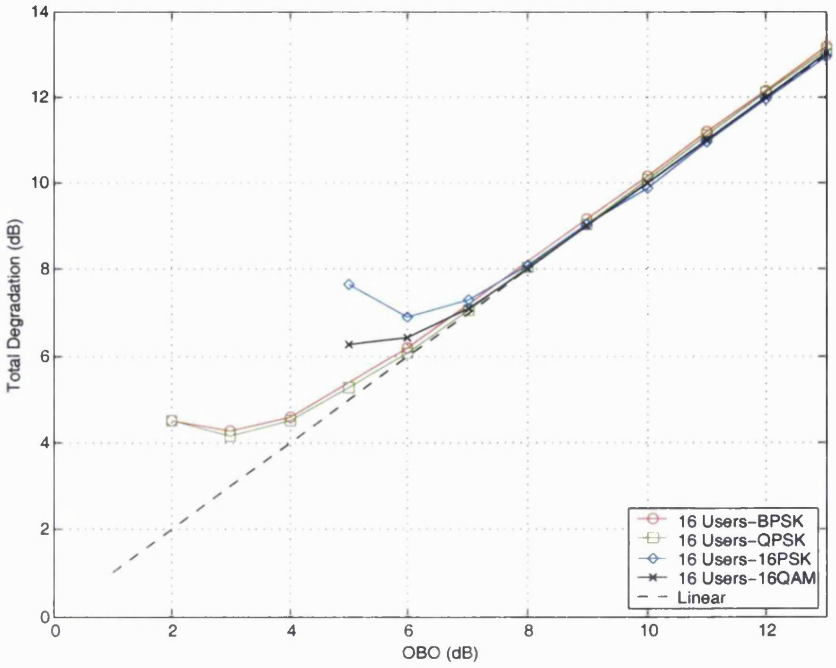

Figure 5.25: Total degradation of MC-DS-CDMA in the presence of SSPA non-linearity for different mapping schemes, with 16 active users

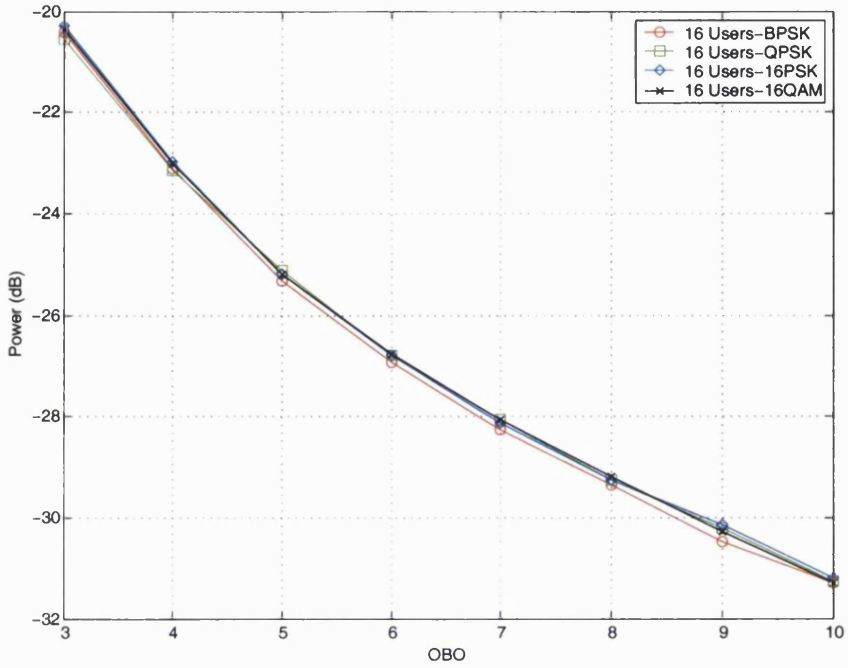

Figure 5.26: Power in the adjacent sidebands of the non-linearly amplified MC-DS-CDMA signal, with different mapping schemes

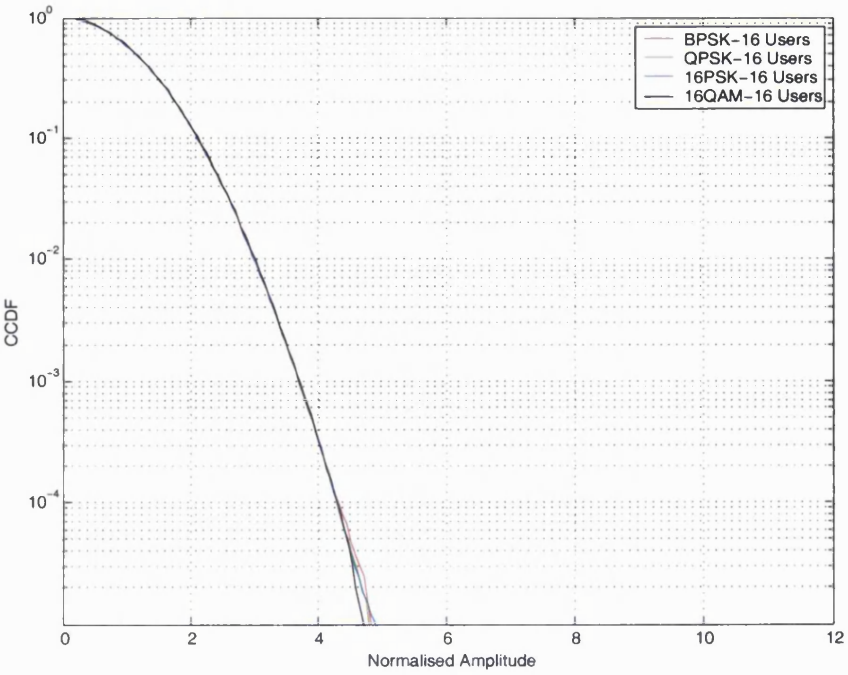

Figure 5.27: CCDF of the normalised amplitudes of MC-DS-CDMA signal at the output of the transmitter, for different PSK/QAM schemes with 16 active users

Table 5.2: Minimum total degradation, $T_{D_{min}}$ for MC-CDMA and MC-DS-CDMA

	Number of active users	Modulation	OBO_{opt} (dB)	$T_{D_{min}}$ (dB)
MC-CDMA	16	BPSK	5	6.49
	16	QPSK	5	7.41
	16	16PSK	10	10.25
	16	16QAM	10	10.58
	32	BPSK	3	4.45
MC-DS-CDMA	1	BPSK	3	3.88
	16	BPSK	3	4.26
	16	QPSK	3	4.15
	16	16PSK	6	6.88
	16	16QAM	5	6.41
	32	BPSK	3	4.71

5.3.3 Discussion of MC-CDMA and MC-DS-CDMA in the presence of HPA non-linearities

Section 5.3.1 and 5.3.2 presented the performance of MC-CDMA and MC-DS-CDMA in the presence of SSPA non-linearities. The key difference between the two multi-carrier CDMA schemes is the way in which the user data is spread and modulated onto the subcarriers. Comparison of the performance of the two multi-carrier CDMA schemes for 16 and 32 active users is shown in Figure 5.28 and Figure 5.29. From these figures it can be observed that for 16 users, MC-DS-CDMA experiences lower total degradation and spectral spreading as compared to MC-CDMA, whereas for 32 users, the difference between the performance of the two schemes is not very significant. Plotting the CCDF of the signal amplitudes at the input of the HPA (Figure 5.30) shows that as the number of active users increase, the CCDF of the signal amplitude of both schemes become similar. Hence it can be concluded that for small number of active users, MC-DS-CDMA experiences lower in-band and out-of-band distortion compared to MC-CDMA, however, for large number of active users, the performance of both multi-carrier CDMA schemes is the same.

Figure 5.31 and 5.32 present the total degradation and spectral spreading of MC-CDMA and MC-DS-CDMA for different PSK/QAM mapping schemes. Observation of the figures reveals that for all mapping schemes, the total degradation and spectral spreading for MC-DS-CDMA is lower than that for MC-CDMA. Comparing the CCDF of the signal amplitudes at the input of the HPA (Figure 5.33) reveals that the amplitudes of MC-DS-CDMA signal are lower than the amplitudes of MC-CDMA signal for all mapping schemes. It is important to point out

that the comparisons have been done for 16 active users. As seen above, the variation in the performance of the two schemes decreases with an increase in the number of active users, hence, for larger number of active users, this difference may not be as significant.

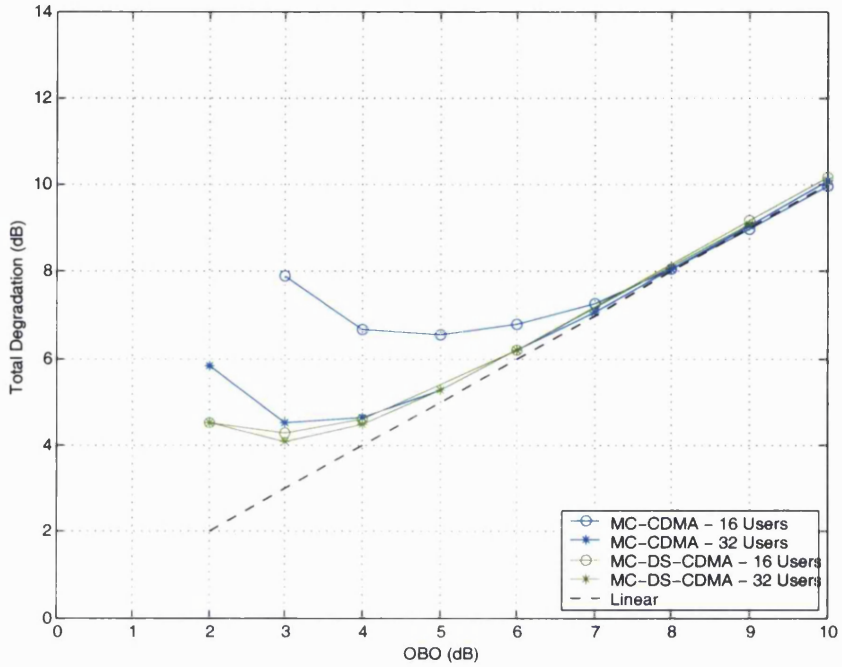

Figure 5.28: Comparison of the total degradation of MC-CDMA/BPSK and MC-DS-CDMA/BPSK for different number of active users

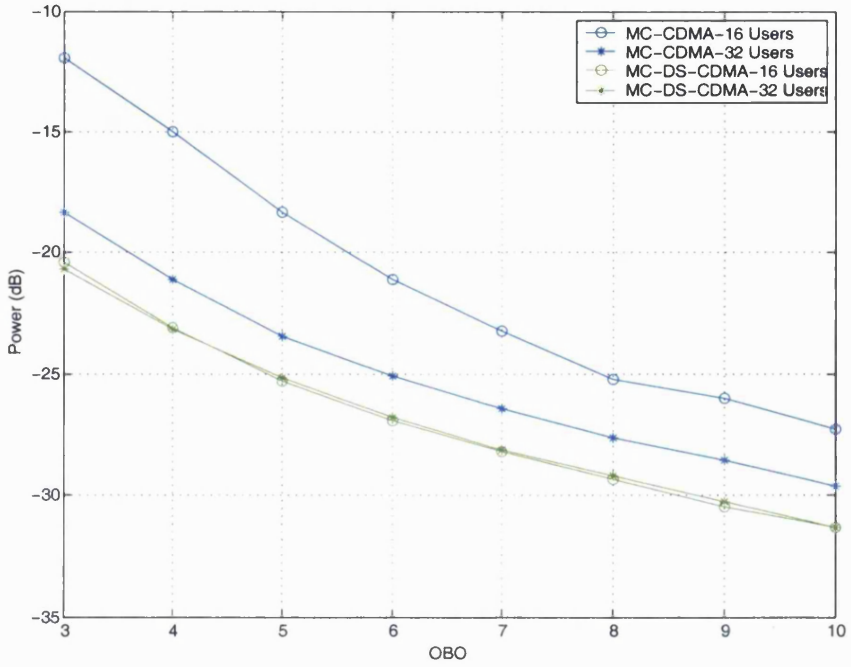

Figure 5.29: Power in the adjacent sidebands of the MC-CDMA and MC-DS-CDMA signal for different OBOs, with different number of active users

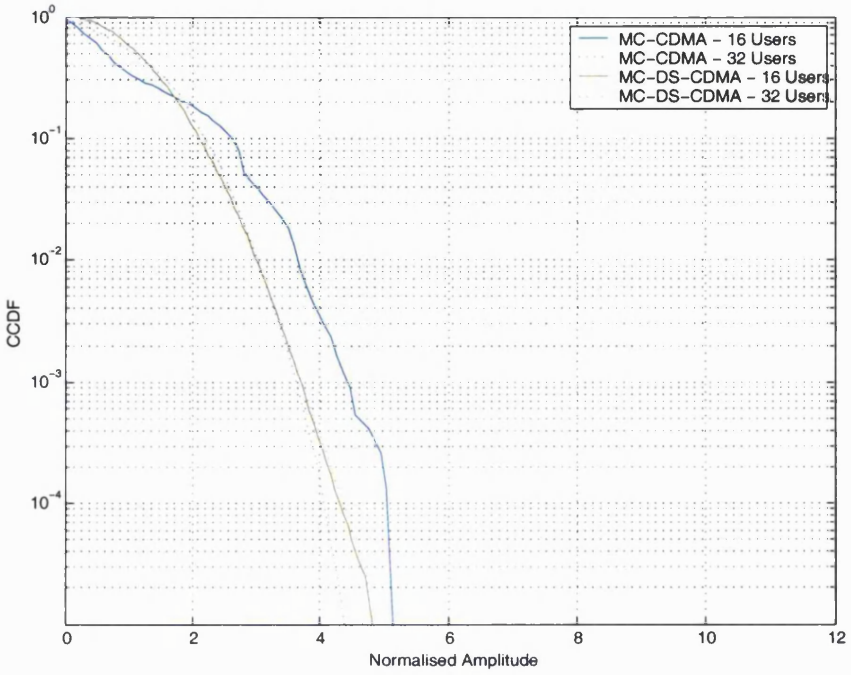

Figure 5.30: Comparison of the CCDF of the normalised amplitudes of MC-CDMA/BPSK and MC-DS-CDMA/BPSK signal for different number of active users

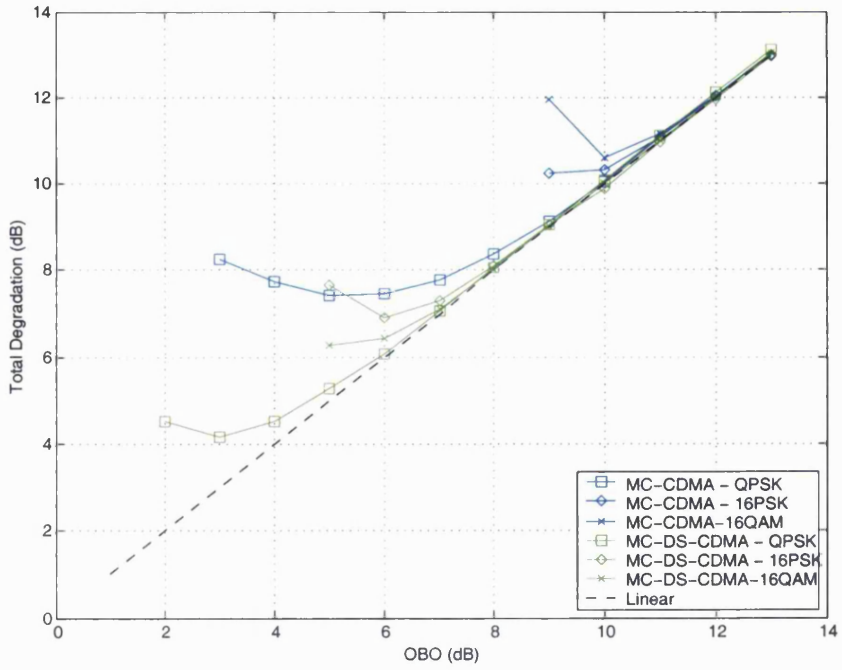

Figure 5.31: Comparison of the total degradation of MC-CDMA and MC-DS-CDMA for different mapping schemes

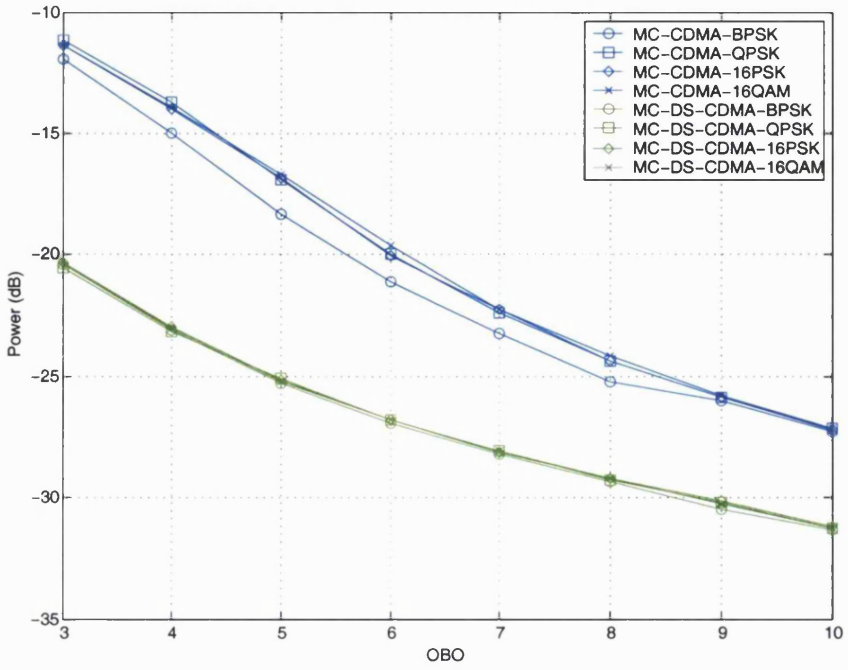

Figure 5.32: Power in the adjacent sidebands of the MC-CDMA and MC-DS-CDMA signal for different OBOs, with different mapping schemes

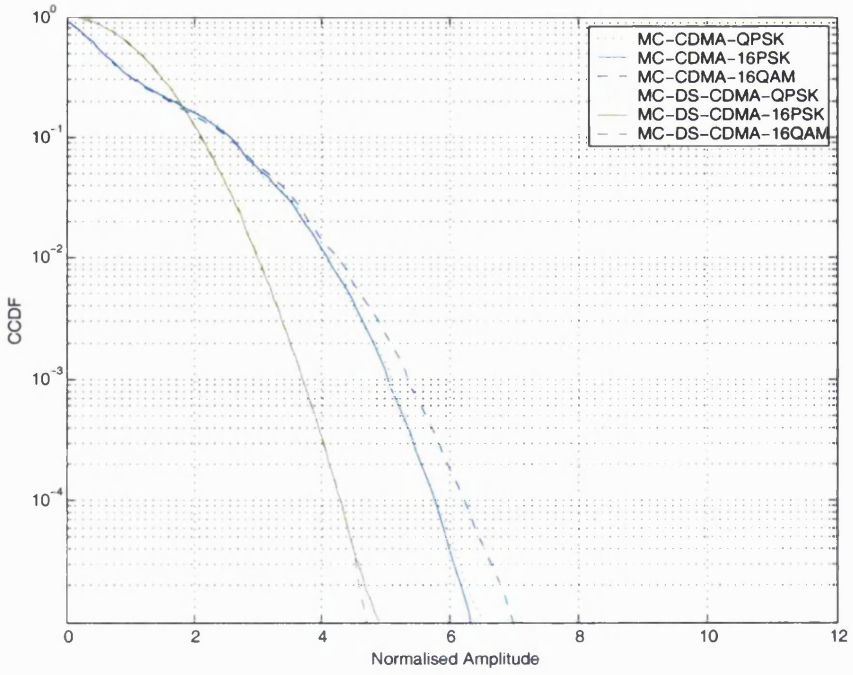

Figure 5.33: Comparison of the CCDF of the normalised amplitudes of MC-CDMA and MC-DS-CDMA signal with different mapping schemes

The trends observed in this research for multi-carrier CDMA with higher order mapping are similar to those observed in [72] and [73] for OFDM with higher order M-QAM mapping. In [72], the performance of M-QAM/OFDM systems is evaluated using a semi-analytical technique. The results show that as the value of M increases, the minimum total degradation, $T_{D_{min}}$ also increases. Increasing the mapping from 4-PSK to 16-QAM results in an increase in $T_{D_{min}}$ of 2 dB. Increasing the mapping from 4-PSK to 16-QAM in MC-DS-CDMA also results in an increase in $T_{D_{min}}$ of 2 dB. In the case of MC-CDMA, changing the mapping from 4-PSK to 16-QAM resulted in a greater increase in the $T_{D_{min}}$ (3dB).

In [73], the BER performance of M-QAM/OFDM schemes has been investigated in the presence of HPA non-linearities and phase noise. The results show that increasing the order of mapping results in an increase in the signal-to-noise ratio required for a given BER. This is similar to the observations made for MC-CDMA and MC-DS-CDMA in this work.

To the best of the author's knowledge, limited research has been carried out into the performance of MC-CDMA and MC-DS-CDMA systems in the presence of HPA non-linearities [64, 65] and hence a comprehensive comparison with the work of other researchers in the field cannot be carried out.

5.4 Summary

The performance of multi-carrier CDMA systems in the presence of HPA non-linearities was presented in this chapter. The effects of HPA non-linearities on an input signal with varying amplitude can be classified in terms of in-band distortion (resulting in BER degradation) and out-of-band distortion (resulting in spectral spreading). The level of in-band distortion and out-of-band distortion caused by the HPA non-linearities when MC-CDMA and MC-DS-CDMA signals are used as inputs was investigated in terms of total degradation and spectral spreading (power in the adjacent sidebands).

The performance of both multi-carrier CDMA systems was investigated for different number of active users and different mapping schemes. The MC-CDMA and MC-DS-CDMA models used for the investigation are similar to the CIT implementations in Section 3.1 and Section 4.1, respectively.

The chapter began with background on HPA non-linearities (Section 5.1). It described the effects of HPA non-linearities on system performance and discussed techniques for modelling HPA non-linearities. Section 5.2 described the parameters used to measure the distortion caused by HPA non-linearities (namely total degradation (T_D) and spectral spreading). The performance of the MC-CDMA and MC-DS-CDMA system in the presence of HPA was presented in Section 5.3.

In the case of MC-CDMA, increasing the number of active users resulted in a reduction in the in-band and out-of-band distortion caused by the SSPA non-linearities. Changing the

mapping scheme from BPSK to QPSK/16PSK and 16QAM showed that the in-band distortion of higher order mapping schemes (16PSK, 16QAM) was much worse than BPSK and QPSK. This trend was explained by the fact that in order to compare the different schemes at the same OBO, the power of the MC-CDMA signal at the input of the HPA has to be the same in all cases. Under these circumstances, the distance between the constellation points for the higher order schemes is smaller than that for lower order schemes. The out-of-band distortion of MC-CDMA with different mapping schemes was observed to be the same.

In the case of MC-DS-CDMA, increasing the number of active users had no significant effect on the performance of the system, i.e., the in-band distortion and out-of-band distortion for different number of active users was observed to be the same. Changing the mapping schemes from BPSK to QPSK/16PSK and 16QAM showed that, as in the case of MC-CDMA, the in-band distortion for higher order mapping schemes was much worse than BPSK and QPSK, due to the fact that the comparison between the different schemes had been performed for the same OBO and hence the same transmitted power. The out-of-band distortion of MC-DS-CDMA for all mapping schemes was observed to be the same.

Comparing the performance of the two multi-carrier CDMA schemes revealed that for small number of active users, MC-DS-CDMA experienced lower distortion (both in-band and out-of-band) than MC-CDMA however, for large number of active users, the distortion experienced by both schemes was approximately the same.

The next chapter investigates the performance of MC-CDMA and MC-DS-CDMA in the presence of HPA non-linearities using different WH code allocation techniques. Three different allocations of WH codes have been considered in order to determine whether the allocation of the WH codes to different users has an effect on the amplitudes of the transmitted signal (and hence the performance of the system in the presence of HPA non-linearities).

Chapter 6

Effects of WH code allocation on the systems performance in the presence of HPA non-linearities

In the previous chapter, it was observed that the performance of multi-carrier CDMA systems in the presence of HPA non-linearities was dependent on the CCDF of the signal amplitudes at the input of the HPA. For example, in the MC-CDMA case, the CCDF of the signal amplitudes decreased with the increase in number of active users and consequently, the performance of the system improved with the number of active users. In the MC-DS-CDMA case, the CCDF of the signal amplitudes remained unchanged for different number of active users and hence the performance of the system in the presence of HPA also remained unchanged.

More specifically, the effect of the HPA non-linearities on the input signal is dependent on the PAPR of the input signal, i.e., the lower the PAPR, the lower the distortion caused by the HPA non-linearity (for a given operating point). The amplifier operating point (IBO, OBO) is set according to the average power of the signal[45] and hence extreme deviations from the average power may result in the signal reaching the saturation region and causing distortion. As mentioned in the previous chapter, this distortion is classified in terms of in-band distortion and out-of-band distortion.

Multi-carrier CDMA systems have a high PAPR. Hence the amplifier operating point has to be "backed off" (as described in 5.1.1) in order to avoid signal distortion. This results in inefficient power conversion within the amplifier. In mobile communications this also results in a

[45] P_{in} and P_{out} in Equation 5.1 and 5.2.

reduction of the coverage area of the transmitter. Accordingly, in applications such as mobile handsets, the benefits of using multi-carrier schemes are often outweighed by the high PAPR of the transmitted signal. Controlling the PAPR of the multi-carrier signal is an important issue.

Much research has been done on controlling the PAPR in OFDM systems and numerous techniques have been proposed for reducing the PAPR [99, 100, 101, 102, 103]. This chapter investigates the variation in PAPR of multi-carrier CDMA signals with different WH code allocation strategies. It has been observed that for the MC-CDMA case, the PAPR variation of the signal is indeed dependent on the WH code allocation scheme whereas for the MC-DS-CDMA case, the PAPR is independent of the WH code allocation.

The variation in PAPR with WH code allocation suggests that the performance of the multi-carrier CDMA system in the presence of HPA non-linearities will also be dependent on the WH code allocation. This is investigated by studying the performance of the two multi-carrier CDMA schemes with different WH code allocation strategies in the presence of SSPA non-linearities.

The chapter begins with an introduction to PAPR (Section 6.1). The section discusses why a low PAPR is desired in a system with non-linear elements such as HPAs. The analytical expression used to calculate the PAPR is presented and the measurement of PAPR using simulation techniques described. The next section discusses the influence of spreading codes on the PAPR of CDMA based systems. It provides some background on spreading codes and then goes on to describe the Walsh-Hadamard codes. The effects of spreading codes on the PAPR performance of the transmitted signal in single and multi-carrier CDMA systems is then discussed. The following section discusses the influence of scrambling codes on the PAPR. It provides some background into the scrambling codes used in current CDMA based systems and then describes the effects of scrambling on the PAPR of MC-CDMA signal. This is followed by a description of the transmission scheme used for the investigation and the techniques used to allocate WH codes to different users. The PAPR performance of the two multi-carrier CDMA systems, for different WH code allocations is then presented together with the performance of both schemes in the presence of HPA non-linearities (in terms of total degradation and spectral spreading). The chapter concludes with a summary.

6.1 Peak-to-average power ratio

The peak-to average power ratio gives the extent of extreme fluctuations in signal power over time. All signals (single or multi-carrier, modulated or unmodulated) have a peak-to-average power ratio. The PAPR of some common wireless standards is given in Table 6.1 [104].

Table 6.1: PAPR for common wireless standards

	Modulation	PAPR(dB)
Analogue	FM	0
GSM	GMSK	1.5
W-CDMA	QPSK/DSSS	8-9
IEEE 802.11a[46]	OFDM	18
DAB/DVB[47]	OFDM	30

In a multi-carrier scheme, high PAPR occurs when the signals in several subchannels add in phase. Figure 6.1 shows the amplitude fluctuation of an MC-CDMA signal for one symbol duration. As can be seen from this figure, the amplitude fluctuations vary significantly, even within one symbol duration.

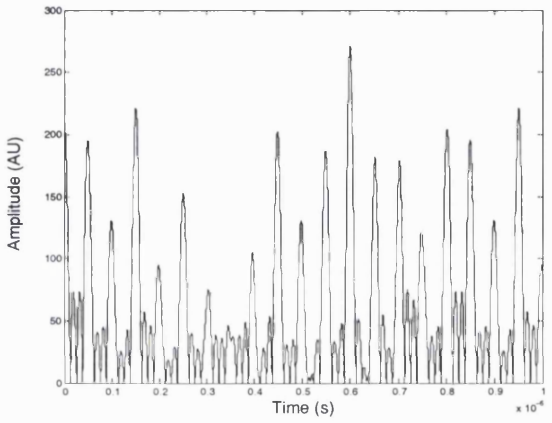

Figure 6.1: Amplitude variation of an MC-CDMA/16QAM symbol with 16 active users

High PAPR results in signal distortion at the transmitter, due to the non-linearity of the amplifier (which is caused by the fact that the amplifier is designed to accommodate the average signal power and not the extreme values). To avoid this distortion, the power of the signal at the input of the amplifier is reduced. This power reduction (or 'back-off') results in inefficient operation of the amplifier.

As described in Section 3.2.2, the PAPR of a bandpass signal, S(t) is given by:

$$PAPR = \frac{P_{peak}}{P_{average}} \tag{6.1}$$

where P_{peak} is the peak power of S(t) and $P_{average}$ is the average power of S(t).

The peak power of a bandpass signal S(t) is, by definition, the average power that would be obtained if the envelope of the equivalent baseband signal ($|\tilde{s}(t)|$) was held constant at its peak value, $\max[|\tilde{s}(t)|]$. This is equivalent to evaluating the average power in an unmodulated

[46] worse case PAPR with 64 subcarriers.
[47] worse case PAPR with 1024 subcarriers

sine wave that has a peak value of $\max[|\tilde{s}(t)|]$ [19, 86][48]. Hence, the peak power of S(t) is given as:

$$P_{peak} = \frac{1}{2}\left[\max|\tilde{s}(t)|\right]^2 \tag{6.2}$$

The average power of a bandpass signal S(t) is given in terms of its equivalent baseband representation, $\tilde{s}(t)$ as:

$$P_{average} = E\left[\lim_{D_{sig.}\to\infty}\left(\frac{1}{D_{sig.}}\int_{D_{sig.}}\frac{1}{2}\left[\tilde{s}(t)\right]^2 dt\right)\right] \tag{6.3}$$

where E[.] is the expectation operator and $D_{sig.}$ is the duration of the signal.

From Equation 6.2 and Equation 6.3, the PAPR is given by:

$$PAPR = \frac{\left[\max|\tilde{s}(t)|\right]^2}{E\left[\lim_{D_{sig.}\to\infty}\left(\frac{1}{D_{sig.}}\int_{D_{sig.}}\left[\tilde{s}(t)\right]^2 dt\right)\right]} \tag{6.4}$$

An alternative measure of the variation in envelope fluctuation of a signal is the *Crest Factor (CF)*, which is defined as the maximum signal value divided by the rms signal value. For an unmodulated carrier, the crest factor is 3 dB whereas the PAPR is 0 dB. The 3 dB difference between PAPR and crest factor also applies to other signals, provided that the centre frequency is large in comparison with the signal bandwidth [19, 105].

The crest factor of the signal can be obtained by using the following expression:

$$CF = \sqrt{PAPR}$$

$$CF = \frac{\max[[s(t)[]}{E\left[\lim_{D_{sig.}\to\infty}\sqrt{\left(\frac{1}{D_{sig.}}\int_{D_{sig.}}\frac{1}{2}\left[\tilde{s}(t)\right]^2 dt\right)}\right]} \tag{6.5}$$

6.1.1 Calculating PAPR using simulation

The peak of a bandpass signal S(t) is given by the maximum of its envelope. In a simulation environment, it is difficult to obtain the real maximum of the envelope as the simulation has to be run for a very long period of time (over all symbol space) in order to capture the real peak. Hence, numerous authors present the CCDF of the PAPR instead of the actual PAPR values [67, 106, 107].

[48] The average power of a sine wave with amplitude A is $A^2/2$.

In this work, the PAPR is calculated over a duration of 10000 multi-carrier CDMA symbols. As the main aim of the work is not to obtain the precise value of the PAPR but to present a comparison between the different implementations, 10000 symbols is assumed to be a sufficient duration for the simulation.

In order to confirm the trends observed for the PAPR, the CCDF of the signal amplitudes at the output of the transmitter (input of the HPA) is also presented.

6.1.2 PAPR reduction techniques

The literature on PAPR reduction for multi-carrier transmission is fairly recent. These techniques were first proposed in the mid 1990s. It is difficult to classify all the proposed schemes into simple categories. The most accepted classification is to divide the schemes proposed into PAPR reduction with distortion and PAPR reduction without distortion. In the first case, the transmitter is not designed for the maximum PAPR range and the transmitted symbols are distorted. In the second case, the PAPR is reduced before the HPA and the transmitted symbols are not distorted.

PAPR reduction with distortion

The simplest way to reduce PAPR is to clip the signal at the transmitter to the desired level. However, this approach degrades the BER and increases the out-of-band radiation (as shown in [101]). The out-of-band radiation can be reduced by filtering the signal after clipping but in this case the signal peaks are partially reintroduced [108].

An alternative approach is peak windowing [100] where large signal peaks are multiplied by a certain window [100, 101]. In [100] a Gaussian shaped window has been employed, but in fact any window can be used (Cosine, Hamming, Kaiser) provided it has good spectral properties. Results presented in [100] and [101] show that peak windowing can reduce the PAPR without significantly increasing the out-of-band radiation. The effect of peak windowing on BER degradation is minor (It is slightly worse than clipping for small values of PAPR [101]).

Distortionless PAPR reduction

These techniques employ some form of coding to reduce the PAPR prior to the non-linear device. The main advantage of these techniques is that they do not cause an increase in the BER degradation or spectral spreading [99, 109]. However, these techniques cause a reduction in throughput. Numerous coding schemes have been proposed to date to reduce the PAPR of the transmitted multi-carrier signal. These include the use of block coding [99, 110], Golay complimentary code sequences [111] and the use of codes with error correcting capabilities [112].

Recently, much research has been done into the use of Partial Transmit Sequence (PTS) [102] and Selective Mapping (SLM) [103] for distortionless PAPR reduction. In PTS, the

transmitter constructs it's transmit signal with low PAPR by coordinated addition of appropriately phased rotated signal parts. In SLM, the transmitter selects one transmitter signal from a set of sufficiently different signal which represent the same signal. In both cases, the PAPR is reduced without distorting the transmitted signal. The main advantage of these schemes over schemes based on coding is the fact that they introduce little redundancy. However, this is at a cost of increased complexity.

6.2 Influence of spreading codes on PAPR

Spreading refers to the operation of multiplying a data sequence by a code sequence. At the transmitter, the user data is spread using the user specific spreading code and at the receiver the data is despread using a replica of the same spreading code. The basic properties of the spreading codes have been presented in Section 2.1.3.

In this work, WH spreading codes have been used as they provide excellent performance in synchronous channels.

WH codes can be constructed using the iterative procedure given by [20]:

$$H_1 = [0], H_2 = \begin{bmatrix} 0 & 0 \\ 0 & 1 \end{bmatrix}, H_4 = \begin{bmatrix} 0 & 0 & 0 & 0 \\ 0 & 1 & 0 & 1 \\ 0 & 0 & 1 & 1 \\ 0 & 1 & 1 & 0 \end{bmatrix} \tag{6.6}$$

$$H_{2N} = \begin{bmatrix} H_N & H_N \\ H_N & \overline{H_N} \end{bmatrix} \tag{6.7}$$

where N is a power of 2 and the over score denotes the binary complement of the bits in the matrix.

Each row of the matrix in (6.6) represents a user specific WH code sequence. For example, in the case of H_4 there are 4 user specific spreading codes. The WH code for user 1 (WH(1)) is [0 0 0 0], WH code for user 2 (WH(2)) is [0 1 0 1] and so on.

A number of authors have studied the influence of spreading codes on the PAPR of the transmitted signal in CDMA based systems. In [113] it has been shown that the PAPR of a CDMA 2000 signal is dependent on the runlength[49] of the WH codes and the PAPR can be reduced by appropriate allocation of the WH code to the next active user. Lau [114] deals with the PAPR variation of IS-95 and CDMA2000 signals for different assignments of the WH codes and concludes that the PAPR of IS-95 and CDMA2000 can be reduced by selectively combining and assigning WH codes (from a set of codes) to different users. Popovic [77] has studied and compared the crest factor and the dynamic range of a number of different classes of spreading code sequences (including Gold codes, Orthogonal Gold codes and Zadoff-Chu codes) for MC-CDMA. Finally, Ochiai and Imai [21] have investigated the PAPR variation of MC-CDMA using

[49] The runlength of the binary WH sequence is given as the number of continuous 0s or continuous 1s in the sequence.

different orthogonal codes (WH codes and Complementary codes) and have shown that for a small number of active users WH codes have a significantly higher PAPR than Complementary codes whereas for a fully loaded system Complementary codes have a marginally higher PAPR than WH codes. The authors also propose a PAPR reduction technique based on the adaptive use of the two orthogonal codes.

This work investigates the PAPR variation of multi-carrier CDMA systems (MC-CDMA and MC-DS-CDMA) with the order of WH code allocation. Section 6.4 presents the PAPR performance of MC-CDMA for different allocations of WH codes and investigates its performance in the presence of HPA non-linearities using the different allocations whereas Section 6.5 presents the PAPR variation of MC-DS-CDMA for different allocations of WH codes and investigates its performance in the presence of HPA (for the different allocations).

In this work (as in the case of the work presented in [21, 113, 114]), multi-cell operation has not been considered (i.e., the data is not multiplied by scrambling code before transmission). However, the following section provides some background on scrambling codes and their effects on the PAPR of the transmitted signal in a CDMA based system.

6.3 Influence of scrambling codes on PAPR

In a multi-cell environment, the user data is multiplied by a base station specific scrambling code as well as a user specific spreading code. The basic concept of scrambling was introduced in Section 2.3.3. Data scrambling is achieved by multiplying the data to be transmitted by a PN code. M-sequence codes and Gold codes are commonly used as scrambling codes in CDMA based systems.

M-sequence codes are generated using linear shift registers with feedback taps (as illustrated in Figure 6.2). For a shift register of size m, the period of the m-sequence code is equal to 2^m-1. The number of possible codes is dependent on the number of feedback connections that produce an m-sequence. A list of the feedback connections for different shift register size is provided in numerous references [75, 76]. Unlike the WH codes described in the previous section, m-sequence codes are not orthogonal. However, they do have a number of useful properties. One of the properties which is exploited in CDMA systems is that for each m-sequence code, a time shifted version of the code is distinct. Hence, the number of codes is equal to the length of the shift register.

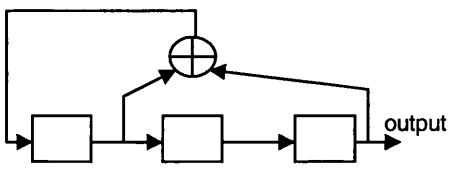

Figure 6.2: M-sequence generator of length 3

Gold codes are generated by combining the output of two m-sequence generators (of the same length) using modulo-2 addition (as shown in Figure 6.3). The number of gold codes is also approximately equal to the period of the codes (2^m+1).

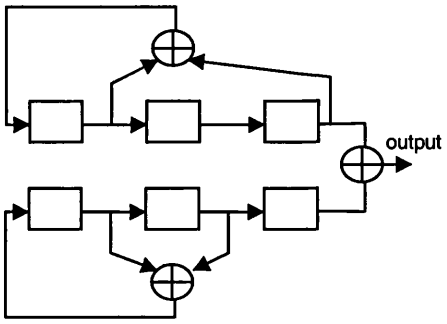

Figure 6.3: Gold code generator of length 3

The influence of scrambling codes on the PAPR of the transmitted MC-CDMA signal has been recently studied at Yeungnam University, Korea. The results show that for a single user case, the PAPR variation is significantly effected by the scrambling code and the WH code allocated to the user. Each WH code has its own optimum scrambling code sequence[50]. For larger number of active users, the PAPR variation is dependent on the scrambling code and the WH code combinations used. Again, each WH code combination has its own optimum scrambling code. Comparison of the peak power of MC-CDMA signal with and without scrambling showed that the peak power of the MC-CDMA signal without scrambling was higher than the peak power of the MC-CDMA signal with scrambling[51].

6.4 MC-CDMA system performance with different WH code allocations

The performance of MC-CDMA with different WH code allocations has been investigated using the transmitter model given in Figure 6.4. (Note that in this work, only BPSK mapping has been considered.) The data at the input of the transmitter is spread and modulated in the same way as the MC-CDMA CIT system described in Chapter 3. However, in this case, the order in which the WH codes are assigned to different users is varied.

[50] Optimum scrambling code refers to the code which provides the lowest PAPR
[51] The material referred to here is based on unpublished work by K. Choi et. al. at Yeungnam University, Korea. The work is expected to be published before the end of 2003.

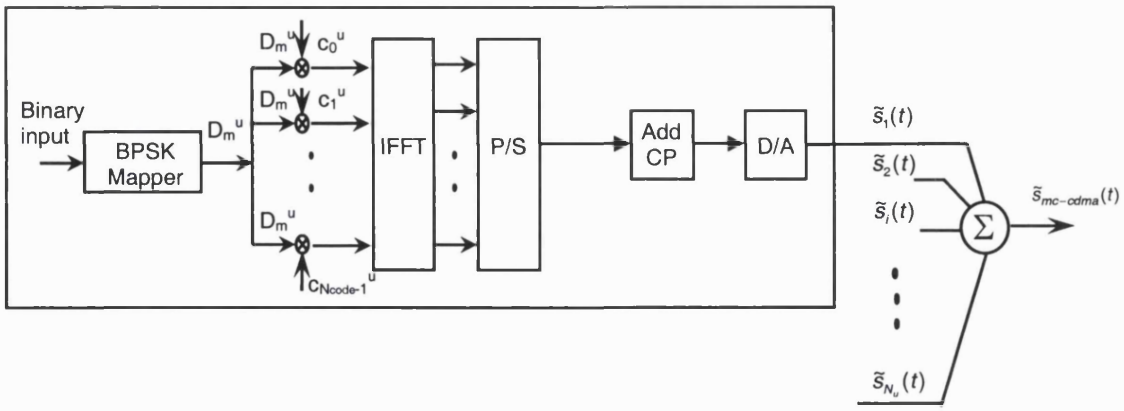

Figure 6.4: Transmitter diagram for the MC-CDMA system

At the receiver, the despreader, knowing the correct allocation of the codes can successfully recover the individual user's data. The receiver used in this work is similar to the receiver model used for MC-CDMA CIT in Section 3.1.1. Hence, it has not been detailed here.

The main system parameters for this investigation are listed in Table 6.2.

Table 6.2: MC-CDMA and MC-DS-CDMA system parameter

Parameter	Value	Parameter	Value
Number of Users, N_{users}	64	Mapping Scheme	BPSK
Spreading code length, N_{code}	N_{users} (64)	FFT size, N_{FFT}	N_{spread}*10*$N_{subcarriers}$
Number of subcarriers, $N_{subcarriers}$	N_{code} (64)	Input sequence	m-sequence
Subcarrier spacing, Δf	$1/(T-T_{cp})$	Data rate	$(\log_2(M))/(T-T_{cp})$
Symbol duration, T	1 μs	Simulation duration	10000 symbols
Cyclic prefix duration, T_{cp}	0.2 μs	Spreading Code	WH Code
Oversampling Factor, N_{spread}	7		

WH code allocation schemes

Three different techniques for the allocations of WH codes have been considered.

WH code allocation scheme-1

This scheme is similar to the allocation scheme used in most CDMA based systems (such as IS-95) where the first WH code, WH(1) is allocated to the first user (user-1), the second WH code, WH(2) is allocated to the second user (user-2) and so on.

WH code allocation scheme-2

This scheme is the inverse of allocation scheme-1. In this case, the last WH code (WH(64))[52] is allocated to user-1, WH(63) is allocated to the user-2 and WH(1) is allocated to user-64.

[52] The maximum number of users and hence the maximum number of codes in the system is 64.

WH code allocation scheme-3

In this scheme, a specific allocation of WH codes has been used. The code allocation was obtained by generating several permutations of the WH code indices (1 to 64) and studying the PAPR of the signal at the output of the transmitter for each permutation. The different permutations considered and the PAPR for each permutation is given in Appendix D. The allocation which produced a low PAPR for small number of active users was chosen for this work.

The WH code indices for each of the three allocation schemes is given in Table 6.3.

Table 6.3: WH code indices for different allocation schemes

User	1	2	3	4	5	6	7	8	9	10	11	12	.....	61	62	63	64
Scheme 1	1	2	3	4	5	6	7	8	9	10	11	12	.....	61	62	63	64
Scheme 2	64	63	62	61	60	59	58	57	56	55	54	53	.....	4	3	2	1
Scheme 3[53]	21	54	3	17	39	50	15	22	45	33	16	62	.....	13	28	55	26

6.4.1 PAPR of MC-CDMA with different WH code allocations

The PAPR of the MC-CDMA signal, $\tilde{s}_{mc-cdma}(t)$ at the output of the transmitter is presented in Figure 6.5 for the three WH code allocation schemes described above.

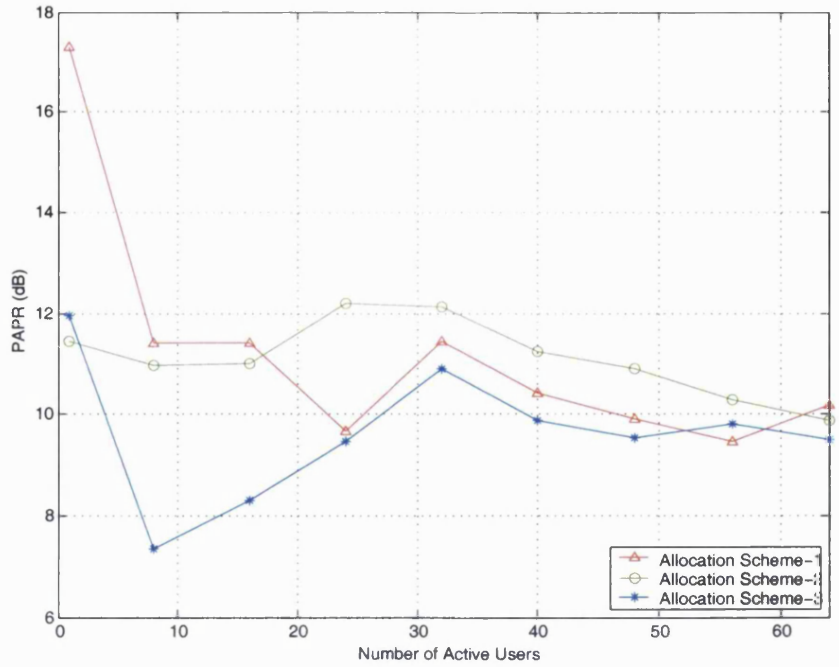

Figure 6.5: PAPR of MC-CDMA signal with different allocations of the WH codes

[53] The complete list for allocation scheme-3:
21 54 3 17 39 50 15 22 45 33 16 62 58 4 20 37 56 43 41 31 57 1 63 51 29 8 34 53 11 12 23 5
40 49 47 18 36 60 7 48 64 42 59 35 14 38 10 30 2 27 46 44 32 9 19 52 25 61 6 24 13 28 55 26

Observation of Figure 6.5 shows that the PAPR performance of the MC-CDMA system is influenced significantly by the WH code sequence allocation, for example, the PAPR of allocation scheme-1 is much higher than that of allocation scheme-3. Obviously this is only the case for a small number of active users. For a large number of active users, any code allocation yields approximately the same PAPR.

As described in Section 6.1.1, in a simulation environment, it is difficult to obtain the real peak (and hence the real PAPR of the signal) as the simulation has to be run for a very long time, over all symbol space. Hence, in order to confirm the trends observed for the PAPR variation, the CCDF of the signal amplitudes at the output of the transmitter have been plotted in Figure 6.6 for different number of active users. The CCDF graphs confirm the trends observed for the PAPR variation in Figure 6.5 (i.e., for a single user case, allocation scheme-2 has the lowest signal amplitudes and hence the lowest PAPR at the output of the transmitter, whereas allocation scheme-1 has the highest signal amplitudes and the highest PAPR at the output of the transmitter. For the 32 user case, allocation scheme-3 has the lowest signal amplitudes and the lowest PAPR at output of the transmitter, whereas allocation scheme-2 has the highest signal amplitudes and hence the highest PAPR).

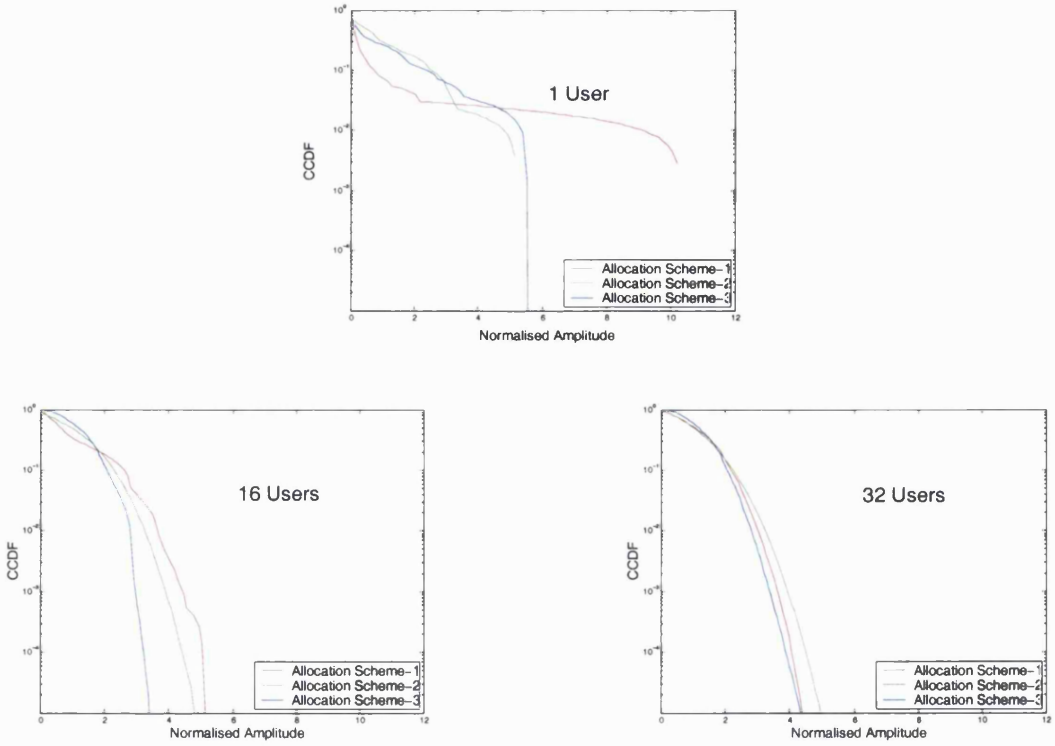

Figure 6.6: CCDF of the MC-CDMA signal amplitudes at the output of the transmitter with different WH code allocations

The variation in the PAPR performance with the allocation of the WH codes can be explained as follows. In an MC-CDMA system (Figure 6.4), the amplitude of the signal at the output of the transmitter is determined by the data transmitted over the individual subcarriers.

More specifically, the amplitude of the signal at the output of the transmitter is determined by $D_m^u c_n^u$ (Figure 6.4). For a given MC-CDMA symbol, the value of D_m^u is the same over all subcarriers. Hence, the amplitude of the signal at the output of the transmitter is dependent on c_n^u, the individual chips of the user specific WH code.

It has been stated in [21, 110] that binary sequences with the same odd and even bit values generate the highest PAPR. In the case of a 64x64[54] WH code matrix (given in [16]), WH(1) consists of all 0s and WH(2) consists of alternate 1s and 0s. Hence, WH(1) and WH(2) generate the highest PAPR.

From Table 6.3, it can be observed that in the case of allocation scheme-1, the *"bad"*[55] WH code sequences appear at the beginning, i.e., they are assigned to user-1 and user-2 (shaded region in Table 6.3). Hence, in this case, the PAPR for the first few active users is very high. In allocation scheme 2, the *"bad"* sequences are allocated to the users at the end. In this case, the transmitted signal consists of the superposition of all the users data and therefore the overall PAPR is much lower than that of allocation scheme-1. In allocation scheme-3, the *"bad"* sequences are allocated to users in the middle (user-22 and user-49). In this case, the transmitted signal consists of the superposition of a number of active user's data and therefore the overall PAPR at the output of the transmitter is lower than that of allocation scheme-1.

Observation of Figure 6.5 also reveals that as the number of users increases, the difference between the PAPR obtained with different allocations reduces. (This trend is also observed for DS-CDMA in [114].) For a fully loaded system, the PAPR of all 3 allocations is approximately the same. This is because of the fact that in a fully loaded system, all three allocation schemes will utilise all 64 codes.

The results presented on Figure 6.5 and Figure 6.6 suggests that in the presence of HPA non-linearities some MC-CDMA signals may perform better than others, depending on the WH code allocation strategy. To be precise, MC-CDMA signals whose code allocation yields a lower PAPR (allocation scheme-3) would perform better than MC-CDMA signals whose code allocation yields a higher PAPR (allocation scheme-1). This has been investigated in the next section.

6.4.2 Performance of MC-CDMA in the presence of non-linearities with different WH code allocations

The performance of MC-CDMA system is investigated in the presence of SSPA non-linearities described in Section 5.1.3 and Section 5.1.4, in terms of total degradation and power in the adjacent sidebands (Section 5.2) for the three WH code allocation schemes described above.

---

[54] A 4x4 WH matrix is given in (6.6).
[55] WH codes sequences consisting of the same odd and even bit values are referred to as "bad" sequences in this work.

The in-band distortion caused by the SSPA non-linearities is given in Figure 6.7, Figure 6.8 and Figure 6.9 in terms of the total degradation, for 1, 16 and 32 active users. Observation of the figure reveals that the performance of MC-CDMA in the presence of SSPA non-linearities is indeed dependent on the WH code allocation technique. The variation in performance is particularly significant for a small number of active users, where the PAPR (and the CCDF of the transmitted signal amplitudes) has been found to vary greatly as a function of the WH code allocation. The variation in performance is not so significant for a larger number of active users (Figure 6.9), where it has been found that any code allocation yields approximately the same PAPR.

Studying the out-of-band distortion of the system in terms of power in the adjacent sidebands (Figure 6.10) reveals that as the number of active users increases, the difference between the power in the adjacent sidebands for different allocations reduces. Hence, as the difference between the PAPR variation for the three allocations reduces, the difference in the out-of-band distortion for the three allocations also reduces.

For a given number of active users, the dependence of spectral spreading on PAPR variation is more evident for small OBO values (<5dB) than large OBO values. For example, for all three allocation schemes, the spectral spreading of the different allocations is in step with the PAPR variation for OBO=3 dB and OBO=4 dB. For OBO values greater than 4dB, this is no longer the case.

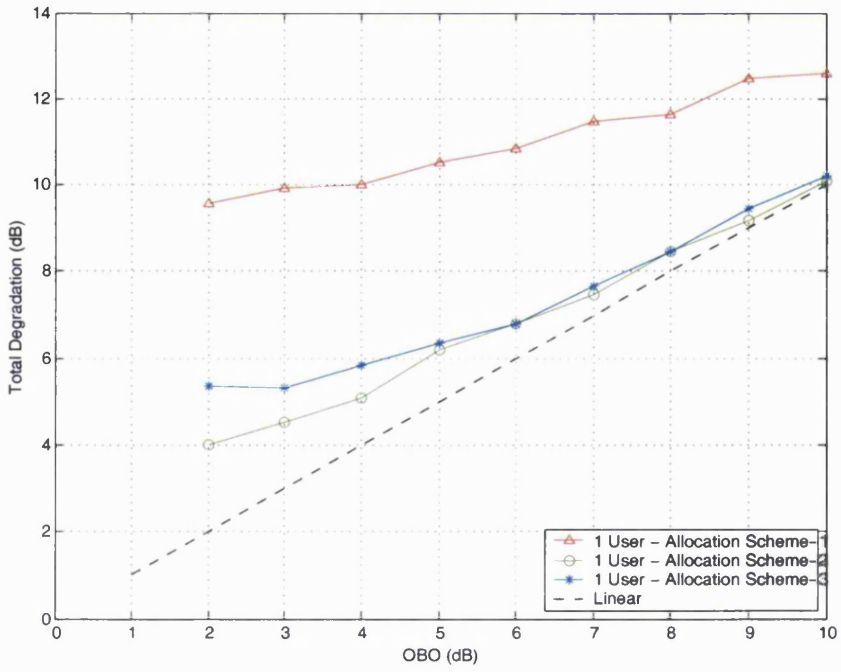

Figure 6.7: Total degradation of MC-CDMA with different allocations of WH codes for 1 active user

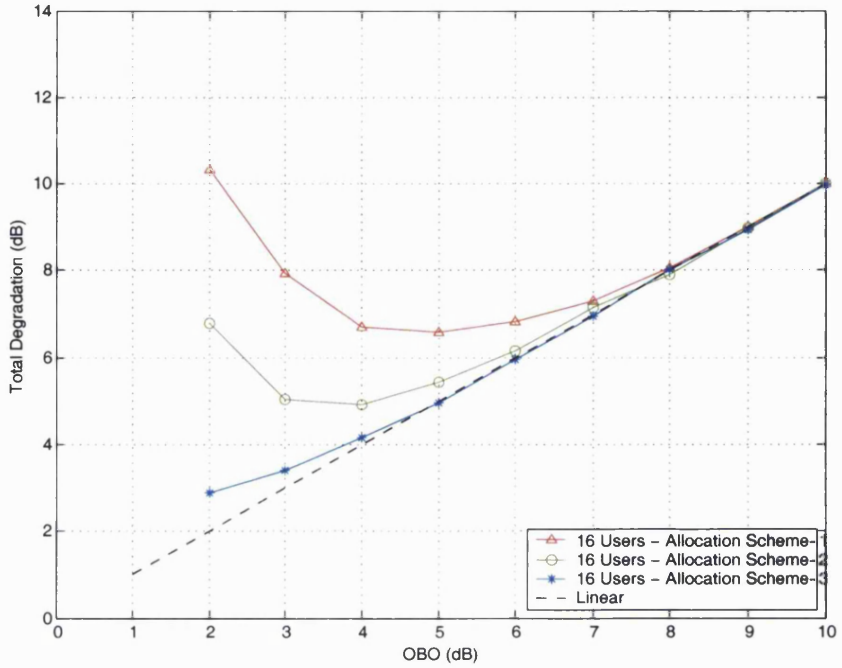

Figure 6.8: Total degradation of MC-CDMA with different allocations of WH codes for 16 active users

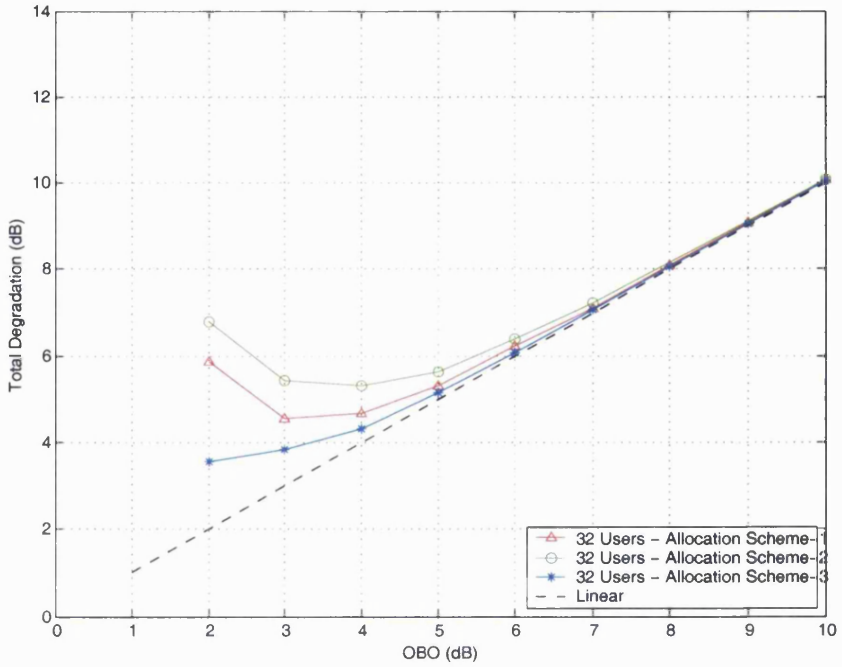

Figure 6.9: Total degradation of MC-CDMA with different allocations of WH codes for 32 active users

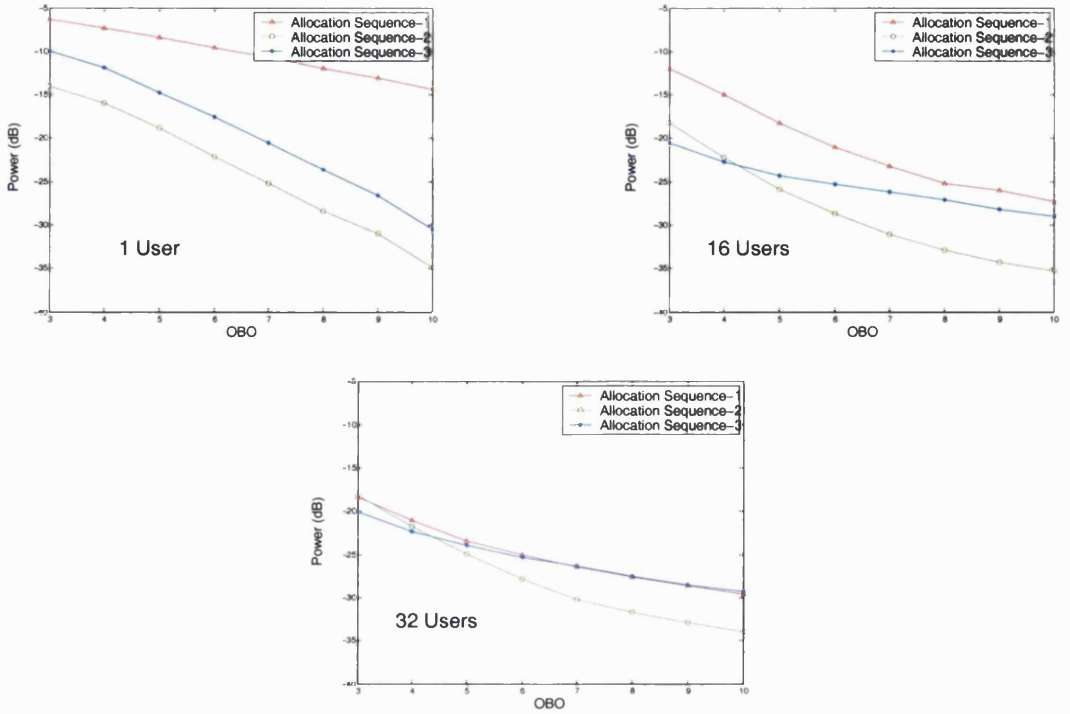

Figure 6.10: Power in the adjacent sidebands of non-linearly amplified MC-CDMA signal with different allocations of the WH code

6.5 MC-DS-CDMA system performance with different WH code allocations

This section describes the performance of MC-DS-CDMA with different allocations of the WH codes. The MC-DS-CDMA scheme employed in this investigation is similar to the MC-DS-CDMA CIT scheme described in Chapter-4. The transmitter model is shown in the figure below.

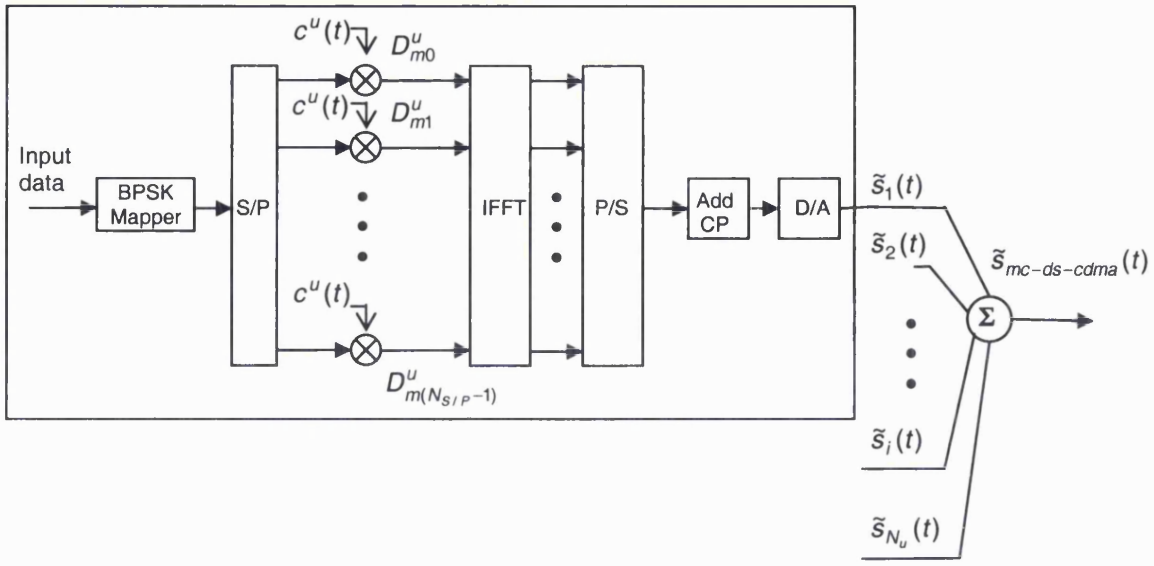

Figure 6.11: MC-DS-CDMA transmitter

The order in which the WH codes are allocated to different users is the same as the allocation schemes described in Section 6.4 for the MC-CDMA case (summarised in Table 6.3).

6.5.1 PAPR of MC-DS-CDMA with different WH code allocations

The PAPR of the MC-DS-CDMA signal at the output of the transmitter, for the three different WH code allocations is presented is Figure 6.12. Observation of the figure reveals that using different allocations of the WH codes does not have a significant effect on the PAPR of the transmitted signal. The CCDF of the MC-DS-CDMA signal amplitudes (Figure 6.13) also shows that the signal amplitudes at the output of the transmitter are independent of the WH code allocation, i.e., for a given number of active users, the CCDF of the signal amplitudes at the output is the same for all three allocations.

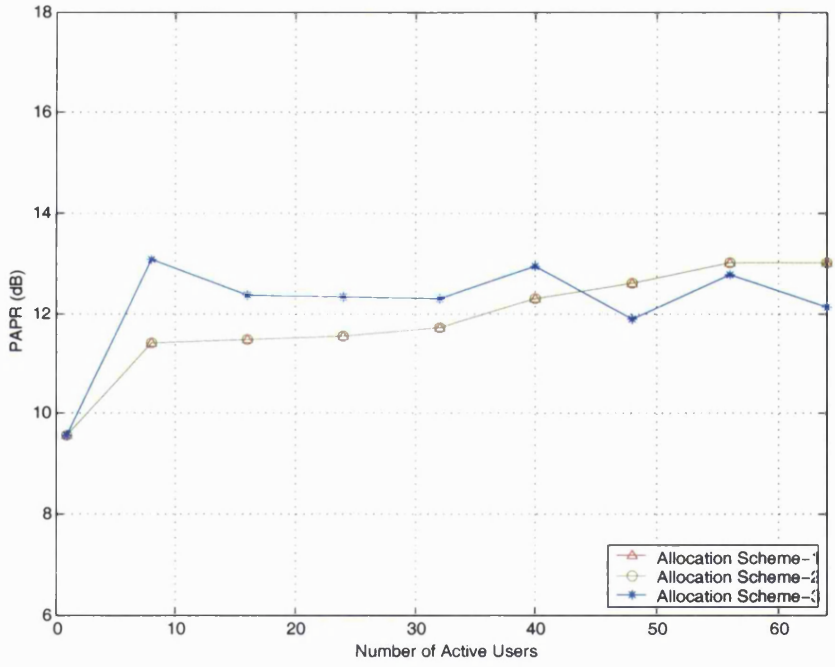

Figure 6.12: PAPR of MC-DS-CDMA signal with different allocations of the WH codes

The trend observed in Figure 6.12 for the PAPR variation with different allocations of the WH codes can be explained as follows. The amplitude of the MC-DS-CDMA signal at the output of the transmitter in Figure 6.11 is determined by the data transmitted over the individual subcarriers, D_{mn}^{u} (Figure 6.11). D_{mn}^{u} is the product of the parallel output of the S/P converter and the user specific WH code. In the case of MC-DS-CDMA, each parallel stream is multiplied by the same copy of the spreading code and therefore, for a given MC-DS-CDMA symbol, the value of c_{m}^{u} is the same over all subcarriers. Hence, the amplitude variation of the signal at the

output of the transmitter is dependent on the parallel output of the S/P converter. The user data at the input of the S/P converter is random in nature and therefore the possibility of getting an input sequence with the same odd and even bit values for the length $N_{S/P}$ is very small.

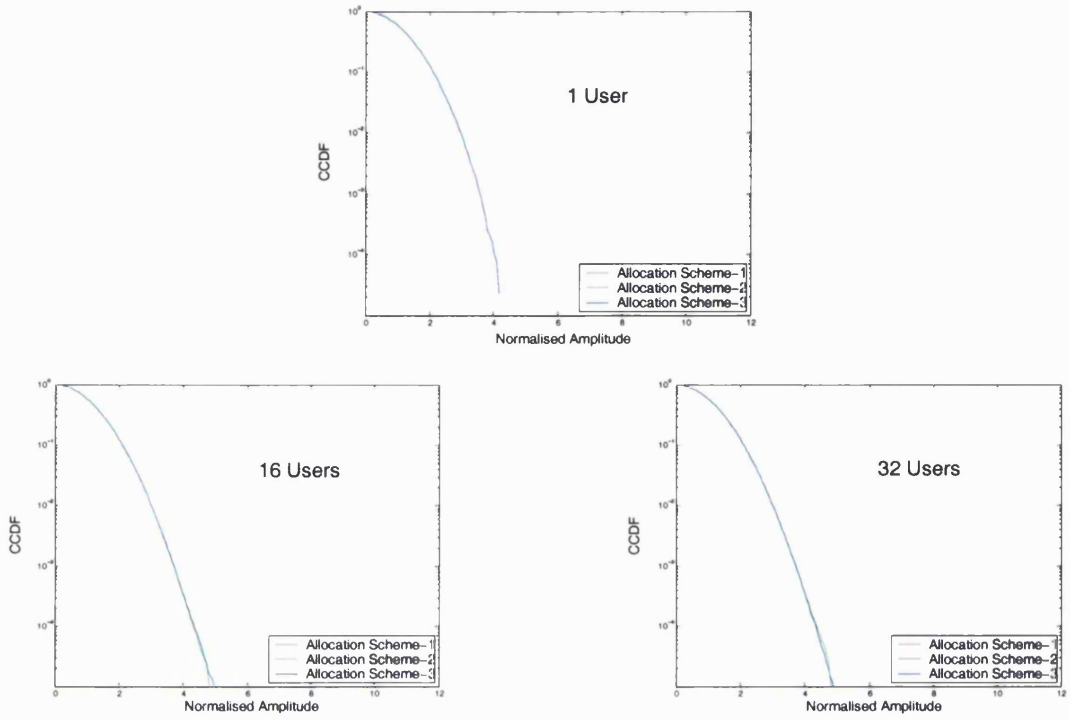

Figure 6.13: CCDF of the MC-DS-CDMA signal amplitudes at the output of the transmitter with different WH code allocations

The nearly constant PAPR for the different allocation schemes suggests that the performance of MC-DS-CDMA signal in the presence of HPA non-linearities is independent of the WH code allocation scheme. This is investigated in the next section.

6.5.2 Performance of MC-DS-CDMA in the presence of non-linearities with different WH code allocations

As in the MC-CDMA case, the performance of MC-DS-CDMA in the presence of SSPA non-linearities is studied for 1, 16 and 32 users in terms of total degradation and spectral spreading. Figure 6.14, Figure 6.15 and Figure 6.16 show the total degradation of the MC-DS-CDMA system for 1, 16 and 32 users, respectively. Observation of these figures reveals that the in-band distortion of MC-DS-CDMA (in terms of T_D) is indeed nearly independent of the WH code allocation scheme.

The spectral spreading of the MC-DS-CDMA system in terms of the power in the adjacent sidebands is given in Figure 6.17. The results presented in this figure show that the out-of-band distortion of MC-DS-CDMA system is also independent of the WH code allocation, i.e., for a

given number of active users, the power in the adjacent sidebands is the same for all three allocation schemes.

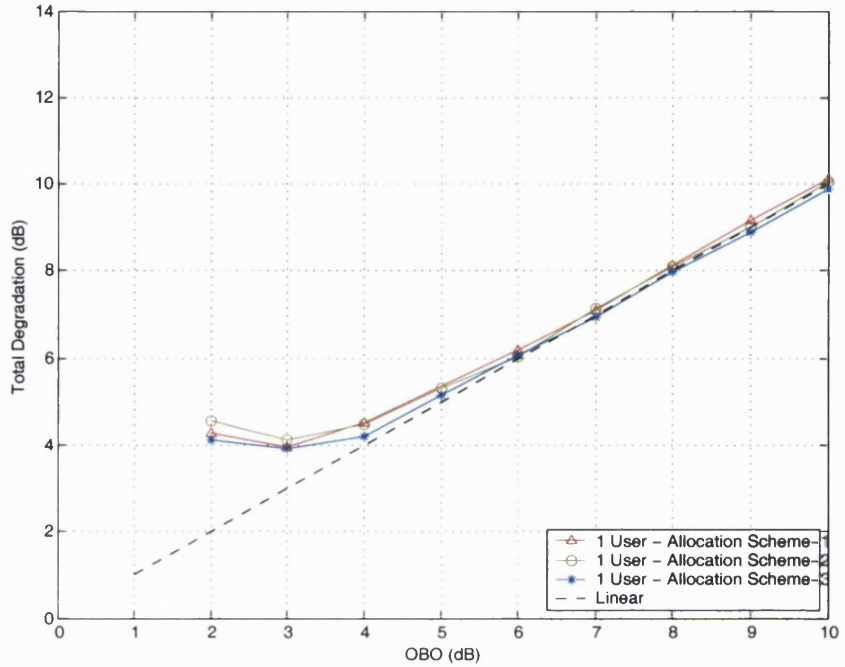

Figure 6.14: Total degradation of MC-DS-CDMA with different allocations of WH codes for 1 user

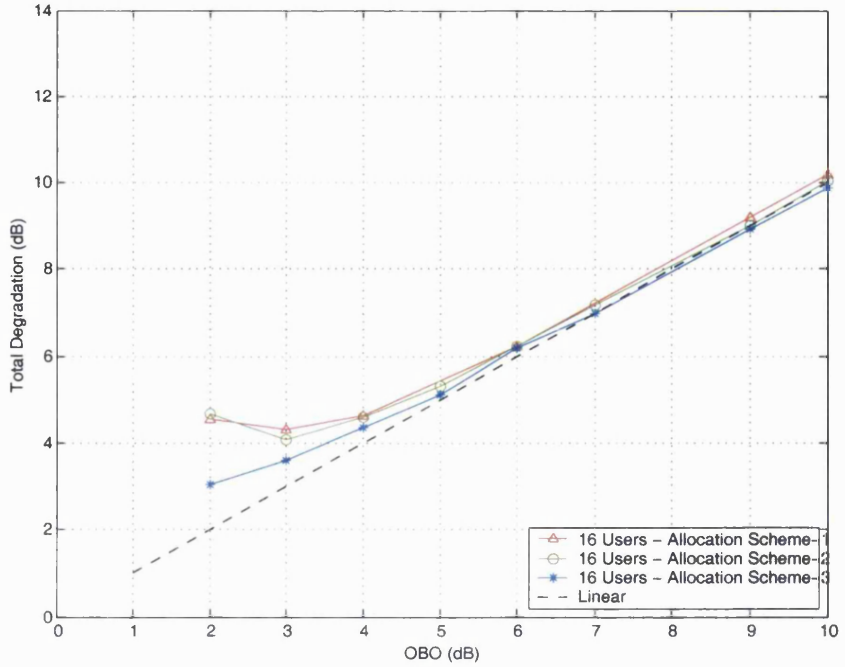

Figure 6.15: Total degradation of MC-DS-CDMA with different allocations of WH codes for 16 users

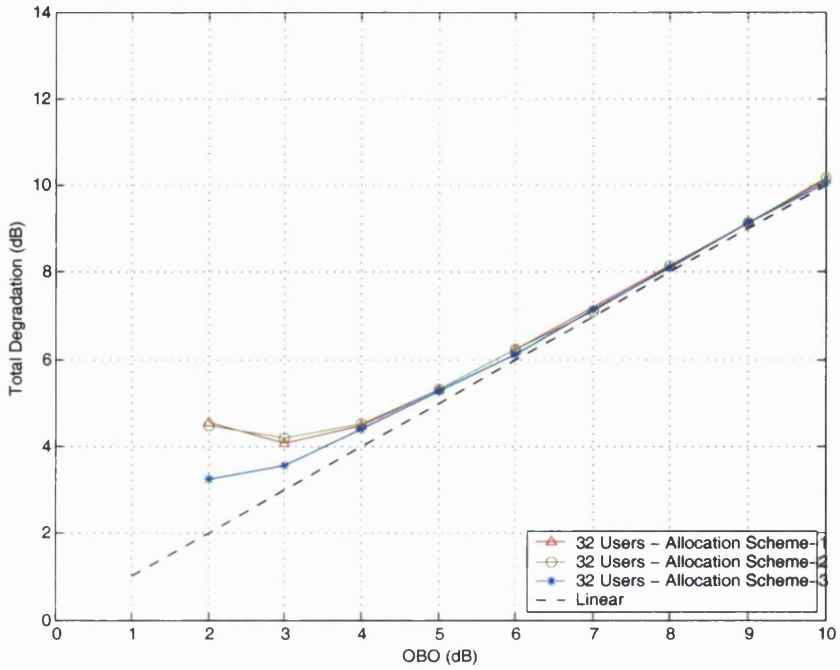

Figure 6.16: Total degradation of MC-DS-CDMA with different allocations of WH codes for 32 users

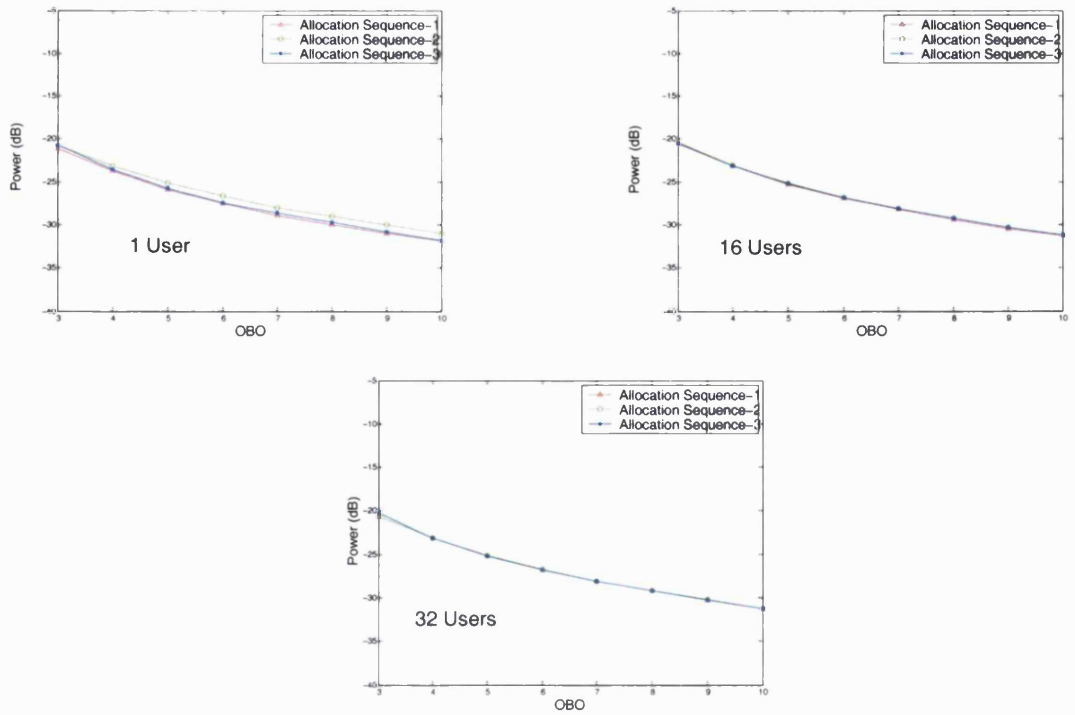

Figure 6.17: Power in the adjacent sidebands of non-linearly amplified MC-DS-CDMA signal with different allocations of WH code

It is important to point out that the results presented in this chapter have been obtained for a system which does not include scrambling codes. As stated in Section 6.3, the PAPR of

the multi-carrier CDMA signal is influence by the scrambling process as well as the spreading process. Hence, the PAPR variation and the performance of the system in the presence of non-linearities will differ when a multi-cell scenario is considered. Further work is required to analyse the effects of the spreading code allocation strategies in a multi-carrier CDMA system with scrambling.

6.6 Summary

The performance of multi-carrier CDMA systems with different WH code allocation schemes was investigated in this chapter. Three different schemes for the allocation of WH codes to different users were considered and their effects on the PAPR of the transmitted signal investigated. It was observed that in the case of MC-CDMA, the PAPR of the transmitted signal was significantly influenced by the WH code allocation scheme, particularly when the number of active users was small. For large number of active users, all allocation schemes produce the same PAPR. In the case of MC-DS-CDMA, changing the allocation of the WH codes had no significant effect on the PAPR of the transmitted MC-DS-CDMA signal.

As the performance of a signal in the presence of HPA non-linearities is dependent on the PAPR of the signal at the input, the performance of the two multi-carrier CDMA schemes with different WH code allocations was investigated in the presence of HPA non-linearities. The results showed that for the MC-CDMA case, the in-band and out-of-band distortion of the system was effected by the allocation of the WH code, especially when the number of active users was small. In the MC-DS-CDMA case, changing the allocation of the WH code made little difference to the in-band and out-of-band distortion of the system.

The work presented in this chapter introduces a technique for reducing the PAPR of the MC-CDMA system (and hence improvement in the performance of the system in the presence of HPA non-linearities) by appropriate allocation of the WH codes to different users in the system. Unlike most of the PAPR reduction schemes, this technique does not result in reduction in throughput or increased complexity. Further work is now required to analyse the effects of the spreading code allocation strategies in a multi-carrier CDMA system with scrambling.

The next chapter presents concluding remarks and summarises the main outcomes of the research work, together with suggestions for further work.

Chapter 7

Concluding remarks

Design issues related to multi-carrier CDMA systems have been addressed in this thesis. The combination of multi-carrier CDMA with higher order PSK/QAM mapping schemes has been investigated by the modelling and simulation of various architectures in the presence of AWGN and HPA non-linearities.

The concept of multi-carrier CDMA was introduced in Chapter 2. The chapter outlined the fundamentals of CDMA and MCM and detailed the three main multi-carrier CDMA schemes proposed in the literature (namely, MC-CDMA, MC-DS-CDMA and MT-CDMA).

The combination of multi-carrier CDMA with higher order PSK/QAM mapping schemes was investigated through the study of a generic architecture and the proposals of new implementation strategies in Chapter 3 and Chapter 4.

Two different architectures for combining MC-CDMA with PSK/QAM mapping were presented in Chapter 3. The first architecture combined the input data in serial format and was termed *combining in time (CIT)* whereas the second architecture combined the data in parallel format and was termed *combining in frequency (CIF)*. Increasing the order of the PSK/QAM scheme in the first case results in an increase in the number of data bits transmitted over a given timeslot whereas increasing the order of the mapping in the second case resulted in a reduction in the number of subcarriers (and hence a reduction in the transmitted signal bandwidth).

Investigation of the performance of the two implementations (in terms of power efficiency, PAPR, spectral efficiency and implementation complexity) showed that increasing the order of PSK/QAM scheme in MC-CDMA CIT resulted in a degradation in the power efficiency and an increase in the spectral efficiency. The PAPR also increased for higher order mapping schemes however, this was only significant for small number of active users. The implementation complexity for different mapping schemes remained unchanged. Hence, increasing the order of

the mapping scheme in the MC-CDMA CIT case resulted in better spectral efficiency, at a cost of reduced power efficiency.

Increasing the order of the PSK/QAM mapping scheme in MC-CDMA CIF case resulted in severe degradation in the BER performance and an improvement in the spectral efficiency and implementation complexity. The PAPR showed slight variation the different mapping schemes. Hence, in the case of MC-CDMA CIF, increasing the order of mapping results in better spectral efficiency and reduced implementation complexity, at a cost of reduced power efficiency.

Comparison of the performance of the two MC-CDMA implementations (CIT and CIF), for a given PSK/QAM mapping scheme showed that CIT provided better BER performance compared to CIF, however, CIF provided considerable reduction in terms of the implementation complexity (given throughout this thesis in terms of MOPS) and a small advantage in terms of the PAPR.

The BER comparison for the two implementations was carried out for a single user case as the simple receiver structure proposed for CIF could only successfully operate for a single user case. Multiuser structures were not studied here and should be the subject of future research.

The performance of MC-DS-CDMA incorporating higher order PSK/QAM mapping was the subject of Chapter 4. In the case of MC-DS-CDMA, three different implementations for incorporating PSK/QAM mapping into the MC-DS-CDMA scheme were considered. The first implementation was similar to the MC-CDMA CIT implementation in which the input data was combined in serial format before being spread and multi-carrier modulated and was referred to as CIT-SC. The second implementation was a modification of the first in which the input data was combined in parallel before being spread and multi-carrier modulated. This implementation was referred to as CIT-PC. The final implementation was similar to the CIF implementation of MC-CDMA in which the data was combined in parallel after being spread but before being multi-carrier modulated.

Investigating the performance of the three MC-DS-CDMA implementations for different PSK/QAM schemes showed that in the case of CIT-SC, increasing the order of mapping resulted in increased spectral efficiency. However, it also resulted in greater BER degradation. The PAPR variation and MOPS requirements remained unchanged for the different mapping schemes.

Increasing the order of the mapping scheme in CIT-PC resulted in improved spectral efficiency and reduced implementation complexity at the cost of increased BER degradation.

In the case of MC-DS-CDMA CIF, increasing the order of the mapping scheme reduced the number of subcarriers. It also resulted in improved spectral efficiency and reduced implementation complexity. However, it also caused degradation in the BER performance.

Comparing the performance of the three MC-DS-CDMA implementations showed that for a given mapping scheme, CIT-SC and CIT-PC provided the same spectral efficiency and power

efficiency, however, CIT-SC could accommodate higher number of data bits over a given symbol duration whereas CIT-PC could provide reduced implementation complexity. An advantage of using CIT-PC instead of CIT-SC is that it performs the mapping at a lower rate.

The effects of HPA non-linearities on the performance of multi-carrier CDMA systems incorporating higher order PSK/QAM mapping was the subject of Chapter 5. The effects of an HPA on an input signal with varying signal amplitude are classified in terms of in-band distortion (resulting in BER degradation) and out-of-band distortion (resulting in spectral spreading). The level of in-band and out-of-band distortion caused by the HPA (when MC-CDMA and MC-DS-CDMA signals were used as inputs) was investigated in terms of total degradation (T_D) and power in the adjacent sidebands.

The performance of the two multi-carrier CDMA schemes was analysed for 1, 16 and 32 active users in order to study the effect of changing the number of active users on the performance of the system. In the MC-CDMA case, it was observed that the in-band distortion of the system improved with an increase in the number of active users. This trend was explained through the study of the CCDF of the signal amplitudes, at the input of the HPA. The study showed that as the number of active users increased, the range of amplitudes present in the transmitted MC-CDMA signal decreased and hence the probability of the signal reaching the saturation region also decreased.

In the MC-DS-CDMA case, it was observed that changing the number of active users did not have an effect on the in-band distortion of the system. This was observed to be due to the fact that the range of amplitudes present in the transmitted MC-DS-CDMA signal were independent of the number of active users.

Comparison of the performance of the two multi-carrier CDMA systems for different number of active users showed that MC-DS-CDMA experienced lower in-band distortion as compared to MC-CDMA systems, for small number of active users. For large number of active users, the difference in performance of the two systems was not significant.

The out-of-band distortion of MC-CDMA was observed to improve with the number of active users (due to the fact that as the number of active users increased, the amplitudes of the transmitted signal reduced). The out-of-band distortion of MC-DS-CDMA was observed to be independent of the number of active users. Overall, the out-of-band distortion of MC-DS-CDMA was lower than MC-CDMA. Hence, if adjacent channel interference is a critical issue in the system, MC-DS-CDMA should be preferred over MC-CDMA.

Investigating the performance of the two multi-carrier CDMA systems in the presence of HPA non-linearities with different PSK/QAM mapping schemes showed that in both systems (MC-CDMA and MC-DS-CDMA), increasing the order of mapping increased the total degradation, T_D, of the system. Overall, the total degradation for MC-DS-CDMA was much lower than that for MC-CDMA. Increasing the order of the mapping scheme did not have a significant effect on the out-of-band distortion of either scheme. This was attributed to the fact that the amplitudes of the transmitted signal for different PSK/QAM mapping remained

unchanged (for a given multi-carrier CDMA scheme). It was concluded that increasing the data rate of the system by using higher order mapping did not affect the adjacent channel interference of the system and only caused an increase in the BER degradation.

The variation of multi-carrier CDMA system performance with the allocation of WH codes was studied in Chapter 6. The investigation concluded that in the MC-CDMA case, changing the allocation of the WH code sequence affected the BER performance and spectral spreading of the system in the presence of HPA non-linearities (particularly for a small number of active users). In the MC-DS-CDMA case, changing the allocation of the WH codes did not cause a significant change in the BER performance of the system nor did it affect the spectral spreading of the transmitted signal. The results showed that the performance of an MC-CDMA system in the presence of HPA non-linearities can be improved by simply changing the allocation of the WH codes to different users. Judicious choice of the WH codes is expected to result in improvement in the performance without reduction in throughput or increase complexity.

7.1 Recommendations for future work

Based on the knowledge and experience acquired during this work, several areas for future research can be suggested. These are:

- Development of a receiver architecture (based on soft demodulation) to facilitate the successful demodulation of multiuser signal for implementation-2 (CIF) in Chapter 3 and Chapter 4.

- Extension of the work presented in Chapter 5 to consider the effects of a multipath fading channel. The performance of MC-CDMA and MC-DS-CDMA incorporating different mapping schemes, in the presence of AWGN and AWGN-HPA has been studied in this work, assuming a non-fading channel. However, consideration of the performance of these PSK/QAM schemes in the presence of AWGN, HPA and multipath is an important area of research for wireless system.

- The multi-carrier CDMA systems used in this research have been assumed to be synchronous. In order to acquire further insight into the performance of multi-carrier CDMA systems with higher order mapping, the effects of frequency offset and timing offset should also be considered.

- The investigation presented in Chapter 6 showed that the performance of the MC-CDMA system in the presence of HPA non-linearities was significantly influenced by the allocation of the WH codes to different users. Hence, the degradation caused by the HPA can be

reduced by appropriate allocation of the WH codes. Further work is required to develop a scheme for code allocation.

- This work has employed the WH codes for user separation. Research can be extended to investigate the variation of PAPR (and the performance of the MC-CDMA system in the presence of HPA no-linearities) using other orthogonal code sets such as complementary codes.

Appendix A

MC-CDMA CIF receiver

The simple receiver model proposed for MC-CDMA implementation-2 (CIF) in Chapter 3 can only successfully demodulate data for a single user case due to the fact that HDD is performed before user separation (despreading). This appendix demonstrated how HDD before user separation can result in demodulation errors. A simple set-up is considered with two receiver models (one with HDD and one without HDD) and it is shown that the receiver without HDD can successfully demodulate data for a multiple user case whereas the one with HDD produces errors.

Figure A.1 shows the simplified transmitter model for MC-CDMA implementation 2 (CIF).

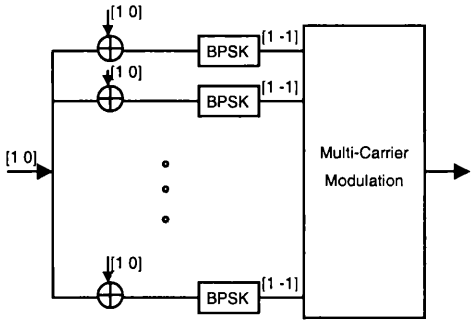

Figure A.1: MC-CDMA CIF transmitter- model A

If the data at the input of the transmitter is of the form [1 -1] and the code chips are of the form [-1 1] (as shown in Figure A.2), then the product of the two will be the same as the data at the output of the BPSK mapper in Figure A.1, provided the following mapping rule is used.

	Model A	**Model B**
Data bit	0	-1
	1	1
Code chip	0	1
	1	-1

In order to distinguish between the two cases, the transmitter model presented in Figure A.1 is referred to as model A and the transmitter model presented in Figure A.2 is referred to as model B.

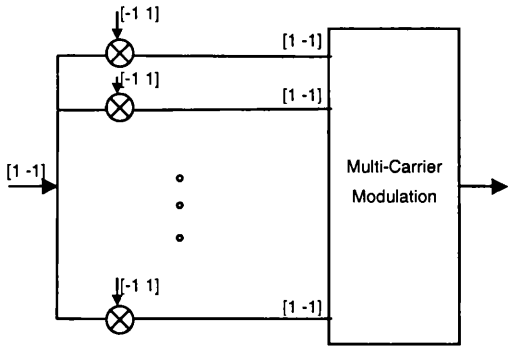

Figure A.2: MC-CDMA CIF transmitter-model B

For the two transmitter models shown above, the corresponding receiver models are presented in Figure A.3 and Figure A.4.

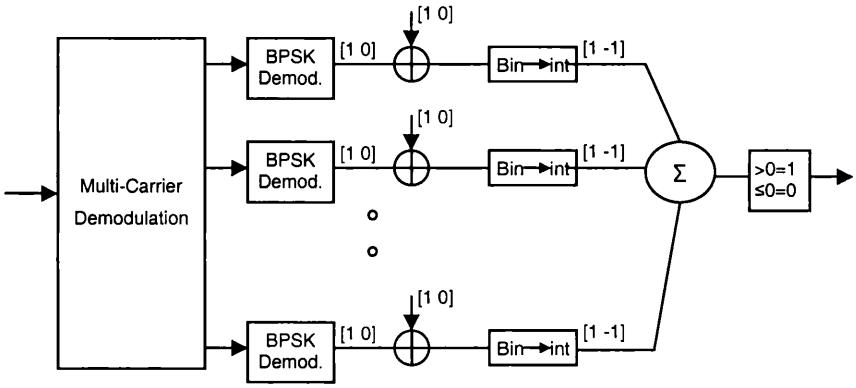

Figure A.3: MC-CDMA CIF receiver-model A

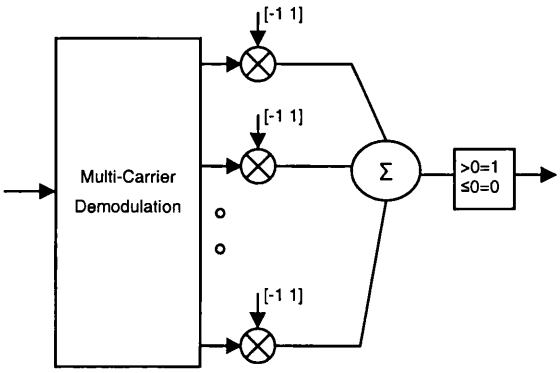

Figure A.4: MC-CDMA CIF receiver-model B

As the transmitted data is the same in both cases, it can be demodulated by either one of the receivers shown in Figure A.3 and A.4.

Consider a system with two active users and a perfect channel, with the following parameters:

Maximum number of users	4
Length of WH code	4
Number of subcarriers	4
Input	
Model A	0 or 1
Model B	(-1) or 1
WH code for user-1	
Model A	0 0 0 0
Model B	1 1 1 1
WH code for user 2	
Model A	1 0 1 0
Model B	-1 1 -1 1

For a system with 2 active users, there are 4 possible input scenarios (Table A.1).

Table A.1: Input scenarios for two active users

	Scenario-1	**Scenario-2**	**Scenario-3**	**Scenario-4**
User	Model-A(Model-B)	Model-A(Model-B)	Model-A(Model-B)	Model-A(Model-B)
1	0(-1)	1(1)	1(1)	0(-1)
2	1(1)	1(1)	0(-1)	0(-1)

The following sections present the data at various points in the transmitter and receiver for the 4 possible input scenarios, for model A and model B.

A.1 Model A

Scenario-1

Transmitter

	Input	WH Code	Input ⊕ Code	BPSK Mod.
User-1	0	0000	0000	-1 -1 -1 -1
User-2	1	1010	0101	-1 1 -1 1
Transmitted data				-2 0 -2 0

Receiver

	Received Data	BPSK Splice	Demod. Demap	WH Code	Decoded output	Bin-to-int	Σ	>0=1 ≤0=0
User-1	-2 0 -2 0	-1 1 -1 1	0 1 0 1	0000	0101	-1 1 -1 1	0	0
User-2	-2 0 -2 0	-1 1 -1 1	0 1 0 1	1010	1111	1111	4	1

In this case, the user data is successfully recovered at the receiver.

Scenario-2

Transmitter

	Input	WH Code	Input ⊕ Code	BPSK Mod.
User-1	1	0000	1111	1111
User-2	1	1010	0101	-1 1 -1 1
Transmitted data				0 2 0 2

Receiver

	Received Data	BPSK Splice	Demod. Demap	WH Code	Decoded output	Bin-to-int	Σ	>0=1 ≤0=0
User-1	0 2 0 2	1111	1111	0000	1111	1111	4	1
User-2	0 2 0 2	1111	1111	1010	0101	-1 1 -1 1	0	0

In this case, the recovered data at the output of the receiver (for user-2) is not the same as the transmitted data and hence an error has occurred.

Scenario-3

Transmitter

	Input	WH Code	Input ⊕ Code	BPSK Mod.
User-1	1	0000	1111	1111
User-2	0	1010	1010	1 -1 1 -1
Transmitted data				2 0 2 0

Receiver

	Received Data	BPSK Splice	Demod. Demap	WH Code	Decoded output	Bin-to-int	Σ	>0=1 ≤0=0
User-1	2 0 2 0	1111	1111	0000	1111	1111	4	1
User-2	2 0 2 0	1111	1111	1010	0101	-1 1 -1 1	0	0

Scenario-4

Transmitter

	Input	WH Code	Input ⊕ Code	BPSK Mod.
User-1	0	0000	0000	-1 -1 -1 -1
User-2	0	1010	1010	1 -1 1 -1
Transmitted data				0 -2 0 -2

Receiver

	Received Data	BPSK Splice	Demod. Demap	WH Code	Decoded output	Bin-to-int	Σ	>0=1 ≤0=0
User-1	0 -2 0 -2	1 -1 1 -1	1010	0000	1010	1 -1 1 -1	0	0
User-2	0 -2 0 -2	1 -1 1 -1	1010	1010	0000	-1-1-1-1	-4	0

From the tables above, it can be seen that in the case of scenario-1, 3 and 4 the transmitted user data is recovered correctly at the receiver. However, in the case of scenario 2, the second user's data is not recovered correctly and hence an error has occurred.

In order to confirm that the error in demodulation occurs due to the hard decision demapping, model B employs a receiver which does not require hard decision demapping before user separation.

The next section considers the 4 input scenarios for model B. The mapping of the input data and the WH codes is done such that the data transmitted on each subcarrier is the same for model A and model B.

A.2 Model B

Scenario-1

Transmitter

	Input	WH Code	Input x Code
User-1	-1	1111	-1 -1 -1 -1
User-2	1	-1 1 -1 1	-1 1 -1 1
Transmitted data			-2 0 -2 0

Receiver

	Received Data	WH Code	Decoded data	Σ	>0=1 ≤0=0
User-1	-2 0 -2 0	1111	-2 0 -2 0	-4	-1
User-2	-2 0 -2 0	-1 1 -1 1	2 0 2 0	4	1

Scenario-2

Transmitter

	Input	WH Code	Input x Code
User-1	1	1111	1111
User-2	1	-1 1 -1 1	-1 1 -1 1
Transmitted data			-0 2 0 2

Receiver

	Received Data	WH Code	Decoded data	Σ	>0=1 ≤0=0
User-1	0 2 0 2	1111	0 2 0 2	4	1
User-2	0 2 0 2	-1 1 -1 1	0 2 0 2	4	1

Scenario-3

Transmitter

	Input	WH Code	Input x Code
User-1	1	1111	1111
User-2	-1	-1 1 -1 1	1 -1 1 -1
Transmitted data			2 0 2 0

Receiver

	Received Data	WH Code	Decoded data	Σ	>0=1 ≤0=0
User-1	2 0 2 0	1111	2 0 2 0	4	1
User-2	2 0 2 0	-1 1 -1 1	-2 0 -2 0	-4	-1

Scenario-4

Transmitter

	Input	WH Code	Input x Code
User-1	-1	1111	-1 -1 -1 -1
User-2	-1	-1 1 -1 1	1 -1 1 -1
Transmitted data			0 -2 0 -2

Receiver

	Received Data	WH Code	Decoded data	Σ	>0=1 ≤0=0
User-1	0 -2 0 -2	1111	0 -2 0 -2	-4	-1
User-2	0 -2 0 -2	-1 1 -1 1	0 -2 0 -2	-4	-1

From the tables in this section it can be observed that in the case of model B the recovered data is the same as the transmitted data for all input scenarios.

As the data at the input of the receiver is the same in both cases (model A and model B), it can be concluded that the error in demodulation in model A occurs due to the hard decision demapping before despreading.

Appendix B

Modelling issues

B.1 Setting E_b/N_0

The E_b/N_0 value is calculated by first measuring the energy per bit, E_b for the multi-carrier CDMA signal and then calculating the N_0 for a given E_b/N_0(dB).

$$\left(\frac{E_b}{N_0}\right)_{dB} = 10\log\left(\frac{E_b}{N_0}\right) \tag{B.1}$$

The Energy per symbol is defined as:

$$E_{symb} = E\left[\frac{1}{2}\int_{T_{cp}}^{T}\left|\tilde{s}(t)\right|^2 dt\right] \tag{B.2}$$

The integration is done over T_{cp} to T in order to avoid energy loss due to the CP.

In the case of CIT, each symbol transmits k (where $k=\log_2 M$) input bits per symbol and hence the energy per bit, E_b is defined as:

$$\begin{aligned} E_b &= \frac{E_{symb}}{N_{act}k} \\ &= \frac{E\left[\frac{1}{2}\int_{T_{cp}}^{T}\left|\tilde{s}(t)\right|^2 dt\right]}{N_{act}k} \end{aligned} \tag{B.3}$$

where E[.] denotes the expectation operator and N_{act} is the number of active users in the system.

In the case of CIF, each symbol carriers a single input bit, hence E_b is given as:

$$E_b = \frac{E_{symb}}{N_{act}} = \frac{E\left[\frac{1}{2}\int_{T_{cp}}^{T}\left|\tilde{s}(t)\right|^2 dt\right]}{N_{act}} \tag{B.4}$$

B.2 Setting OBO

The OBO is defined as:

$$OBO = 10\log\left(\frac{P_{sat_{out}}}{P_{out}}\right) = \left(\frac{A_{sat}^2}{E\left[\lim_{D_{sig.}\to\infty}\left(\frac{1}{D_{sig.}}\int_{D_{sig.}}\left|y(t)\right|^2 dt\right)\right]}\right) \tag{B.5}$$

where A_{sat} is the saturation amplitude of the amplifier related to the output, y(t) is the signal at the output of the amplifier and $D_{sig.}$ is the duration of y(t).

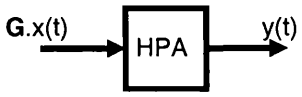

Figure B.1: HPA input/output

The input to the HPA is multiplied by a gain variable, G (Fig. B.1). By altering the value of G, the output power can also be altered and hence the OBO can be set to some predefined value.

Appendix C

BER performance of MC-CDMA CIF

In this appendix, the BER performance of MC-CDMA implementation 2 (CIF) with BPSK mapping is considered for two different receiver models in order to show that the degradation in the BER is due to the fact that the HDD is performed before despreading in the receiver. The first receiver model employs a HDD technique whereas the second model does not employ a HDD technique. The transmitter model and the two receiver models are shown in Figure C.1, C.2 and C.3 respectively.

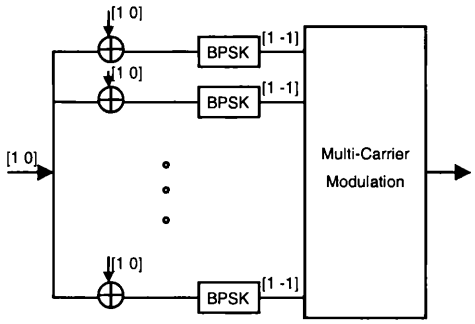

Figure C.1: MC-CDMA CIF transmitter

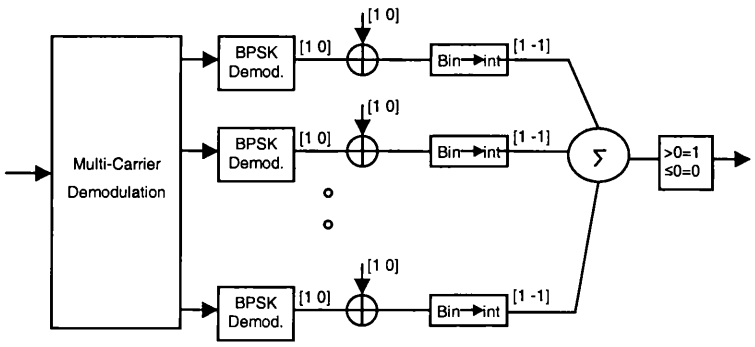

Figure C.2: MC-CDMA CIF receiver-model A

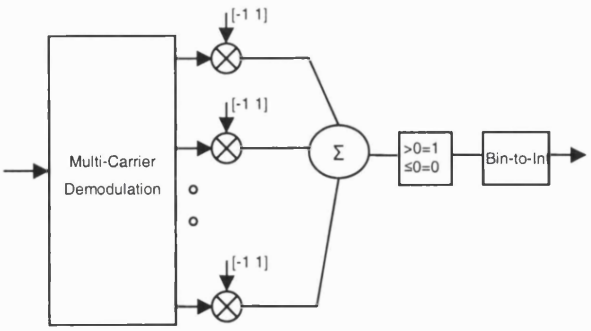

Figure C.3: MC-CDMA CIF receiver-model B

To confirm that the two receivers are similar, a simple set-up with the following parameters is considered:

- No AWGN
- Number of users: 1
- Maximum number of users: 4
- WH code length: 4
- Input: 0 or 1
- WH code allocation for the active user: 1010
- Mapping rule

	Model A	**Model B**
Data bit	0	-1
	1	1
Code chip	0	1
	1	-1

As there is only 1 active user, there are just two possible input scenarios: 1 and 0. The following tables present the data at various points in the transmitter and receivers for the 2 input scenarios.

Transmitter

Input	WH Code	Input ⊕ Code	BPSK Mod.	
0	1010	1010	1 -1 1 -1	1 -1 1 -1
1	1010	0101	-1 1 -1 1	-1 1 -1 1

Receiver – Model A

Received Data	BPSK Splice	Demod. Demap	WH Code	Decoded output	Bin-to-int	Σ	>0=1 ≤0=0
1 -1 1 -1	1 -1 1 -1	1010	1010	0000	-1 -1 -1 -1	-4	0
-1 1 -1 1	-1 1 -1 1	0101	1010	1111	1111	4	1

Receiver – Model B

Received Data	WH Code	Decoded data	Σ	>0=1 ≤0=0	Bin-to-int
1 -1 1 -1	-1 1 -1 1	-1 -1 -1 -1	-4	-1	0
-1 1 -1 1	-1 1 -1 1	1 1 1 1	+4	+1	1

Hence in the absence of AWGN, both receivers demodulate the user data correctly.

Investigating the performance of these two schemes in the presence of AWGN (Figure C.4) shows that in the case of model B, the performance of the system is the same as theoretical performance of BPSK (in a single carrier, single user case) whereas in the case of model A, there is a significant degradation in performance. Hence, from these results it can be concluded that the degradation in BER performance of model A is due to HDD before despreading in the receiver.

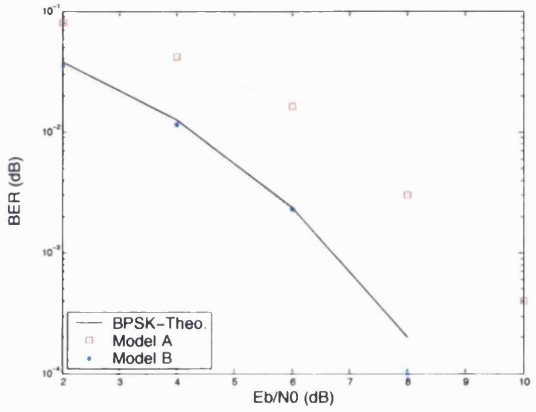

Figure C.4: BER performance of model A and model B in AWGN

Appendix D

Spreading code allocations

Allocation 1

1	2	3	4	5	6	7	8	9	10	11	12	13	14	15	*16*
17	18	19	20	21	22	23	24	25	26	27	28	29	30	31	*32*
33	34	35	36	37	38	39	40	41	42	43	44	45	46	47	*48*
49	*50*	*51*	*52*	*53*	*54*	*55*	*56*	*57*	*58*	*59*	*60*	*61*	*62*	*63*	*64*

Allocation 2

26	63	53	41	60	43	22	12	49	56	28	23	37	47	21	*35*
2	13	50	57	24	30	29	54	11	39	14	20	38	15	32	*44*
40	33	59	10	46	48	58	51	18	5	9	34	45	3	62	*64*
16	*31*	*55*	*1*	*52*	*6*	*61*	*4*	*25*	*7*	*8*	*17*	*19*	*42*	*36*	*27*

Allocation 3

21	54	3	17	39	50	15	22	45	33	16	62	58	4	20	*37*
56	43	41	31	57	1	63	51	29	8	34	53	11	12	23	*5*
40	49	47	18	36	60	7	48	64	42	59	35	14	38	10	*30*
2	*27*	*46*	*44*	*32*	*9*	*19*	*52*	*25*	*61*	*6*	*24*	*13*	*28*	*55*	*26*

Allocation 4

26	39	54	44	31	47	34	19	36	24	20	40	41	53	22	*38*
61	60	62	49	14	43	48	59	10	56	25	35	7	18	50	*12*
2	13	16	23	28	64	63	6	52	8	3	42	4	45	37	*32*
29	*21*	*27*	*55*	*17*	*15*	*46*	*57*	*51*	*1*	*5*	*11*	*9*	*58*	*30*	*33*

Allocation 5

19	49	44	51	27	13	57	33	47	14	40	4	59	10	38	12
11	56	6	28	3	58	9	50	62	45	54	26	52	7	53	30
46	36	34	42	39	25	15	21	20	37	8	43	48	1	16	22
60	*17*	*41*	*23*	*64*	*63*	*31*	*61*	*24*	*35*	*32*	*55*	*5*	*18*	*2*	*29*

Allocation 6

18	21	38	28	22	47	1	50	16	52	7	25	41	54	3	*9*
63	64	40	2	17	59	35	48	4	36	14	45	44	10	27	*43*
8	20	55	58	33	37	60	61	24	42	15	31	51	34	11	*46*
32	*53*	*49*	*6*	*19*	*12*	*13*	*57*	*56*	*5*	*29*	*62*	*26*	*23*	*30*	*39*

Allocation 7

31	28	23	29	5	60	57	41	22	4	37	51	34	8	13	*59*
54	21	63	55	33	27	50	43	19	49	56	15	42	36	52	*17*
18	25	1	11	10	14	24	46	62	47	3	39	44	6	53	*7*
26	*64*	*9*	*32*	*40*	*16*	*30*	*48*	*38*	*2*	*61*	*20*	*12*	*45*	*58*	*35*

Allocation 8

27	63	24	59	40	46	20	36	39	1	52	18	38	35	51	*14*
5	41	30	49	64	53	33	8	6	61	56	31	48	43	2	*62*
45	44	28	10	11	34	55	7	4	22	29	17	12	9	23	*54*
3	*42*	*25*	*58*	*60*	*16*	*26*	*19*	*50*	*57*	*13*	*21*	*47*	*32*	*37*	*15*

Allocation 9

54	4	60	7	36	61	27	43	42	64	44	14	57	28	56	*52*
5	26	48	24	1	10	39	40	34	17	6	62	35	47	2	*9*
25	22	18	33	37	13	30	19	49	59	51	23	20	12	31	*3*
21	46	63	53	55	41	16	11	32	8	15	29	45	38	58	50

Allocation 10

37	22	1	35	33	57	8	26	59	31	53	63	23	47	27	*3*
41	11	40	29	15	39	4	30	34	13	43	45	24	64	42	*12*
46	14	19	32	36	9	48	51	58	21	49	25	38	16	50	*56*
7	*10*	*5*	*61*	*52*	*44*	*54*	*2*	*18*	*6*	*17*	*62*	*60*	*20*	*28*	*55*

Allocation 11

27	3	55	25	54	29	5	31	59	6	42	52	16	33	11	*32*
22	58	60	26	48	40	2	23	46	21	1	47	12	4	7	*10*
17	14	20	56	35	38	43	44	8	57	63	36	50	53	51	*41*
34	*9*	*45*	*62*	*37*	*15*	*64*	*61*	*24*	*30*	*18*	*49*	*39*	*13*	*19*	*28*

Allocation 12

54	12	29	32	62	21	47	59	48	36	13	41	18	10	9	*6*
57	63	56	7	49	60	30	44	40	16	38	23	43	15	37	*24*
53	34	14	4	11	50	46	33	25	35	61	31	8	19	45	*51*
26	*55*	*5*	*42*	*58*	*17*	*22*	*3*	*39*	*20*	*28*	*2*	*64*	*1*	*52*	*27*

Allocation 13

47	37	28	13	59	52	9	64	2	21	51	55	38	31	4	*49*
34	50	11	54	43	3	29	36	5	57	48	30	20	17	53	*15*
19	56	24	35	26	12	44	39	25	8	33	14	1	46	42	*7*
32	*16*	*6*	*45*	*63*	*10*	*58*	*18*	*40*	*41*	*23*	*61*	*60*	*22*	*62*	*27*

Allocation 14

61	27	9	19	15	64	3	39	41	43	21	60	25	13	16	*51*
55	46	57	1	34	53	31	30	49	47	54	11	52	59	7	*42*
38	63	20	5	37	17	23	48	32	40	12	10	56	44	2	*33*
38	*62*	*24*	*26*	*22*	*8*	*36*	*35*	*14*	*45*	*50*	*4*	*18*	*29*	*58*	*6*

Allocation 15

1	14	63	33	40	22	5	42	55	56	8	57	48	2	27	*38*
60	35	25	23	16	34	61	28	13	47	15	18	36	46	64	*7*
43	32	49	6	44	39	37	62	53	9	21	19	31	51	52	*58*
12	*45*	*17*	*3*	*24*	*26*	*54*	*4*	*11*	*50*	*41*	*59*	*29*	*20*	*30*	*10*

Allocation 16

40	3	44	17	5	54	6	12	47	33	7	32	34	61	10	*21*
41	45	46	64	20	22	49	31	14	8	25	56	35	39	37	*2*
26	27	57	15	11	62	51	60	23	43	63	28	1	16	13	*38*
9	*29*	*30*	*58*	*36*	*48*	*50*	*42*	*24*	*18*	*59*	*52*	*19*	*55*	*4*	*53*

Allocation 17

14	12	15	29	41	46	30	43	42	36	55	59	23	20	37	*4*
48	6	1	60	54	38	50	8	32	13	26	31	16	58	61	*52*
11	51	17	57	34	10	24	47	53	56	21	28	9	44	39	*64*
63	*62*	*22*	*19*	*27*	*5*	*7*	*45*	*25*	*3*	*35*	*18*	*2*	*49*	*40*	*33*

Allocation 18

10	45	32	30	23	41	21	51	52	12	3	48	53	34	50	*31*
25	36	46	38	1	17	24	37	61	56	22	55	20	28	42	*2*
59	40	57	64	7	4	47	5	58	44	29	14	15	19	26	*27*
54	*62*	*49*	*35*	*16*	*6*	*33*	*9*	*63*	*60*	*11*	*43*	*39*	*18*	*13*	*8*

Allocation 19

10	9	35	30	7	56	21	12	34	2	28	26	16	15	61	*57*
54	39	53	18	4	45	22	41	32	5	47	29	19	3	6	*64*
49	31	11	40	37	8	38	36	52	60	48	13	62	59	24	*14*
27	*25*	*58*	*23*	*1*	*20*	*43*	*63*	*33*	*51*	*55*	*46*	*42*	*17*	*50*	*44*

Allocation 20

6	52	63	41	37	36	14	17	39	42	58	19	27	51	34	*7*
18	23	30	20	26	11	43	59	12	16	45	48	47	15	29	*61*
56	5	62	13	21	1	8	4	44	35	46	64	53	38	32	*10*
49	*28*	*25*	*33*	*40*	*55*	*54*	*9*	*22*	*57*	*3*	*50*	*24*	*2*	*31*	*60*

Allocation 21

62	22	17	30	27	42	60	56	25	41	12	13	26	21	45	*61*
20	4	29	14	19	57	8	34	52	43	63	47	9	48	33	*38*
6	64	28	36	51	23	11	55	24	15	16	31	1	3	58	*37*
54	*10*	*49*	*53*	*2*	*44*	*59*	*40*	*7*	*39*	*50*	*46*	*32*	*35*	*5*	*18*

Allocation 22

40	11	12	18	41	22	19	63	30	14	2	36	5	17	43	*32*
51	7	29	31	35	9	1	53	52	20	21	39	6	3	46	*48*
8	27	64	38	56	33	34	10	62	61	26	57	13	16	28	*55*
15	*24*	*37*	*54*	*45*	*42*	*23*	*25*	*58*	*59*	*44*	*60*	*4*	*50*	*47*	*49*

Allocation 23

42	38	24	45	36	20	22	15	30	44	41	26	54	50	11	*21*
25	6	49	16	43	5	56	29	13	33	28	2	39	35	32	*57*
7	52	51	61	34	59	31	62	60	27	1	10	19	63	58	*12*
48	*23*	*40*	*55*	*9*	*18*	*3*	*4*	*46*	*14*	*17*	*47*	*53*	*64*	*37*	*8*

Allocation 24

38	31	20	22	45	21	60	4	14	50	56	46	19	54	32	*58*
41	34	57	61	13	16	27	15	17	6	62	39	64	52	24	*29*
26	12	55	35	3	18	28	11	25	49	51	23	33	40	10	*42*
30	*9*	*37*	*59*	*7*	*43*	*48*	*44*	*5*	*2*	*36*	*1*	*53*	*8*	*47*	*63*

Allocation 25

52	8	31	25	40	46	29	21	60	59	16	47	62	12	42	*39*
9	3	55	28	41	2	56	64	33	13	51	15	27	44	48	*24*
50	19	34	17	14	54	23	43	61	37	53	5	45	6	58	*18*
32	*30*	*36*	*22*	*20*	*38*	*49*	*63*	*11*	*26*	*57*	*10*	*4*	*1*	*35*	*7*

Allocation 26

44	36	55	23	57	58	59	10	6	52	41	30	45	16	14	*39*
11	34	48	19	50	3	29	61	43	28	15	63	51	38	26	*60*
62	27	40	56	18	9	37	5	13	47	4	22	12	7	25	*46*
21	*8*	*33*	*31*	*64*	*42*	*35*	*20*	*53*	*54*	*49*	*1*	*24*	*32*	*2*	*17*

Allocation 27

13	7	12	36	52	25	62	14	57	8	15	20	11	30	28	*47*
46	19	5	54	40	56	45	37	1	55	44	3	34	9	6	*42*
60	17	21	58	32	31	51	50	24	63	29	49	53	4	64	*38*
22	*27*	*61*	*48*	*33*	*18*	*10*	*39*	*2*	*23*	*16*	*43*	*41*	*26*	*35*	*59*

Allocation 28

19	3	20	25	22	33	30	40	63	5	50	11	51	8	1	18
36	55	7	59	48	12	60	13	28	41	37	9	29	35	24	49
31	42	58	47	54	64	16	10	34	2	21	27	53	62	6	57
15	*39*	*44*	*43*	*17*	*26*	*38*	*4*	*32*	*14*	*61*	*46*	*52*	*45*	*23*	*56*

Allocation 29

32	4	56	61	41	3	30	22	17	15	14	54	40	8	50	47
26	60	13	39	59	23	43	48	18	62	55	12	5	28	10	51
21	44	7	27	63	33	24	25	20	6	46	31	11	9	64	37
58	*38*	*57*	*45*	*16*	*2*	*53*	*29*	*36*	*49*	*1*	*52*	*19*	*35*	*42*	*34*

Allocation 30

64	63	62	61	60	59	58	57	56	55	54	53	52	51	50	*49*
48	47	46	45	44	43	42	41	40	39	38	37	36	35	34	*33*
32	31	30	29	28	27	26	25	24	23	22	21	20	19	18	*17*
16	*15*	*14*	*13*	*12*	*11*	*10*	*9*	*8*	*7*	*6*	*5*	*4*	*3*	*2*	*1*

PAPR variations of the different random code allocations

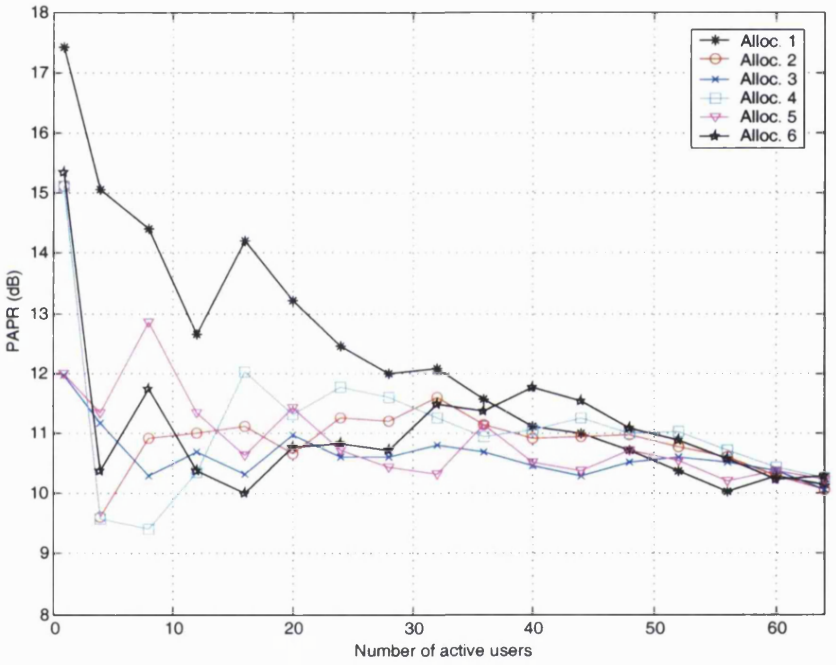

Figure D.1: PAPR of the signal at the output of the MC-CDMA transmitter with different WH code allocations - Allocation-1 to Allocation-6

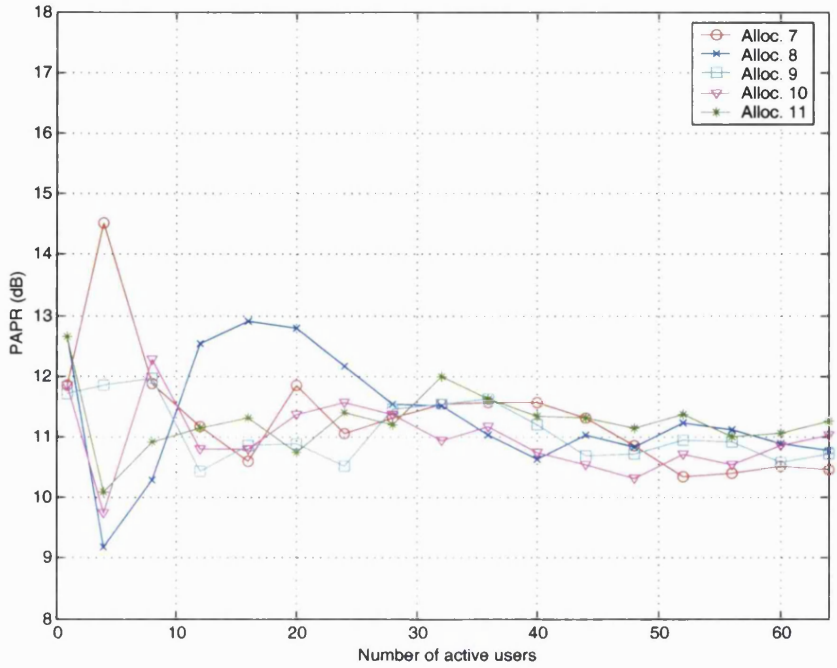

Figure D.2: PAPR of the signal at the output of the MC-CDMA transmitter with different WH code allocations - Allocation-7 to Allocation-11

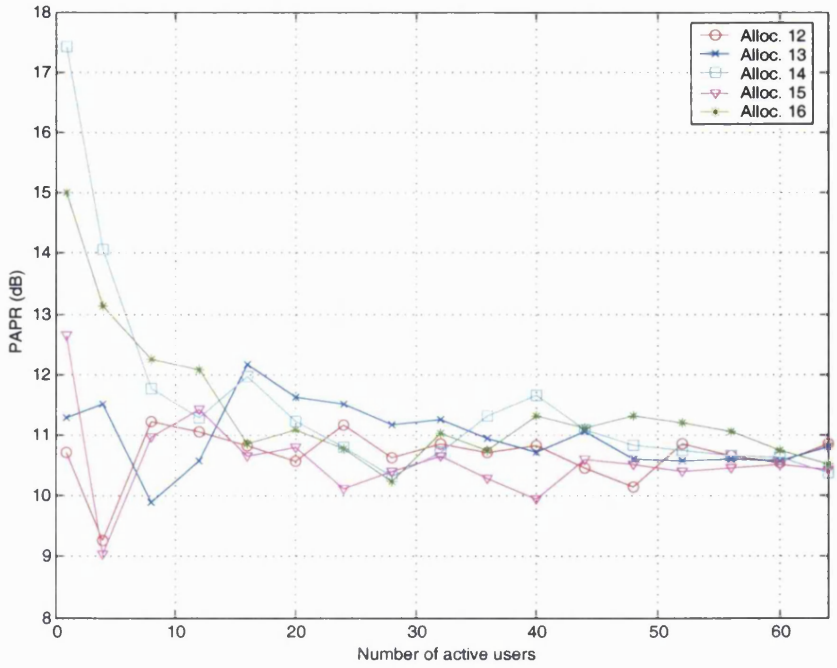

Figure D.3: PAPR of the signal at the output of the MC-CDMA transmitter with different WH code allocations - Allocation-12 to Allocation-16

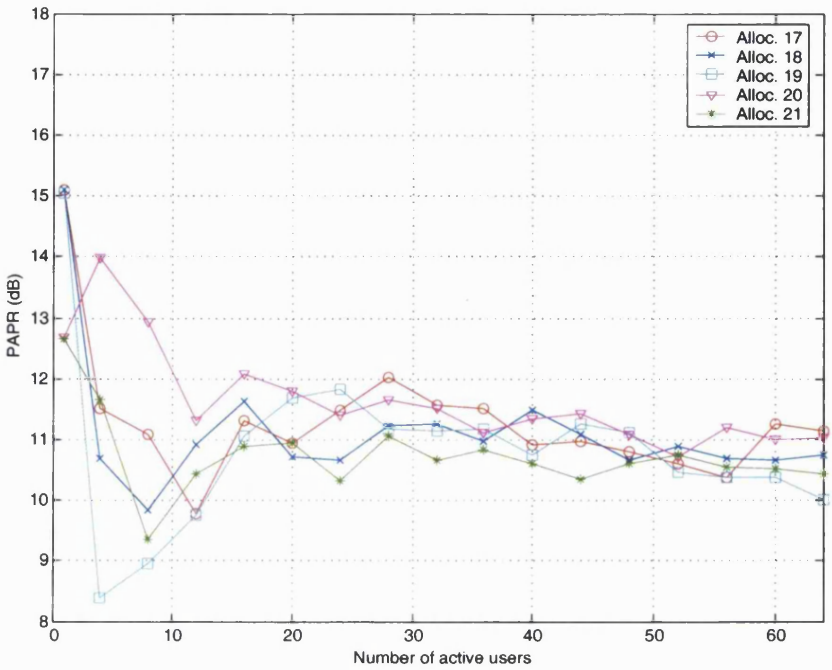

Figure D.4: PAPR of the signal at the output of the MC-CDMA transmitter with different WH code allocations - Allocation-17 to Allocation-21

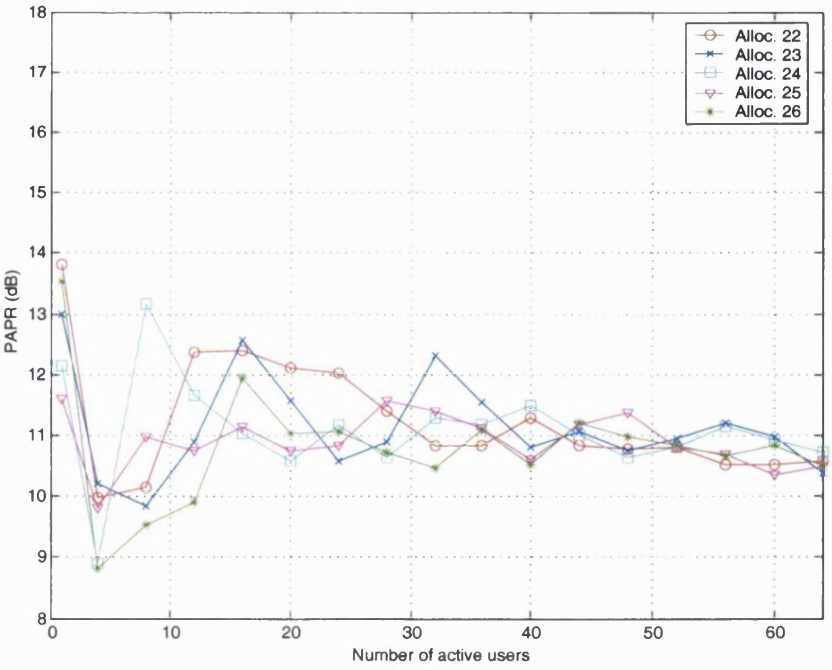

Figure D.5: PAPR of the signal at the output of the MC-CDMA transmitter with different WH code allocations - Allocation-22 to Allocation-26

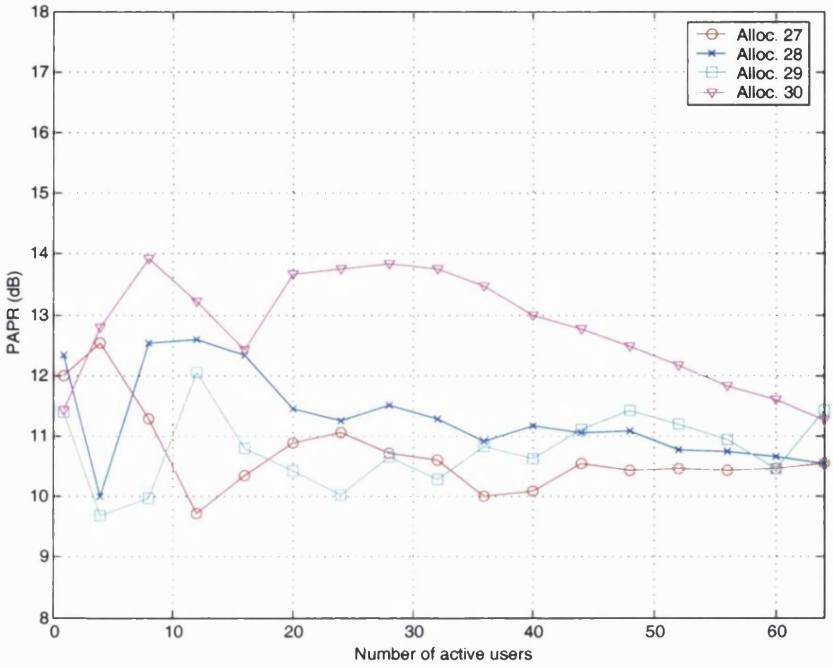

Figure D.6: PAPR of the signal at the output of the MC-CDMA transmitter with different WH code allocations - Allocation-27 to Allocation-30

References

[1] Wireless world research forum, www.wireless-world-research.org.

[2] Fourth generation mobile forum, www.4gmobile.com.

[3] IST Cluster on systems beyond 3G, www.cordis.lu/ist/ka4/mobile/proclu/c/beyond3g.htm.

[4] "Samsung locates 4G wireless research group at its London Seri Lab.," Electronic Engineering Times, Issue 1175, pp. 26, July 2001.

[5] "DoCoMo plans 4G launch by 2006," Network Briefing Daily, April 2001.

[6] "DoCoMo says 4G transmission test successful," RCR Wireless News, Vol. 21, Issue 41, pp. 35, October 2002.

[7] "Getting early handle on 4G," Electronic Engineering Times, Issue 1192, pp. 65, November 2001.

[8] A. Dornan, "Fast forward to 4G?," Network Magazine, Vol. 17, Issue 3, pp. 34-39, March 2002.

[9] N. Mokhoff, "4G wireless challenge raises stakes for DSP," Electronic Engineering Times, Issue 1027, pp. 53-54, February 2002.

[10] M. LeFevre and P. Okrah, "Making the leap to 4G wireless," Communication Systems Design, Vol. 7, Issue 7, pp. 26-32, July 2001.

[11] "Multi carrier code division multiple access," Hughes Software Systems, www.hssworld.com.

[12] H. Atarashi, S. Abeta and M. Sawahashi, "Performance evaluation of coherent high speed TD-OFCDM broadband packet wireless access in forward link employing multi-level modulation and hybrid ARQ," IEICE Transactions Fundamentals, Vol. E84-A, No. 7, pp. 1670-1680, July 2001.

[13] "A conversation with Claude Shannon," interview conducted by R. Price, edited by F. Ellersick, IEEE Communications Magazine, Vol. 22, No. 5, pp. 123-126, May 1984.

[14] G. R. Cooper and R. W. Nettleton, "A spread-spectrum technique for high capacity mobile communications," IEEE Transactions in Vehicular Technology, Vol. 27, No. 4, pp. 264-275, November 1978.

[15] Qualcomm Inc., www.qualcomm.com

[16] M. Y. Rhee, "CDMA cellular mobile communications: Networks and security," Prentice Hall, 1998.

[17] T. Ojanpera and R. Prasad, "Wideband CDMA for third generation mobile communications," Artech House Publishers, 1998.

[18] M. R. Karim, "W-CDMA and CDMA-2000 for 3G mobile networks," McGraw-Hill Publishers, 2002.

[19] R. Nee and R. Prasad, "OFDM for wireless multi-media communications," Artech House Publishers, 2000.

[20] E. H. Dinan and B. Jabbari, "Spreading codes for direct sequence CDMA and Wideband CDMA cellular networks," IEEE Communications Magazine, Vol. 36, No. 9, pp. 48-54, September 1998.

[21] H. Ochiai and H. Imai, "OFDM-CDMA with peak power reduction based on the spreading sequences," Proceedings of IEEE ICC'98, pp. 1299-1303, Atlanta, USA, June 1998.

[22] R. R. Mosier and R. G. Clabaugh, "Kineplex, a bandwidth efficient binary transmission system," AIEE Transactions, Vol. 76, pp. 723-728, January 1958.

[23] R. W. Chang, "Synthesis of band limited orthogonal signals for multi-channel data transmission," Bell System Technical Journal, 45:1775-1796, December 1966.

[24] B. R. Salzberg, "Performance of an efficient parallel data transmission system," IEEE Transactions in Communications, Vol. COM-15, pp. 805-813, December 1967.

[25] S. B. Weinstein and P. M. Ebert, "Data transmission by frequency-division multiplexing using the discrete fourier transform," IEEE Transactions in Communications, Vol. COM-19, pp. 628-634, October 1971.

[26] G. C. Porter, "Error distribution and diversity performance of a frequency differential PSK HF modem," IEEE Transactions in Communications, Vol. COM-16, pp 567-575, August 1968.

[27] M. S. Zimmerman and A. L. Kirsh, "The AN/GSC-10 (KATHRYN) variable rate date modem for HF radio," IEEE Transactions in Communications, Vol. COM-15, pp. 197-205, April 1967.

[28] Hirosaki, B., "A 19.2 kbits voice band data modem based on orthogonal multiplexed QAM techniques," Proceedings of IEEE ICC'85, pp 21.1.1-5, 1985.

[29] S. Hara, M. Mouri, M. Okada and N. Morinaga, "Transmission performance analysis of multi-carrier modulation in frequency selective fast rayleigh fading channel," Wireless Personal Communications, Kluwer Academic Publishers, Vol. 2, No. 4, pp. 335-356, 1996.

[30] P. S. Chow, J. C. Tu and J. M. Cioffe, "Performance evaluation of a multichannel transceiver system for ADSL and VHDSL services," IEEE Journal on Selected Areas in Communications, Vol. SAC-9, No. 6, pp. 909-919, August 1991.

[31] P. S. Chow, J. C. Tu and J. M. Cioffe, "A discrete multitone transceiver system for HDSL applications," IEEE Journal on Selected Areas in Communications, Vol. SAC-9, No. 6, pp. 895-908, August 1991.

[32] Digital video broadcasting website, http://www.dvb.org/

[33] The world forum for digital audio broadcasting, http://www.worlddab.org/

[34] Palowireless HiperLAN resource centre, http://www.palowireless.com/hiperlan2/

[35] Palowireless IEEE 802.11 resource centre, http://www.palowireless.com/i802_11/tutorials.asp

[36] Palowireless IEEE 802.16 resource centre, http://www.palowireless.com/i802_16/tutorials.asp

[37] M. R. D. Rodrigues, "Modelling and performance assessment of OFDM communication systems in the presence of non-linearities," PhD Thesis, University College London, UK, October 2002.

[38] R. Prasad and S. Hara, "Overview of multi-carrier CDMA," IEEE Communications Magazine, pp. 126-133, December 1997.

[39] N. Yee, J-P Linnartz and G. Fettweis, "Multi-carrier CDMA in indoor wireless radio networks," Proceeding of IEEE PIMRC'93, pp109-113, Yokohama, Japan, September 1993.

[40] K. Fazel and L. Papke, "On the performance of convolutionally-coded CDMA/OFDM for mobile communications system," Proceeding of IEEE PIMRC'93, pp. 468-472, Yokohama, Japan, September, 1993.

[41] A. Chouly, A. Brijal and A. Jourdan: " Orthogonal multicarrier techniques applied to direct sequence spread spectrum CDMA systems," Proceedings of IEEE GLOBECOM'93, pp. 1723-1728 , Houston, USA, November 1993.

[42] V. M. DaSilva and E. S. Sousa, "Performance of orthogonal CDMA codes for quassi-synchronous communication systems," Proceedings of IEEE ICUPC'93, pp. 995-999, Ottawa, Canada, October 1993.

[43] L. Vandendorpe, "Multitone direct sequence CDMA system in an indoor wireless environment," Proceedings of IEEE First Symposium of communications and Vehicular Technology, pp. 4.1.1-4.1.8, Delft, The Netherlands, October, 1993.

[44] S. Kaiser, "OFDM-CDMA versus DS-CDMA: performance evaluation of fading channels," Proceedings of IEEE ICC'95, pp. 1722-1726, Seattle, USA, June 1995.

[45] L-L. Yang and L. Hanzo, "Multi-carrier code division multiple access," University of Southampton internal report, 2000.

[46] S. Konda and L. B. Milstein, "Performance of multi-carrier DS-CDMA systems," IEEE Transactions in Communications, Vol. 44, No 2, pp 238-246, February 1996.

[47] E. Sourour and M. Nakagawa, "Performance of orthogonal multi-carrier CDMA in a multipath fading channel," IEEE Transactions in Communications, Vol. 44, No. 3, pp 356-367, March 1996.

[48] T. Rappaport, "Wireless communications: Principles and practice," Prentice Hall Publishers, 1996.

[49] B. Glance and L. J. Greenstein, "Frequency-selective fading effects in digital mobile radio with diversity combining," IEEE Transactions on Communications, pp. 625-635, 1983.

[50] M. C. Jeruchim, P. Balaban and K. Sam Shanmugan, "Simulation of communication systems, modelling, methodology and techniques," Kluwer Academic/Plenum Publishers, 2000.

[51] R. A. Stirling-Gallacher and G. J. R. Povey, "Comparison of MC-CDMA and DS-CDMA using frequency domain and time domain RAKE receivers," Wireless Personal Communications, Kluwer Academic Publishers, pp. 105-119, 1995.

[52] P. Varzakas and G. S. Tombras, "Estimation of spectral efficiency for MC/DS-CDMA in cellular systems," Proceeding of SCVT'00, pp. 62-68, 2000.

[53] H. Steendam and M. Moeneclaey, "Comparison of the sensitivities of MC-CDMA and MC-DS-CDMA to carrier frequency offset," Proceedings of SCVT-2000, pp. 166-173, Leuven, Belgium, October 2000.

[54] S. Abeta, H. Atarashi, M. Sawahashi and F. Adachi, "Coherent multicarrier/DS-CDMA and MC-CDMA for broadband packet wireless access," Proceedings of VTC'00, Vol. 3, pp. 1918-1922, Tokyo, Japan, May 2000.

[55] S. Suwa, H. Atarashi and M. Sawahashi, "Performance comparison between MC/DS-CDMA and MC-CDMA for reverse link broadband packet wireless access," Proceedings of VTC-02, Vol. 4, pp. 2076-2080, Kanagawa, Japan, September 2002.

[56] G. P. Fettweis, A. Nahler and J. Kuhne, "A time domain view to multi-carrier spread spectrum," Proceedings of IEEE ISSTA, New Jersey, USA, September 2000.

[57] H. Kaaranen, A. Ahtiainen, L. Laitinen, S. Naghian and V. Niemi, "UMTS Networks," John Wiley and Sons, 2001.

[58] H. Holma and A. Toskala, "WCDMA for UMTS," John Wiley and Sons Ltd, 2001.

[59] J. Yang, D. Bao and M. Ali, "PN offset planning in IS-95 based CDMA systems," Proceedings of VTC'97, Vol. 3, pp. 1435-1439, Phoenix, Arizona, USA, May 1997.

[60] C. R. Chang, J. Z. Wan and M. F. Yee, "PN offset planning strategies for non-uniform CDMA networks," Proceedings of VTC'97, Vol. 3, pp. 1543-1547, Phoenix, Arizona, USA, May 1997.

[61] S. Faruque, "Directional PN offset reuse for DCMA deployment," Proceedings of IEEE ICPWC'97, pp. 130-132, Mumbai, India, December 1997.

[62] Y-H. Jung and Y. H. Lee, "Scrambling code planning for 3GPP W-CDMA systems," Proceedings of VTC'01, Vol. 4, pp. 2431-2434, Rhodes, Greece, May 2001.

[63] H. Steendam and M. Moeneclaey, "The effect of synchronisation errors on MC-CDMA performance," Proceedings of IEEE ICC'99, pp. 1510-1514, Vancouver, Canada, June 1999.

[64] M. Chrysochoos and J. Kim, "Performance analysis of an MC-CDMA broadcasting system under high power amplifier non-linearities. I. System Proposal," IEEE Transactions on Broadcasting, Vol. 46, No. 4, pp. 256-262, December 2000.

[65] K. Fazel and S. Kaiser, "Analysis of non-linear distortions on MC-CDMA," Proceedings of IEEE ICC'98, pp. 1028-1034, Atlanta, June 1998.

[66] L. Frieberg, A. Annamalai and V. Bhargava, "Crest factor reduction using orthogonal spreading codes in multi-carrier CDMA systems," Proceedings of IEEE PIMRC'97, pp. 120-124, Helsinki, Finland, September 1997.

[67] T. Ginige, N. Rajatheva and K. M. Ahmed, "Dynamic spreading code selection method for PAPR reduction in OFDM-CDMA systems with 4-QAM modulation," IEEE Communications Letters, Vol. 5, No. 10, pp. 408-410, October 2001.

[68] S. Hara and R. Prasad, "DS-CDMA, MC-CDMA and MT-CDMA for mobile multi-media communications," Proceedings of IEEE VTC'96, pp. 1106-1110, Atlanta, USA, May 1996.

[69] L. Tomba and W. A. Krzymien, "Sensitivity of the MC-CDMA access scheme to carrier phase noise and frequency offset," IEEE Transactions on Vehicular Technology, Vol. 48, pp. 1657-1665, September 1999.

[70] S. B. Slimane, "MC-CDMA with quadrature spreading over frequency selective fading channels," Proceedings of IEEE GLOBCOM'97, pp. 315-319, Phoenix, USA, November 1997.

[71] A. Burr, "Modulation and coding for wireless communications," Prentice Hall Publishers, 2001.

[72] G. Santella and F. Mazzenga, "A model for performance evaluation in M-QAM OFDM schemes in the presence of nonlinear distortions," Proceedings of IEEE VTC'95, pp. 830-834, Chicago, USA, July 1995.

[73] E. Costa and S. Pupolin, "M-QAM–OFDM system performance in the presence of a nonlinear amplifier and phase noise," IEEE Transactions on Communications, Vol. 50, No. 3, pp. 462-472, March 2002.

[74] W. Yongbin, E. G. Tiedemann, L. Fuyun and S. Sarkar, "Using multi-level QAM modulation in CDMA System," Proceedings of IEEE VTC'01, pp. 633-636, Greece, May 2001.

[75] S. Haykin, "Communication Systems," John Wiley and Sons Publishers, 2001.

[76] J. Proakis, "Digital communications," McGraw-Hill Publishers, 2001.

[77] B. M. Popovic, "Spreading sequences for multi-carrier CDMA systems," Proceedings of IEE Colloquium on CDMA Techniques and Applications for Third Generation Mobile Systems, pp. 8/1-8/6, London, May 1997.

[78] A. Doufexi, S. Armour, A. Nix and D. Bull, "A comparison of HIPERLAN/2 and IEEE 802.11a physical and MAC layers," Proceedings of Symposium on Communications and Vehicular Technology 2000, pp. 14-20, Belgium, October 2000.

[79] S. Verdu, "Minimum probability of error for asynchronous gaussian multiple-access channels," IEEE Transactions in Information Theory, Vol. IT-32, pp. 85-96, January 1986.

[80] L. K. Rasmussen, T. J. Lim and T. M. Aulin, "Breadth-first maximum likelihood detection in multiuser CDMA," IEEE Transactions in Communications, Vol. 45, No. 10, pp. 1176-1178, October, 1997.

[81] N. Phamdo and F. Alajaji, "Soft-decision demodulation design for COVQ over white, colored and ISI Gaussian channels," IEEE Transactions on Communications, Vol. 48, Issue 9, pp. 1499-1506, September 2000.

[82] F. Tosato and P. Bisaglia, "Simplified soft output demapper for binary interleaved COFDM with application to HIPERLAN/2," Proceedings of ICC'02, Vol. 2, pp. 664-668, April New York City, USA, 2002.

[83] E. Baccarelli, R. Cusani and G. Di Blasio, "A new family of decision delay-constrained MAP decoders for data transmission over noisy channels with ISI and soft decision demodulation," Proceedings of IEEE ISIT'95, pp. 333, September 1995.

[84] S. Verdu, "Multiuser detection," Cambridge University Press, 1998.

[85] M.C. Jeruchim, "Techniques for estimating the bit error rate in the simulation of digital communication systems," IEEE Journal on selected areas in communications, pp. 153-170, January 1984.

[86] J. Pinto, "Studies of predetection filters and error vector magnitude in GSM and EDGE mobile communication systems," PhD Thesis, University of Manchester Institute of Science and Technology, UK, November 2001.

[87] [Sklar1] B. Sklar, "Digital communications, fundamentals and applications," Prentice Hall, 1988.

[88] P. C. Li and E. Geraniotis, "Performance analysis of synchronous M-PSK CDMA multi-tier systems with a nonlinear amplifier," Proceedings of IEEE Symposium on Computers and Communications, pp. 275-279, Egypt, July 1997.

[89] S. Merchan, A Garcia Armada and J. L. Garcia, "OFDM performance in amplifier nonlinearity," IEEE Transactions on Broadcasting, Vol. 44, No. 1, pp. 106-113, March 1998.

[90] S-W Chen, W. Panton and R. Gilmore, "Effects of non-linear distortion on CDMA communication systems," IEEE Transactions on Microwave Theory and Techniques, Vol. 44, No. 12, pp. 2743-2750, December 1996.

[91] G. White, "Mobile Radio Technology," Butterworth-Heinemann Publishers, 1994.

[92] O. Bishop, "Understanding Amplifiers," Butterworth-Heinemann Publishers, 1998.

[93] J. Tellado, "Multicarrier modulation with low PAR: Application to DSL and wireless," Kluwer Academics Publishers, 2000.

[94] C. Rapp, "Effects of HPA-nonlinearity on a 4-DPSK/OFDM-signal for a digital sound broadcasting system," Proceedings of 2nd European Conference on Satellite Communications, Belgium, October 1991.

[95] A. A. Saleh, "Frequency-independent and frequency-dependent non-linear models of TWT amplifiers," IEEE Transactions on Communications, Vol. COM-29, No. 11, pp. 1715-1720, November 1981.

[96] J. Jong, K. Yang, W. E. Stark, and G. I. Haddad, "Power optimization of OFDM systems with dc bias controlled nonlinear amplifiers," Proceedings of IEEE VTC'99 pp. 268-272, September 1999.

[97] G. Santella and F. Mazzenga, "A hybrid analytical-simulation procedure for performance evaluation in M-QAM-OFDM schemes in presence of nonlinear distortions," IEEE Transactions on Vehicular Technology, Vol. 47, No. 1, pp. 142-151, February 1998.

[98] A. N. D' Andrea, V. Lotici, and R. Reggiannini, "RF power amplifier linearization through amplitude and phase predistortion," IEEE Transactions on Communications, Vol. 44, pp. 1477-1484, November 1996.

[99] A. E. Jones, T. A. Wilkinson and S. K. Barton, "Block coding schemes for reduction of peak-to-mean envelope power ratio of multicarrier transmission scheme," Electronics letters, Vol. 30, No. 25, pp. 2098-2099, December 1994.

[100] M. Pauli and H. P. Kuchenbecker, "Minimization of the intermodulation distortion of a nonlinearly amplified OFDM signal," Wireless Personal Communications, Kluwer Academic Publishers, Vol. 4, No. 1, pp. 93-101, January 1997.

[101] R. Van Nee and A. De Wild, "Reducing the peak-to-average power ratio of OFDM," Proceedings of IEEE VTC'98, pp. 2072-2076, Ottawa, Canada, May 1998.

[102] S. Muller and J. Huber, "OFDM with reduced peak-to-average power ratio by optimum combination of partial transmit sequences," Electronics letters, Vol. 33, No. 5, pp. 368-369, February 1997.

[103] R. Bauml, R. Fischer and J. Huber, "Reducing the peak-to-average power ratio of multi-carrier modulation by selected mapping," Electronics letters, Vol. 32, No. 22, pp. 2056-2057, October 1996.

[104] Multi-carrier power amplifiers for W-CDMA wireless systems, Powerwave technologies, www.powerwave.com/mcpa.pdf

[105] N. Pothecray, "Feedback linear power amplifiers," Artech House Publishers 1999.

[106] T. Fujii and M. Nakagawa, "Code selecting peak power reduction for MC-CDMA," Proceedings of Wireless communications and networking conference, Vol. 1, pp. 482-486, Florida, USA, March 2002.

[107] H. Ochiai and H. Imai, "On the distribution of the peak-to-average power ratio in OFDM signals," IEEE Transactions on communications, Vol. 49, No. 2, pp. 282-289, February 2001.

[108] X. Li and L. J. Cimini, "Effects of clipping and filtering on the performance of OFDM," IEEE Communications Letters, pp. 131-133, May 1998.

[109] R. Van Nee, "OFDM codes for peak-to-average power reduction and error correction," Proceedings of IEEE GLOBECOM'96, pp. 740-744, London, UK, November 1996.

[110] S. Fragiacomo, C. Matrakidis and J. J. O'Reilly, "Multicarrier transmission peak-to-average power reduction using simple block code," Electronics Letters, Vol. 34, Issue 10, pp. 953-954, May 1998.

[111] B. M. Popovic, "Synthesis of power efficient multitone signals with flat amplitude spectrum," IEEE Transactions on communications, Vol. 39, pp. 1031-1033, July 1991.

[112] J. A. Davis and J. Jedwab, "Peak-to-mean power control in OFDM, Golay complementary sequences and Reed-Muller codes," IEEE Transactions on information theory, Vol. 45, pp. 2397-2417, November 1997.

[113] A. G. Shanbhag and E. G. Tiedemann, "Peak-to-average reduction via optimal walsh code allocation in third generation CDMA systems," Proceedings of IEEE ISSTA'00, pp. 560-564, Parsippany, USA, September 2000.

[114] V. K. N. Lau, "Peak to average ratio (PAR) reduction by walsh-code selection for IS-95 and CDMA2000 systems," IEE Proceedings on Communications, Vol. 147, No. 6, pp. 361-364, December 2000.